



---

# TECHNICAL REPORT

---

**97-19**

**Assessment of a spent fuel disposal  
canister**

**Assessment studies for a copper canister  
with cast steel inner component**

Alex E Bond, Andrew R Hoch, Gareth D Jones,  
Aleks J Tomczyk, Richard M Wiggin, William J Worraker

AEA Technology, Harwell, UK

May 1997

---

**SVENSK KÄRNBRÄNSLEHANTERING AB**  
*SWEDISH NUCLEAR FUEL AND WASTE MANAGEMENT CO*

P.O.BOX 5864 S-102 40 STOCKHOLM SWEDEN  
PHONE +46 8 459 84 00  
FAX +46 8 661 57 19

# **ASSESSMENT OF A SPENT FUEL DISPOSAL CANISTER**

## **ASSESSMENT STUDIES FOR A COPPER CANISTER WITH CAST STEEL INNER COMPONENT**

*Alex E Bond, Andrew R Hoch, Gareth D Jones,  
Aleks J Tomczyk, Richard M Wiggin, William J Worraker*

**AEA Technology, Harwell, UK**

May 1997

This report concerns a study which was conducted for SKB. The conclusions and viewpoints presented in the report are those of the author(s) and do not necessarily coincide with those of the client.

Information on SKB technical reports from 1977-1978 (TR 121), 1979 (TR 79-28), 1980 (TR 80-26), 1981 (TR 81-17), 1982 (TR 82-28), 1983 (TR 83-77), 1984 (TR 85-01), 1985 (TR 85-20), 1986 (TR 86-31), 1987 (TR 87-33), 1988 (TR 88-32), 1989 (TR 89-40), 1990 (TR 90-46), 1991 (TR 91-64), 1992 (TR 92-46), 1993 (TR 93-34), 1994 (TR 94-33), 1995 (TR 95-37) and 1996 (TR 96-25) is available through SKB.

# **ASSESSMENT OF A SPENT FUEL DISPOSAL CANISTER**

## **ASSESSMENT STUDIES FOR A COPPER CANISTER WITH CAST STEEL INNER COMPONENT**

*Alex E Bond, Andrew R Hoch, Gareth D Jones, Aleks J Tomczyk,  
Richard M Wiggan and William J Worraker*

**AEA Technology, Harwell, UK**

May 1997

# ABSTRACT

The proposed design for a final repository for spent fuel and other long-lived residues in Sweden, is based on the multi-barrier principle. The waste will be encapsulated in sealed cylindrical canisters, which will then be placed in vertical storage holes drilled in a series of caverns excavated from the granite bedrock at a depth of about 500m. Each canister will be surrounded by compacted bentonite clay.

In this report, a simple model of the behaviour of the canister subsequent to a first breach in its copper overpack is developed. This model is used to predict:

- the ingress of water to the canister (as a function of the size and shape of the initial defect, the buffer conductivity, the corrosion rate and the pressure inside the canister);
- the build-up of corrosion product in the canister (as a function of the available water in the canister, the corrosion rate and the properties of the corrosion product);
- the effect of corrosion on the structural integrity of the canister.

A number of different scenarios for the location of the breach in the copper overpack are considered.

## SAMMANFATTNING

Den föreslagna designen för ett djupförvar för använt kärnbränsle och annat lång-livat avfall i Sverige är baserad på multi-barriär principen. Avfallet kommer att inkapslas i förseglade cylindriska kapslar, vilka kommer att placeras i vertikala deponeringshål i en serie av tunnlar i granitiskt urberg på ett djup av cirka 500 m. Varje kapsel kommer att omges av kompakterad bentonitlera.

I den här rapporten presenteras en enkel modell för kapselns utveckling efter ett första genombrott i kapseln ytterhölje av koppar. Modellen används för att prediktera:

- intrånget av vatten i kapseln (som en funktion av storlek och form på defekten, buffertens konduktivitet, korrosionshastigheten och trycket inuti kapseln);
- Uppbyggnaden av korrosionsprodukter inuti kapseln (som en funktion av tillgängligt vatten i kapseln, korrosionshastigheten och korrosionsprodukternas egenskaper);
- effekten av korrosionsprodukterna på kapselns strukturella integritet.

Ett antal scenarier för placeringen av skadan i kopparhöljet har studerats.

# TABLE OF CONTENTS

	Page	
<b>1</b>	<b>INTRODUCTION</b>	<b>1</b>
<b>2</b>	<b>CANISTER</b>	<b>3</b>
2.1	CANISTER DESIGN	3
2.2	BENTONITE BUFFER	3
<b>3</b>	<b>THE ASSESSMENT MODEL</b>	<b>6</b>
3.1	INTRODUCTION	6
3.2	ASSUMPTIONS	6
3.2.1	Geometry	6
3.2.2	Processes outside the canister	7
3.2.3	Processes inside the canister	8
3.3	THE SEQUENCE OF EVENTS	9
3.4	RESULTS	10
3.4.1	Definition of scenarios	10
3.4.2	$a = 5 \cdot 10^{-6} \text{ m}^2$ , and $\mu = 0.1 \text{ micron/year}$	12
3.4.3	$a = 2 \cdot 10^{-5} \text{ m}^2$ , and $\mu = 0.1 \text{ micron/year}$	15
3.4.4	$a = 5 \cdot 10^{-6} \text{ m}^2$ , and $\mu = 0.01 \text{ micron/year}$	19
3.4.5	$a = 0.1791 \text{ m}^2$ , AND $\mu = 1 \text{ micron/year}$	28
<b>4</b>	<b>THE DIFFUSION MODEL</b>	<b>34</b>
4.1	INTRODUCTION	34
4.2	ASSUMPTIONS	34
4.3	REVIEW OF THE STRESS CORROSION MODEL	35
4.4	THE COMPUTER MODEL	36
4.5	RESULTS AND DISCUSSION	37
4.6	CONCLUSIONS	41
<b>5</b>	<b>THE STRESS MODEL</b>	<b>51</b>
5.1	INTRODUCTION	51
5.2	ASSUMPTIONS	52
5.2.1	Canister	52
5.2.2	Repository	55
5.2.3	Penetration	57
5.2.4	Material properties	57
5.2.5	Corrosion	60
5.2.6	Corrosion product properties	62
5.2.7	Loading	63

5.3	CANISTER ANALYSES	63
5.3.1	Model	64
5.3.2	Results	68
5.3.3	Discussion	69
5.4	INFLUENCE OF CORROSION PRODUCT PROPERTIES	82
5.4.1	Model	82
5.4.2	Results	82
5.4.3	Discussion	83
5.5	DETAILED ANALYSES	88
5.5.1	Model	88
5.5.2	Results	89
5.5.3	Discussion	98
5.6	INFLUENCE OF DEFECT GEOMETRY	98
5.6.1	Model	98
5.6.2	Method of analysis	99
5.6.3	Results	100
5.7	VAULT ANALYSES	109
5.7.1	Model	109
5.7.2	Results	110
5.7.3	Discussion	111
5.8	CORROSION AT THE LID INTERFACE	120
5.8.1	Introduction	120
5.8.2	Results	120
<b>6</b>	<b>TIME SCALE FOR THE STRESS MODEL</b>	<b>121</b>
6.1	INTRODUCTION	121
6.2	RESULTS	121
<b>7</b>	<b>CONCLUSIONS</b>	<b>139</b>
	<b>REFERENCES</b>	<b>143</b>
	<b>APPENDICES</b>	<b>146</b>

## SUMMARY AND CONCLUSIONS

The proposed design for a final repository for spent fuel and other long-lived residues in Sweden, is based on the multi-barrier principle. The waste will be encapsulated in sealed cylindrical canisters, which will then be placed in vertical storage holes drilled in a series of caverns excavated from the granite bedrock at a depth of about 500m. Each canister will be surrounded by compacted bentonite clay.

The canister design is based on a thick cast steel inner container, designed to provide mechanical strength and to keep individual fuel bundles at a safe distance from one another, thereby minimising the risk of criticality. The steel container is fitted inside an inherently corrosion resistant copper overpack (the wall of which is approximately 50 mm thick) that is designed to provide containment over the long time scales required.

As part of the safety case for the repository, one of the scenarios being addressed by SKB involves the mechanical failure of the outer copper overpack, allowing water to enter the canister and corrode the inner steel container. The seals in the inner container are also assumed to have failed, allowing groundwater access to the fuel channels. The consequences of this failure are:

- water or water vapour can penetrate the canister;
- anaerobic corrosion of the inner container generates hydrogen;
- the long-term build up of corrosion product induces stresses in the spent fuel canister.

A model has been developed for the inflow of water to a canister with a penetration in its copper overpack, resulting in anaerobic corrosion of the cast steel inner container and the generation of hydrogen. This model describes the interactions between the supply of water, corrosion, hydrogen production, pressure inside the canister and the flows of water and hydrogen.

Broadly, the sequence of events is as follows:

- Water flows into the annulus through the penetration in the copper overpack, causing anaerobic corrosion on the outer and inner surfaces of the inner container. This generates hydrogen which causes the pressure inside the canister to rise, thereby gradually reducing the rate of water inflow. Since water is being consumed by corrosion at an almost constant rate, the internal water inventory reaches a maximum and then declines. Depending on the hole size, the corrosion rate, and the height

of the crack in the inner container, the water in the annulus may also spill over into the inner container.

- What happens next is determined by the maximum water inventory inside the canister, which depends mainly on the hole size and the corrosion rate. The distribution of water between the annulus and inner container is relatively unimportant. There are three possibilities:

(1) If the hole is so small that the initial (i.e. peak) rate of water ingress cannot match the corrosion rate, then there is no build-up of liquid water in the vessel. Corrosion proceeds at a rate limited by the supply of water, which decreases as the hydrogen pressure inside the canister rises. The internal pressure approaches the external pressure asymptotically from below, while the corrosion rate falls asymptotically to zero. No hydrogen escapes from the canister. Assuming a hole of circular cross-section, a simple calculation based on the rate of water supply that is required to support the postulated corrosion rate, shows that the hole radius is directly proportional to the corrosion rate and inversely proportional to the external pressure. At a corrosion rate of  $10^{-7}$  m/year and a pressure of 5 MPa, the hole radius below which no water collects in the canister is calculated as 1.62 mm, corresponding to an area of  $8.25 \text{ mm}^2$ .

(2) If the hole is larger in comparison with the corrosion rate than in case (1), but still sufficiently small, there will be a build-up of liquid water inside the canister, but this water will be completely consumed before the pressure inside the canister reaches the external pressure. After this, corrosion proceeds at a rate limited by the supply of water to the canister, which decreases as the internal pressure rises, as in case (1). Thus, as before, the internal pressure approaches the external pressure asymptotically from below, while the corrosion rate falls asymptotically to zero. Once again, no hydrogen escape from the canister.

(3) If the hole is sufficiently large in comparison with the corrosion rate, the hydrogen pressure inside the canister will reach the external pressure while there is still water left in the vessel. If the water level in the annulus is below the penetration in the copper overpack, hydrogen starts to escape, keeping the internal pressure constant and cutting off the external pressure-driven water supply. However, if the water level in the annulus is above the penetration, the pressure inside the canister rises further, and water is expelled until the water level in the annulus falls below the penetration. At this point the excess pressure is relieved, and hydrogen is vented. In both cases, once hydrogen is being expelled from the

canister, corrosion proceeds as before until the water inventory inside the canister is exhausted. The total amount of hydrogen expelled from the canister is largely determined by the water inventory inside the canister at the point when hydrogen starts to escape.

The calculation halts when

- either the internal water inventory is exhausted, and diffusion suddenly becomes the sole means of water supply;
- or the annulus fills with corrosion residue.

After any liquid water in the canister has been consumed, corrosion of the steel container continues because water vapour can diffuse into the canister from outside. A numerical model of this diffusion limited corrosion process, which took into account:

- the change in size of the annular gap as corrosion progresses;
- possible suppression of the corrosion rate;
- the flow of hydrogen generated by the corrosion process;

was developed to predict the corrosion residue profile in the annulus. Suppression of the corrosion rate, characterised by a length scale of the order of  $1\ \mu\text{m}$ , has a considerable influence on the build-up of corrosion residue in the annulus.

The annular fitting gap between the cast steel inner container and the copper overpack will eventually fill with magnetite ( $\text{Fe}_3\text{O}_4$ ). A set of finite element calculations has analysed the implications of the build-up of corrosion product for the structural integrity of the canister.

The analyses considered an extreme corrosion scenario, with corrosion occurring globally on the outer surface of the cast insert, and a more likely scenario, with corrosion restricted to a region around the initial defect.

In the case of restricted corrosion, the stress analyses showed no loss of long term structural integrity of the canister. The copper overpack fails locally when the strain reaches 50%. This occurs at the edge of the region of corrosion product build-up, when the displacement in the copper overpack is 0.5 mm. At this point the groundwater gains access to the fuel channels in the cast insert, and corrosion starts to occur globally.

In the case of restricted corrosion, the geometry of the initial defect could have been important. The results of a stress analysis showed that, other than locally near the edge of the defect, plastic strains are low for both a circular hole and a longitudinal crack in the copper overpack. The stresses near the

defect are not significantly larger than the stresses elsewhere, and so significant dilation of the hole is unlikely. The copper overpack is likely to fail locally near the edge of the region of corrosion product build-up, regardless of the geometry of the initial defect, and corrosion then starts to occur globally.

In the case of global corrosion, the inner container maintains its structural integrity for a displacement loading of at least 0.5 mm. For a displacement loading of 0.2 mm, stress concentrations in the rim of the copper overpack cause plasticity. The copper overpack yields more generally at a displacement loading of 0.25 mm. Despite this plasticity, the copper overpack is likely to remain intact until after the time at which corrosion of the inner container causes a breach of the fuel storage channels.

Allowing for compression of the corrosion product does not lead to a significant decrease in the canister stresses. The introduction of voids in the corrosion product results in a slight reduction in the maximum stresses in the inner container and the copper overpack. This reduction is small, about 1%, although assuming an extreme bound on the properties of the corrosion product did give a 10% reduction. Basing an estimate of the lifetime of the canister on the time at which the copper overpack begins to fail, thus allowing the groundwater access to the fuel channels in the cast insert, we note that:

- the lifetime is unchanged if we assume that the corrosion product is compressible;
- the lifetime is a factor 1.03 greater if the corrosion product is assumed to have voids;
- the lifetime is a factor 1.1 greater if an extreme bound is used to define the properties of the corrosion product.

It is likely that corrosion will take place at the interface between the steel container and its lid, inducing bending stresses in the lid and tensile stresses in its fixing bolt. This build-up of stress could be sufficient to cause the lid fixing to fail, allowing the lid to come free and giving the groundwater access to the exposed fuel channels. Indeed, the assessment model assumes (conservatively) that there is a 1 mm wide crack in the inner container. A stress analysis showed that the central bolt fixing the lid of the BWR canister insert is likely to resist the loads induced by the build-up of corrosion product at the interface, at least until the point when the build-up of corrosion product on the external surface of the lid starts to exert a balancing force. The flow of groundwater through the fuel channels of the canister will be restricted. The PWR canister design is likely to be similarly satisfactory.

A final study considered the effect on the repository of the expansion of the canister due to corrosion. This stress analysis assumed that corrosion was

occurring globally on the outer surface of the cast insert (a worst case), and identified the bottom corner of the deposition hole as a region where cracks might initiate in the rock. However, bentonite acts as an extremely efficient buffer for displacement loadings of up to 55mm (equivalent to corrosion of the entire thickness of steel to the fuel channels).

# 1 INTRODUCTION

The proposed design for a final repository for spent fuel and other long-lived residues in Sweden, is based on the multi-barrier principle. The waste will be encapsulated in sealed cylindrical canisters, which will then be placed in vertical storage holes drilled in a series of caverns excavated from the granite bedrock at a depth of about 500 m. Each canister will be surrounded by compacted bentonite clay. Once full, the facility will be backfilled and sealed with a mixture of bentonite and sand.

The canister concept is based on a thick cast steel inner container, designed to provide mechanical strength and to keep individual fuel bundles at a safe distance from one another, thereby minimising the risk of criticality. The primary loading on the inner container will be a pressure of about 10 MPa, resulting from the hydrostatic pressure of 5 MPa and a bentonite swelling pressure of 5 MPa. The steel container is fitted inside an inherently corrosion resistant copper overpack (the wall of which is approximately 50 mm thick) that is designed to provide containment over the long time scales required.

As part of the safety case for the repository, one of the scenarios being addressed by SKB involves the mechanical failure of the outer copper overpack, allowing water to enter the canister and corrode the inner steel container. The consequences of this failure are:

- water or water vapour can penetrate the canister;
- anaerobic corrosion of the inner container generates hydrogen;
- the long-term build up of corrosion product induces stresses in the spent fuel canister.

In previous assessments of the performance of the repository this scenario has been simplified; it is assumed that saturated conditions develop immediately throughout a canister once it has failed. The aim of the present study is to develop a simple model of the behaviour of the canister subsequent to a first breach in the copper overpack. This model is used to predict:

- the ingress of water to the canister (as a function of the size and shape of the initial defect, the buffer conductivity, the corrosion rate and the pressure inside the canister);

- the build-up of corrosion product in the canister (as a function of the amount of water in the canister, the corrosion rate, the available metal surface area and the properties of the corrosion product);
- the effect of corrosion on the structural integrity of the canister.

The layout of this report is as follows. The design of the canister, and the functional specification of the bentonite buffer are described in Section 2. Section 3 develops the model of the behaviour of the canister subsequent to mechanical failure of the copper overpack. After any liquid water that has entered the canister has been consumed, corrosion continues as a result of water vapour diffusing into the canister, as discussed in Section 4. Section 5 analyses the implications of the build-up of corrosion product for the structural integrity of the canister. In Section 6, the results of the stress analyses are presented as a function of time. Finally, our conclusions are summarised in Section 7.

## **2 CANISTER**

### **2.1 CANISTER DESIGN**

The canister is a fundamental engineered barrier in the repository system. It should retain its integrity over a long time.

The canister concept is based on a thick cast steel inner container, designed to provide mechanical strength and to keep individual fuel bundles at a safe distance from one another, thereby minimising the risk of criticality. The primary loading on the inner container will be a pressure of about 10 MPa, resulting from the hydrostatic pressure of 5 MPa and a bentonite swelling pressure of 5 MPa. The steel container is fitted inside an inherently corrosion resistant copper overpack (the wall of which is approximately 50 mm thick) that is designed to provide containment over the long time scales required. The details of the canister design have not yet been finalised; modifications may be made in response to the requirements of the fabrication and encapsulation process. A possible design /2-1/ is shown in Figure 2-1.

The cast steel insert will be fabricated in two parts, each with half the total length, and welded together in the middle. The outer copper shell will be fabricated either as a seamless tube by extrusion, or from two plates that have been formed into tube halves and welded together by longitudinal electron beam welds. The lid and bottom will be fabricated by working from thick plate or will be forged and machined to their final shape.

### **2.2 BENTONITE BUFFER**

Each canister will be surrounded by compacted bentonite clay. The purpose of this buffer is to:

- support the canister (and provide mechanical protection);
- restrict groundwater flow;
- allow hydrogen gas to escape.

The bentonite swells as it takes up water; in the deposition hole swelling is hindered, and so a 'swelling pressure' is exerted on the confining boundaries.

The hydraulic conductivity of the bentonite /2-2/ is designed to be very small,  $10^{-13}$  m/s.

The mechanism for significant gas transport in water-saturated bentonite is believed to be that one or more channels are opened through interconnected spaces between the dense bentonite particles. Laboratory experiments show that gas passage occurs at a 'critical' pressure. Typically, this pressure is equal to the hydrostatic pressure plus a pressure that is between 60% and 90% of the bentonite's swelling pressure. The gas transport capacity becomes as great as needed to allow entrapped gas to pass through the channels that are opened in the buffer. The quantity of water that accompanies the gas is small, which means that the bentonite remains water-saturated.

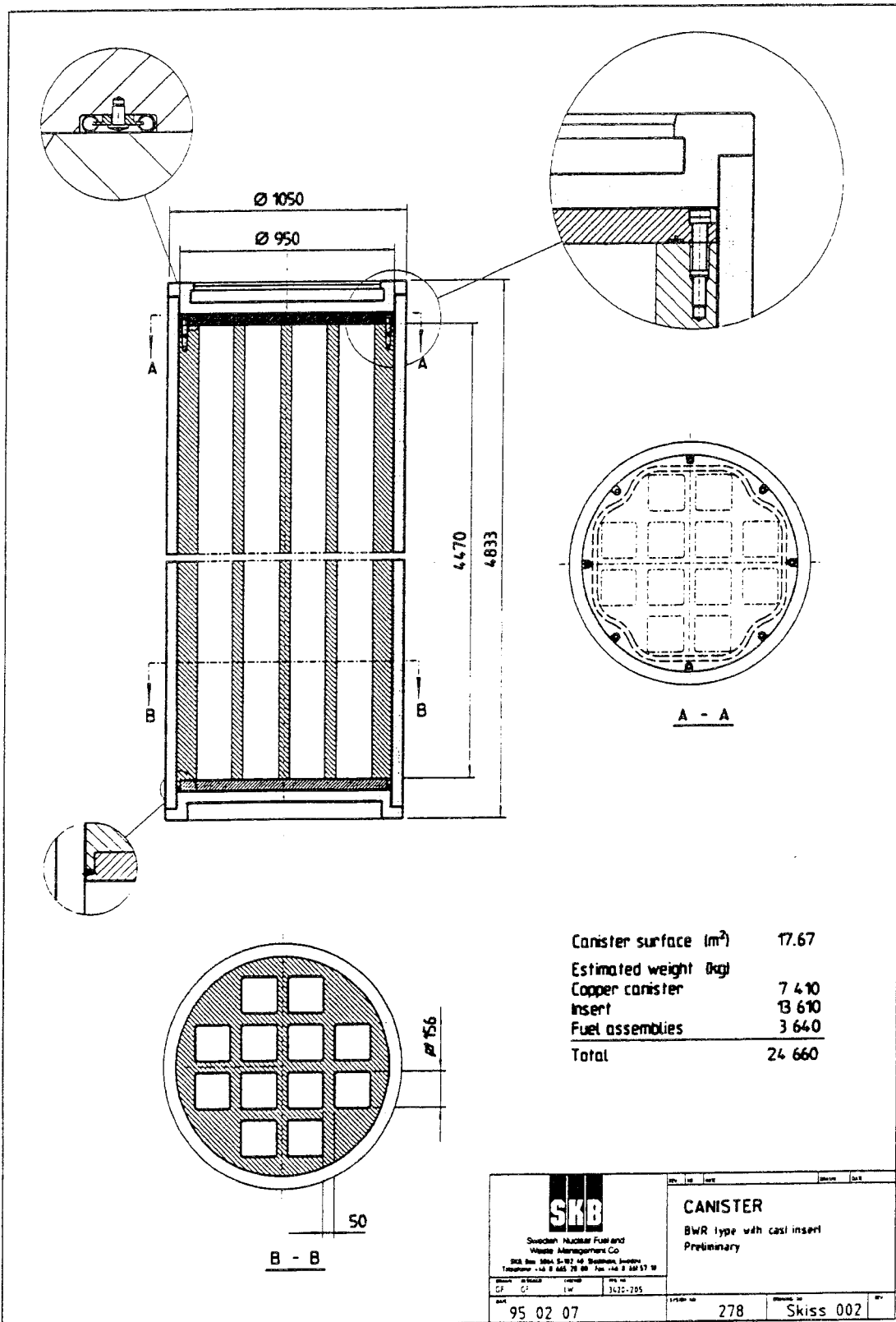


Figure 2-1. Design of the BWR canister.

## 3 THE ASSESSMENT MODEL

### 3.1 INTRODUCTION

The assessment model considers the inflow of water to a canister with a penetration in its copper overpack, resulting in anaerobic corrosion of the cast steel inner container and the generation of hydrogen. It describes the interactions between the supply of water, corrosion, hydrogen production, pressure inside the canister and the flows of water and hydrogen.

### 3.2 ASSUMPTIONS

#### 3.2.1 Geometry

In the model, the proposed spent fuel canister is represented as having an internal depth of 4.47m and an outer radius of 0.525m. It consists of a cast steel inner container of 0.473m radius inside a 50mm thick copper overpack. There is an annular gap of 2mm between the inner container and the overpack /2-1/. In the BWR canister type investigated here, the spent fuel is contained in 12 square section vertical channels of width 0.156m. On closure, the remaining void volume in the inner container is 0.4m<sup>3</sup>.

As in previous corrosion studies /3-1/ the inner container is assumed to be penetrated by a circumferential crack of width 1mm at height  $h_1$ ; this height is one of the key parameters in the model. However, by contrast, we now assume that the copper overpack is penetrated by a hole rather than a circumferential crack. The reference value for the cross sectional area of the hole is 5mm<sup>2</sup>, in agreement with the value used in a recent stress analysis study /3-2/, but the effect of increasing the hole size is also investigated in the present model.

Although the results are quoted for a hole of given cross sectional area  $a = \pi r_h^2$ , they also apply to the case of a circumferential crack of width  $2r_i$ . We note that the volume flow rate through a circular hole /3-3/ is given by

$$q = 2\pi r_h \frac{k}{\mu} (p - p_\infty) \quad 3-1$$

where  $r_h$  is the radius of the hole,  $k$  is the permeability of the bentonite outside the hole,  $\mu$  is the viscosity, and  $(p - p_\infty)$  is the pressure drop

between a far boundary (usually taken to be the rock-bentonite interface) and the hole. Similarly, the volume flow rate through a circumferential crack /3-4/ is

$$q = 2 \pi \frac{\pi R}{\ln\left(\frac{r_\infty}{r_i}\right)} \frac{k}{\mu} (p - p_\infty) \quad 3-2$$

where  $R$  is the radius of the canister,  $r_\infty$  is the distance to the far boundary and  $r_i$  is the half-width of the crack. Comparing Equations 3-1 and 3-2, it follows that the crack width which gives the same transport properties as the hole is

$$\ln \frac{r_\infty}{r_i} = \frac{\pi R}{r_h} \quad 3-3$$

$h_2$ , the height of the hole in the copper overpack, is another key parameter in the model.

### 3.2.2 Processes outside the canister

The canister is assumed to be buried in granite at a depth of 500m inside a vertical hole backfilled with compacted sodium bentonite to a thickness of 0.5m. The hydrostatic pressure of water at this depth is 5MPa, and in all the calculations involving the transport of water to or from the canister this is taken to be the effective external pressure.

The flow of water from the surrounding bentonite into a punctured canister is represented as flow through a porous medium of low permeability. The case of flow to a circular hole has been analysed in /3-3/. The result is given in terms of the volume inflow of water per unit time per unit pressure drop between the far field and the outside edge of the hole. Since the flow resistance of the hole is many orders of magnitude smaller than the flow resistance of the bentonite, the relevant pressure difference may be taken as that between the far field and the interior of the canister. For a given hole size and external pressure, the supply of water to the canister is directly proportional to the bentonite permeability.

The bentonite swelling pressure of 5MPa contributes to the total external pressure of 10MPa which must be overcome before hydrogen can escape from the canister /3-5/. In the present model, no attempt is made to determine what happens to the hydrogen expelled from the canister, other than to keep track of its total inventory (in moles).

### 3.2.3 Processes inside the canister

The corrosion product is assumed to be mainly magnetite ( $\text{Fe}_3\text{O}_4$ ). The volume increase in forming magnetite from iron is estimated from the relative densities of the two materials (i.e. the expansion factor is 2.1:1).

It is assumed that any water that enters the canister can take part in the corrosion process. An imbalance between the supply of water and that demanded by the total rate of corrosion

- if an excess, adds to the internal liquid water inventory;
- if a shortfall, reduces the corrosion rate uniformly over the entire steel surface.

Any change in the internal liquid water inventory is distributed as follows:

- if there is a reduction in the quantity of water in the canister, and if there is water in both the annulus and the inner container, then the water levels fall together (this is also assuming a common rate of evaporation of water per unit area, that maintains saturated conditions inside the canister);
- if there is an increase in the internal liquid water inventory, and if the water level in the annulus is below the crack in the inner container, the additional water is assigned to the annulus;
- if there is an increase in the internal liquid water inventory, and if the water level in the annulus coincides with the crack but the water level in the inner container is below the crack, the additional water is assigned to the inner container;
- if there is an increase in the internal liquid water inventory, and if the water levels in both the annulus and the inner container are above the crack, the additional water is apportioned so that the levels rise together.

The corrosion rate in the annulus is galvanically enhanced by a factor

$$\left(1 + \frac{\text{height of water in annulus}}{\text{height of annulus}}\right) \quad 3-4$$

Corrosion residue due to this enhanced rate of corrosion is distributed uniformly over the surface of the annulus (i.e. the thickness of magnetite in the annulus is a function of time but not of position).

The transient calculations assume that the transport of water within the canister is fast compared to the time step used. This assumption is discussed further in Appendix A.1.3.

### 3.3 THE SEQUENCE OF EVENTS

Broadly, the sequence of events is as follows:

- Water flows into the annulus through the penetration in the copper overpack, causing anaerobic corrosion on the outer and inner surfaces of the inner container. This generates hydrogen which causes the pressure inside the canister to rise, thereby gradually reducing the rate of water inflow. Since water is being consumed by corrosion at an almost constant rate, the internal water inventory reaches a maximum and then declines. Depending on the hole size, the corrosion rate, and  $h_1$ , the water in the annulus may also spill over into the inner container.
- What happens next is determined by the maximum water inventory inside the canister, which depends mainly on the hole size and the corrosion rate. The distribution of water between the annulus and inner container is relatively unimportant. There are three possibilities:
  - (1) If the hole is so small that the initial (i.e. peak) rate of water ingress cannot match the corrosion rate, then there is no build-up of liquid water in the vessel. Corrosion proceeds at a rate limited by the supply of water, which decreases as the hydrogen pressure inside the canister rises. The internal pressure approaches the external pressure asymptotically from below, while the corrosion rate falls asymptotically to zero. No hydrogen is found outside the canister. Assuming a hole of circular cross-section, a simple calculation based on the rate of water supply that is required to support the postulated corrosion rate, shows that the hole radius is directly proportional to the corrosion rate and inversely proportional to the external pressure. At a corrosion rate of  $10^{-7}$  m/year and a pressure of 5MPa, the hole radius below which no water collects in the canister turns out to be 1.621 mm, corresponding to an area of  $8.25 \text{ mm}^2$ .
  - (2) If the hole is larger in comparison with the corrosion rate than in case (1), but still sufficiently small, there will be a build-up of liquid water inside the canister, but this water will be completely consumed before the pressure inside the canister reaches the external pressure. After this, corrosion proceeds at a rate limited by the supply of water to the canister, which decreases as the internal pressure rises, as in case (1). Thus, as before, the internal pressure approaches the external pressure asymptotically from below, while the corrosion rate falls asymptotically to zero. Once again no hydrogen is found outside the canister.
  - (3) If the hole is sufficiently large in comparison with the corrosion rate, the hydrogen pressure inside the canister will

reach the external pressure while there is still water left in the vessel. If the water level in the annulus is below the penetration in the copper overpack, hydrogen starts to escape, keeping the internal pressure constant and cutting off the external pressure-driven water supply. However, if the water level in the annulus is above the penetration, the pressure inside the canister rises further, and water is expelled until the water level in the annulus falls below the penetration. At this point the excess pressure is relieved, and hydrogen is vented. In both cases, once hydrogen is being expelled from the canister, corrosion proceeds as before until the water inventory inside the canister is exhausted. The total amount of hydrogen expelled from the canister is largely determined by the water inventory inside the canister at the point when hydrogen starts to escape.

- There are no critical events for regimes (1) or (2). However, at some point the rate of water supply by diffusion through the hole in the overpack will exceed the pressure-driven supply and canister corrosion will then be ‘diffusion controlled’, as described in the following section. Execution of the computer model is halted at this point.

If regime (3) is terminated by exhaustion of the water inside the canister, diffusion becomes the sole means of water supply, and as for regimes (1) and (2) the computer model is stopped at this point. However, it is possible for the annulus to fill with corrosion residue before this point. If this occurs while there is still some water in the inner container, then corrosion in the inner container will continue at the original rate until either the water is exhausted or the remaining void space is full of corrosion product. Execution of the computer model is halted if the annulus fills with corrosion residue.

## **3.4 RESULTS**

### **3.4.1 Definition of scenarios**

The computer model described in Appendix A was used to calculate output for a number of different scenarios. These were defined by the values of a key set of parameters, namely:

- the cross-sectional area  $a$  (reference value  $5 \cdot 10^{-6} \text{ m}^2$ ) of the penetration in the copper overpack;
- the corrosion rate  $\mu$  (reference value  $0.1 \mu \text{ m/year}$ );
- the height of the circumferential crack in the inner canister,  $h_1$  (m);
- the height of the penetration in the copper overpack,  $h_2$  (m).

The most important of these are  $a$ , which determines the rate of supply of water to the canister, and  $\mu$ , which determines the rate at which water is consumed by corrosion.  $h_1$  determines how soon water enters the inner canister, i.e. it determines the distribution of water between inner canister and annulus. Since corrosion will occur more rapidly in the annulus the greater the depth of water there (as a result of galvanic coupling between the inner container and the copper overpack),  $h_1$  also affects the time for the annulus to fill with magnetite.  $h_2$  is important only when the internal pressure reaches the external pressure: if at this time the level of water in the annulus is above the outer penetration, water has to be expelled before hydrogen can be expelled. This causes a delay in the accumulation of hydrogen outside the canister, and occasionally a significant rise in the internal pressure.

Five scenarios for the locations of the crack in the inner container and the penetration in the copper overpack were selected for consideration:

- Scenario one:  $h_1 = 4.3\text{ m}$ ,  $h_2 = 2.235\text{ m}$  (i.e. the circumferential crack is at the top of the inner container, and the outer penetration is halfway up the copper overpack);
- Scenario two:  $h_1 = 0.0\text{ m}$ ,  $h_2 = 2.235\text{ m}$  (i.e. the circumferential crack is at the bottom of the inner container, and the outer penetration is halfway up the copper overpack);
- Scenario three:  $h_1 = 0.0\text{ m}$ ,  $h_2 = 0.0\text{ m}$  (i.e. the circumferential crack is at the bottom of the inner container, and the outer penetration is at the bottom of the copper overpack);
- Scenario four:  $h_1 = 4.3\text{ m}$ ,  $h_2 = 0.0\text{ m}$  (i.e. the circumferential crack is at the top of the inner container, and the outer penetration is at the bottom of the copper overpack);
- Scenario five:  $h_1 = 4.3\text{ m}$ ,  $h_2 = 4.3\text{ m}$  (i.e. the circumferential crack is at the top of the inner container, and the outer penetration is at the top of the copper overpack).

For each of these five scenarios, we investigated the effect on the results of varying the outer penetration size  $a$  and the corrosion rate  $\mu$ . Table 3-1 summarises the suite of calculations that was carried out. The results are classified according to the three regimes described in Section 3.3.

**Table 3-1. Table summarising the set of parameter variations that were used in the canister assessment model. The results have been classified according to the regimes (1), (2) and (3) described in Section 3.3.**

Scenario	Parameters			
	$a = 5 \cdot 10^{-6} \text{ m}^2$ , $\mu = 0.1 \text{ } \mu\text{m/year}$	$a = 2 \cdot 10^{-5} \text{ m}^2$ , $\mu = 0.1 \text{ } \mu\text{m/year}$	$a = 5 \cdot 10^{-6} \text{ m}^2$ , $\mu = 0.01 \text{ } \mu\text{m/year}$	$a = 0.1791 \text{ m}^2$ , $\mu = 1 \text{ } \mu\text{m/year}$
One	(1)	(2)	(3)	(3)
Two	(1)		(3)	(3)
Three	(1)	(2)	(3)	
Four	(1)		(3)	
Five	(1)		(3)	(3)

The various cases are discussed approximately in this order: regime (1), regime (2) and regime(3).

#### 3.4.2 $a = 5 \cdot 10^{-6} \text{ m}^2$ , and $\mu = 0.1 \text{ micron/year}$

In the case of the first scenario, with  $a = 5 \cdot 10^{-6} \text{ m}^2$  and  $\mu = 0.1 \text{ micron/year}$ , there is no build up of water inside the canister. The pressure inside the canister increases asymptotically to the external value (see Figure 3-1), and the internal hydrogen inventory increases asymptotically to a value of about 0.83 kg - moles (i.e. 1.67 kg, see Figure 3-2). There is no accumulation of hydrogen outside the canister.

Similar results were obtained for the other four scenarios with these values of  $a$  and  $\mu$ , and also for all five scenarios if the corrosion rate was increased to 1 micron/year. In the case of the first scenario, increasing the penetration area to  $a = 2 \cdot 10^{-5} \text{ m}^2$  and the corrosion rate to 1 micron/year also did not affect the results.

These results all belong to regime (1) of Section 3.3. This is consistent with the calculation that regime (1) will apply for  $a < 8.25 \cdot 10^{-6} \text{ m}^2$  (see Section 3.3). In the case of an increased corrosion rate of 1 micron/year, the corresponding limit is  $a < 8.25 \cdot 10^{-4} \text{ m}^2$ , and so even for  $a = 2 \cdot 10^{-5} \text{ m}^2$  regime (1) is expected to apply.

In all of these cases, program execution was halted when the rate of supply of water by diffusion exceeded the rate of supply due to Darcy flow. For  $a = 5 \cdot 10^{-6} \text{ m}^2$  and  $\mu = 0.1$  or 1 micron/year this occurs after 5110 years, while for scenario one with  $a = 2 \cdot 10^{-5} \text{ m}^2$  and  $\mu = 1 \text{ micron/year}$  it occurs after 2140 years (this difference is a result of the difference in the rates of supply of water, i.e. the different penetration areas).

**Scenario One: Penetration Area 5 mm<sup>2</sup>, Corrosion Rate 10<sup>-7</sup> m/year  
Internal Canister Pressure**

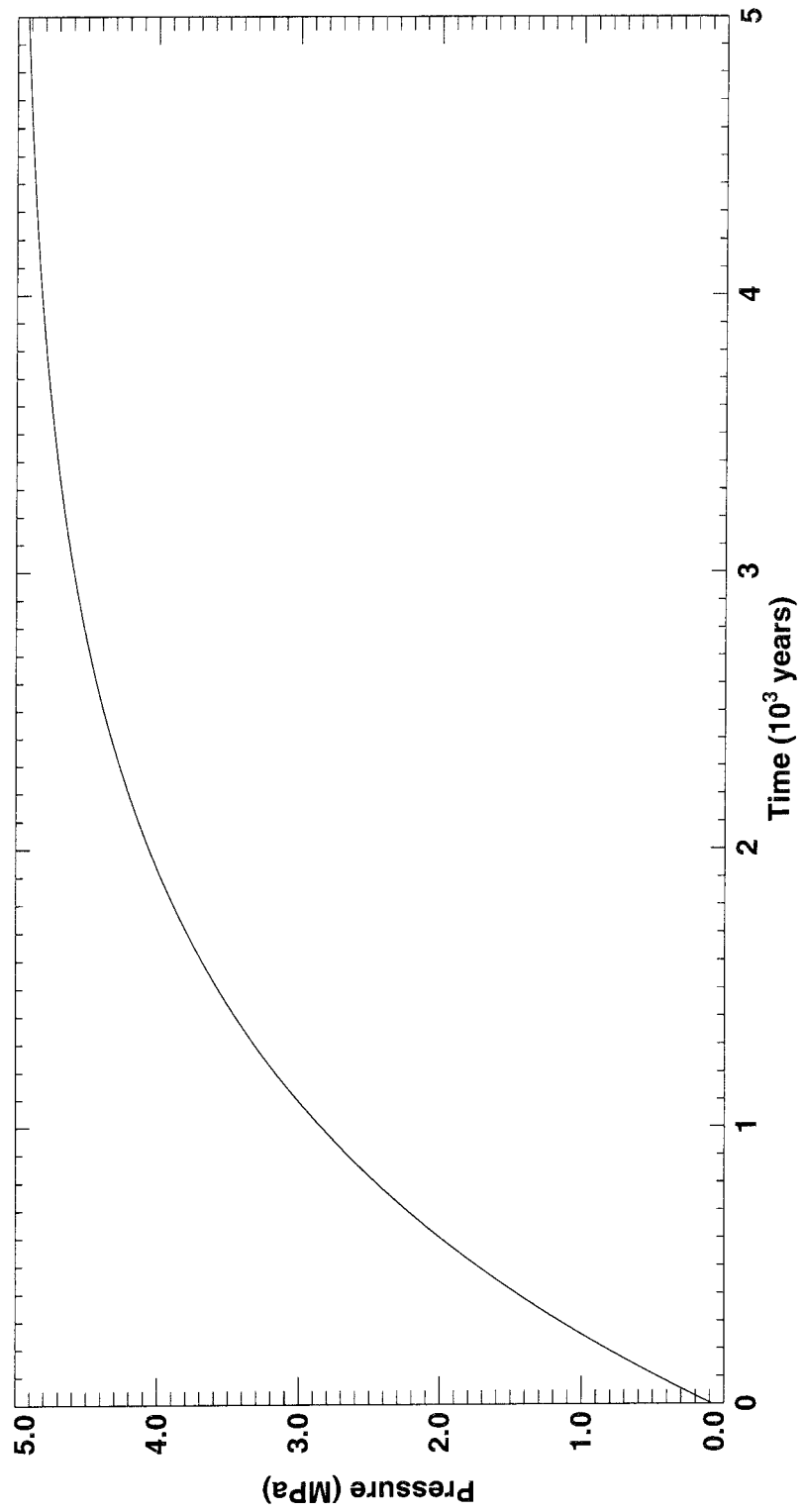


*Figure 3-1. The pressure inside the canister for scenario one, with  $a = 5 \cdot 10^{-6} \text{ m}^2$  and  $\mu = 0.1 \text{ micron/year}$ .*

**Scenario One: Penetration Area  $5 \text{ mm}^2$ , Corrosion Rate  $10^{-7} \text{ m/year}$   
Amount of Hydrogen in the Inner Canister and Annulus**

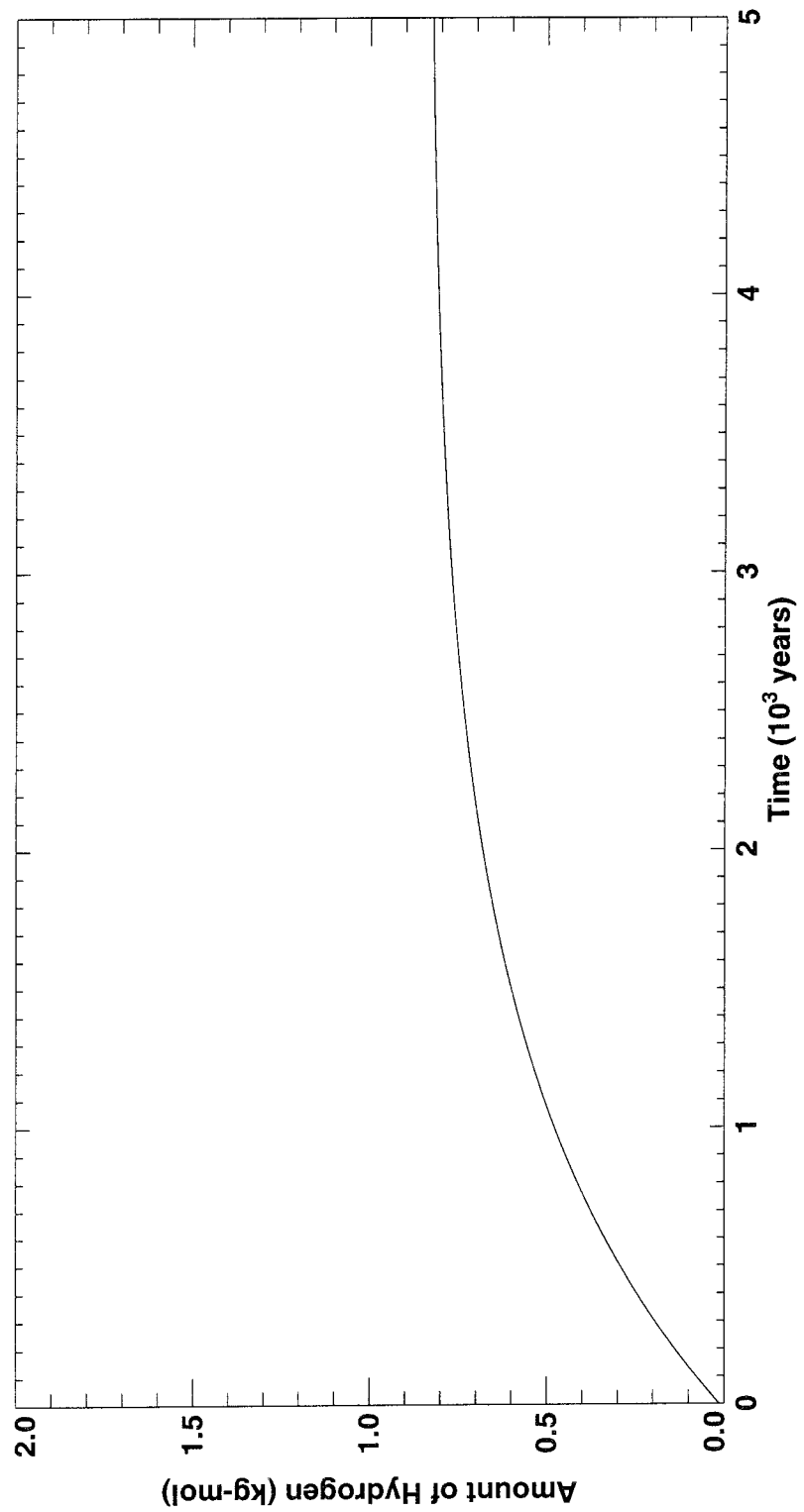


*Figure 3-2. The amount of hydrogen inside the canister for scenario one, with  $a = 5 \cdot 10^{-6} \text{ m}^2$  and  $\mu = 0.1 \text{ micron/year}$ .*

### 3.4.3 $a = 2 \cdot 10^{-5} \text{ m}^2$ , and $\mu = 0.1 \text{ micron/year}$

In the case of the first scenario, with  $a = 2 \cdot 10^{-5} \text{ m}^2$  and  $\mu = 0.1 \text{ micron/year}$ , water accumulates in the annulus but not in the inner container. The maximum depth of water in the annulus is 0.266 m at 314 years. This water has dried out by 628 years (see Figure 3-3), after which the pressure and the hydrogen inventory inside the canister increase asymptotically (see Figures 3-4 and 3-5). Again there is no accumulation of hydrogen outside the canister. The program halts after 2070 years because the supply of water to the canister has become dominated by diffusion. This case clearly conforms to regime (2) of Section 3.3.

The results for scenario three with these values of  $a$  and  $\mu$  belong to the same regime, but are slightly different in that the levels of water in the annulus and the inner container rise and fall together. The maximum depth of water in the canister is only  $1.56 \cdot 10^{-2} \text{ m}$  at 322 years, and this water has dried out by 644 years. The program halts because the supply of water to the canister has become dominated by diffusion after 2070 years.

Despite the differences due to varying the penetration area and the height of the crack in the inner container, in these cases the final hydrogen inventory is virtually the same as for regime (1); this is expected, since the hydrogen inventory is effectively determined by the internal volume of the canister and the asymptotic value of the pressure inside the canister (indeed, the ideal gas law gives a final hydrogen inventory of 0.845 kg - moles for all of these cases).

**Scenario One: Penetration Area 20 mm<sup>2</sup>, Corrosion Rate 10<sup>-7</sup> m/year  
Height of Water in Annulus**

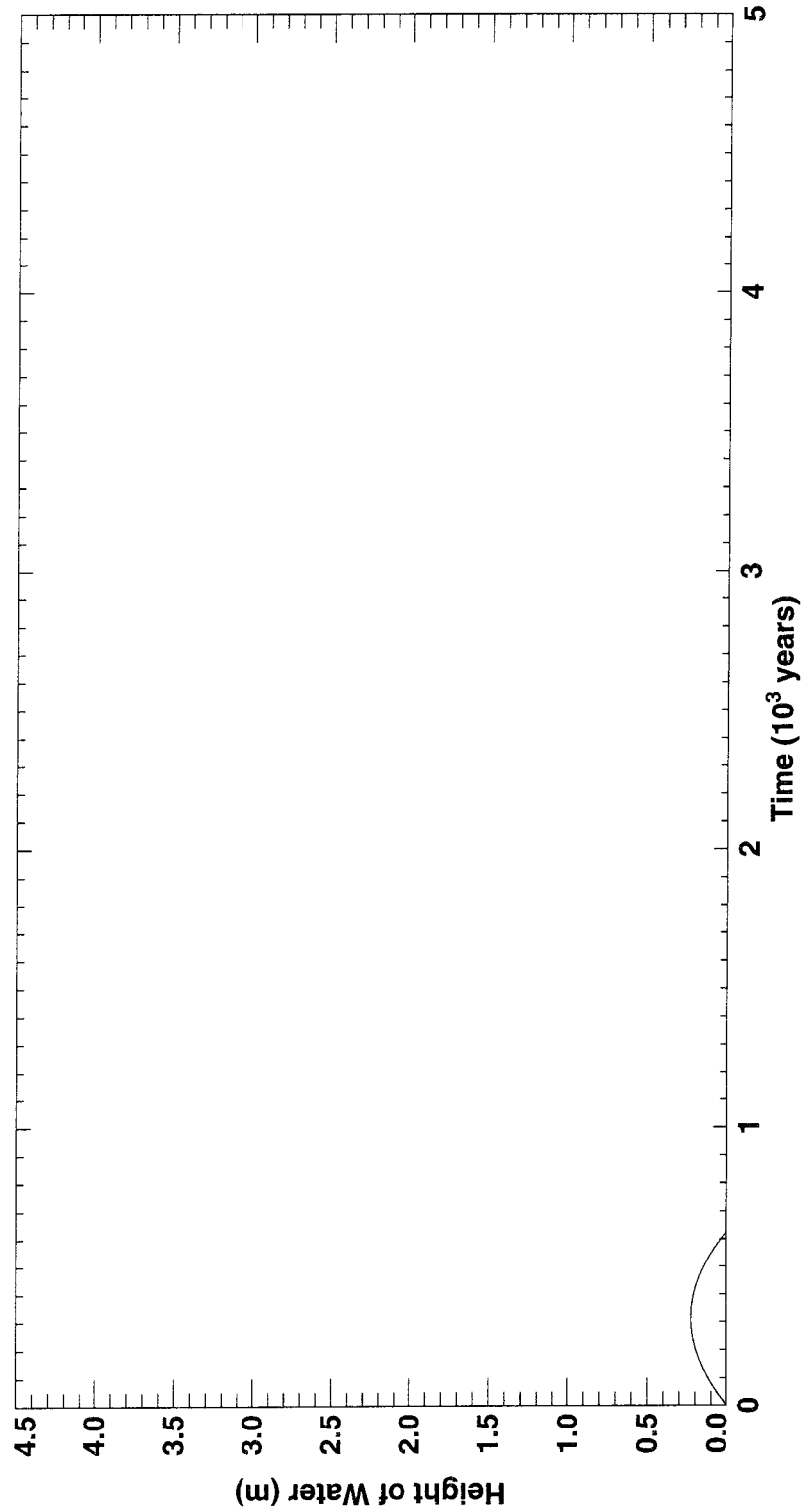


*Figure 3-3. The height of water in the annulus for scenario one, with  $a = 2 \cdot 10^{-5} \text{ m}^2$  and  $\mu = 0.1 \text{ micron/year}$ .*

**Scenario One: Penetration Area 20 mm<sup>2</sup>, Corrosion Rate 10<sup>-7</sup> m/year  
Internal Canister Pressure**

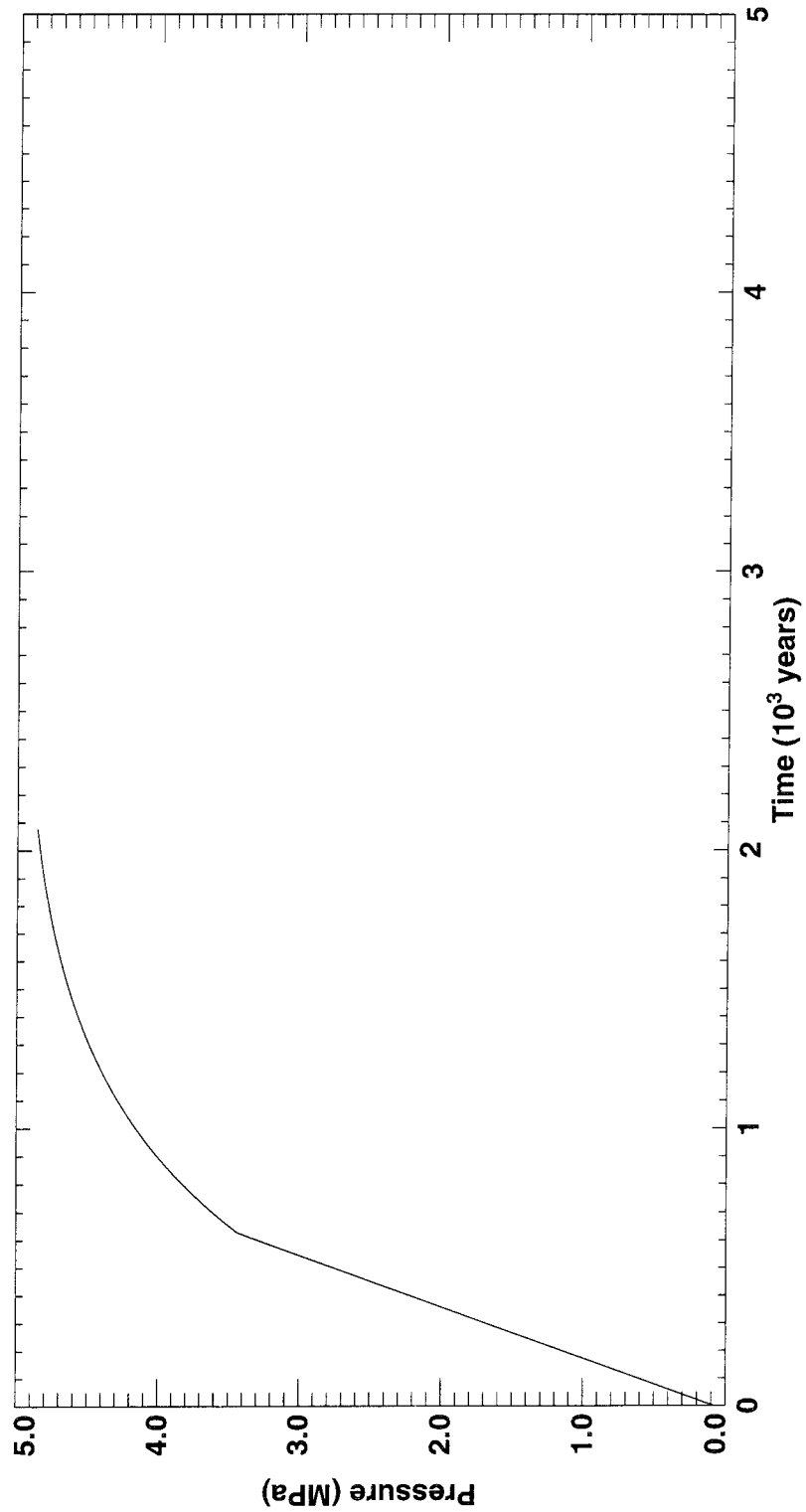


*Figure 3-4. The pressure inside the canister for scenario one, with  $a = 2 \cdot 10^{-5} \text{ m}^2$  and  $\mu = 0.1 \text{ micron/year}$ .*

**Scenario One: Penetration Area  $20 \text{ mm}^2$ , Corrosion Rate  $10^{-7} \text{ m/year}$   
Amount of Hydrogen in the Inner Canister and Annulus**

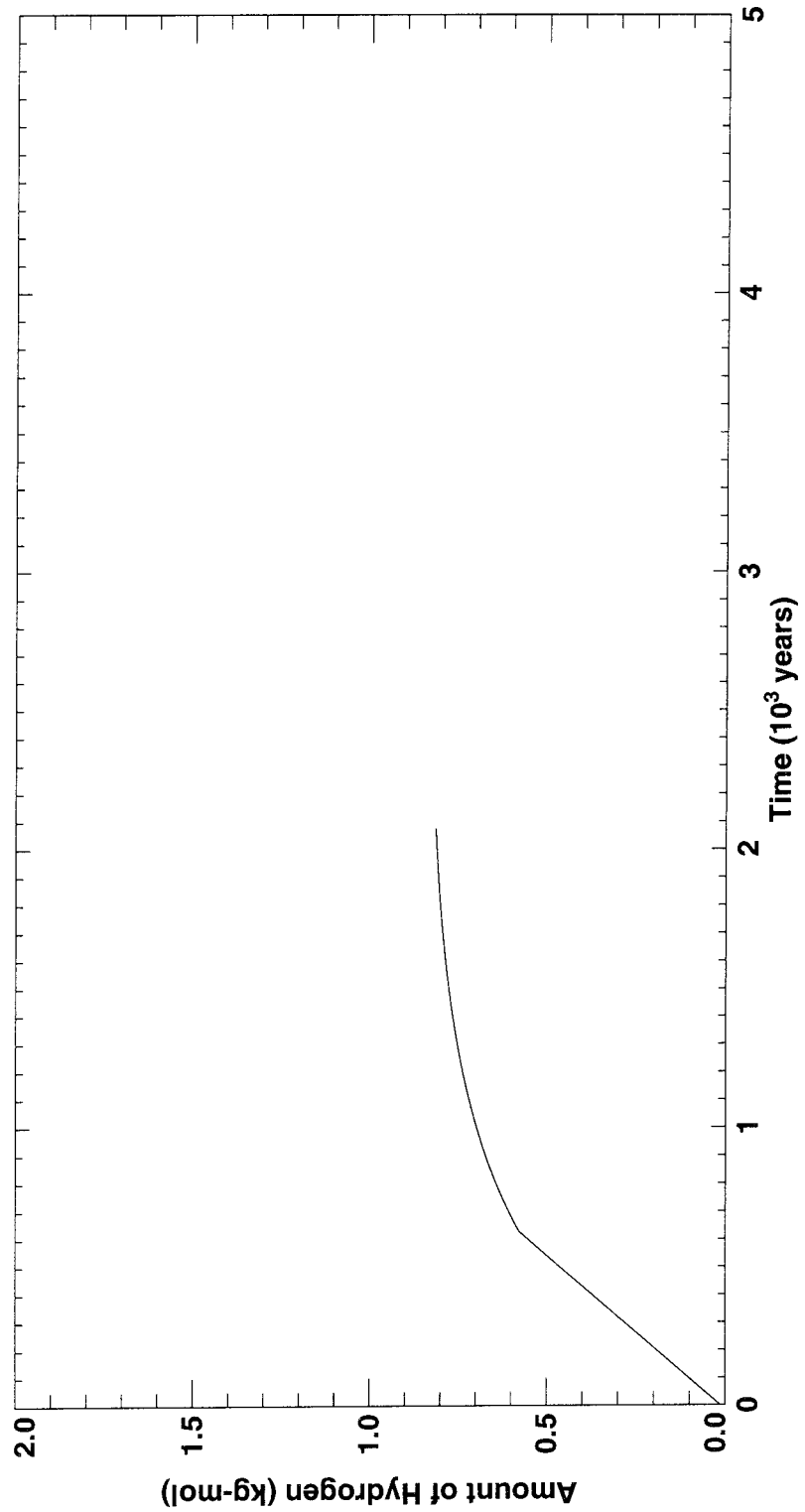


*Figure 3-5. The amount of hydrogen inside the canister for scenario one, with  $a = 2 \cdot 10^{-5} \text{ m}^2$  and  $\mu = 0.1 \text{ micron/year}$ .*

#### 3.4.4 $a = 5 \cdot 10^{-6} \text{ m}^2$ , and $\mu = 0.01 \text{ micron/year}$

In the case of the first scenario, with  $a = 5 \cdot 10^{-6} \text{ m}^2$  and  $\mu = 0.01 \text{ micron/year}$ , water enters the canister. The water level in the annulus reaches the crack after 3070 years, and water spills over into the inner container. The water in the inner container reaches its maximum depth of 0.102m at 6070 years, after which the level falls; the inner container finally dries out after 11120 years. In the meantime, the pressure inside the canister has reached the external hydrostatic pressure at 7046 years, and continues to increase until at 15440 years it becomes equal to the total external pressure of 10 MPa. At this point hydrogen begins to emerge from the canister, while the internal pressure remains constant at the value of 10 MPa. Eventually, after 18010 years the annulus dries out and the program halts because the supply of water to the canister is dominated by diffusion (see Figures 3-6, 3-7 and 3-8). This case belongs to regime (3) in Section 3.3. The total hydrogen inventory outside the canister at the point at which the calculation ends is 0.222 kg - moles (i.e. 0.448 kg; see Figure 3-9).

In the case of the second scenario with these values of  $a$  and  $\mu$ , the water level in both the annulus and the inner canister reaches its maximum depth of 0.448m after 7180 years. The pressure inside the canister reaches the external hydrostatic pressure after 8260 years, and the total external pressure of 10 MPa after 17070 years, at which point hydrogen begins to be expelled. The water level inside the canister falls continuously from its maximum value, and the canister dries out after 31680 years, at which point the program halts because the supply of water to the canister is dominated by diffusion (see Figures 3-10, 3-11 and 3-12). The total hydrogen inventory outside the canister (1.245 kg - moles, see Figure 3-13) is greater than for scenario one. The difference is that in the present case no water has been expelled from the canister, and so corrosion continues for longer before the diffusion limit is reached.

Scenario three is identical to scenario two, up to the point at which the pressure inside the canister reaches the external hydrostatic pressure (8260 years). However, in the present case the canister dries out after 14770 years, when the internal pressure is 8.126MPa. The program halts because the supply of water to the canister is dominated by diffusion. No hydrogen is expelled because the internal pressure does not reach the total external pressure of 10 MPa.

In scenario four, the events of scenario two are repeated, except that since the penetration in the copper overpack is at the bottom of the annulus pressure relief does not occur. The annulus dries out after 12270 years, when the internal pressure has reached 7.971MPa. No hydrogen is expelled from the canister.

**Scenario One: Penetration Area 5 mm<sup>2</sup>, Corrosion Rate 10<sup>-8</sup> m/year  
Height of Water in Inner Canister**

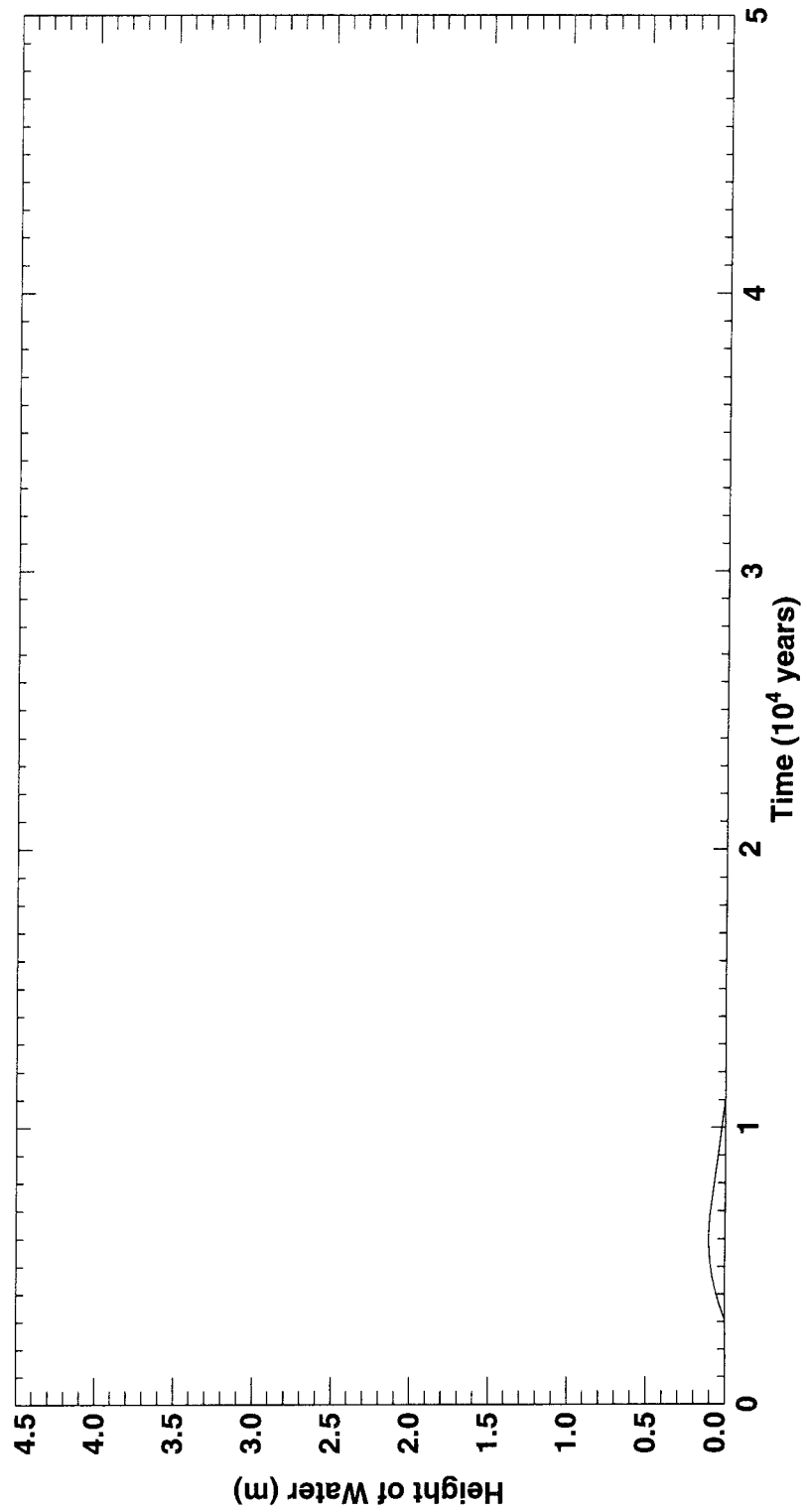


*Figure 3-6. The height of water in the inner container for scenario one, with  $a = 5 \cdot 10^{-6} \text{ m}^2$  and  $\mu = 0.01 \text{ micron/year}$ .*

**Scenario One: Penetration Area 5 mm<sup>2</sup>, Corrosion Rate 10<sup>-8</sup> m/year  
Height of Water in Annulus**

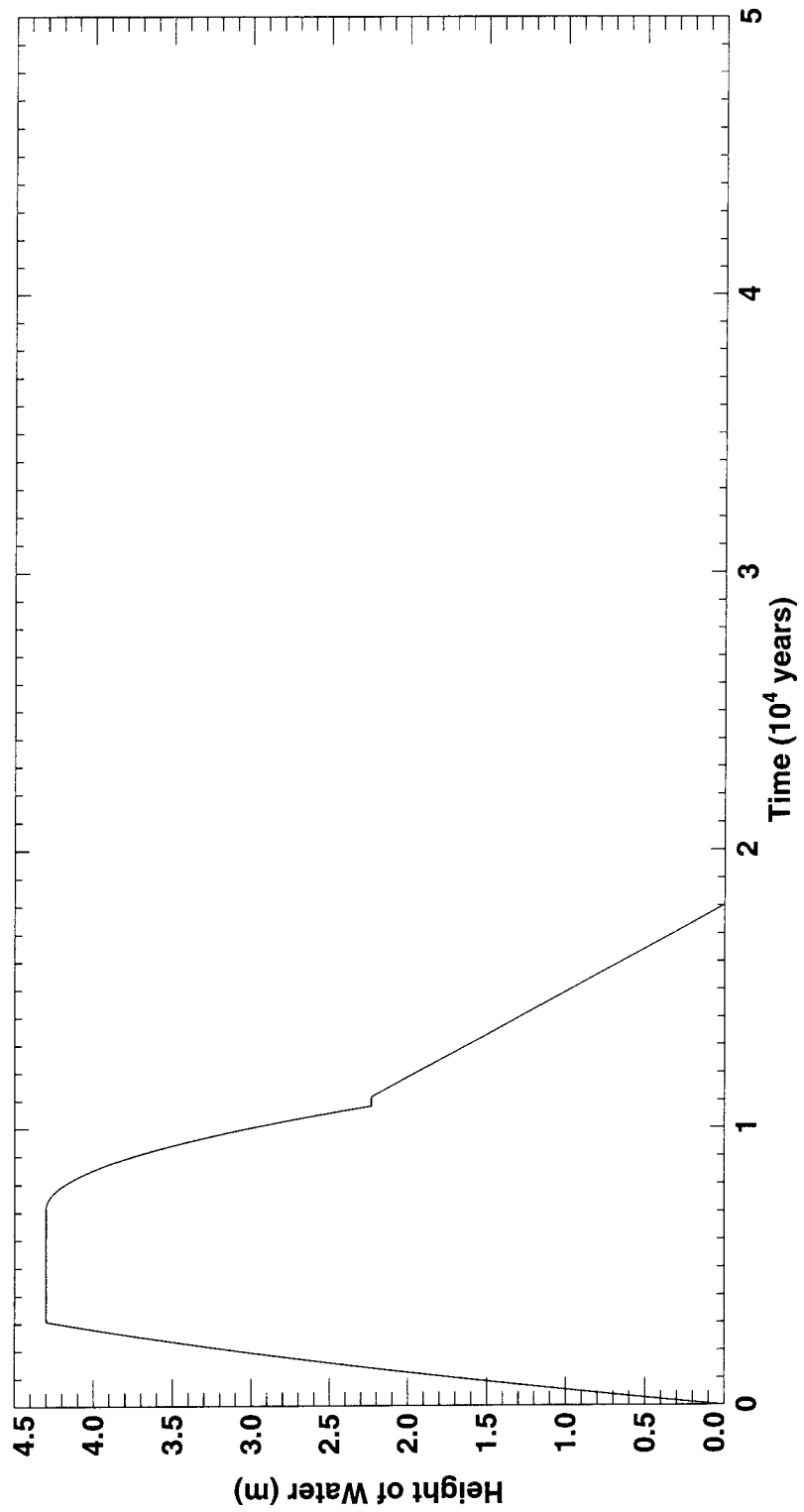


*Figure 3-7. The height of water in the annulus for scenario one, with  $a = 5 \cdot 10^{-6} \text{ m}^2$  and  $\mu = 0.01 \text{ micron/year}$ .*

**Scenario One: Penetration Area 5 mm<sup>2</sup>, Corrosion Rate 10<sup>-8</sup> m/year  
Internal Canister Pressure**

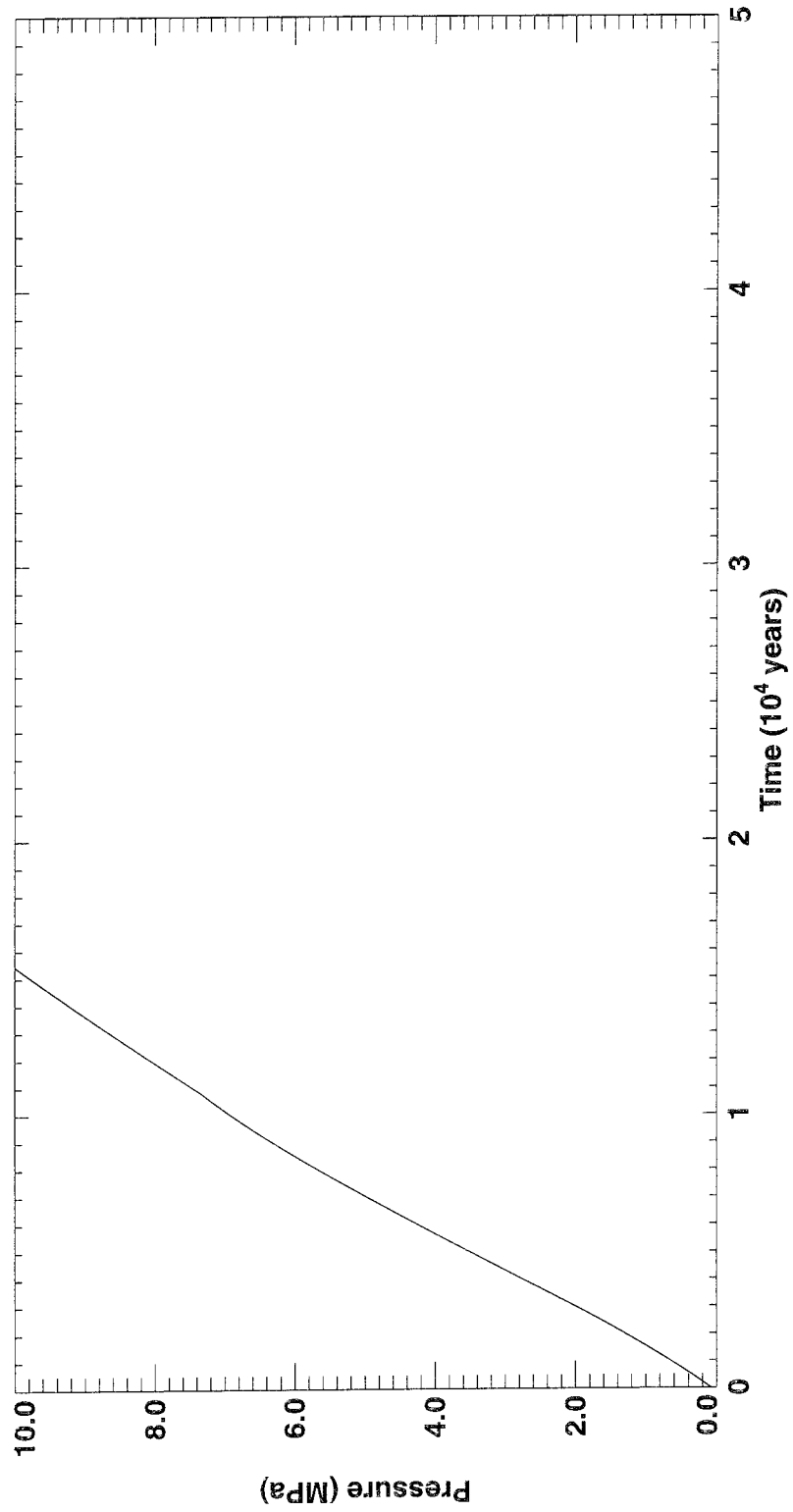


*Figure 3-8. The pressure inside the canister for scenario one, with  $a = 5 \cdot 10^{-6} \text{ m}^2$  and  $\mu = 0.01 \text{ micron/year}$ .*

**Scenario One: Penetration Area 5 mm<sup>2</sup>, Corrosion Rate 10<sup>-8</sup> m/year  
Amount of Hydrogen Expelled from the Canister**

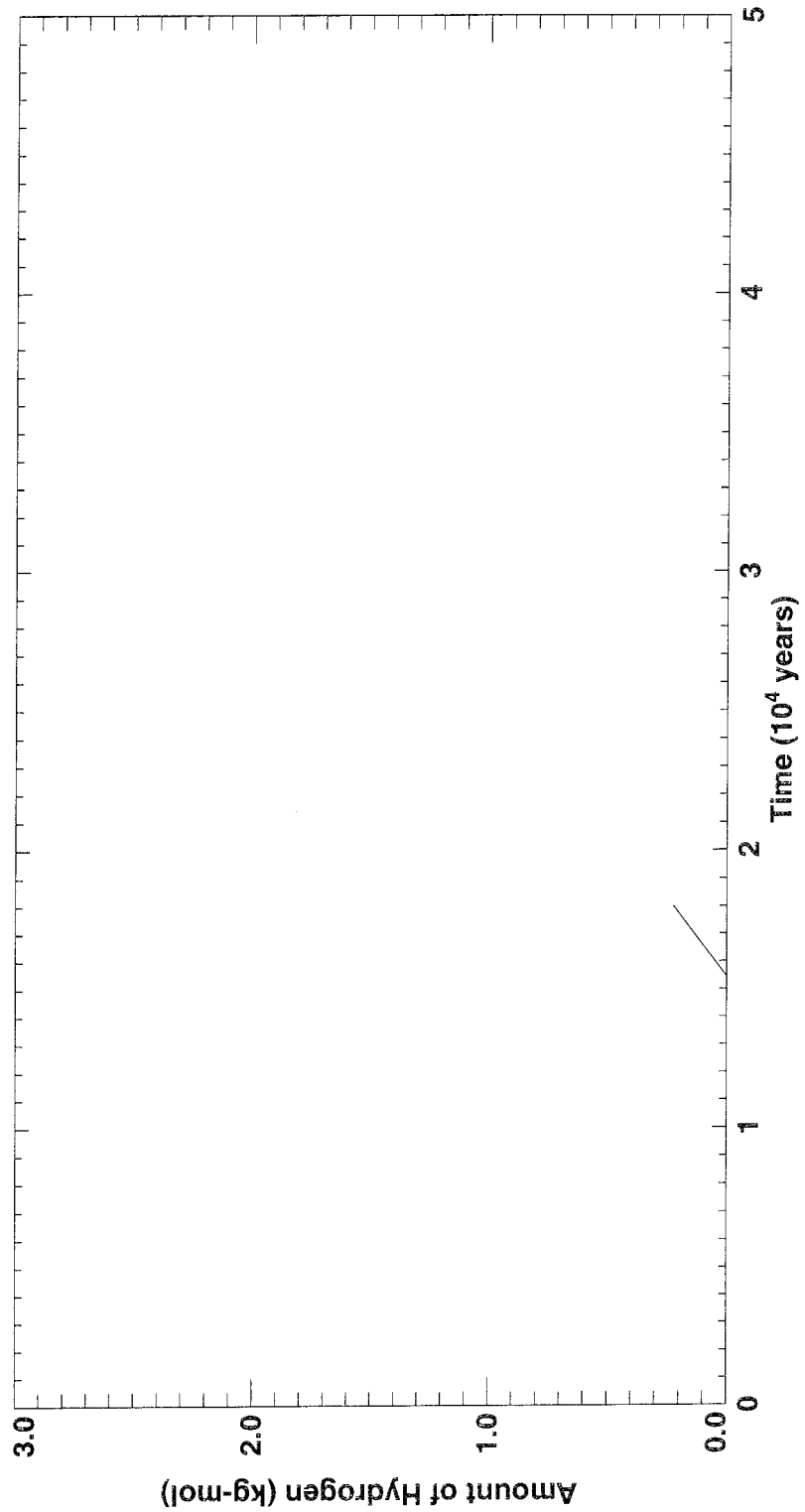


*Figure 3-9. The amount of hydrogen outside the canister for scenario one, with  $a = 5 \cdot 10^{-6} \text{ m}^2$  and  $\mu = 0.01 \text{ micron/year}$ .*

**Scenario Two: Penetration Area 5 mm<sup>2</sup>, Corrosion Rate 10<sup>-8</sup> m/year  
Height of Water in Inner Canister**

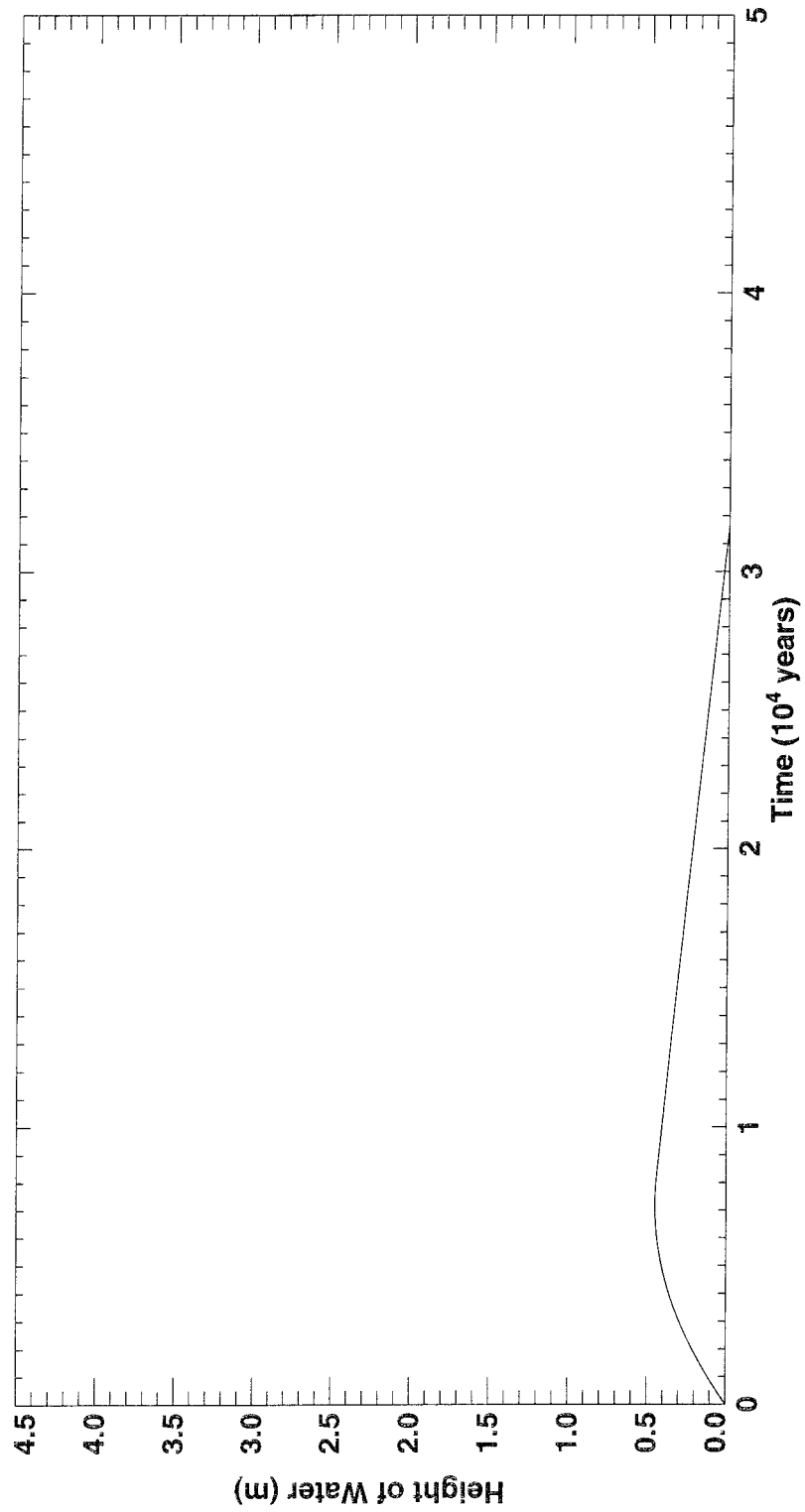


*Figure 3-10. The height of water in the inner container for scenario two, with  $a = 5 \cdot 10^{-6} \text{ m}^2$  and  $\mu = 0.01 \text{ micron/year}$ .*

**Scenario Two: Penetration Area  $5 \text{ mm}^2$ , Corrosion Rate  $10^{-8} \text{ m/year}$   
Height of Water in Annulus**

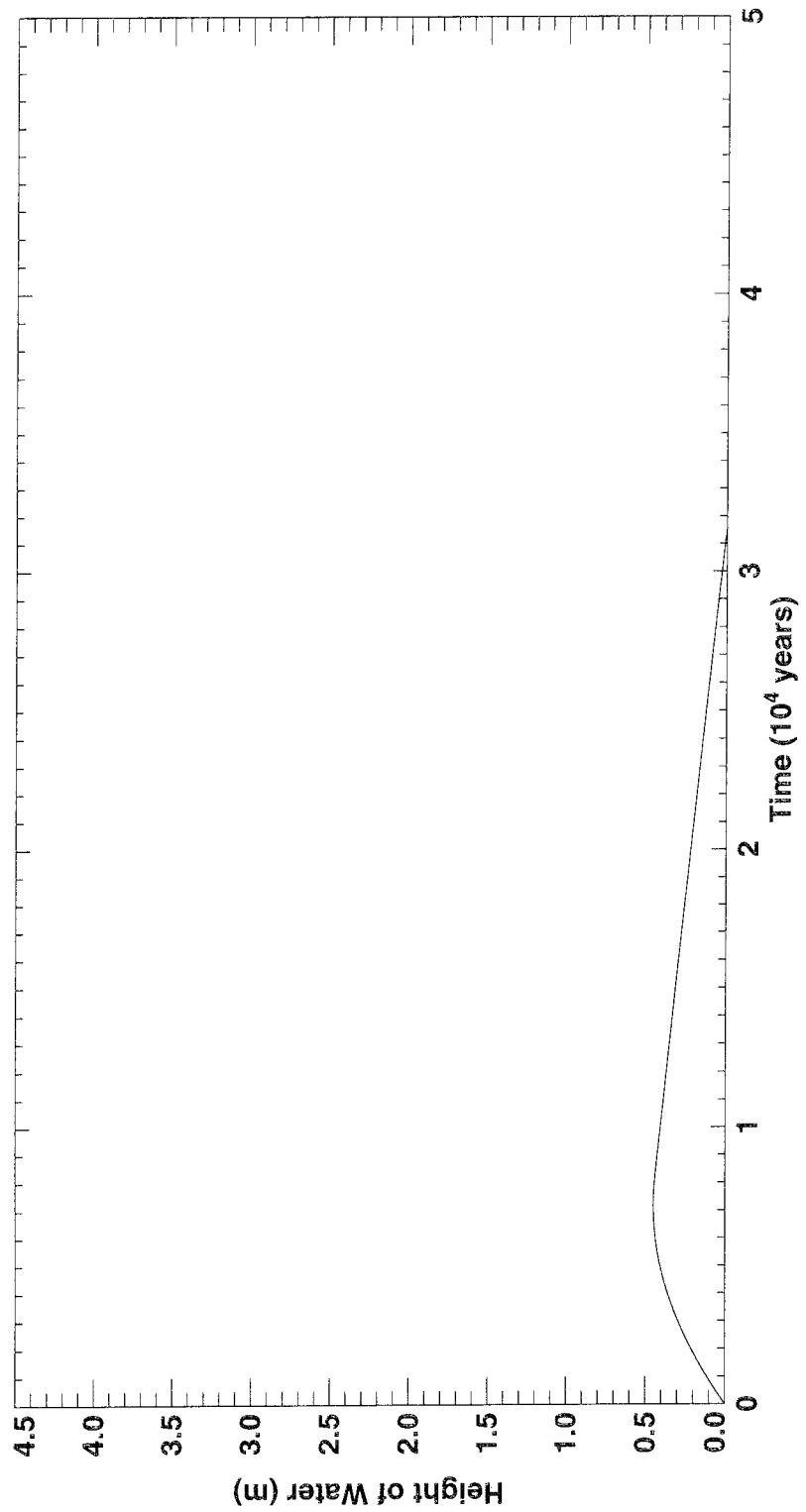


*Figure 3-11. The height of water in the annulus for scenario two, with  $a = 5 \cdot 10^{-6} \text{ m}^2$  and  $\mu = 0.01 \text{ micron/year}$ .*

**Scenario Two: Penetration Area 5 mm<sup>2</sup>, Corrosion Rate 10<sup>-8</sup> m/year  
Internal Canister Pressure**

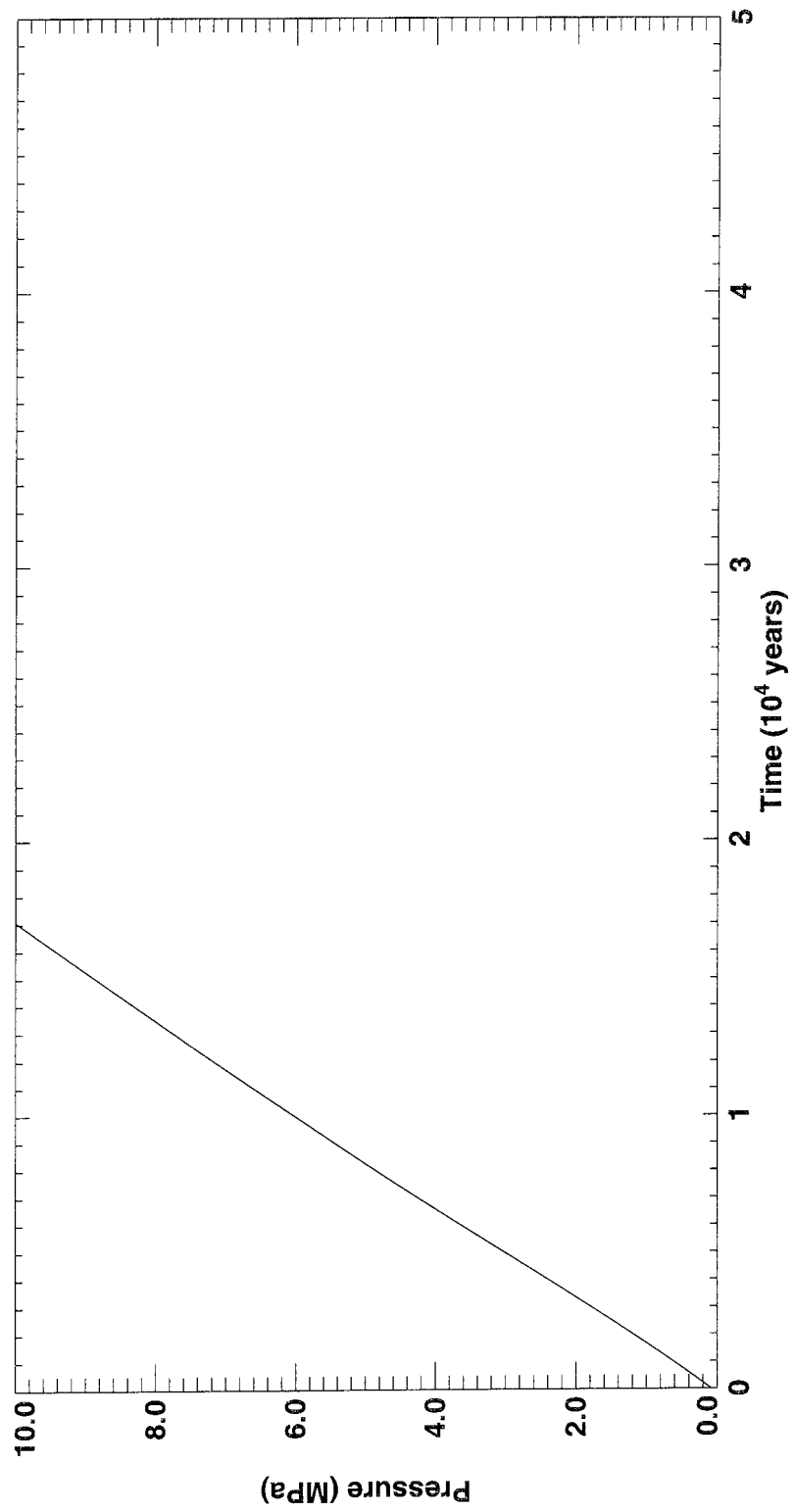


*Figure 3-12. The pressure inside the canister for scenario two, with  $a = 5 \cdot 10^{-6} \text{ m}^2$  and  $\mu = 0.01 \text{ micron/year}$ .*

**Scenario Two: Penetration Area  $5 \text{ mm}^2$ , Corrosion Rate  $10^{-8} \text{ m/year}$   
Amount of Hydrogen Expelled from the Canister**

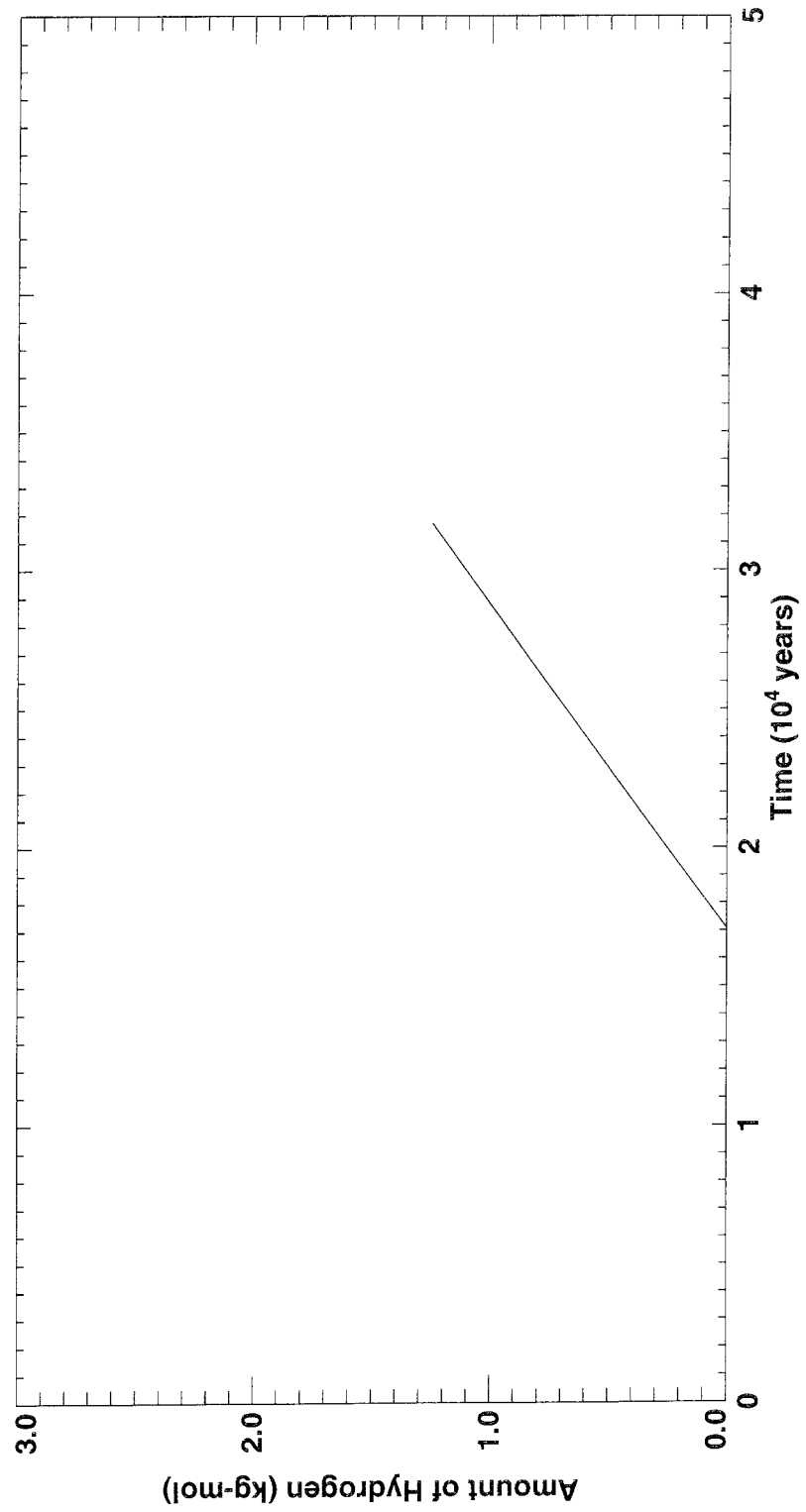


*Figure 3-13. The amount of hydrogen outside the canister for scenario two, with  $a = 5 \cdot 10^{-6} \text{ m}^2$  and  $\mu = 0.01 \text{ micron/year}$ .*

In scenario five, the events of scenario two are repeated. The pressure inside the canister reaches the external hydrostatic pressure after 7040 years, and pressure relief begins at 14080 years when the internal pressure becomes equal to the total external pressure of 10 MPa. The inner container dries out after 11280 years, but because of the extended period for which the annulus is nearly full of water, and therefore undergoing galvanic enhanced corrosion, the program halts when the annulus fills with magnetite after 93550 years. The hydrogen inventory outside the canister is then 9.086 kg - moles.

In summary, these cases which belong to regime (3) of Section 3.3 show the effect of the location of the penetration in the copper overpack in determining the maximum pressure, the amount of hydrogen expelled, and the time scale for various events. A key factor is the amount of water forced out of the canister before hydrogen can be expelled, since this reduces the amount of water available for the corrosion reaction.

### 3.4.5 $a = 0.1791 \text{ m}^2$ , and $\mu = 1 \text{ micron/year}$

This case mimics a previous assessment study /3-4/ in which the penetration in the copper overpack was envisaged as a circumferential crack  $10^{-3} \text{ m}$  in width. The area of the penetration in the copper overpack has been chosen to give the same relationship between water flow to the canister and pressure drop between the far field and the canister. As a result of the very large penetration area, notwithstanding the relatively high corrosion rate, these cases belong to regime (3) of Section 3.3. Thus *a priori* we expect that there will be a considerable water inventory inside the canister and, because of the high corrosion rate, time scales will be shorter than in the cases described in Section 3.4.4.

In the case of the first scenario, with  $a = 0.1791 \text{ m}^2$  and  $\mu = 1 \text{ micron/year}$ , events do indeed occur rapidly. The water level in the annulus reaches the crack after only 13 years, while the water level in the inner container reaches its maximum depth of 0.495m after 58 years. The pressure inside the canister exceeds the external hydrostatic pressure after 63 years, and the total external pressure of 10 MPa after 139 years, when hydrogen starts to be expelled. The inner container dries out after 292 years. The annulus dries out after 349 years, when the program halts because the supply of water to the canister is dominated by diffusion (see Figures 3-14, 3-15 and 3-16). The hydrogen inventory outside the canister is 1.980 kg - moles (i.e. 3.992 kg, see Figure 3-17).

In the case of the second scenario with these values of  $a$  and  $\mu$ , the water level in both the annulus and the inner canister reaches its maximum depth of 0.877m after 68 years. The pressure inside the canister reaches the external hydrostatic pressure after 73 years, and the total external pressure of

10 MPa after 150 years, when hydrogen starts to be expelled. The water level inside the canister falls continuously from its maximum value, and the canister dries out after 534 years, at which point the program halts because the supply of water to the canister is dominated by diffusion). The total hydrogen inventory outside the canister is 3.316 kg - moles . The difference between the present case and scenario one is that no water has been expelled from the canister, and so corrosion continues for longer before the diffusion limit is reached. The pressure inside the canister also takes slightly longer to reach the external hydrostatic pressure than in scenario one, probably because there is less galvanic enhancement of the corrosion process.

In scenario five, the pressure inside the canister reaches the external hydrostatic pressure after 63 years and the total external pressure of 10 MPa after 129 years. The inner container dries out after 289 years, but because of the extended period for which the annulus is nearly full of water, and therefore undergoing galvanic enhanced corrosion, the program halts when the annulus fills with magnetite after 931 years. The hydrogen inventory outside the canister is 9.052 kg - moles , virtually the same as for scenario five in Section 3.4.3 (where the corrosion rate is 100 times slower, and the time to fill the annulus is 100 times longer).

It appears that the main difference between these cases, and the cases presented in Section 3.4.3, is the time scale for various events (much shorter for the cases in this section).

**Scenario One: Penetration Area  $1.791 \cdot 10^5 \text{ mm}^2$ , Corrosion Rate  $10^{-6} \text{ m/year}$   
 Height of Water in Inner Canister**

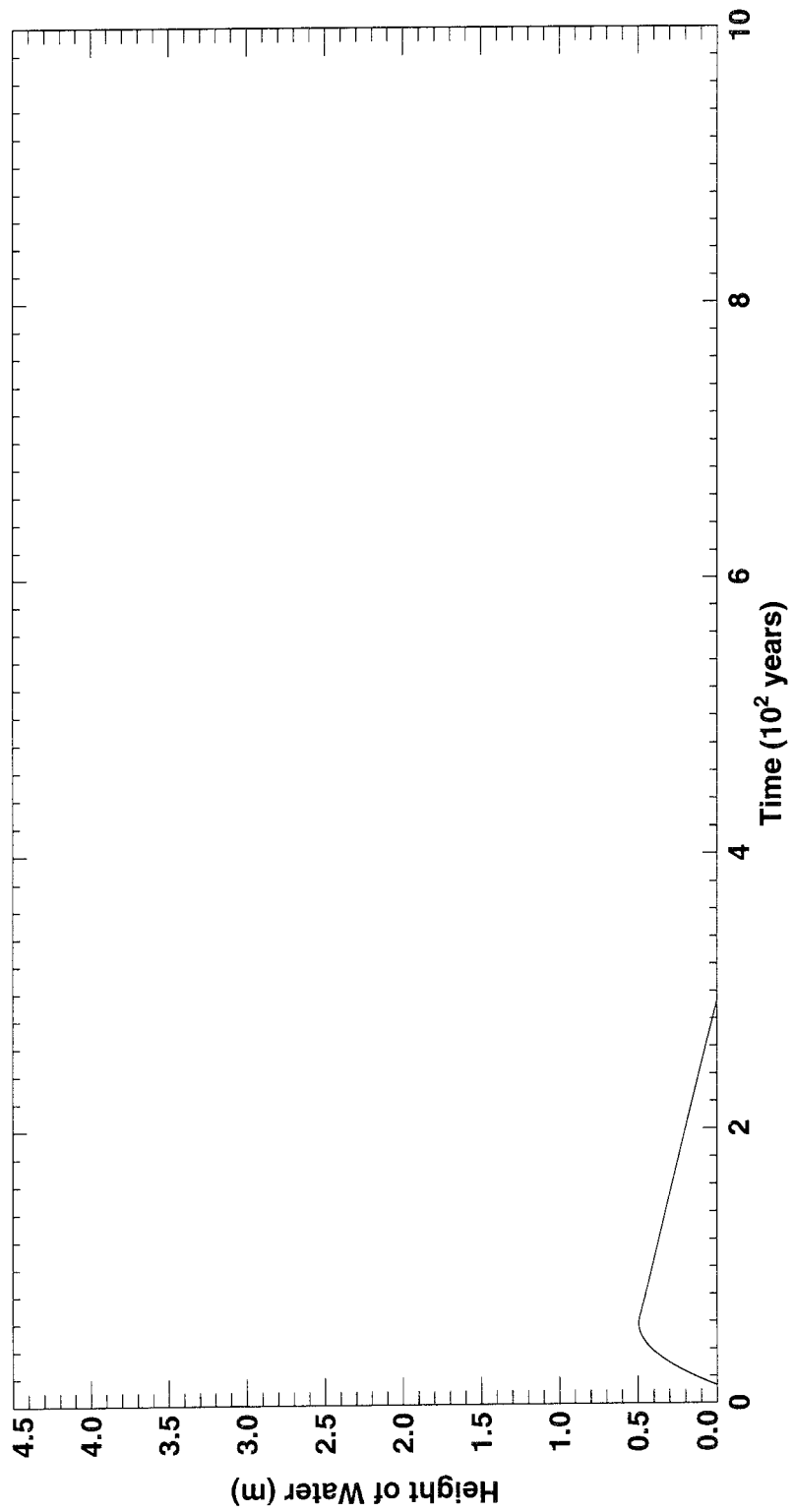


*Figure 3-14. The height of water in the inner container for scenario one, with  $a = 0.1791 \text{ m}^2$  and  $\mu = 1 \text{ micron/year}$ .*

**Scenario One: Penetration Area  $1.791 \cdot 10^5 \text{ mm}^2$ , Corrosion Rate  $10^{-6} \text{ m/year}$   
Height of Water in Annulus**

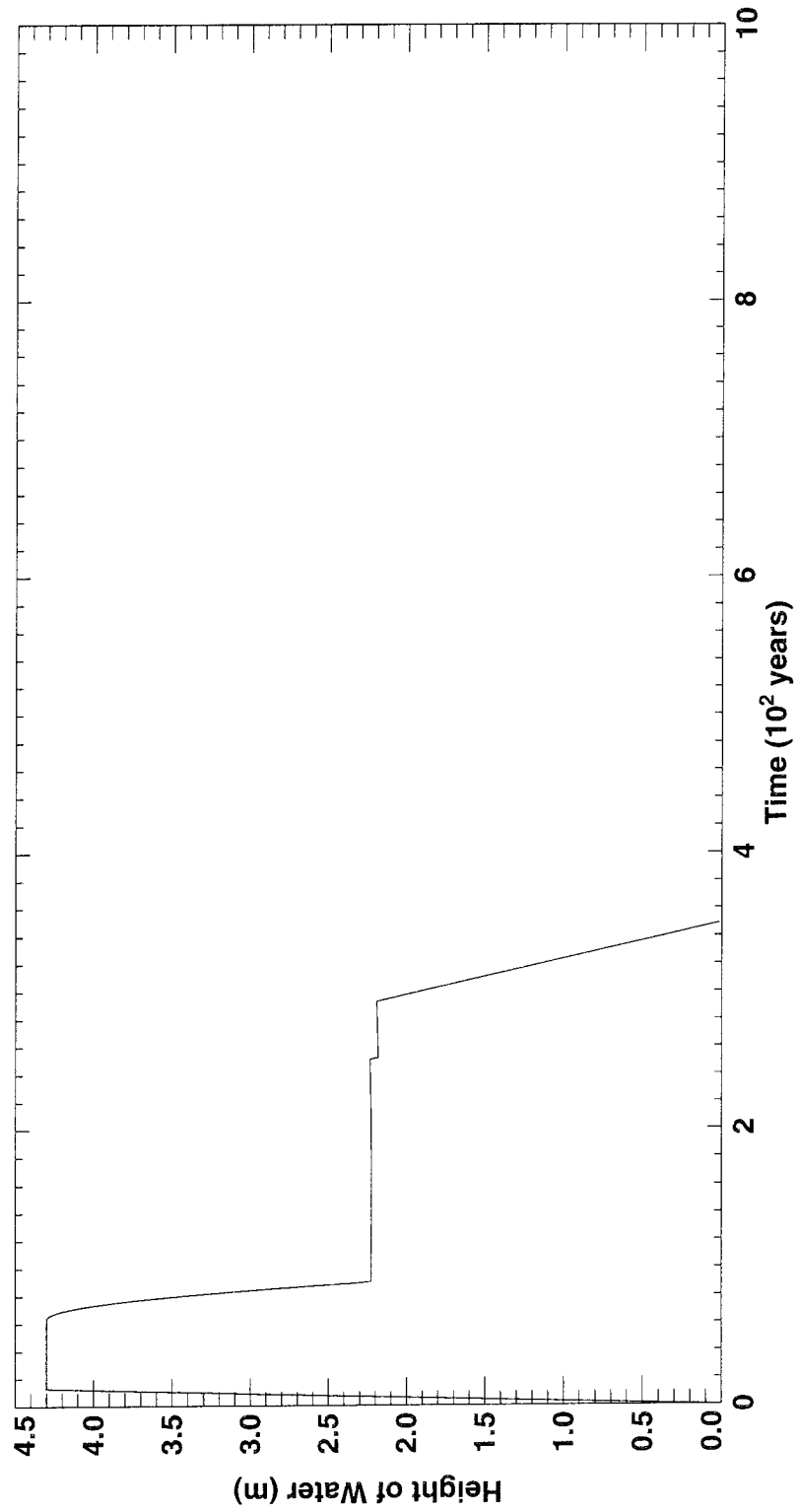


*Figure 3-15. The height of water in the annulus for scenario one, with  $a = 0.1791 \text{ m}^2$  and  $\mu = 1 \text{ micron/year}$ .*

**Scenario One: Penetration Area  $1.791 \cdot 10^5 \text{ mm}^2$ , Corrosion Rate  $10^{-6} \text{ m/year}$   
Internal Canister Pressure**

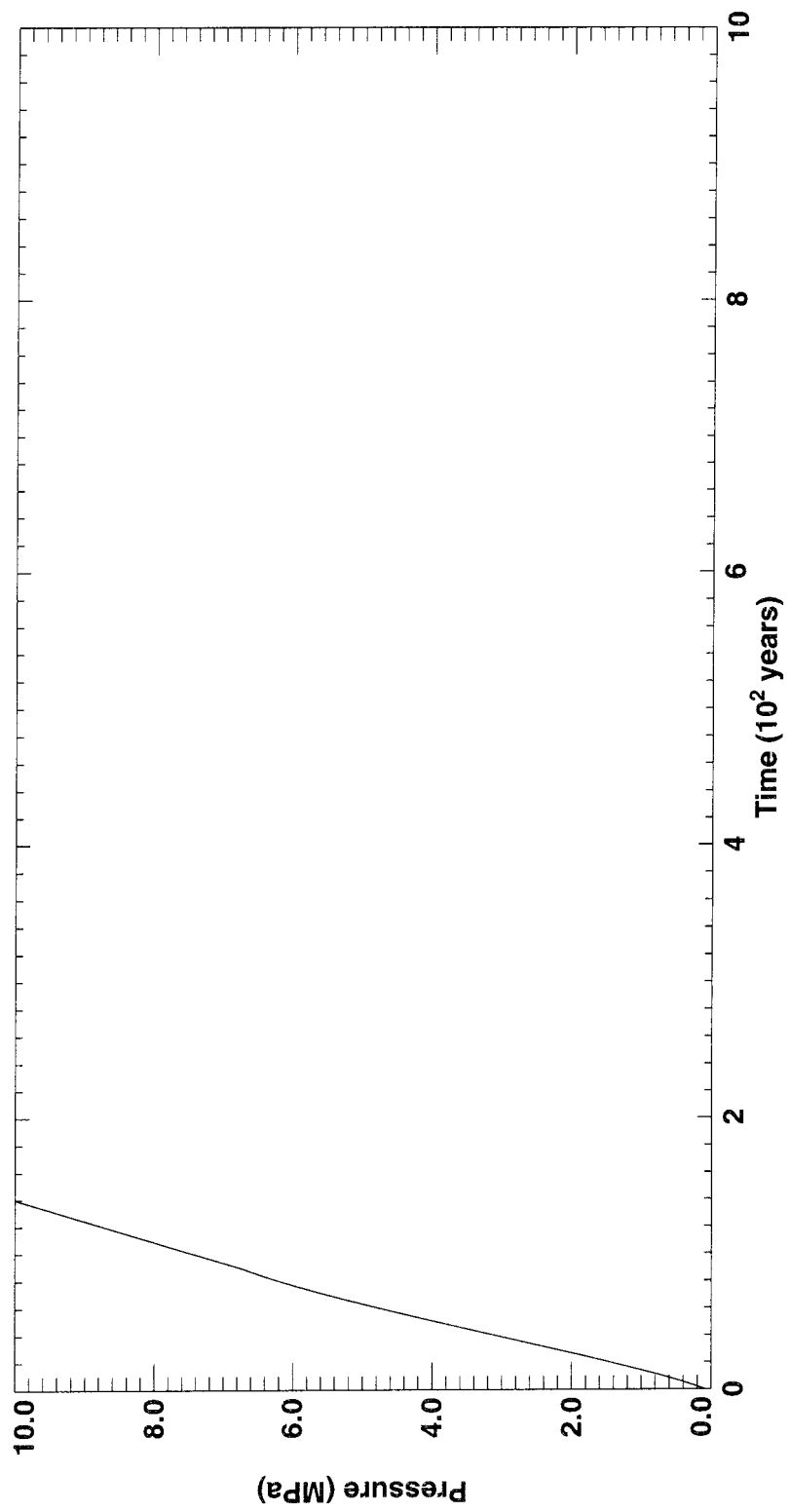


*Figure 3-16. The pressure inside the canister for scenario one, with  $a = 0.1791 \text{ m}^2$  and  $\mu = 1 \text{ micron/year}$ .*

**Scenario One: Penetration Area  $1.791 \cdot 10^5 \text{ mm}^2$ , Corrosion Rate  $10^{-6} \text{ m/year}$   
Amount of Hydrogen Expelled from the Canister**

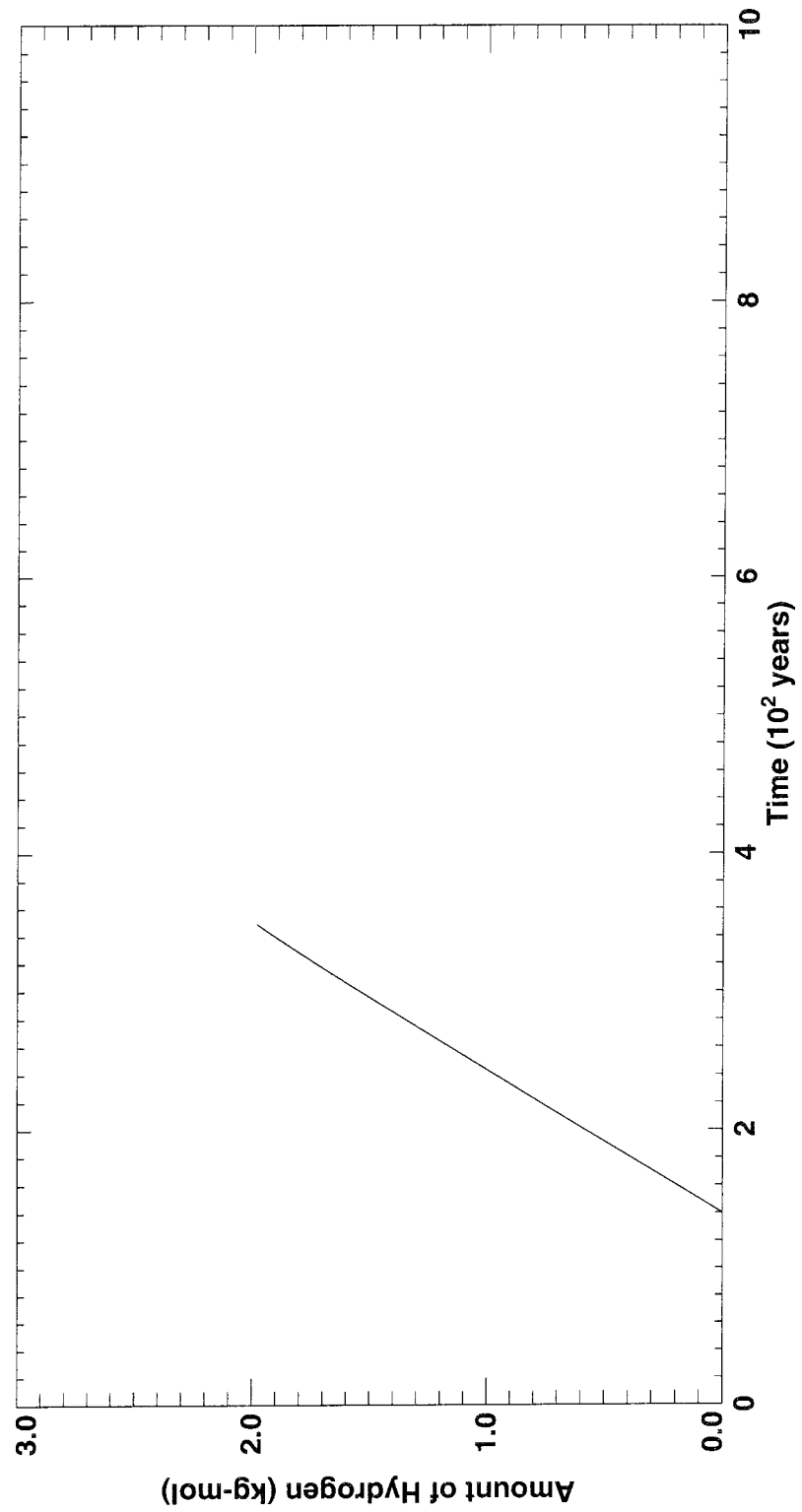


*Figure 3-17. The amount of hydrogen outside the canister for scenario one, with  $a = 0.1791 \text{ m}^2$  and  $\mu = 1 \text{ micron/year}$ .*

## 4 THE DIFFUSION MODEL

### 4.1 INTRODUCTION

After any liquid water in the canister has been consumed (see Section 3), corrosion of the steel container continues because water vapour can diffuse into the canister from outside. This section describes a numerical model of the diffusion limited corrosion process, which takes into account:

- the change in size of the annular gap as corrosion progresses;
- possible suppression of the corrosion rate;
- the flow of hydrogen generated by the corrosion process.

The aim of this modelling study is to calculate:

- the corrosion residue profile in the annulus;
- the extent of corrosion on the surface of the steel container (referred to as the corrosion radius  $r_c$ ).

### 4.2 ASSUMPTIONS

The annulus is assumed initially to be free of corrosion residue. A transient calculation predicts the thickness of corrosion residue as a function of position and time, and the corrosion radius as a function of time. The equation parameters change with time as a result of the build-up of magnetite and consequent reduction in size of the annular gap. The calculation continues until the annulus is blocked.

The model geometry consists of a 1D penetration (characterised by a length and cross-sectional area) connected at right angles to the centre of a disk representing the annular gap. The thickness of the disk corresponds to the initial size of the annular gap, while its radius corresponds to the area of the outer surface of the inner container. Both

- the diffusion of water vapour from outside the canister through the penetration and annular gap to the surface of the corroding inner container,
- and the counterflow of hydrogen produced by corrosion,

are included in the model. The computer code developed here solves the 1D diffusion equation for water vapour in the region (the flow of hydrogen adds no significant complexity); i.e. variations in water vapour density, water vapour flux and hydrogen velocity across the width of the annulus are ignored. The consequences of this approximation were explored by comparing against the results of a 2D finite element analysis (see Sections 4.3 and 4.5).

The diffusion coefficient is  $D \sim 9 \cdot 10^{-7} \text{ m}^2/\text{s}$  (see Section 5.2.5). The calculation uses a steady-state solution for the density and flux of water vapour in the annulus, i.e. it is assumed that changes in the distribution of water vapour are practically instantaneous compared to the time step used to determine the growth of the magnetite layer (this assumption is justified in Appendix A.1.3).

It is possible that the corrosion rate may be suppressed by the presence of a thick magnetite layer [3-4]. Qualitative insight into this behaviour can be gained by assuming a simple model for the corrosion rate

$$\frac{\mu}{1 + \frac{t_R}{l_s}} \quad 4-1$$

where  $\mu$  is the initial corrosion rate,  $t_R$  is the thickness of the magnetite layer and  $l_s$  is a 'suppression length'. The consequences of this assumption for the corrosion residue profile and the corrosion radius were investigated.

The following parameter values were considered to be of practical interest:

- the initial corrosion rate,  $\mu$ , was chosen to lie in the range  $0.001 \mu\text{m}/\text{year}$  to  $25.8 \mu\text{m}/\text{year}$ ;
- the suppression length,  $l_s$ , was chosen to be  $0.1 \mu\text{m}$ ,  $1 \mu\text{m}$ ,  $10 \mu\text{m}$  or  $\rightarrow \infty$ ;
- the penetration area,  $a$ , was chosen to be  $5 \text{ mm}^2$  or  $20 \text{ mm}^2$  (corresponding to the two smaller sizes considered in Section 3).

### 4.3 REVIEW OF THE STRESS CORROSION MODEL

The present study is concerned with the build-up of corrosion product in the annulus. A related study (see Section 5.2.5) was concerned with a simpler question:

*Assuming that the annulus has filled with magnetite, corrosion can continue only as a result of the diffusion of either water or*

*water vapour through this corrosion residue. Where in the annulus will corrosion occur?*

The 2D steady state diffusion equation for water in the penetration and annulus was solved using a finite element approach. The results are presented in Table 5-2, and show the corrosion radius as a function of a dimensional parameter  $\Lambda$  ( $\Lambda$  is the ratio of the corrosion rate and the diffusion coefficient). For a penetration in the lid of the canister, it was predicted that for  $\Lambda < 10^{-5} \text{ m}^{-1}$  corrosion would occur over the whole of the steel container. At the largest value of  $\Lambda$  considered,  $10^{-1} \text{ m}^{-1}$ , the corrosion radius was predicted to be 0.013 m.

Equation B-9 in Appendix B shows how  $\Lambda$  can be related to the parameters used in this Section.

## 4.4 THE COMPUTER MODEL

Appendix B sets out:

- the water and hydrogen balance equations which determine the location of corrosion in the annulus;
- analytical solutions which are available in the case of constant gap width (in general, the gap width is only constant within a certain limited radius beyond which the analytical solutions do not apply).
- the modifications required to model corrosion rate suppression.

The computer code reads in the model data and then, for a number of time steps until the annulus blocks, calculates the thickness of corrosion residue, water vapour flux, water vapour density and hydrogen velocity at a sequence of radial positions in the annulus.

The key mathematical problem is to find the correct steady-state values for the corrosion radius  $r_c$  and flux of water vapour in the penetration  $F_1$ .

In the case of a constant gap width, this can be done by Newton-Raphson iteration of equation B-20 (this gives the value of  $q \equiv F_1/S_c$ , where  $S_c$  is the flux of water vapour consumed by corrosion, whence  $r_c$  and  $F_1$  follow).

In the more general, but more difficult, case of a varying gap width, an iterative procedure is used. Equation B-11, or more generally B-25, is integrated numerically outward from the last point at which the gap width is constant to give the discretised form of  $G_2 \equiv rF_2$ , where  $F_2$  is the outward flux of water vapour in the annulus. Similarly, equation B-7 is integrated outward to give the discretised form of the water vapour density  $\rho_2$ . These integrations are continued, while moving out through the sequence of

discrete radial positions, until an interval is found in which  $G_2$  becomes negative. An estimate of  $r_c$  is then found by interpolation within this interval. If  $\rho_2(r_c)$  is zero (to within a tolerance), and there are no points at smaller radii where  $\rho_2$  has changed sign, then the loop is considered to have converged giving both  $r_c$  and the corresponding value of  $F_1$ . If  $\rho_2(r_c)$  is not zero, then its value is used to update  $F_1$  and another iteration is started. This algorithm is modified slightly to handle cases where:

- $\rho_2$  changes sign at a smaller radius than  $r_c$  ;
- $r_c$  reaches the last point in the sequence of discrete radial positions.

## 4.5 RESULTS AND DISCUSSION

The computer model described in Section 4.4 was first verified against the results of the 2D finite element analysis (see Section 5.2.5). In particular, the corrosion radii  $r_c$  predicted by equations B-16 and B-20 for the case of an uncorroded annulus (i.e. in the absence of corrosion suppression) were compared with the values in Table 5-2. Note that the present model accounts for countercurrent hydrogen flow, but that this has a negligible impact on the results.

The results of this comparison are shown in Table 4-1. Note that the ‘equivalent’ maximum radius in the 2D finite element analysis is 1.544 m, i.e. smaller than in the present 1D analysis where it is 2.1624 m. That is the reason for the difference between the two models when  $\Lambda = 10^{-5} \text{ m}^{-1}$ . At higher values of  $\Lambda$ , the 1D model predicts a value of  $r_c$  between 21% and 36% larger than that obtained in the 2D finite element model. We believe this to be a measure of the degree of approximation introduced by using 1D rather than 2D. The trend in  $r_c$  as a function of  $\Lambda$  is the same in both models.

**Table 4-1. Table showing the corrosion radius  $r_c$  as a function of corrosion rate (or  $\Lambda$ ) as determined by a 2D finite element analysis and the present 1D analysis.**

Corrosion rate ( $\mu \text{ m/year}$ )	$\Lambda$ ( $\text{m}^{-1}$ )	$r_c$ (m) (2D analysis)	$r_c$ (m) (1D analysis)
$2.5845 \cdot 10^{-4}$	$10^{-6}$	Whole container	Whole container
$2.5845 \cdot 10^{-3}$	$10^{-5}$	Whole container	1.740
$2.5845 \cdot 10^{-2}$	$10^{-4}$	0.454	0.552
$2.5845 \cdot 10^{-1}$	$10^{-3}$	0.129	0.175
$2.5845 \cdot 10^0$	$10^{-2}$	0.040	0.056
$2.5845 \cdot 10^1$	$10^{-1}$	0.013	0.018

Following this, the present 1D model was used to calculate corrosion radii and corrosion residue profiles for a number of cases listed in Table 4-2.

The calculations were discretised as follows:

- the time, going up to a time just before the annulus blocks, was divided into  $10^5$  timesteps of equal size;
- radially the model was discretised into 2000 equal intervals: the innermost point corresponds to the penetration radius  $r_0$ , and the outermost to either the largest corrosion radius found in a preliminary calculation or the maximum annulus radius  $r_{\max}$ .

**Table 4-2. Table showing the individual cases considered in the calculations of corrosion radii and corrosion residue profiles.**

Case	Initial Corrosion Rate, $\mu$ ( $\mu$ m/year)	Suppression Length, $l_s$ ( $\mu$ m)	Penetration Area, $a$ ( $m^2$ )
1	1	$\rightarrow \infty$	$5 \cdot 10^{-6}$
1a	1	1	$5 \cdot 10^{-6}$
1b	1	10	$5 \cdot 10^{-6}$
1c	1	0.1	$5 \cdot 10^{-6}$
2	$10^{-3}$	$\rightarrow \infty$	$5 \cdot 10^{-6}$
2a	$10^{-3}$	1	$5 \cdot 10^{-6}$
3	25.845	$\rightarrow \infty$	$5 \cdot 10^{-6}$
3a	25.845	1	$5 \cdot 10^{-6}$
4	1	$\rightarrow \infty$	$2 \cdot 10^{-5}$
4a	1	1	$2 \cdot 10^{-5}$

The resulting profiles for the corrosion residue thickness are shown in Figures 4-1 to 4-9.

### Case 1 (Figure 4-1)

In Case 1 the corrosion radius  $r_c$  decreases monotonically from its initial value of  $8.94 \cdot 10^{-2}$  m, the decrease being most rapid immediately before the annulus blocks at  $1.823 \cdot 10^3$  years. In this variant, which has no corrosion suppression, the corrosion radius is only affected by the gap width  $h_g$  and as predicted in Appendix B.1.4  $r_c$  decreases as  $h_g$  decreases. At all times the gap has uniform width within the corrosion radius, and the corrosion residue

profile is rounded towards its outer edge only because of the shrinkage in  $r_c$  as  $h_g$  decreases.

#### **Case 1a (Figure 4-2)**

In Case 1a the corrosion radius increases rapidly to the maximum possible value of  $r_{\max} = 2.1624$  m (i.e. the case of corrosion over the whole outer surface of the inner container) after  $2.430 \cdot 10^5$  years, and remains at this value almost until the time the annulus blocks at  $3.487 \cdot 10^6$  years. The small deviation of the profile from uniformity reflects the limited time for which corrosion is not taking place over the whole steel surface.

#### **Case 1b (Figure 4-3)**

In Case 1b the corrosion radius increases with time, slowly at first (in the direction indicated in Appendix B.1.4) and then more rapidly until it reaches a maximum of 2.13 m (i.e. not quite reaching  $r_{\max}$ ) after  $3.390 \cdot 10^5$  years. It then decreases rapidly until the annulus blocks after  $3.503 \cdot 10^5$  years. In contrast with Case 1a, the proportionally longer time spent by the system at small corrosion radius is reflected in the strongly non-uniform profile.

#### **Case 1c (Figure 4-4)**

In Case 1c, the variation of corrosion radius with time is qualitatively similar to Case 1a. The corrosion radius reaches  $r_{\max}$  at about  $3.010 \cdot 10^5$  years, and the annulus blocks at  $3.485 \cdot 10^7$  years, so the proportion of the total time spent with the corrosion radius less than the maximum is smaller than in Case 1a; hence the more uniform profile.

#### **Case 2 (Figure 4-5)**

In Case 2 the corrosion radius is initially at its maximum allowed value of 2.1624 m, but falls below this and decreases rapidly from  $1.692 \cdot 10^6$  years; the annulus blocks at  $1.823 \cdot 10^6$  years. The late shrinkage of the corrosion radius is reflected in a slightly non-uniform profile.

#### **Case 2a**

In Case 2a the corrosion radius is 2.1624 m almost until the annulus blocks, which occurs after  $3.487 \cdot 10^9$  years. The resulting profile is practically uniform (and therefore not shown) as would be expected given

the very low initial rate of corrosion and the significant corrosion suppression.

### **Case 3 (Figure 4-6)**

In Case 3, the corrosion radius behaves similarly to that observed in Case 1. There is monotonic, and increasingly rapid, shrinkage of  $r_c$  from an initial value of  $1.77 \cdot 10^{-2}$  m; the time for the annulus to block at this high corrosion rate is 70.54 years. As expected, the profile is qualitatively similar to that obtained in Case 1.

### **Case 3a (Figure 4-7)**

In Case 3a, the corrosion radius behaves similarly to that observed in Case 1b, i.e. it increases, slowly at first and then more rapidly, reaching a maximum of 1.38 m after  $1.328 \cdot 10^5$  years and then decreasing rapidly until the annulus blocks after  $1.349 \cdot 10^5$  years. As in Case 1b, the resulting profile is far from uniform.

### **Case 4 (Figure 4-8)**

In Case 4 the corrosion radius decreases monotonically from an initial value of 0.17 m, until the annulus blocks after  $1.823 \cdot 10^3$  years. Note that the time to blockage is the same as in Case 1, and the initial value of  $r_c$  is approximately double that in Case 1. These comparisons are as expected, since the only change in going from Case 1 to Case 4 is a doubling of the penetration area. The profiles are similar for the two cases, being a little less sharp at the outer boundary in the present case.

### **Case 4a (Figure 4-9)**

In Case 4a the corrosion radius increases to 2.1624 m after  $2.520 \cdot 10^4$  years, and then starts to decrease after  $3.442 \cdot 10^6$  years. The annulus blocks after  $3.487 \cdot 10^6$  years. This case is comparable to Case 1a; the time to blockage is identical, and the behaviour of the corrosion radius and the profile are very similar. The profile is a little more uniform in the present case because the ratio ( $r_{\max}/r_0$ ) is smaller; i.e. in units of  $r_0$ , water vapour flow and corrosion occur over a smaller distance.

If there is no corrosion suppression (e.g. Cases 1, 2, 3 and 4), the following arguments from first principles give the dependence of the corrosion radius  $r_c$  on the penetration radius  $r_0$  and the corrosion rate, characterised by  $\Lambda$  :

- if the corrosion rate (and hence  $\Lambda$ ) is increased by an arbitrary factor  $\kappa_1$ , then the area over which a given quantity of water can diffuse will correspondingly decrease by  $\kappa_1$ ;
- if  $r_0$  is increased by an arbitrary factor  $\kappa_2$ , then the quantity of water able to flow in through the penetration increases by  $\kappa_2^2$ , and the area over which the water can diffuse will correspondingly increase by  $\kappa_2^2$ .

These arguments suggest that the corrosion radius should scale like  $r_c \sim r_0/\Lambda^{0.5}$ , provided there is no corrosion suppression. This observation is approximately supported by the results from Cases 1, 2, 3 and 4.

## 4.6 CONCLUSIONS

Our results lead to the following general conclusions:

- up to a limit corresponding to the total available surface area of the inner container, the extent of corrosion as measured by the corrosion radius is approximately proportional to the penetration radius and inversely proportional to the square root of the corrosion rate (as expected from first principles, and assuming there is no corrosion suppression);
- corrosion suppression, characterised by a length scale of the order of 1 micron, has very considerable effects in:
  - (1) increasing the time for the annulus to block by orders of magnitude;
  - (2) increasing the area over which corrosion proceeds, in many cases so that it covers the total available surface area of the inner container;
  - (3) modifying the corrosion profiles from rounded ‘top hat’ profiles to much wider profiles, in many cases nearly uniform as a function of radius.
- at the high pressure ( $10^7$  Pa) of interest, the influence of hydrogen flow out of the canister is negligible.

**Thickness of Corrosion Product in Annulus  
Profile at the Time when Annulus Blocks**

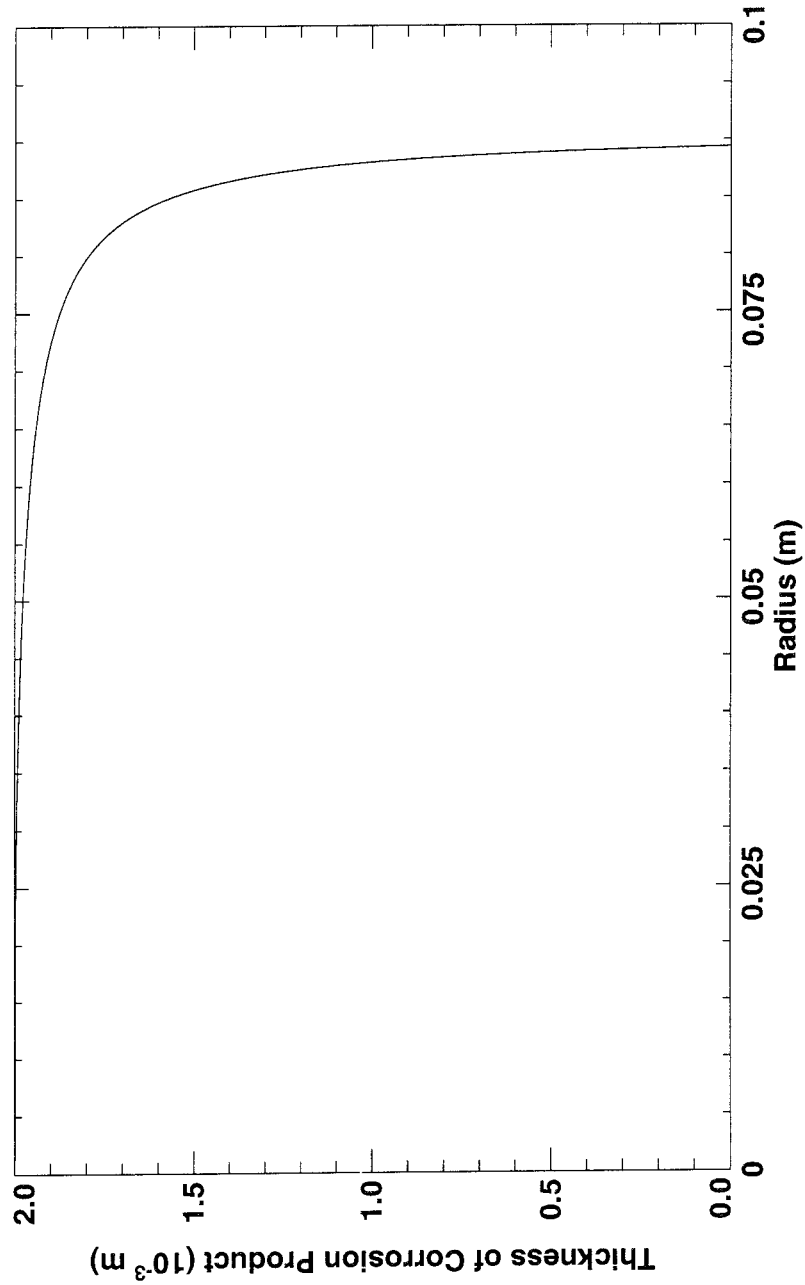
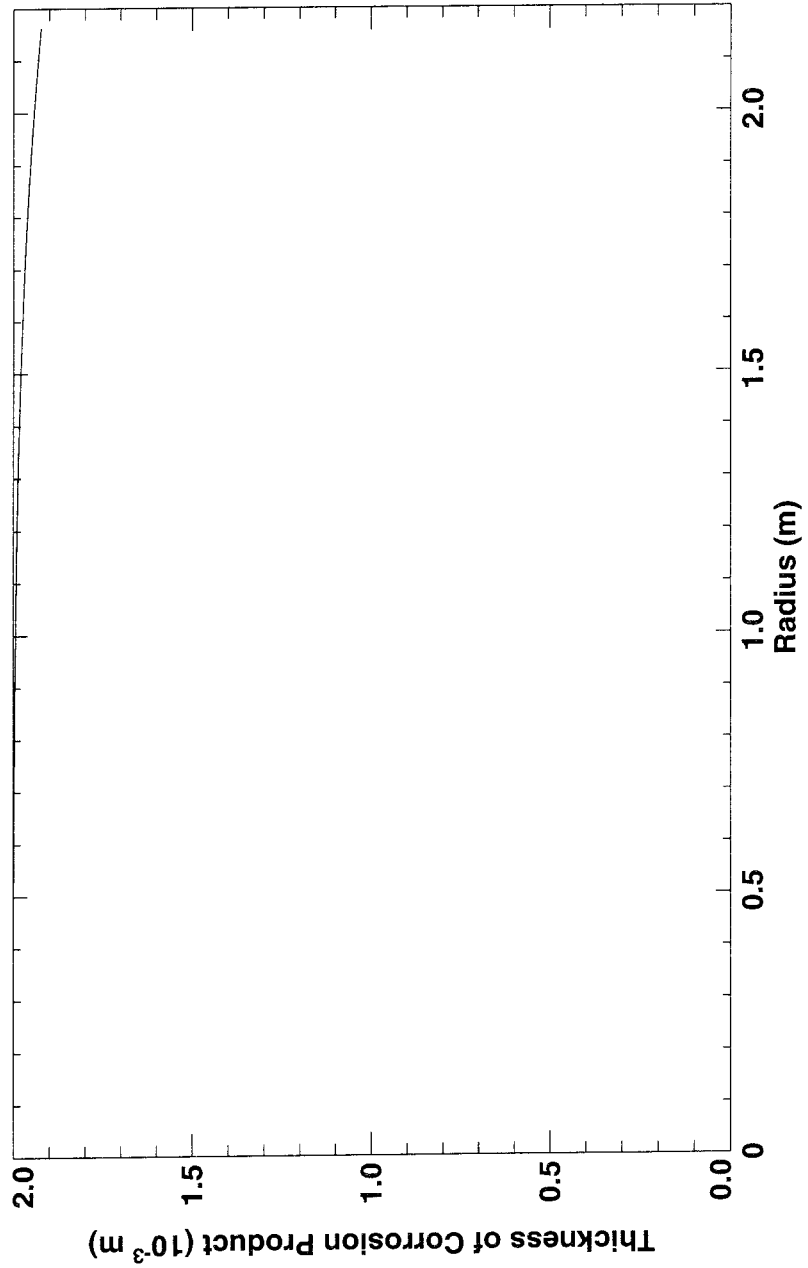


*Figure 4-1. Corrosion residue profile at the time when the annulus blocks for  $\mu = 1$  micron/year,  $l_s \rightarrow \infty$  and  $a = 5 \cdot 10^{-6} \text{ m}^2$ .*

**Thickness of Corrosion Product in Annulus  
Profile at the Time when Annulus Blocks**



Penetration Area (mm<sup>2</sup>):  
5.0

Base Corrosion Rate (m/year):  
10<sup>-6</sup>

Suppression Length (m):  
10<sup>-6</sup>

Time (years):  
3.487 10<sup>6</sup>

*Figure 4.2. Corrosion residue profile at the time when the annulus blocks for  $\mu = 1$  micron/year,  $l_s = 1$  micron and  $a = 5 \cdot 10^{-6} \text{ m}^2$ .*

**Thickness of Corrosion Product in Annulus  
Profile at the Time when Annulus Blocks**

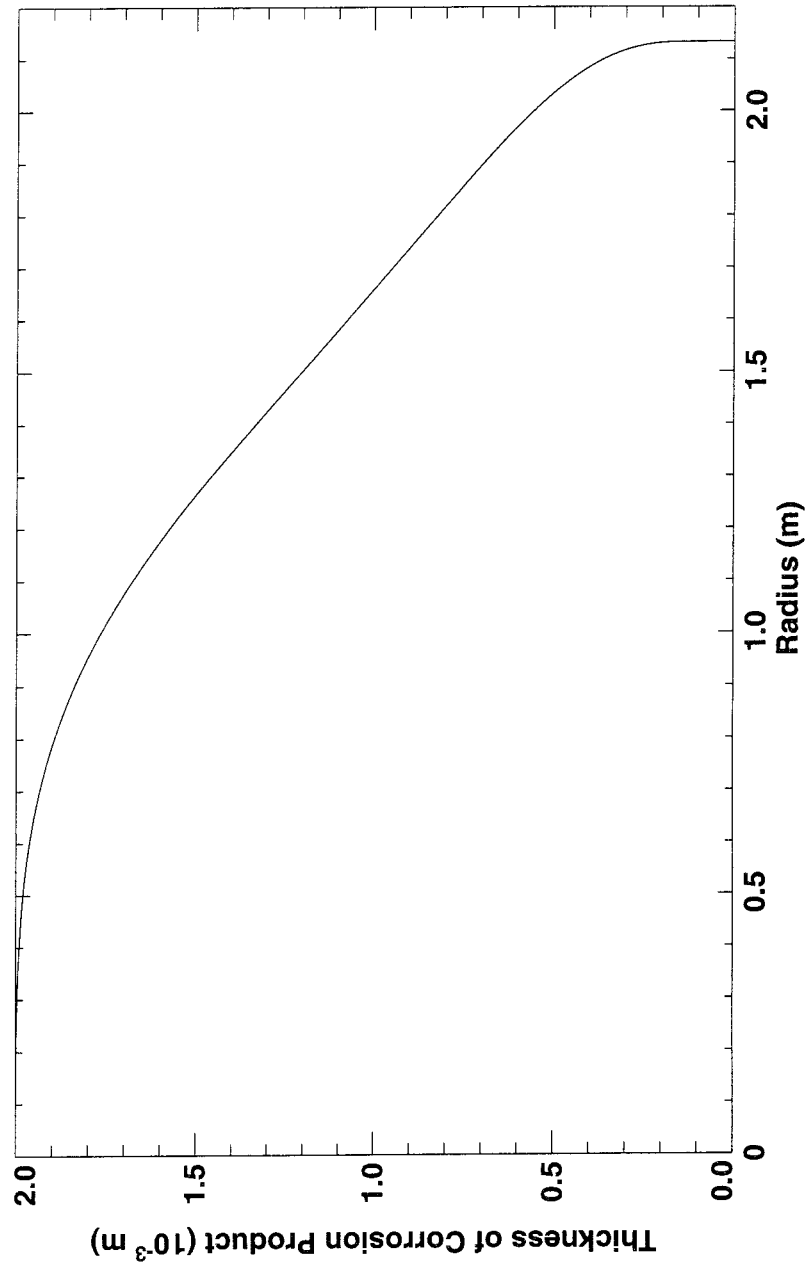
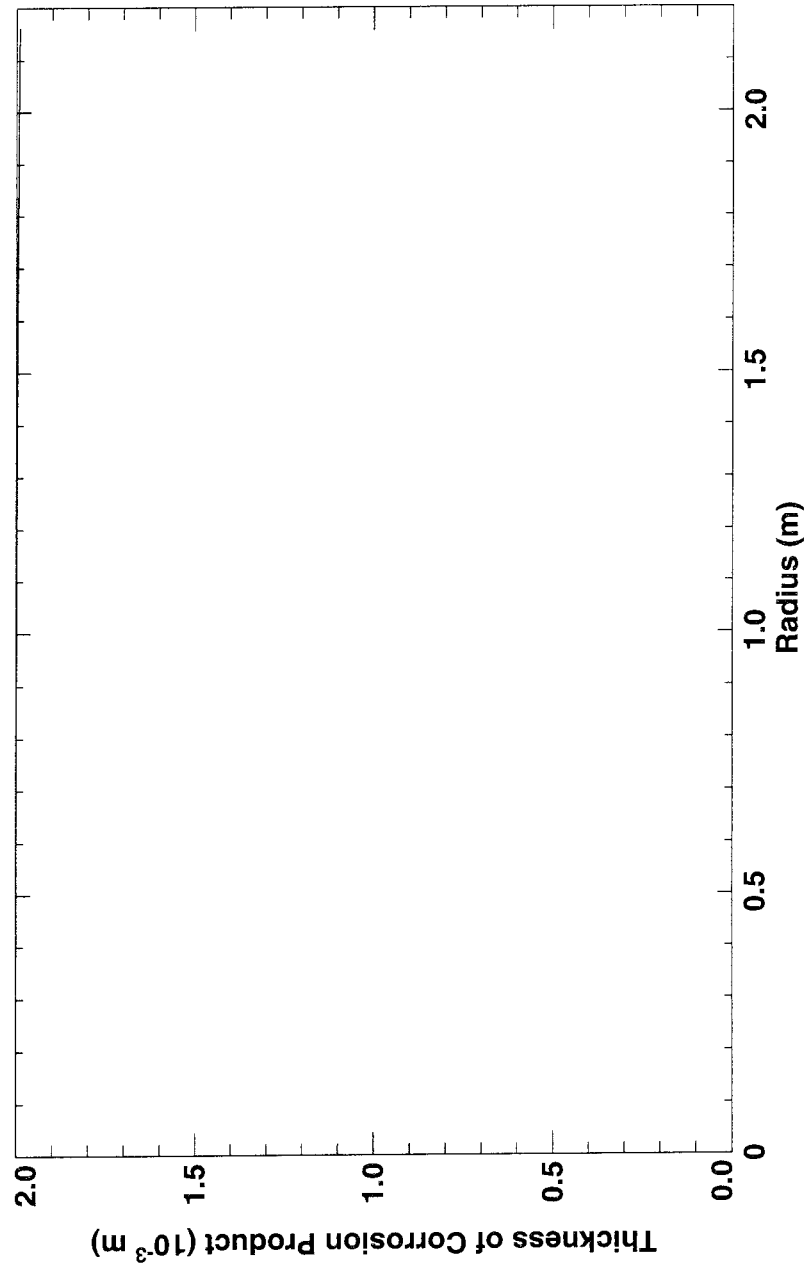


*Figure 4-3. Corrosion residue profile at the time when the annulus blocks for  $\mu = 1$  micron/year,  $l_s = 10$  micron and  $a = 5 \cdot 10^{-6} \text{ m}^2$ .*

**Thickness of Corrosion Product in Annulus  
Profile at the Time when Annulus Blocks**



Penetration Area (mm<sup>2</sup>):  
5.0

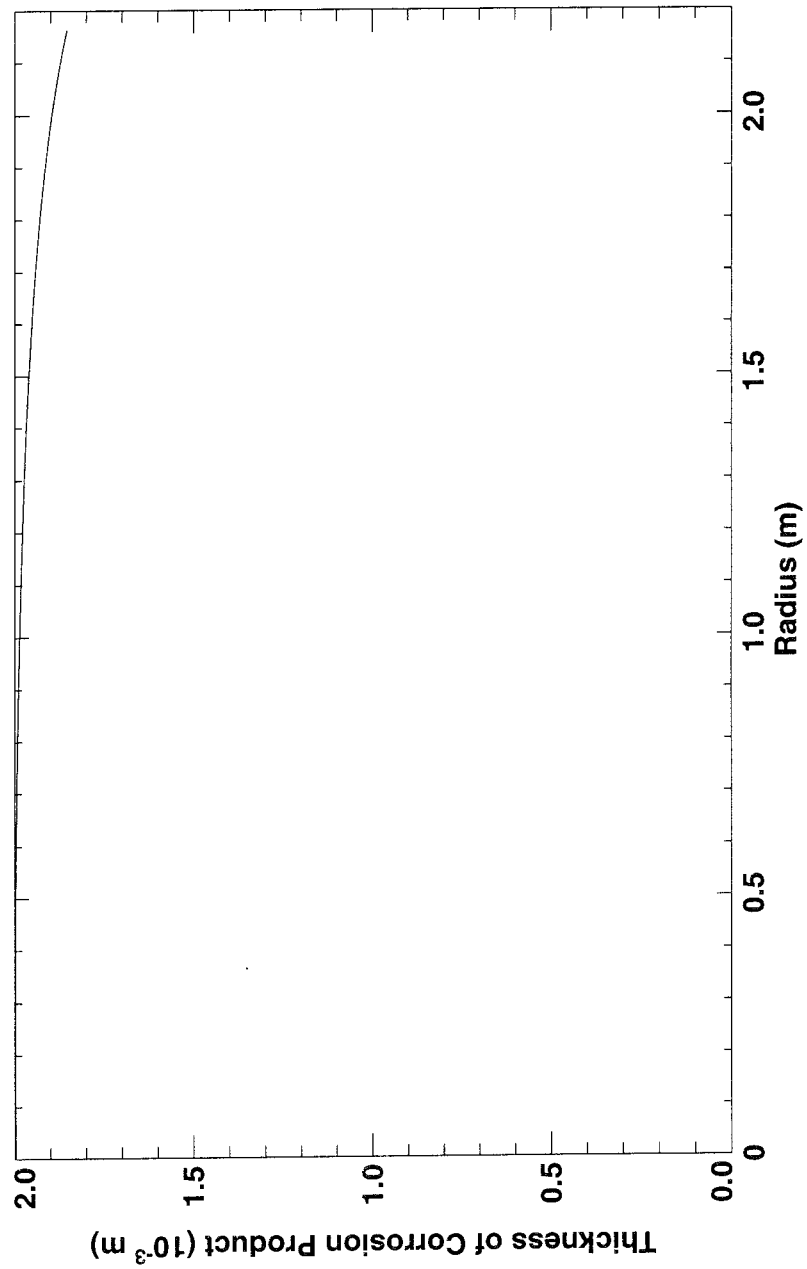
Base Corrosion Rate (m/year):  
 $10^{-6}$

Suppression Length (m):  
 $10^{-7}$

Time (years):  
 $3.485 \cdot 10^7$

*Figure 4-4. Corrosion residue profile at the time when the annulus blocks for  $\mu = 1$  micron/year,  $l_s = 0.1$  micron and  $a = 5 \cdot 10^{-6} \text{ m}^2$ .*

**Thickness of Corrosion Product in Annulus  
Profile at the Time when Annulus Blocks**



**Penetration Area (mm<sup>2</sup>):**  
5.0

**Base Corrosion Rate (m/year):**  
 $10^{-9}$

**Suppression Length (m):**  
 $10^6$

**Time (years):**  
 $1.823 \cdot 10^6$

*Figure 4-5. Corrosion residue profile at the time when the annulus blocks for  $\mu = 0.001$  micron/year,  $l_s \rightarrow \infty$  and  $a = 5 \cdot 10^{-6}$  m<sup>2</sup>.*

**Thickness of Corrosion Product in Annulus  
Profile at the Time when Annulus Blocks**

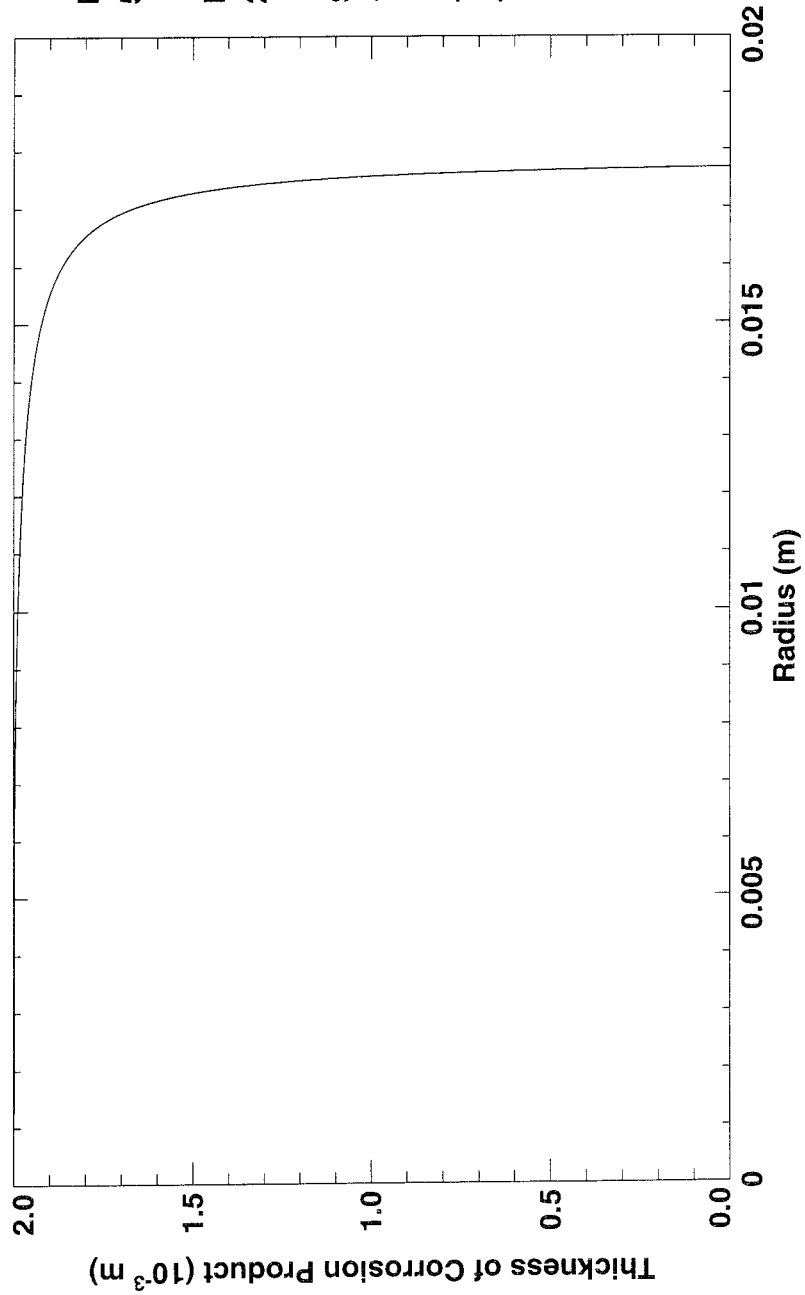
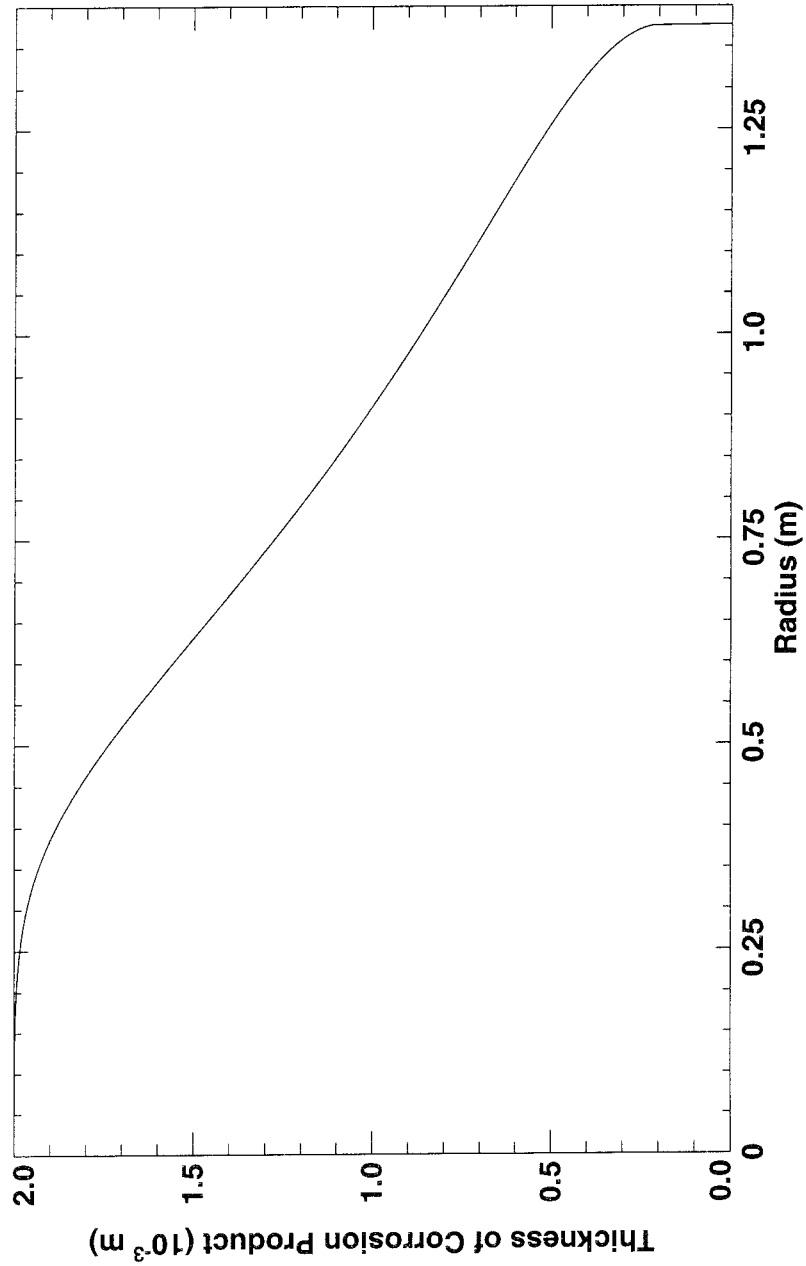


*Figure 4-6. Corrosion residue profile at the time when the annulus blocks for  $\mu = 25.845$  micron/year,  $l_s \rightarrow \infty$  and  $a = 5 \cdot 10^{-6}$  m<sup>2</sup>.*

**Thickness of Corrosion Product in Annulus  
Profile at the Time when Annulus Blocks**



**Penetration Area ( $\text{mm}^2$ ):**  
5.0

**Base Corrosion Rate (m/year):**  
 $2.58 \cdot 10^{-5}$

**Suppression Length (m):**  
 $10^{-6}$

**Time (years):**  
 $1.349 \cdot 10^5$

*Figure 4-7. Corrosion residue profile at the time when the annulus blocks for  $\mu = 25.845$  micron/year,  $l_s = 1$  micron and  $a = 5 \cdot 10^{-6}$   $\text{m}^2$ .*

**Thickness of Corrosion Product in Annulus  
Profile at the Time when Annulus Blocks**

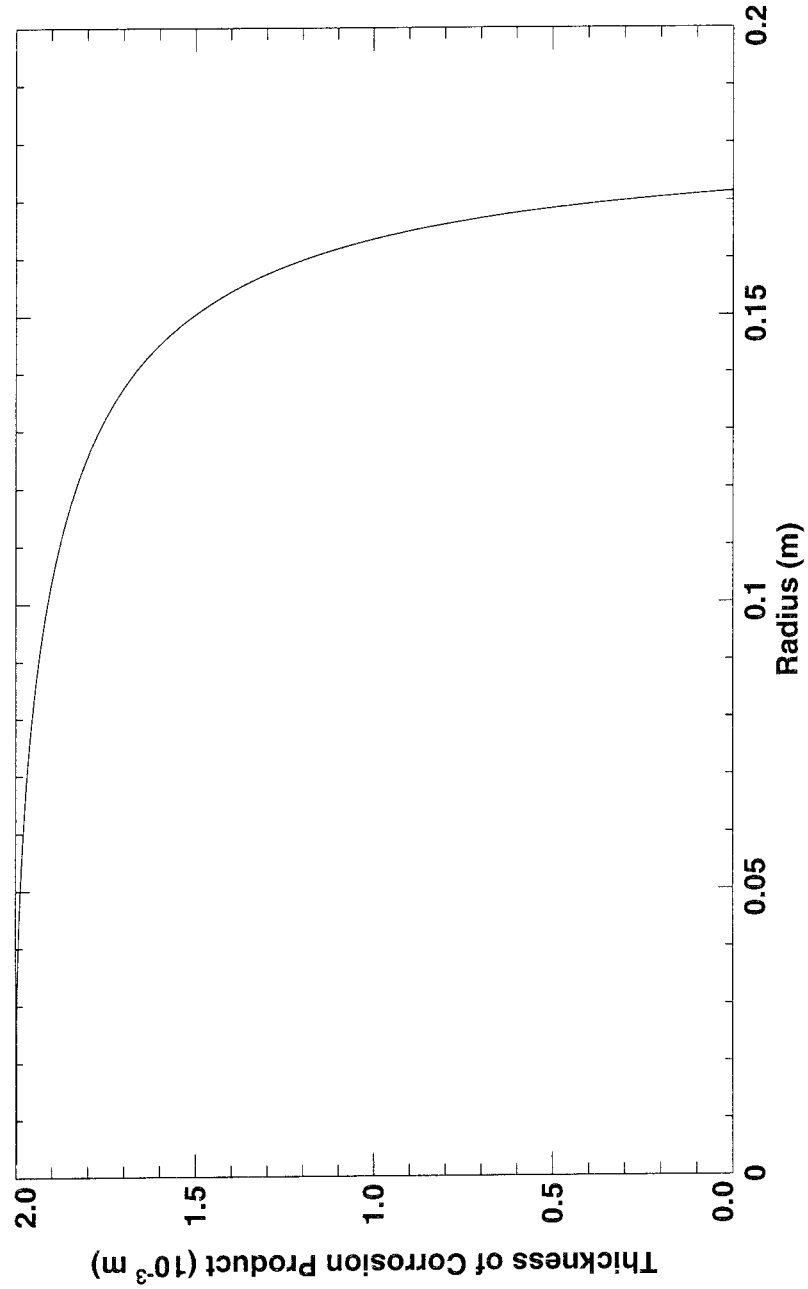


*Figure 4-8. Corrosion residue profile at the time when the annulus blocks for  $\mu = 1$  micron/year,  $l_s \rightarrow \infty$  and  $a = 2 \cdot 10^{-5} \text{ m}^2$ .*

**Thickness of Corrosion Product in Annulus  
Profile at the Time when Annulus Blocks**

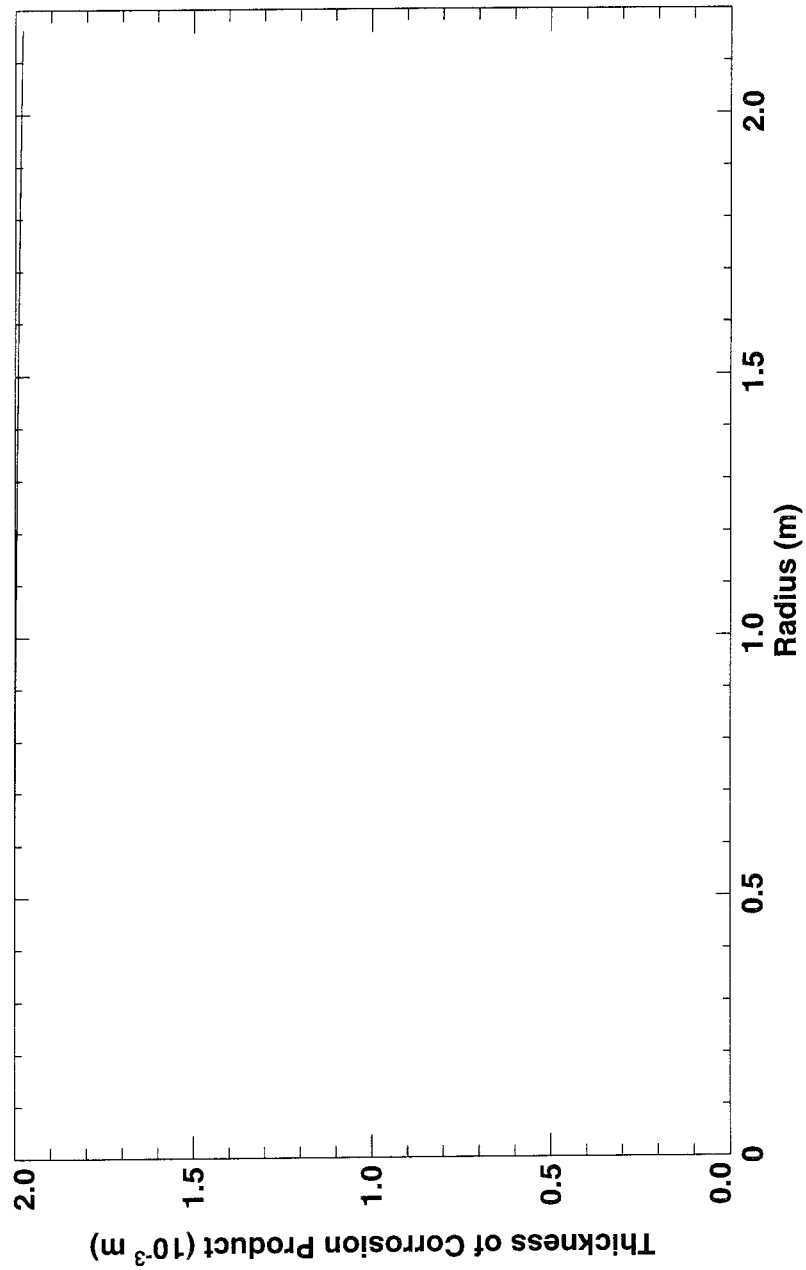


*Figure 4-9. Corrosion residue profile at the time when the annulus blocks for  $\mu = 1$  micron/year,  $l_s = 1$  micron and  $a = 2 \cdot 10^{-5} \text{ m}^2$ .*

## 5 THE STRESS MODEL

### 5.1 INTRODUCTION

In Section 3, a model was developed for the inflow of water to a canister with a penetration in its copper overpack, resulting in anaerobic corrosion of the cast steel inner container and the generation of hydrogen. This model described the interactions between the supply of water, corrosion, hydrogen production, pressure inside the canister and the build-up of corrosion product.

For several of the cases discussed in Section 3, a point is reached in which the supply of water taking part in corrosion is controlled by the diffusion of vapour through an hydrogen atmosphere filling the available space inside the canister. Section 4 shows how the continued corrosion of the canister fills the annular fitting gap with corrosion product (assuming that this has not already happened while liquid water is present in the canister).

This section assumes that the annular fitting gap between the cast steel inner container and the copper overpack has filled with magnetite ( $\text{Fe}_3\text{O}_4$ ), and analyses the implications of a further build-up of corrosion product for the structural integrity of the canister. In particular, three key issues are addressed:

- how does corrosion affect the structural performance of the steel inner container;
- what are the stresses in the canister local to the penetration in the copper overpack, and is the original defect likely to grow;
- can the stresses induced by corrosion of the canister in the surrounding rock cause the deposition hole to fail?

Corresponding to the issues, finite element stress analyses were carried out at three different levels of detail:

- **canister models:** the canister was modelled in 3D (the inner container was modelled using solid elements, and the copper overpack using shell elements) to examine the overall structural integrity of the canister;
- **detailed models:** a small region of the canister was modelled in detail in order to examine the stresses in the canister local to the penetration in the copper overpack;

- **vault models:** the copper overpack, bentonite buffer and rock were all modelled to examine the stresses induced by corrosion of the canister in the surrounding rock.

These stress analyses used the finite element code ABAQUS 5.5, which is particularly suited to modelling the non-linear material properties and geometric complexity prevalent in this study.

In addition, a number of subsidiary issues were also considered:

- does the geometry of the penetration in the copper overpack affect the canister's performance;
- are the results presented in Section 5.3.3 overly pessimistic because the magnetite has been assumed to be incompressible;
- can corrosion cause the lid fixing of the inner container to fail, thereby allowing groundwater free access to the radioactive waste?

Throughout most of this section, our results are presented in terms of a strain field estimated from the build up of corrosion product, and are independent of time (and any uncertainty about the rate of corrosion). However, in Section 6 a 'best estimate' corrosion rate is used to relate the thickness of corrosion product to time, and the behaviour of the canister is discussed as a function of time.

## **5.2 ASSUMPTIONS**

### **5.2.1 Canister**

The canister geometry is taken from the PASS report /2-1/. Both the BWR and PWR designs for the canister were analysed (see Figures 5-1 and 5-2). A number of simplifying assumptions were made to allow the stress analyses to be carried out using conventional finite element techniques. These are summarised below.

The 'canister' and 'detailed' models assume symmetry between the top and the bottom half of the canister. However, in the 'vault' model the bottom half of the canister and the surrounding rock are modelled explicitly, as this is the most constrained region where the highest stresses are likely to occur. The detailed design of the canister lid and the fixing method (e.g. welding, bolts) is neglected, since the purpose of the stress analyses is to assess the long term behaviour of the canister. The curvature at the corners of the fuel channels is not modelled, leading to a slight overestimate of the stresses at these points.

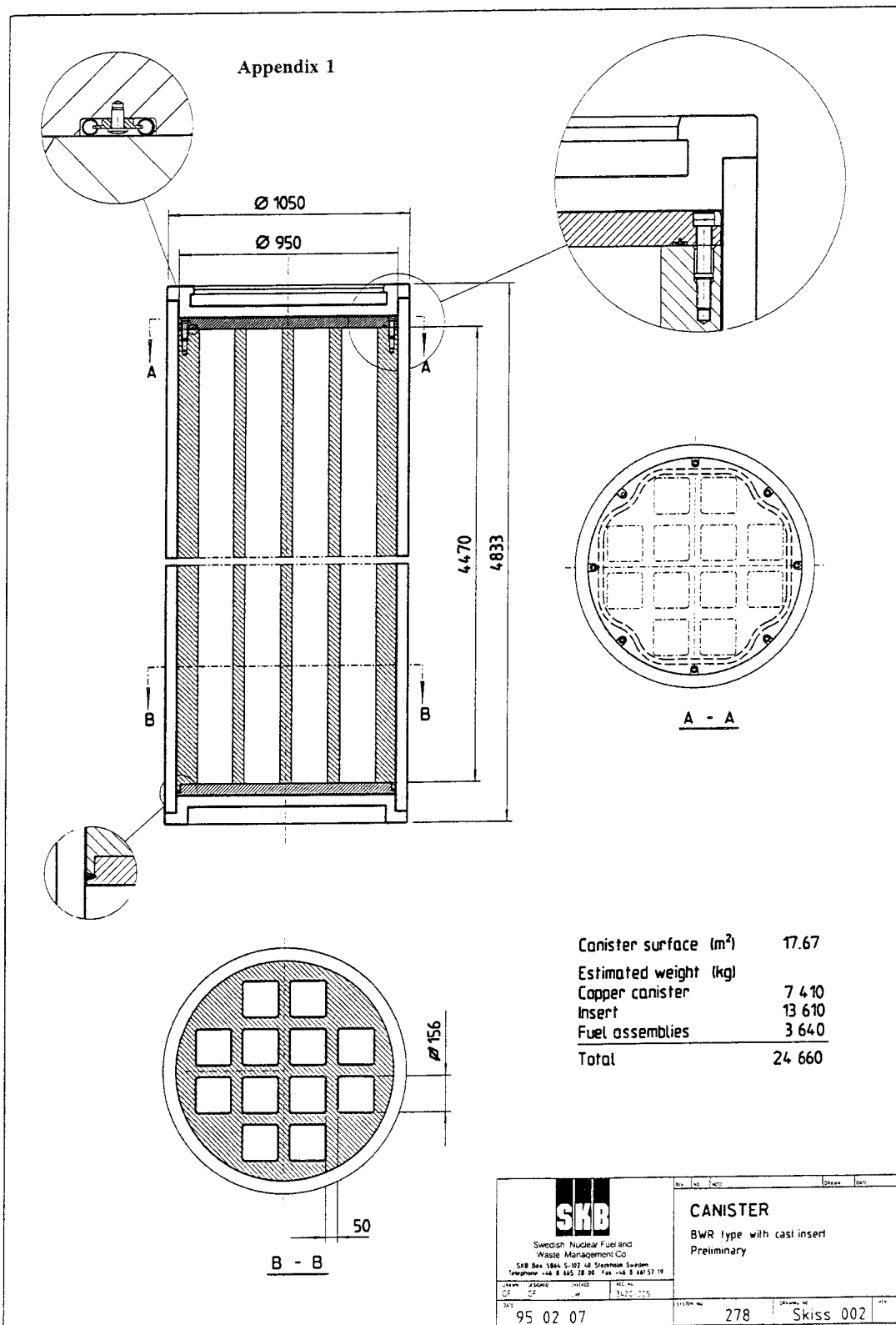
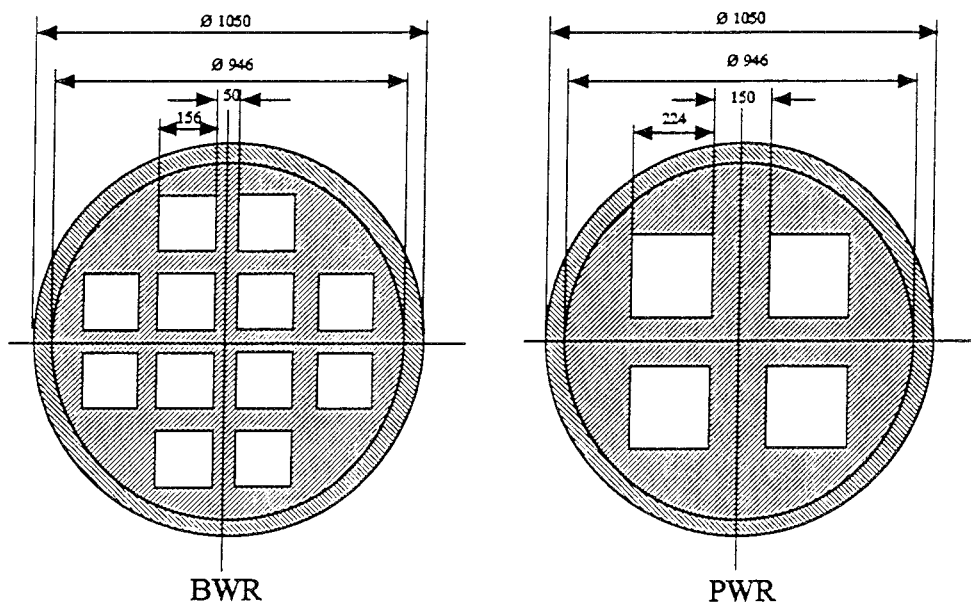


Figure 5-1. Design of the BWR canister.



*Figure 5-2. Storage configuration in cast inserts for BWR and PWR type fuel.*

The stress analyses carried out here assume a 2 mm 'fitting gap' between the copper overpack and the inner container. However, a previous calculation /5-2/ showed that the overpack will creep and come into contact with the inner container after resaturation of the repository. In this report, the stresses in the copper overpack and inner container are calculated in terms of the strain applied by the corrosion product, and remain valid whichever assumption is made. The only difference is in the discussion of time scales (see Section 6) when the time to fill the annulus is either present or absent.

The possibility that the inner container may be positioned eccentrically with respect to the copper overpack is ignored. In the long term, the major effect of any eccentricity could be local differences in the corrosion rate, but the impact is likely to be small.

The canister is assumed to be initially free of stress. However, residual stresses within the cast inner container will influence the stress at which failure initiates. In addition, stresses associated with welds or bolts will affect the canister locally. In practice, these stresses are likely to be small compared to the stresses induced by corrosion.

The radioactive waste has been neglected, i.e. the fuel channels have been modelled as voids. This is likely to be the case, although corrosion of the waste might pressurise the fuel channel slightly (which would reduce the effect of the stresses on the inner container).

### 5.2.2 Repository

According to the KBS-3 concept /2-1/, the canister will be placed in a chamber drilled in volcanic rock in one of an array of vertical storage holes. The canister will then be surrounded by compacted bentonite (Figure 5-3). In the 'vault' analyses, it was assumed that the bentonite is fully saturated. Any effects of the migration of hydrogen gas (produced by corrosion) on the bentonite are neglected. As a consequence, the elastic/plastic properties of the bentonite remain constant over the time scale of the analyses. Geostatic stresses are not considered because they are small compared to the bentonite swelling pressure.

The 'canister' and 'detailed' models did not explicitly include the bentonite, since it was assumed that the stresses due to the bentonite would be much smaller than those due to the stiffness of the inner container. The result is that the stresses in the copper overpack are slightly overestimated, and the stresses in the inner container are slightly underestimated. As the copper overpack is strained, the void ratio decreases and the stiffness of the bentonite increases (i.e. the error between the calculated stresses and the true values increases). The formation of 20 mm of corrosion product typically results in a doubling of the hydrostatic pressure.

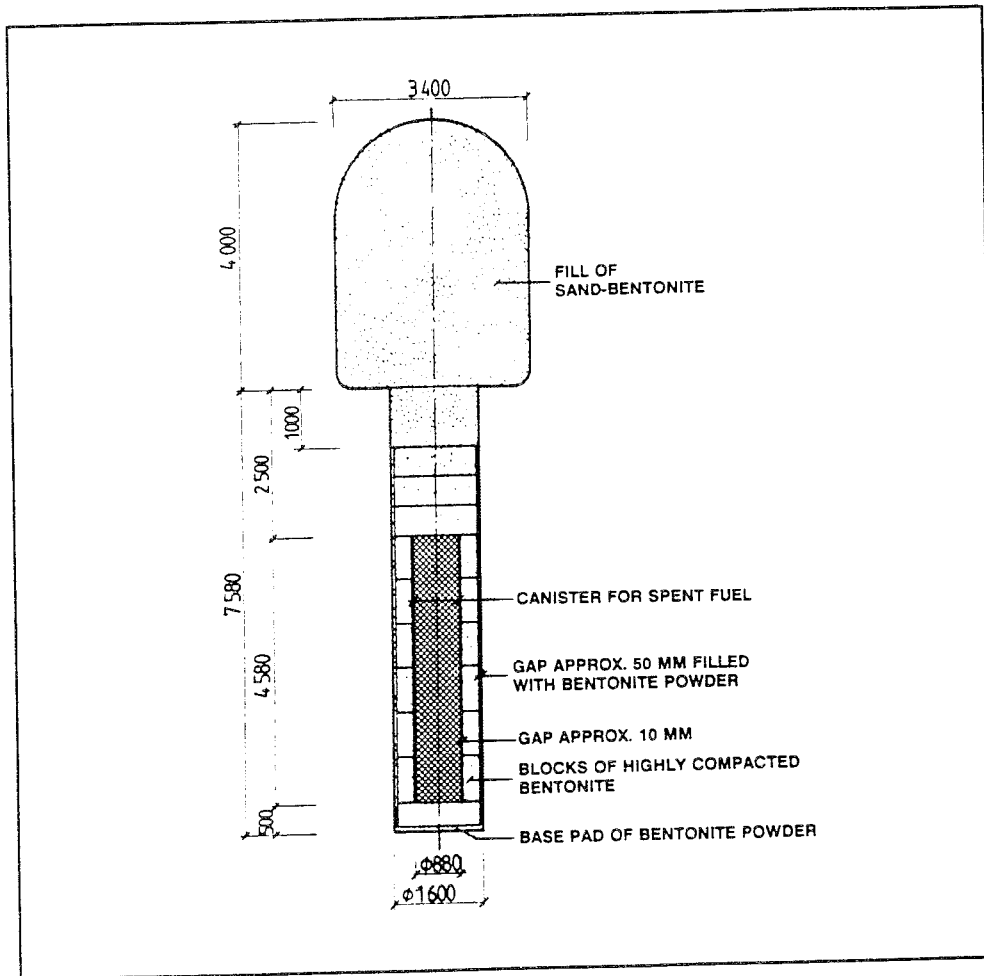


*Figure 5-3. Deposition hole with copper/steel canister and bentonite buffer.*

### **5.2.3 Penetration**

The stress analyses assume the presence of a defect with area  $5 \text{ mm}^2$  in the copper overpack. This nominal hole size was specified by SKB, and is intended to represent a worst case failure in the welding of the copper.

The hole size will affect:

- the corrosion behaviour of the canister;
- the stresses local to the defect as calculated in the ‘detailed’ analyses.

This size of defect is such that any pressures exerted on the inner and outer surfaces of the copper overpack are assumed to be equal.

The influence of the defect geometry on the predicted stresses is discussed in Section 5.6

### **5.2.4 Material properties**

Material properties were supplied by SKB /5-1, 5-2/, and are summarised in Table 5-1.

**Table 5-1. Summary of the material properties.**

<b>Material</b>	<b>Elastic Modulus (GPa)</b>	<b>Poisson's Ratio</b>	<b>Yield Stress (MPa)</b>	<b>Tensile Strength (MPa)</b>	<b>Post Yield Properties</b>
Copper	117	0.3	65 (0.2% proof)	200	Tensile Multi-Linear Plastic (True) Stress (MPa)      (True) Plastic Strain 60      0.000 80      0.015 130      0.065 180      0.154 200      0.288
Steel	206	0.3	200 (0.2% proof)	400	Not modelled
Bentonite	0.1	0.4	0.133	N/A	Compressive Drucker-Prager (Linear) Hardening Characteristics: friction angle, $\beta = 20^\circ$ yield stress, $d = 133$ kPa dilation angle, $\psi = 2^\circ$ flow stress ratio, $K = 0.9$ (True) Stress (kPa)      (True) Plastic Strain 113      0.000 138      0.005 163      0.020 188      0.040 213      0.100
Rock	5	0.2	Assumed brittle	N/A Compressive strengths 80→270 MPa /5-3, 5-4/	Not modelled

The copper overpack was modelled as:

- an elastic multi-linear plastic material, to allow for the behaviour at the canister rim, in the ‘canister’ and ‘detailed’ analyses,;
- a linear elastic material in the ‘vault’ analyses.

The stress-strain curve for copper is shown in Figure 5-4, and was parameterised as in Table 5-1. Once the final plasticity data point on the stress-strain curve has been reached, ABAQUS extrapolates the curve assuming elastic perfectly-plastic behaviour. This enables strains to continue at a fixed stress (in this particular case, 200 MPa). The failure

strain for copper is about 29% ; strains larger than this indicate failure, and a redistribution of stress. The models are inaccurate near such points. The effects of creep and thermal expansion were not included in the models.

The visco-plastic nature of copper on the long time scales being considered here, means that the stresses in the canister will tend to be overestimated and the life expectancy of the canister will be underestimated.

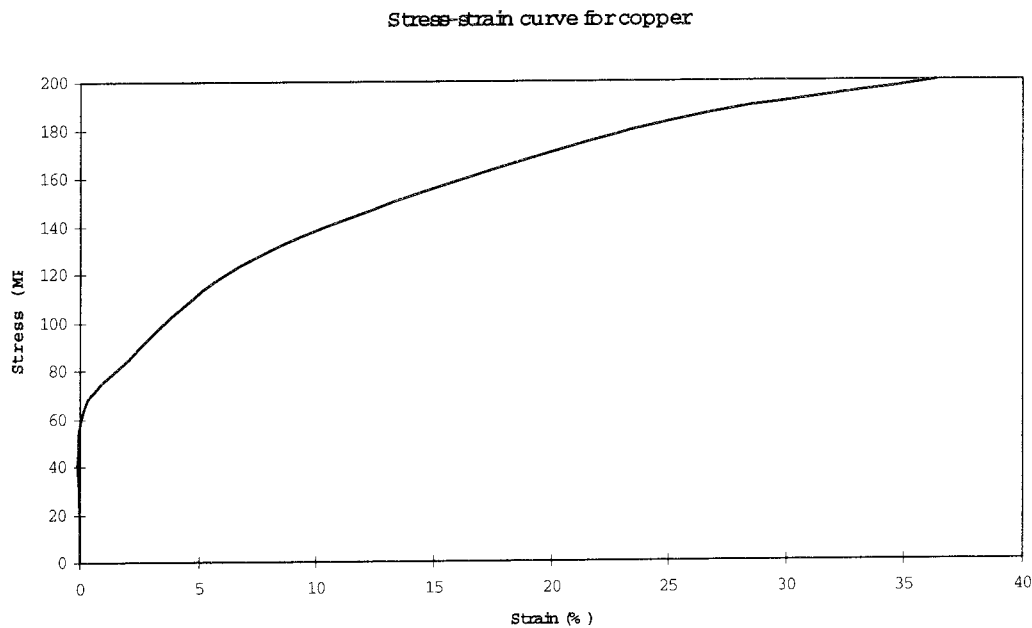


**Figure 5-4.** Stress-strain curve for copper

The steel inner container was modelled as a linear elastic material with the properties in Table 5-1. In view of the relative stiffnesses of the steel inner container and the copper overpack, it was assumed that the stresses in the steel would remain below yield (this view was subsequently confirmed in the analyses).

The bentonite backfill was modelled as an elastic plastic material with Drucker-Prager hardening using the properties determined by SKB /5-2/, and listed in Table 5-1. The bentonite's swelling pressure of 5 MPa corresponds to a dry density of about  $1800 \text{ kg/m}^3$  /5-5/. Assuming that the bentonite remains fully saturated, this density allows an (constant) elastic modulus of 0.1 GPa to be determined /5-5/. A simple elastic regime was defined using this modulus and the given Poisson's ratio of 0.4 /5-1/.

The mechanical properties of the volcanic rock surrounding the canister were defined by SKB /5-2/. The rock was modelled as a linear elastic material. In evaluating our results, the rock was assumed to have compressive strength (see Table 5-1), but no tensile strength (because fissures and cracks, either inherent in the geology or caused by excavation, are present).

### 5.2.5 Corrosion

Corrosion in the vicinity of the hole is controlled by the diffusion of 'reactant' through the corrosion residue and into the annular gap between the cast steel inner container and the copper overpack. It is assumed that conditions in the repository will be anaerobic, and so the 'reactant' is either water vapour, if the evolution of hydrogen gas by corrosion has forced the groundwater away from the canister, or water.

Since the surface of the cast steel inner container moves on a much longer time scale than the characteristic time of the diffusion process, it is legitimate to use the steady-state diffusion equation in two-dimensional cylindrical planar co-ordinates  $(r, z)$  to describe the diffusion of 'reactant' through the corrosion residue.

The diffusion equation is

$$D \frac{1}{r} \frac{\partial}{\partial r} \left( r \frac{\partial c}{\partial r} \right) + D \frac{\partial^2 c}{\partial z^2} = 0 \quad 5-1$$

where  $D$  is the diffusion coefficient and  $c$  is the concentration of 'reactant'. This equation is to be solved subject to the boundary conditions that:

- the concentration of 'reactant' at the mouth of the hole in the copper overpack is given by  $C_o$ ;
- (in the absence of detailed knowledge of the corrosion process) there is a constant flux of 'reactant'  $i/nF$  on the inner surface of the annulus. Here  $i$  is the corrosion current,  $n = 3/4$  is determined from the stoichiometry of the corrosion reaction  $3\text{Fe} + 4\text{H}_2\text{O} \leftrightarrow \text{Fe}_3\text{O}_4 + 4\text{H}_2$ , and  $F$  is Faraday's constant. The corrosion current  $i$  has been measured in the range  $0.01 - 1.0 \mu\text{m}/\text{year}$  /5-6/.

These boundary conditions can be expressed in equations as

$$\begin{aligned} c &= C_o \quad \text{at the mouth of the hole in the copper overpack} \\ -D \nabla c &= \frac{i}{nF} H(c) \quad \text{on the inner surface of the annulus} \end{aligned} \quad 5-2$$

where  $H(c)$  is Heaviside's function. Zero flux boundary conditions are set elsewhere.

The equations can be simplified by introducing the scaled concentration

$$c' = \frac{c}{C_o} \quad 5-3$$

It can then be seen that only the flux boundary condition on the inner surface of the annulus has any dependence on the physical properties, and it is a function of the single parameter

$$\Lambda = \frac{i}{nFC_oD} \quad 5-4$$

Under conditions of anaerobic corrosion the corrosion current is initially measured to be  $1.0 \mu\text{m}/\text{year}$ , and reduces to  $0.1 \mu\text{m}/\text{year}$ . The latter value corresponds to a flux of  $\text{H}_2\text{O}$

$$\frac{i}{nF} = 4.5 \cdot 10^{-10} \text{ mol}/\text{m}^2/\text{s} \quad 5-5$$

If hydrogen gas produced by the corrosion reaction forces the groundwater away from the canister, then corrosion will be sustained by the diffusion of water vapour. At  $25^\circ\text{C}$  the saturation concentration of water vapour in hydrogen gas is  $C_o = 1.3 \text{ mol}/\text{m}^3$ . This saturation concentration is relatively insensitive to pressure. The diffusion coefficient of water vapour in hydrogen gas at 1 atm and  $25^\circ\text{C}$  is  $0.9 \cdot 10^{-4} \text{ m}^2/\text{s}$ . The diffusion coefficient of water vapour in hydrogen gas at  $p$  atm can be estimated from

$$D(p \text{ atm}) = \frac{1}{p} D(1 \text{ atm}) \quad 5-6$$

The effect of magnetite blocking the annulus might be to reduce this diffusion coefficient by up to a few of orders of magnitude. This analysis suggests that for corrosion caused by the diffusion of water vapour we should consider values in the range

$$4 \cdot 10^{-4} < \Lambda < 4 \cdot 10^{-1} \text{ m}^{-1} \quad 5-7$$

Alternatively, diffusion of water might cause the corrosion of the cast steel inner container. The concentration of the water is  $C_o = 5 \cdot 10^4 \text{ mol}/\text{m}^3$ , and the diffusion coefficient of water in magnetite might lie in the range  $10^{-12} \text{ m}^2/\text{s}$  to  $10^{-10} \text{ m}^2/\text{s}$ . This analysis suggests that for corrosion caused by the diffusion of water we should consider values in the range

$$10^{-4} < \Lambda < 10^{-2} \text{ m}^{-1} \quad 5-8$$

A 2-D axisymmetric finite element model of the annular fitting gap was used to determine the point at which the concentration of 'reactant' (either

water vapour or water) becomes zero. The results of the calculations are summarised in Table 5-2.

**Table 5-2. Table showing the position at which the reactant concentration becomes zero as a function of  $\Lambda$ . The case considered here assumes that the copper overpack has a penetration located at the centre of the canister lid.**

$\Lambda$	Position ( $r, z$ ) at which concentration becomes zero
$10^{-6}$	all of the container corrodes
$10^{-5}$	all of the container corrode
$10^{-4}$	corrosion to a radius 0.454 m on the lid of the container
$10^{-3}$	corrosion to a radius 0.129 m on the lid of the container
$10^{-2}$	corrosion to a radius 0.040 m on the lid of the container
$10^{-1}$	corrosion to a radius 0.013 m on the lid of the container

Two corrosion scenarios are considered:

- **restricted case:** (this is the more likely scenario) corrosion occurs within a 4 cm radius of the penetration in the copper overpack;
- **global case:** corrosion occurs over the entire surface of the inner container.

### 5.2.6 Corrosion product properties

The initial stress analyses assumed, pessimistically, that the corrosion product was incompressible. This assumption was made because of a lack of measured mechanical properties for corrosion product formed under conditions in the repository. A further analysis attempted to bound the effects of corrosion product compressibility, based on best estimates of the likely mechanical properties.

The corrosion product was assumed to be mainly  $\text{Fe}_3\text{O}_4$ . A literature search revealed some useful properties, although none for the thicknesses (up to 5 mm) of corrosion product considered here, and certainly not for  $\text{Fe}_3\text{O}_4$  formed at the pressures ( $\approx 10\text{MPa}$ ) in the canister under which corrosion takes place. This data provided the basis for specifying bounds on the properties of the corrosion product. ‘Upper bound’, ‘best estimate’ and ‘lower bound’ corrosion product properties were obtained.

For the upper bound, it was assumed that the magnetite layer is solid (i.e. has no voids) and has a constant elastic modulus. This is the highest elastic modulus that could be expected, given available data. The data for a single crystal of  $\text{Fe}_3\text{O}_4$  [5-7] suggests the values:

- Young’s modulus,  $E = 208 - 210\text{GPa}$  (a value of 210 GPa was used);

- Bulk modulus,  $K = 162 \text{ GPa}$  ;
- Shear modulus,  $G = 89 \text{ GPa}$  ;
- Poisson's ratio,  $\nu = 0.29$  .

A 'best estimate' for the properties of the corrosion product is found by assuming that the  $\text{Fe}_3\text{O}_4$  has been formed with voids, and is likely to compress with a low modulus until the void space is zero, and thereafter with the modulus of crystalline  $\text{Fe}_3\text{O}_4$  . The low modulus was chosen to be  $5 \text{ GPa}$  , which is the micro-hardness level quoted by Nicholls et al /5-7/ for iron oxide on mild steel. The compression at which the modulus change occurs was selected to be 15% . This figure is arbitrary, and is based upon previous corrosion modelling experience. Although this is significantly above the  $0.1\% \rightarrow 0.4\%$  failure strains quoted for iron oxide in the literature /5-8, 5-9/, it represents the maximum likely void space.

An additional stress analysis was performed using the low modulus of  $5 \text{ GPa}$  at all strains, which represents a lowest (optimistic) bound on the properties of the corrosion product.

### 5.2.7 Loading

In the 'canister' and 'detailed' models, the load is generated by the growth of the corrosion product layer. The volume increase in forming magnetite from iron can be estimated from the relative densities of the two materials. This suggests an expansion factor of 2.1:1, i.e. if corrosion removes 1 unit of thickness of steel, 2.1 units of thickness of corrosion product are formed. The expansion leads to a load being exerted on the canister.

At the onset of corrosion, the annular fitting gap between the inner container and the copper overpack is a nominal  $2 \text{ mm}$  . Corrosion product fills this gap (when about  $1.818 \text{ mm}$  of steel has been removed), and then starts to exert a strain on the steel inner container and the copper overpack. The relative stiffnesses of the canister components determines the displacements, and hence material stresses.

The 'canister' analyses were used to determine the displacement in the copper overpack corresponding to a given amount of corrosion for input to the 'vault' model.

## 5.3 CANISTER ANALYSES

The purpose of the 'canister' analyses was to determine how corrosion affects the structural integrity of the inner container.

### 5.3.1 Model

Models were constructed for both the BWR and PWR canister geometries.

The inner container was modelled using second order 3D brick elements, and the copper overpack using second order general shell elements. The corner nodes in the shell elements were linked to corresponding nodes in the inner container by truss elements. The truss elements were oriented either radially or axially. The model did not use diagonal truss elements at the canister corners; this corresponds to the fact that corrosion product exerts less of a load at the corners, and stresses are transferred through the shell. The load was introduced by a thermal expansion of the connection between the two portions of the model. This approach avoids the need for a large 3D model, which would have been required if the canister geometry had been represented using only 3D solid elements.

This approach, using truss elements, was compared with the more usual approach, using 3D solid elements, in a small test model /3-2/. The results from the test model showed the desired behaviour, and the truss elements gave a more uniform expansion than 3D solid elements.

The stiffness of each truss element is a function both of the area of the element and the desired corrosion product properties. In the initial analyses the trusses were treated as rigid, and assigned a stiffness 1000 times greater than the inner container (the influence of different corrosion product properties on the stresses in a canister is discussed in more detail in Section 5.4).

An eighth of the canister (symmetrically constrained so as to represent the whole canister) was modelled, i.e. a quarter of the circular cross section and half the height. The penetration was not represented explicitly, as the effects on the stress field remain local to the hole, and are therefore easier to assess in the 'detailed' model. In the case of 'local' corrosion, this implies that the model is simulating the behaviour of a canister with a pair of penetrations located diametrically opposite one another. Again, because of the local influence of a hole, the behaviour of a canister with a single penetration is similar (this was confirmed using the 'detailed' model, as described in section 5.5.3). The bentonite backfill was also neglected. The low elastic modulus of the bentonite makes this a reasonable simplification.

Figures 5-5 to 5-7 show the PWR finite element mesh. The red and green elements correspond to the steel inner container; the pink and dark blue elements to the steel lid of the inner container; the light blue elements to the wall of the copper overpack, and the yellow elements to the lid of the copper overpack. The truss elements are not shown.

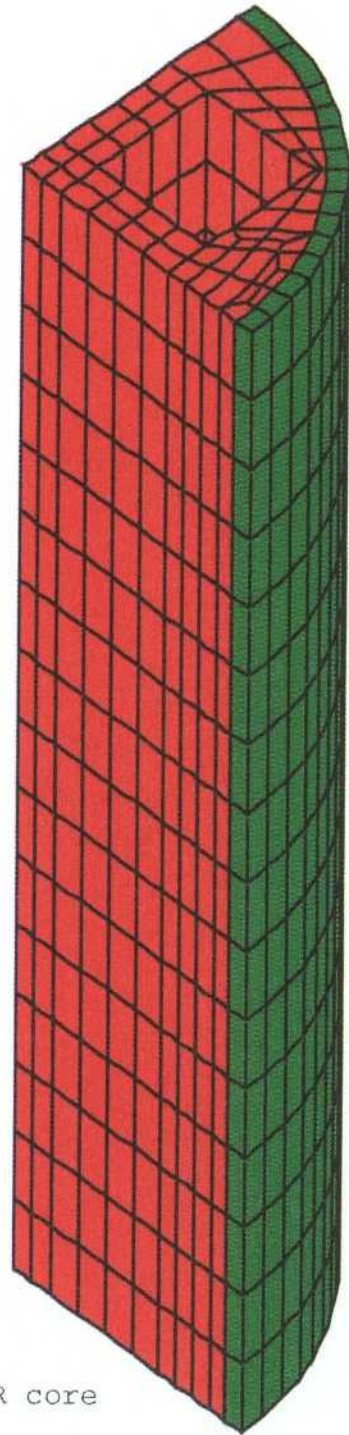


Figure 5-5 Core model, mesh of PWR core

*Figure 5-5. Canister model: finite element mesh of PWR core.*

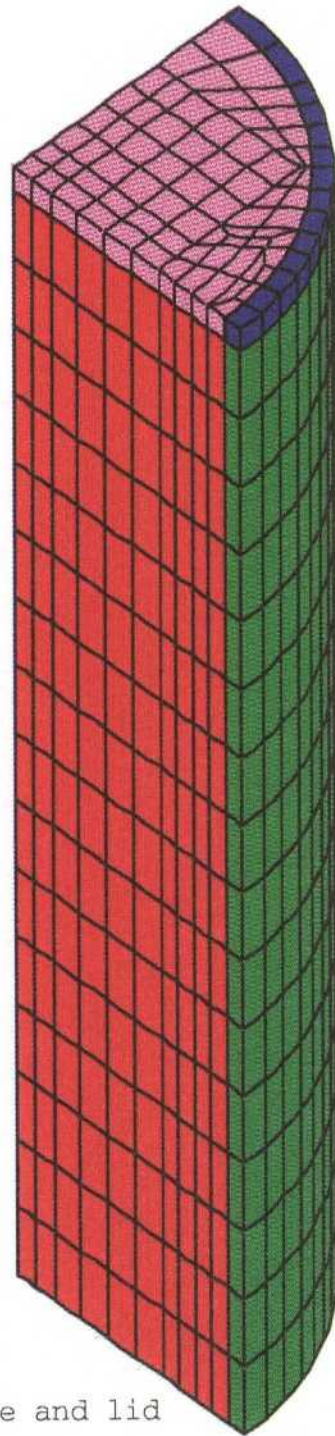


Figure 5-6 Core model, mesh of PWR core and lid

*Figure 5-6. Canister model: finite element mesh of PWR core and lid.*

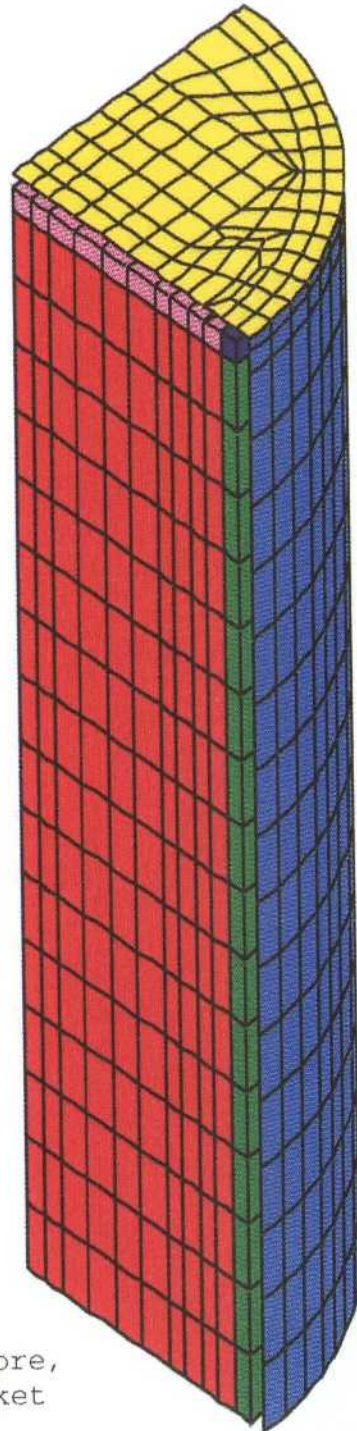


Figure 5-7 Core model, mesh of PWR core, lid and copper jacket

*Figure 5-7. Canister model: finite element mesh of PWR core, lid and copper overpack.*

The following corrosion scenarios were considered:

- corrosion over the entire surface of the inner container;
- corrosion within a radius of a circular penetration located in the centre of the lid of the copper overpack;
- corrosion within a 4 cm radius of a circular penetration located in the middle of the wall of the copper overpack.

In the restricted corrosion cases, the displacement was applied at a single truss element, the adjacent truss elements had a nominal stiffness of 205 GPa (i.e. steel) and the remaining truss elements had no stiffness.

In all of the analyses, the load is applied in the form of a growth in corrosion product, and so the results are independent of the corrosion rate. By assuming a particular corrosion rate, the time corresponding to a given strain and hence set of stresses can be determined (see Section 6). The material properties for steel and copper are listed in Table 5-1. The analyses assumed that 2.273 mm of steel had been corroded away from the inner container (this corresponds to an applied displacement of 0.5 mm in the annulus; this value was selected as preliminary calculations indicated that stresses approaching yield would occur in the copper overpack by this displacement). Assuming a corrosion rate of  $0.1 \mu\text{m}/\text{year}$ , this occurs at  $0.23 \cdot 10^5$  years. At earlier times less steel will have been corroded away, and the predicted stresses in the inner container will be higher than they should be.

### 5.3.2 Results

In the global corrosion scenario, results were similar for both BWR and PWR geometries.

Figure 5-8 shows the Mises stresses in the BWR inner container assuming a 0.5 mm expansion in the annular gap. In the region of the rim, stresses occur that will cause some localised plastic deformation. The fuel storage channels create concentrations of stress, both between and at the corners of the channels. However, none of these stresses affect the structural integrity of the inner container.

Figure 5-9 includes the lid of the inner container, and shows the change in stress parallel to the axis of the canister caused by the changing stiffness of the inner container due to the fuel channels. Stress concentrations in the lid above the fuel channels are also visible. It can also be seen that at larger radii, regions of the lid are nearing the yield stress of 200 MPa, but the lid is not likely to fail over the ends of the fuel channels. It should be remembered that the detailed geometry of this region was not modelled.

Figure 5-10 shows the Mises stresses in the copper overpack induced by a 0.2 mm expansion in the annular gap (occurring after  $0.20 \cdot 10^5$  years assuming a corrosion rate of  $0.1 \mu\text{m}/\text{year}$ ). Stresses approaching yield are being generated around the rim of the copper overpack. Figure 5-11 shows the same region for a 0.3 mm expansion in the annular gap (occurring after  $0.21 \cdot 10^5$  years assuming a corrosion rate of  $0.1 \mu\text{m}/\text{year}$ ), and a bending effect is creating stresses above yield at the rim. Plastic deformation initiates at the rim of the copper overpack, and eventually the copper will fail. In order to determine the time at which this occurs, a more detailed analysis increasing the strain in the copper to 29% is required. This is carried out for one scenario in Section 6.

Figures 5-12 and 5-13, for the PWR inner container, are similar to Figures 5-8 and 5-9. Higher peak stresses occur at the corners of the fuel channels in the PWR design. Although this is largely a function of the sharp corners in our model, the geometry of the fuel channels does increase the stresses in the PWR design.

Figures 5-14 to 5-18 show the stresses for the restricted corrosion scenarios and a 0.5 mm expansion in the annular gap. As expected, the stresses are very localised; the effects have died away far from the channels, producing no significant stresses in the inner container.

In several of the analyses, significant gradients of stress occur over a small number of elements (e.g. at the lid). This region has not been modelled in detail (see Section 5.2.1), and as a result the calculated stresses should be treated with caution. The purpose of our analyses is to assess the general suitability of the canister, and the simplifications are not thought to significantly affect the conclusions. Clearly, once the canister design is finalised, more detailed analyses should be carried out.

### 5.3.3 Discussion

In the global corrosion scenario, the structural integrity of the inner container remains intact. The first notable event is yield at the rim of the copper overpack, which occurs for a displacement of about 0.2 mm. The effect of this on the structural integrity of the inner container is minimal. As the corrosion continues (and certainly for a displacement of about 0.5 mm), the copper overpack yields more globally. Subsequent loads on the inner container are then due to the non-linear elastic behaviour of copper. Finally, the bending caused by the relative displacements of the wall and the lid causes the copper overpack to fail at the rim. The canister stresses at this stage are difficult to evaluate, and cannot be determined with the current model. The stresses in the inner container may remain constant or decrease as an increasing proportion of the load in the annular gap is taken up by

displacement of the copper and bentonite. Eventually, the yield in the copper and the stress concentrations lead to the rim being peeled off.

In the restricted corrosion scenario, neither location of the penetration (in the lid or in the wall of the copper overpack) leads to stresses that are significant for the structural integrity of the inner container. Section 5.5 analyses this scenario in more detail, with a view to determining if the stresses can cause a change from a case of restricted corrosion to one of global corrosion. The two penetration locations were intended to lead to worst cases for the structural integrity of the copper overpack. However, given the results of this section, a hole closer to the rim of the canister lid might lead to an earlier failure of the copper overpack. The design of the copper overpack's rim would need to be modelled in this case.

The analyses suggest that at a displacement load of 0.5 mm (for both global and restricted corrosion scenarios) localised yield occurs in the lid of the inner container, but structural failure is unlikely. Further corrosion is necessary before the fuel channels are exposed to groundwater; a more sophisticated finite element model would be needed to determine the exact amount of corrosion.

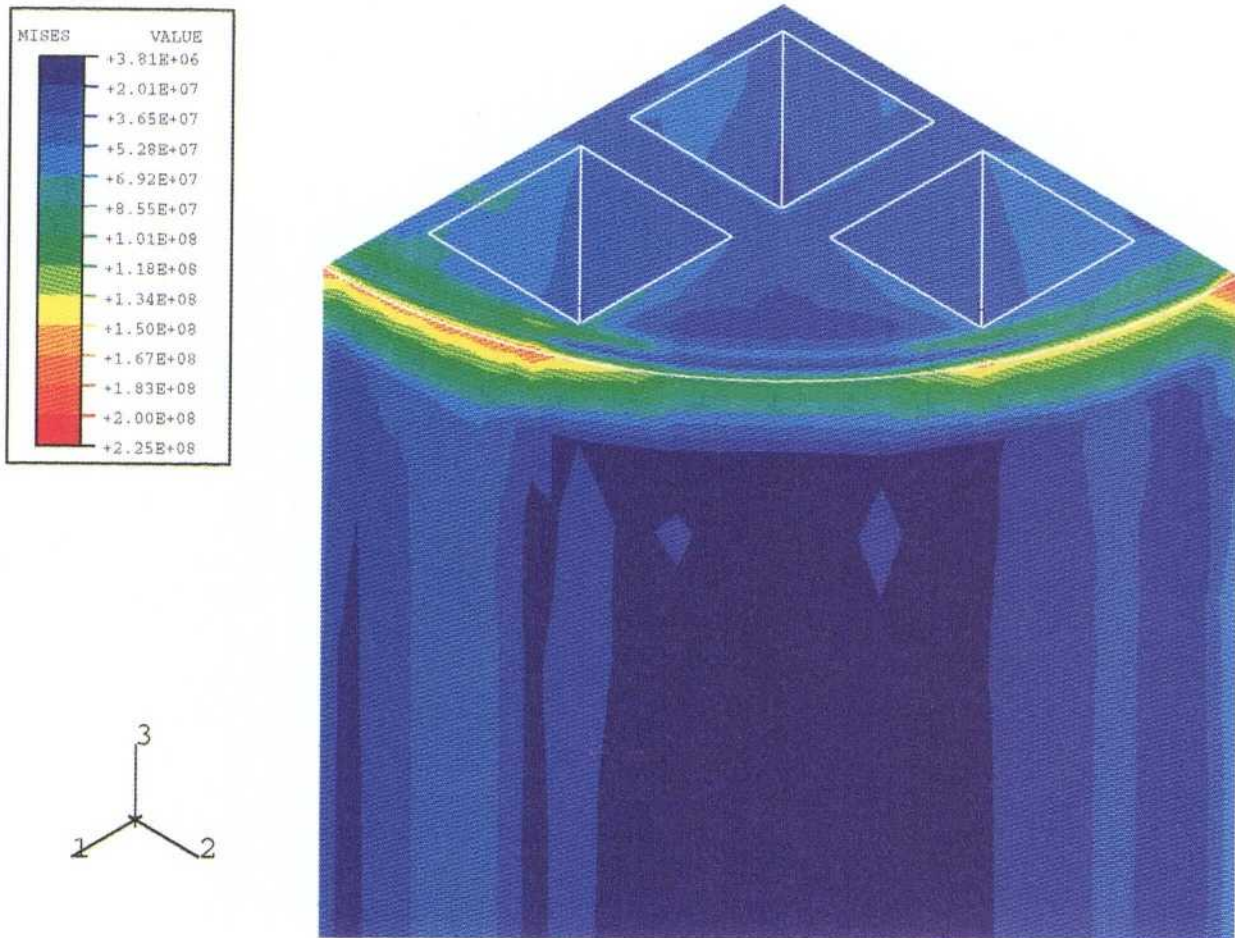


Figure 5-8: Mises Stress in BWR core at 0.5 mm displacement load

*Figure 5-8. Mises stress in the BWR inner container at 0.5 mm displacement load.*

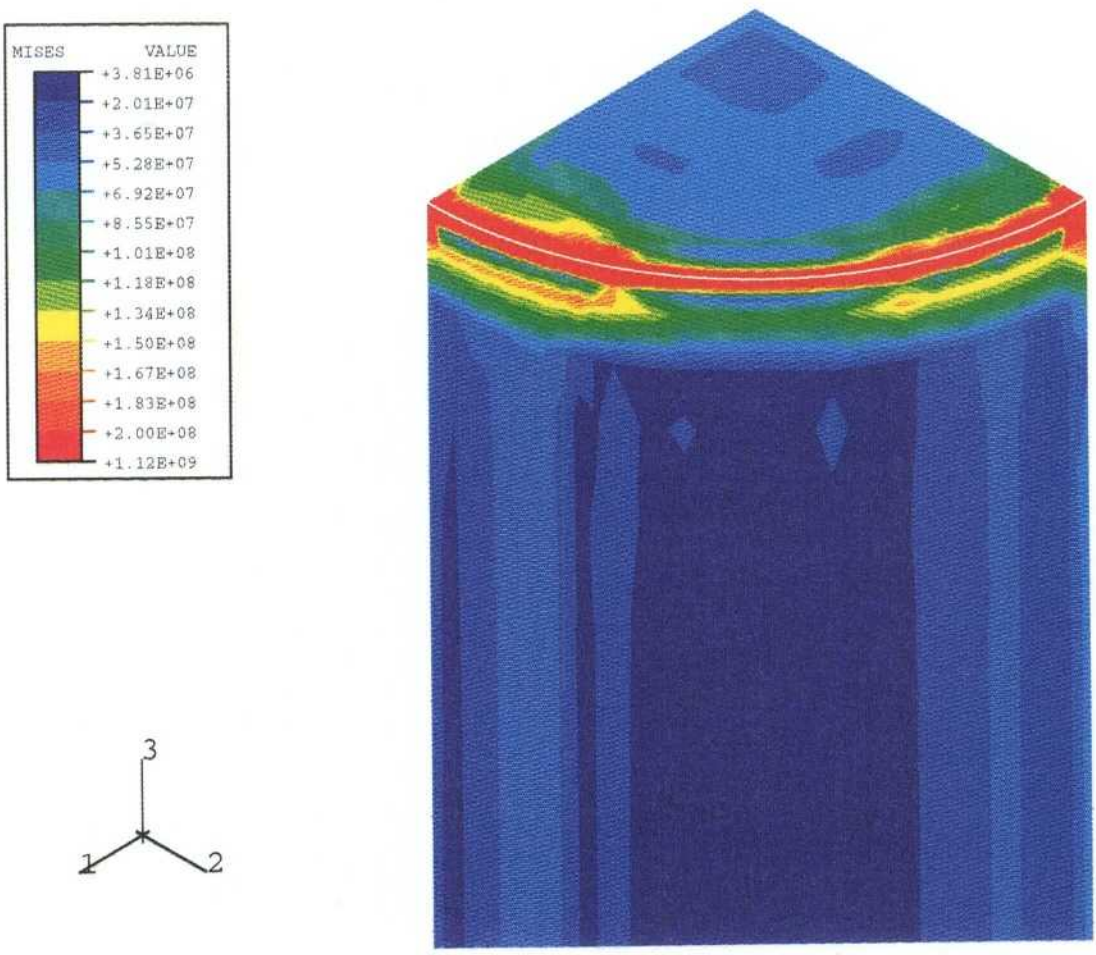
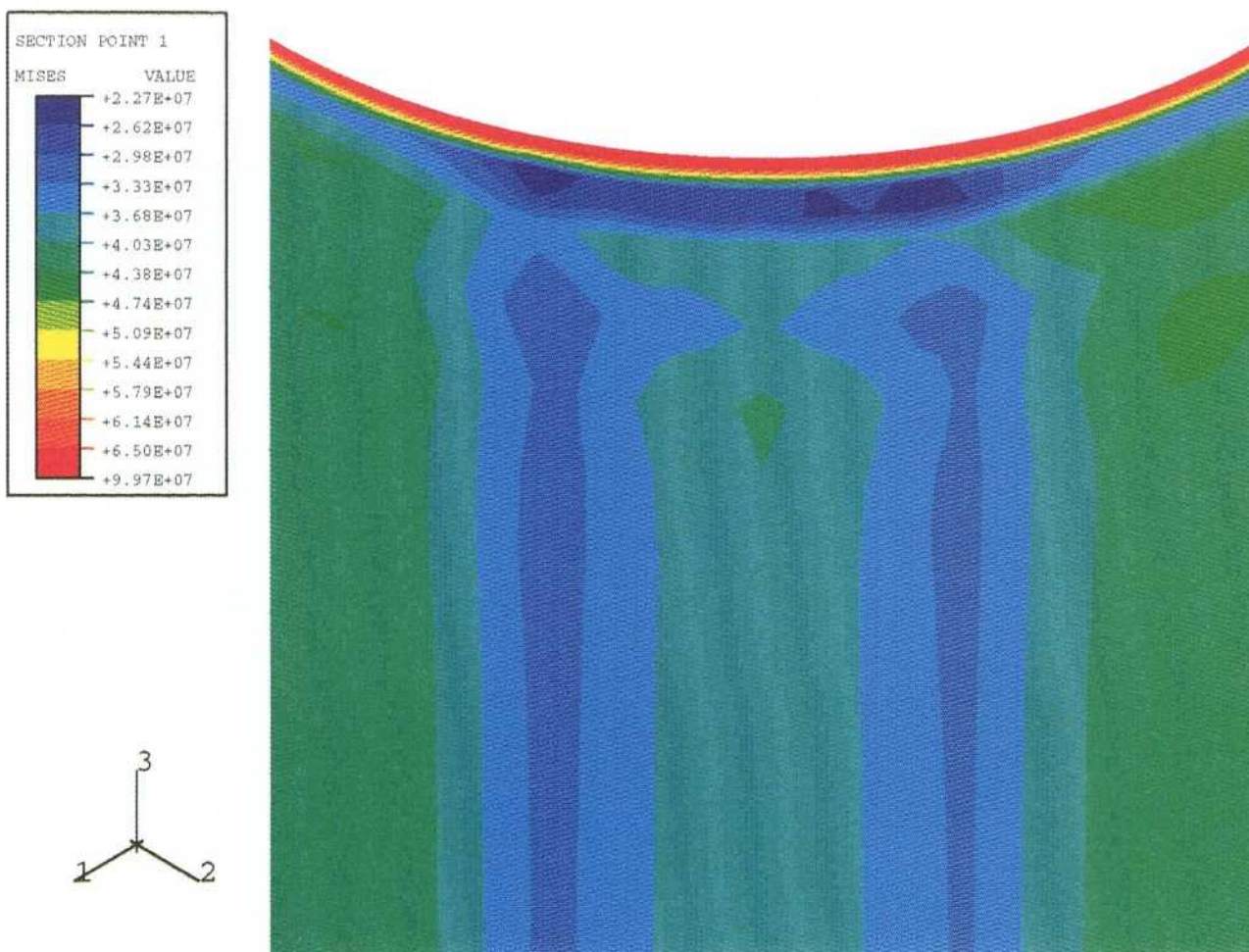
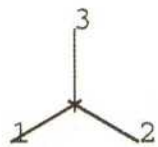
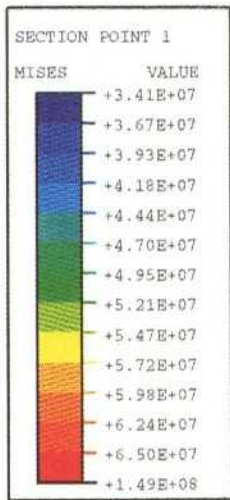


Figure 5-9: Mises Stress in BWR core and core lid at 0.5 mm displacement load

*Figure 5-9. Mises stress in the BWR inner container and lid at 0.5 mm displacement load.*



**Figure 5-10.** Mises stress on the inner surface of the BWR copper overpack at 0.2 mm displacement load.



**Figure 5-11.** Mises stress on the inner surface of the BWR copper overpack at 0.3 mm displacement load.

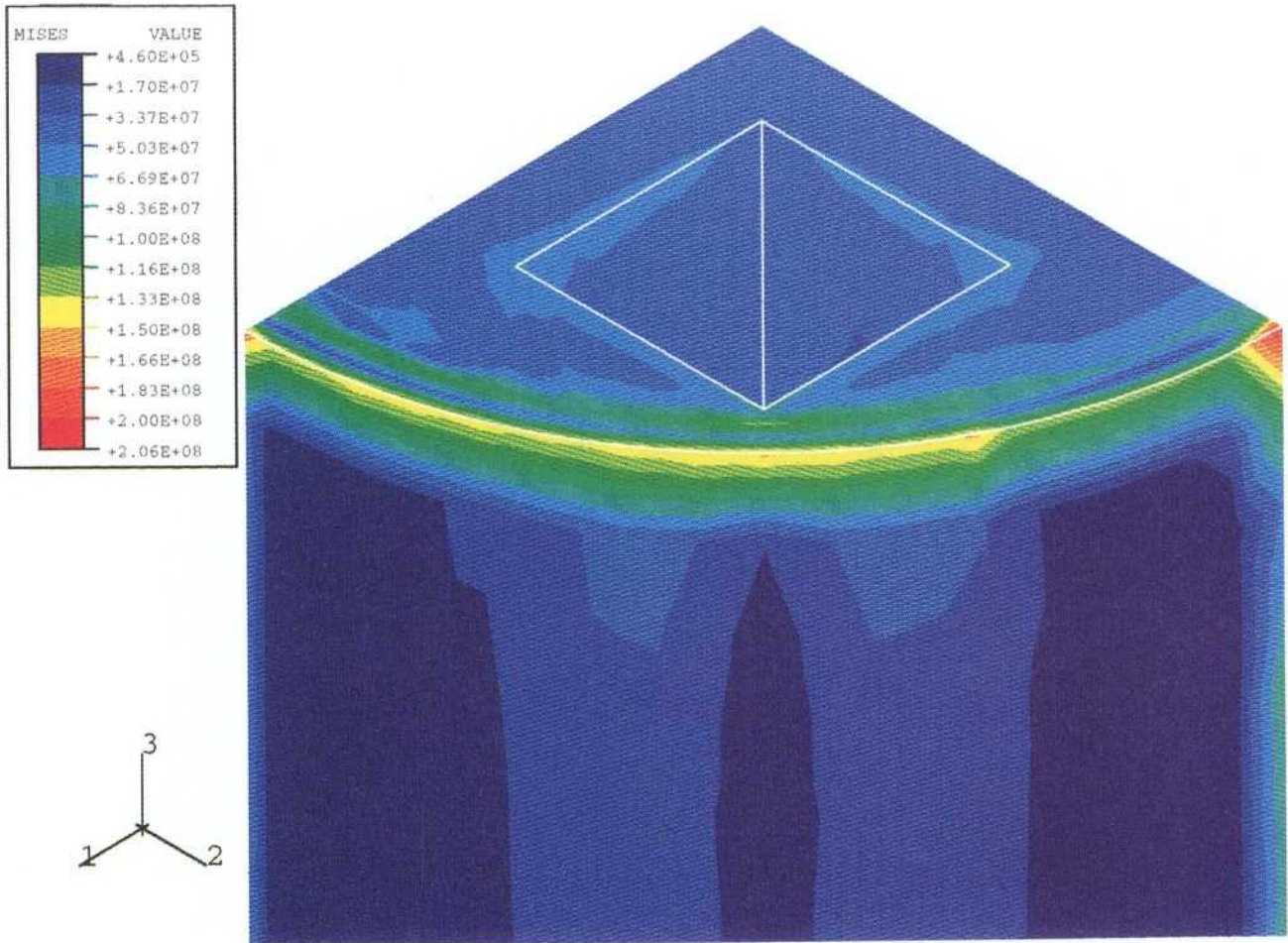


Figure 5-12: Mises stress in PWR core at 0.5 mm displacement load

*Figure 5-12. Mises stress in the PWR inner container at 0.5 mm displacement load.*

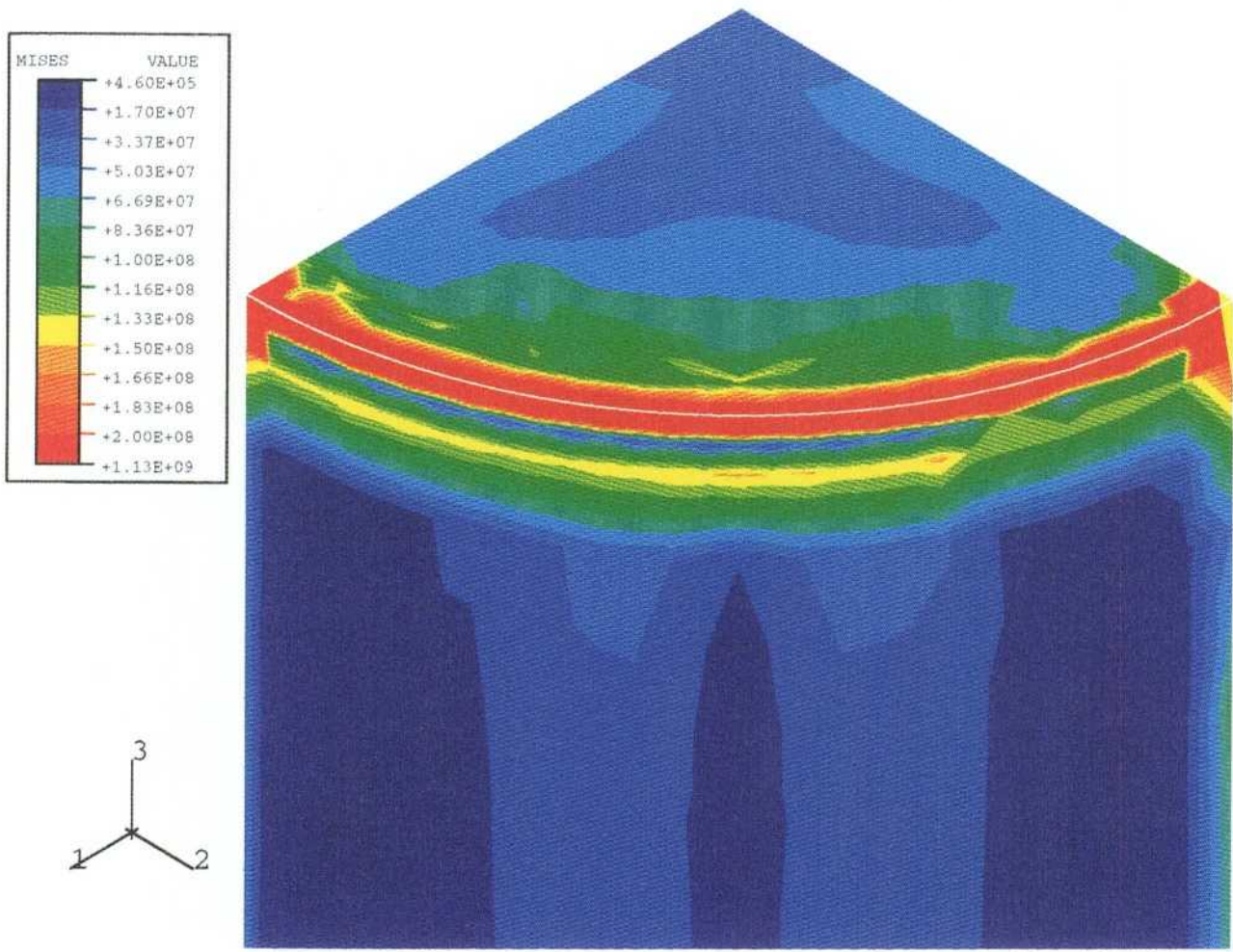


Figure 5-13: Mises stress in PWR core and lid at 0.5 mm displacement load

*Figure 5-13. Mises stress in the PWR inner container and lid at 0.5 mm displacement load.*

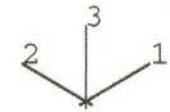
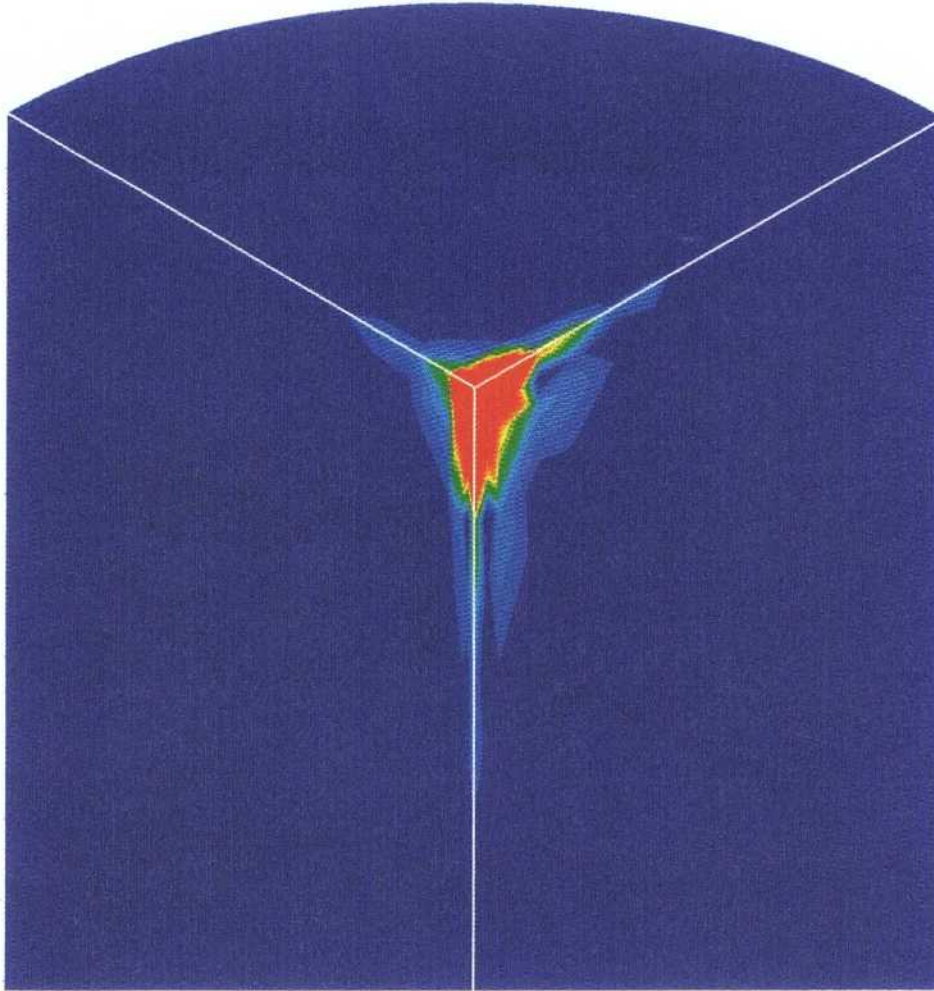
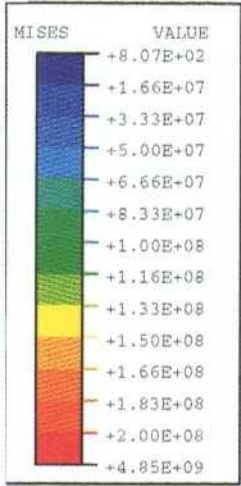


Figure 5-14: Mises stress in BWR core and lid, local corrosion at centre point of lid at 0.5 mm displacement load

*Figure 5-14. Mises stress in the BWR inner container and lid for restricted corrosion scenario and 0.5 mm displacement load.*

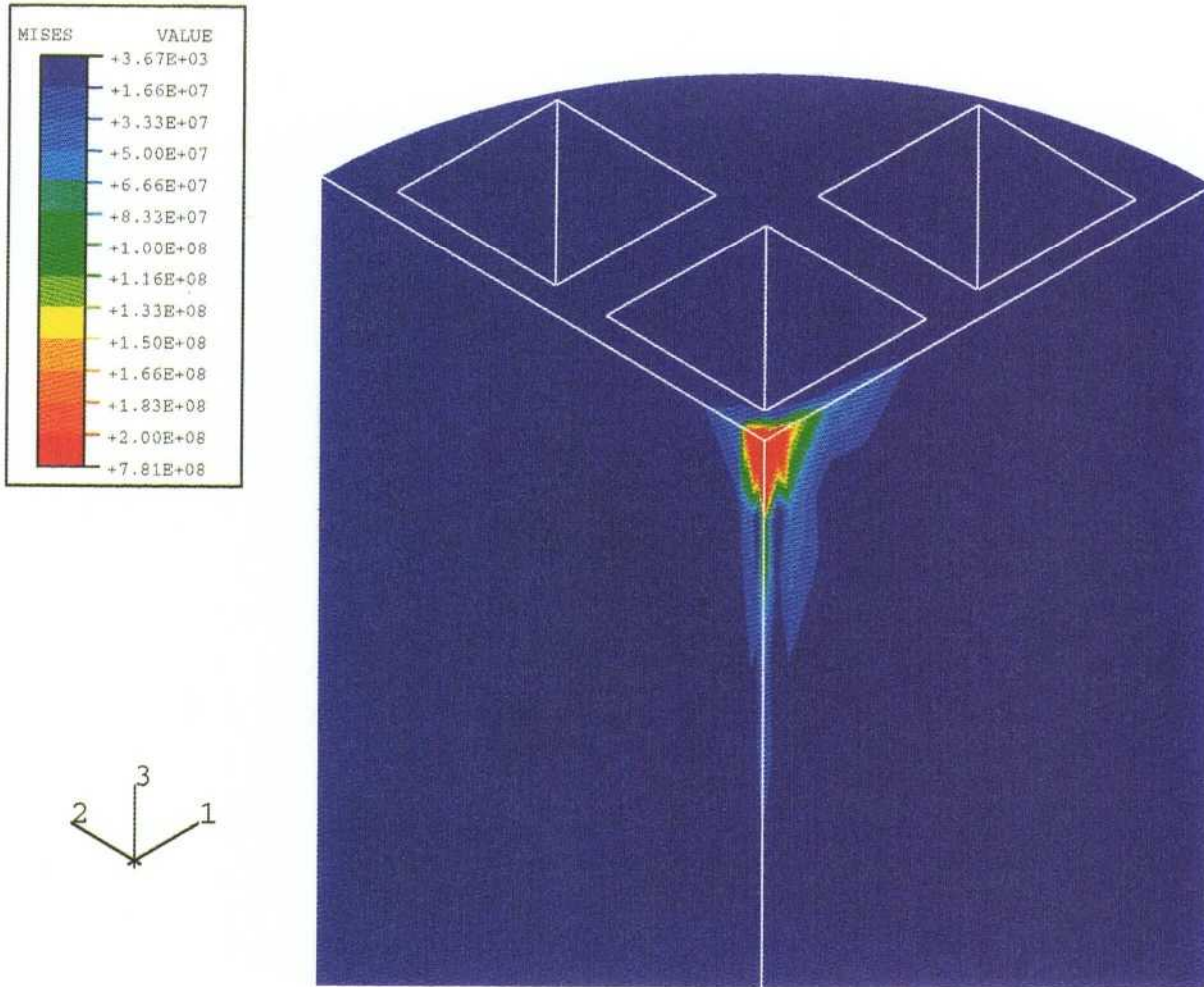


Figure 5-15: Mises stress in BWR core, local corrosion at centre point of lid at 0.5 mm displacement load

*Figure 5-15. Mises stress in the BWR inner container for restricted corrosion scenario and 0.5 mm displacement load.*

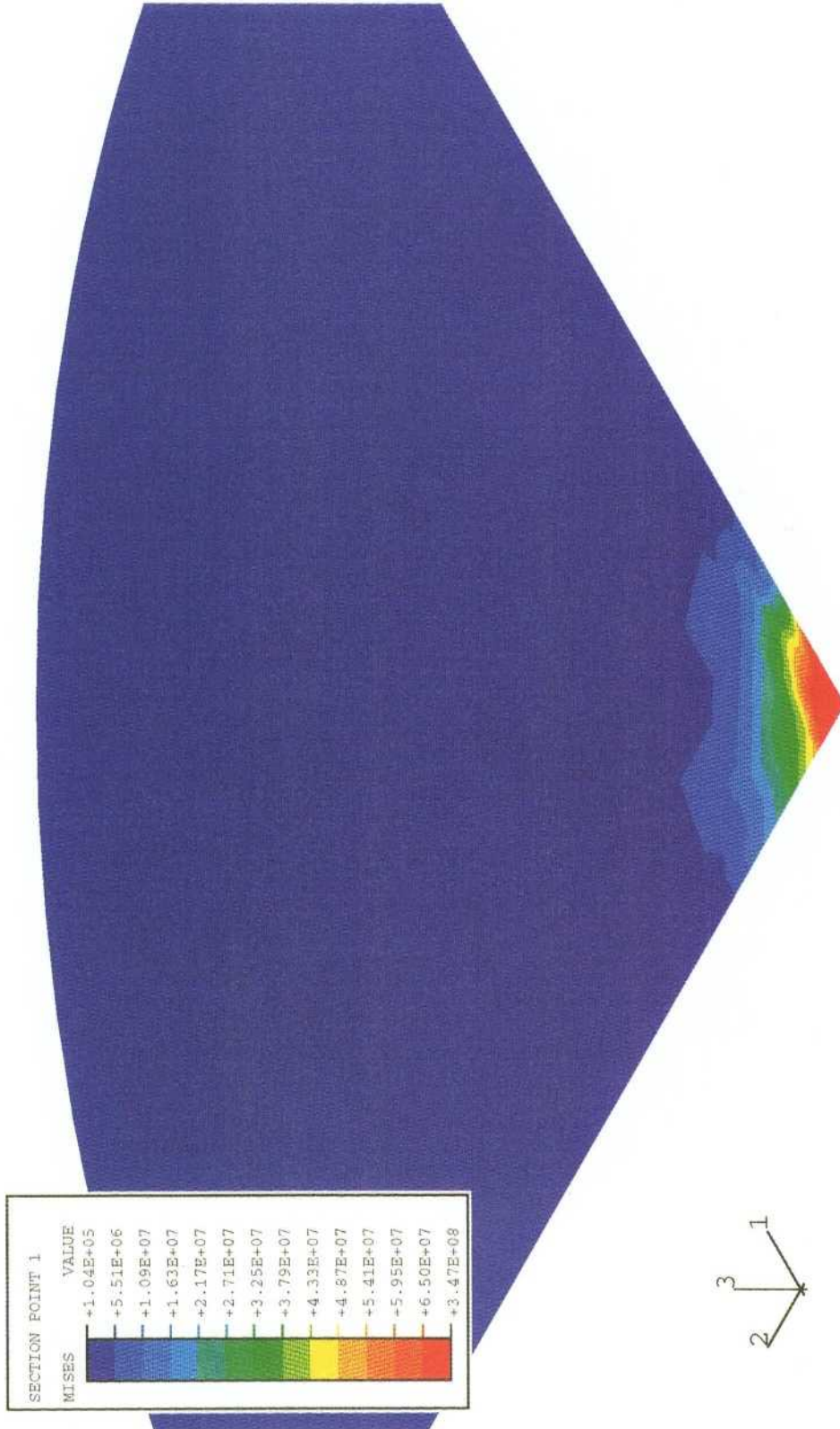
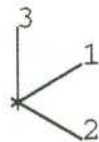
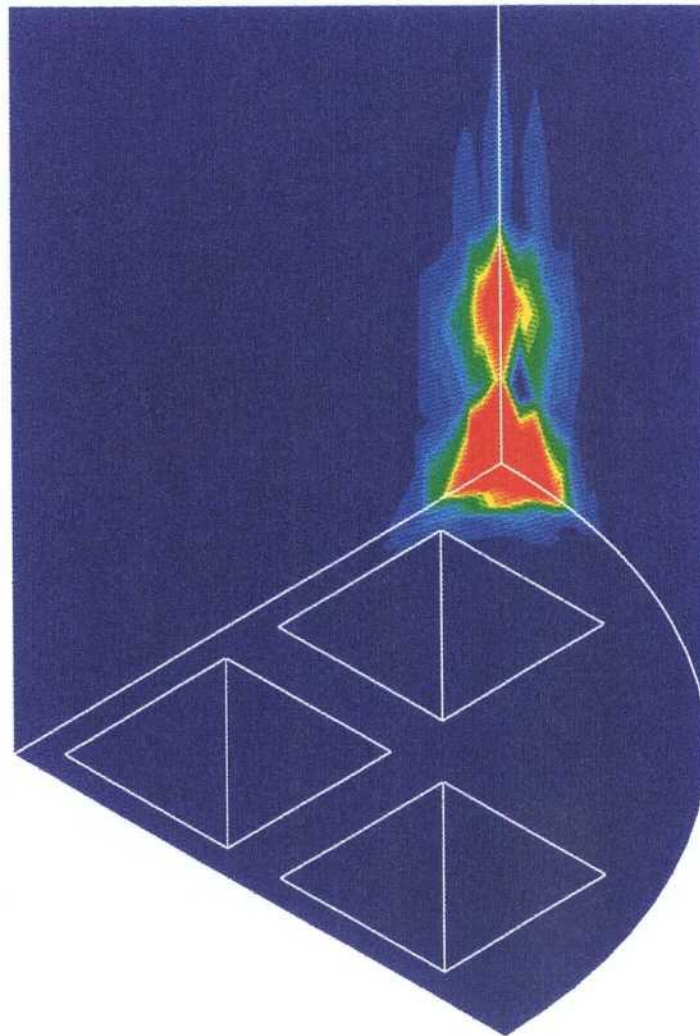
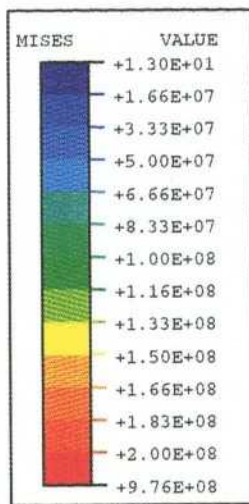
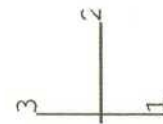
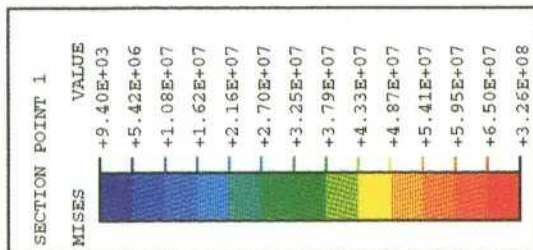
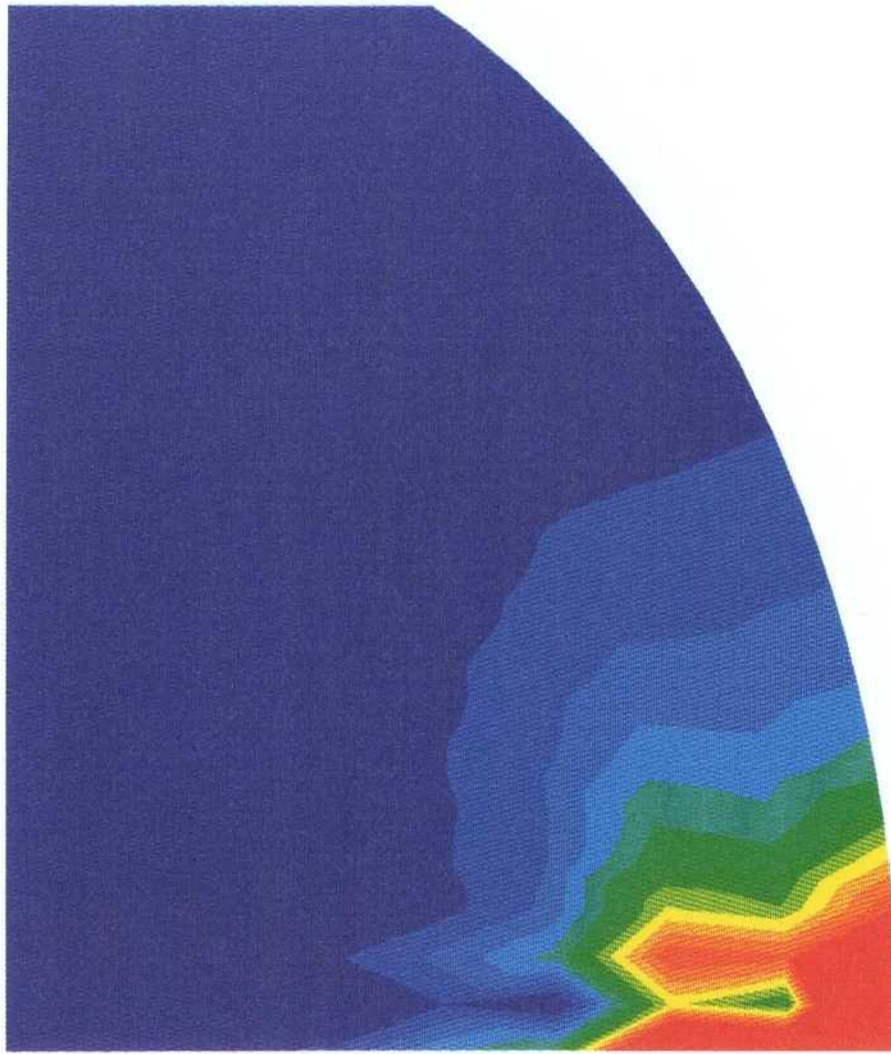


Figure 5-16: Mises stress on inner surface of copper jacket lid of BWR canister. local corrosion at centre of lid, 0.5 mm displacement load

**Figure 5-16.** Mises stress on the inner surface of the BWR copper overpack lid for restricted corrosion scenario and 0.5 mm displacement load.



*Figure 5-17. Mises stress in the BWR inner container for restricted corrosion scenario on wall and 0.5 mm displacement load.*



*Figure 5-18. Mises stress on the inner surface of the BWR copper overpack for restricted corrosion scenario and 0.5 mm displacement load.*

## 5.4 INFLUENCE OF CORROSION PRODUCT PROPERTIES

The above stress analyses assumed, pessimistically, that the corrosion product is incompressible. This assumption was made because of a lack of measured mechanical properties for corrosion product formed under conditions in the repository. In the following analyses, the effects of more realistic corrosion product properties on the canister's structural integrity are quantified. The BWR design undergoing global corrosion was studied, since this represents a worst case for the structural integrity of the canister.

### 5.4.1 Model

As discussed in Section 5.2.4, 'upper bound', 'best estimate' and 'lower bound' corrosion product properties were considered in the analyses.

The model is identical to that used in the 'canister' analyses, except for the addition of spring elements in series with the trusses to model the stiffness of the corrosion product. As before, a displacement of up to 0.5mm was applied to the copper overpack by invoking a thermal expansion of the truss elements (this corresponds to the corrosion of 2.273 mm of steel from the inner container). The model was then used to calculate the stresses in the canister. Since compression of the corrosion product occurs only after the annulus is full, and assuming the upper bound elastic moduli for the corrosion product, the calculated stresses at displacements less than 0.5mm will be pessimistic. Conversely, assuming the lower bound elastic moduli for the corrosion product will give slightly optimistic stresses at displacements less than 0.5mm. Modelling the full interaction was beyond the scope of this study.

### 5.4.2 Results

Allowing for compression of the corrosion product did not lead to a significant decrease in the stresses (cf. Section 5.3). Figure 5-19 shows the Mises stress in the inner container for the upper bound case; the maximum stress of 223 MPa is similar to the peak stress from the previous analysis (i.e. 225 MPa if the corrosion product is incompressible). The maximum stress in the copper overpack is also not significantly different from the previous analysis. The onset of large scale yield (at 65 MPa) does not occur until the growth of corrosion product has reached 0.31mm (see Figure 5-20), which is about the same result as was obtained with the rigid model. Given that Young's modulus for the corrosion product is similar to that of steel, but the stiffness of the copper overpack is significantly less, these results are as expected.

The introduction of voids in the corrosion product (which have been modelled as non-linear springs, with an initial low stiffness) reduces the

maximum stress in the inner container by only 1%. The onset of yield in the copper overpack is delayed until the growth of corrosion product has reached 0.32 mm . Increasing the void space in the corrosion product should continue to reduce the stresses in both the cast steel insert and the copper overpack. Using the low modulus of 5 GPa at all strains (which represents a true lowest bound on the properties of the corrosion product), gives a 10% reduction in the stresses in the copper overpack (see Figure 5-21) and in the inner container (see Figure 5-22).

### 5.4.3 Discussion

The predicted decrease in the stresses does not lead to a significant increase in the lifetime of the canister . Basing our estimate of the lifetime of the canister on the time at which the copper overpack begins to fail, thus allowing the groundwater access to the fuel channels in the cast insert, we note that:

- the lifetime is unchanged if we assume that the corrosion product is compressible;
- the lifetime is a factor 1.03 greater if the corrosion product is assumed to have voids.
- the lifetime is a factor 1.1 greater if an extreme bound is used to define the properties of the corrosion product.

Given these results, it is recommended that future work should concentrate on obtaining accurate values for the compressibility of the corrosion product. Exact figures for the final stiffness of the corrosion product are of less significance to the long term integrity of the canister.

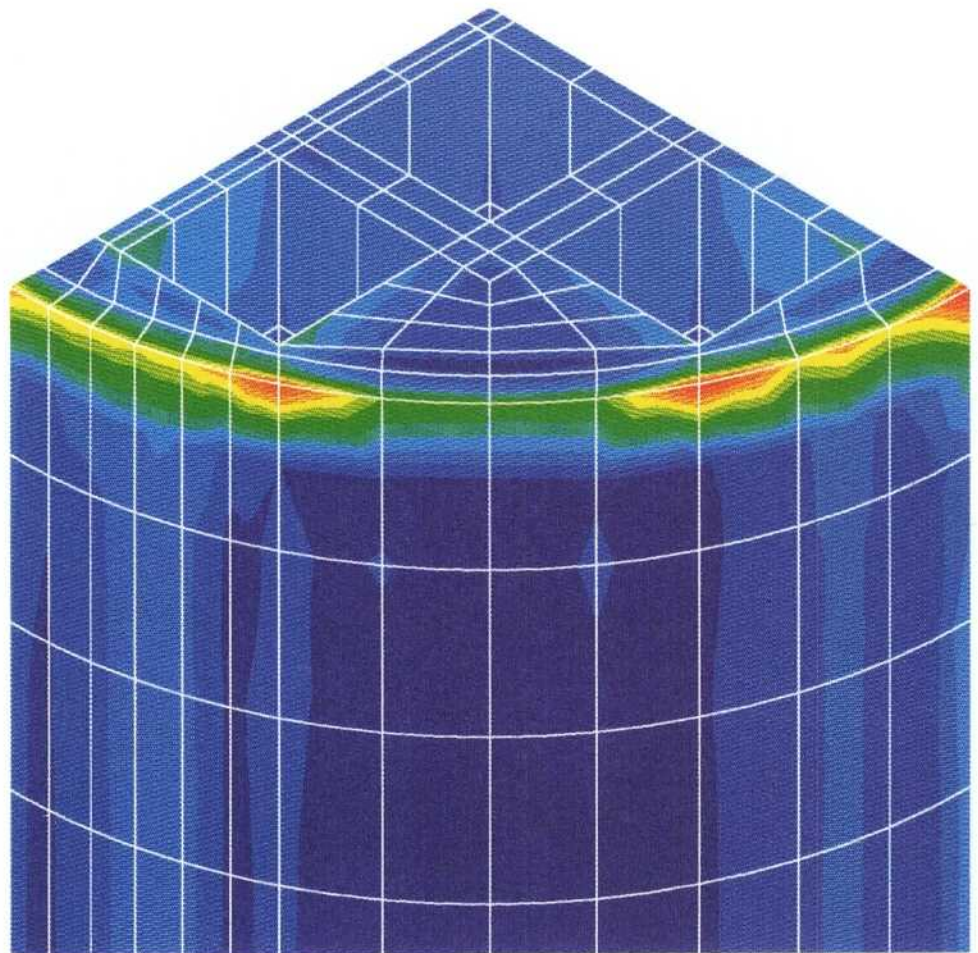
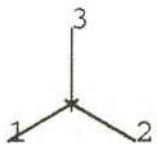
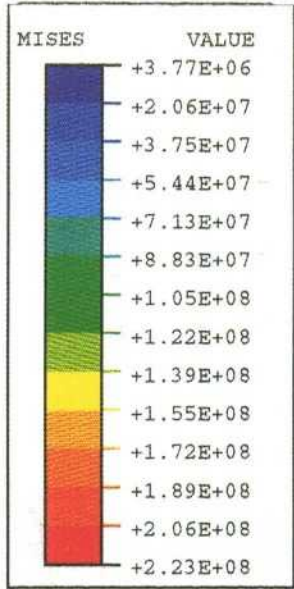


*Figure 5-19. Mises stress in the inner container using the 'upper bound' properties for the corrosion product.*

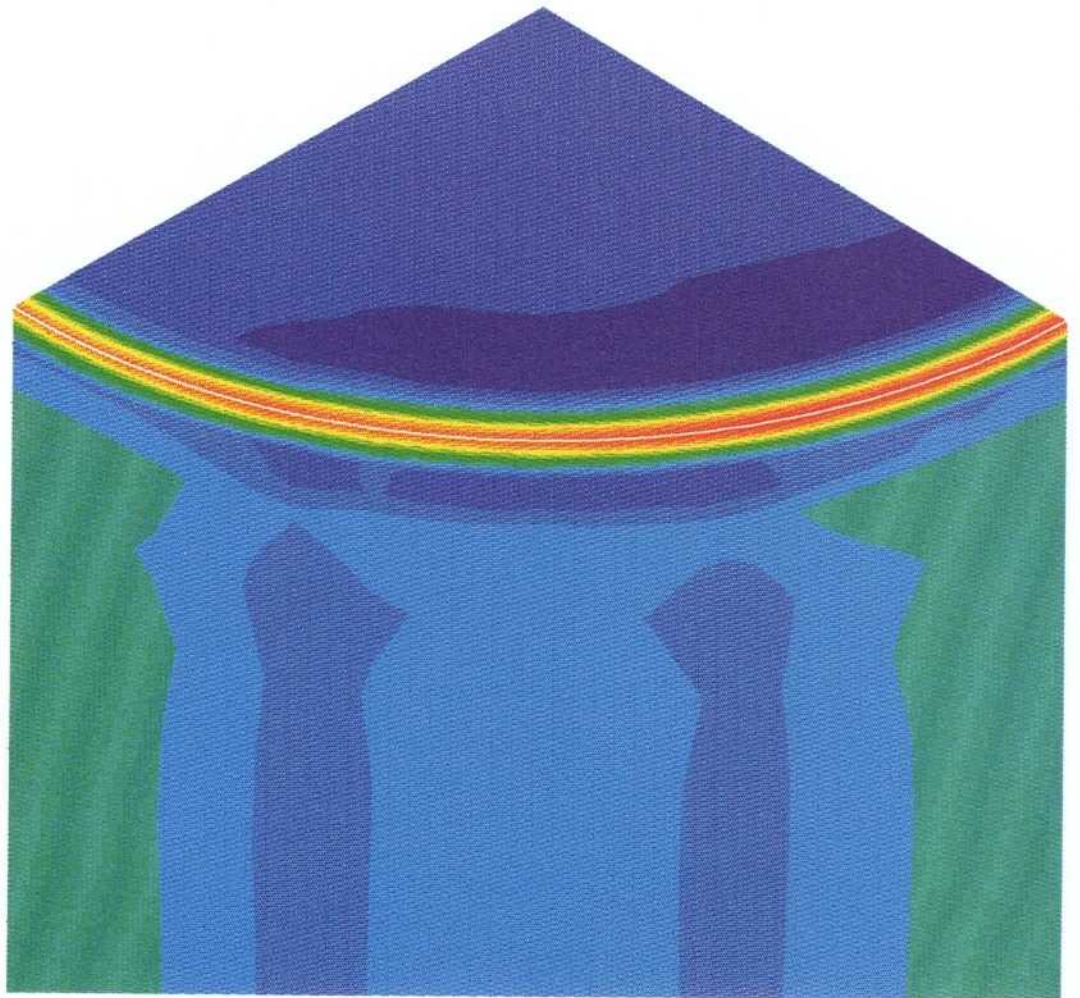
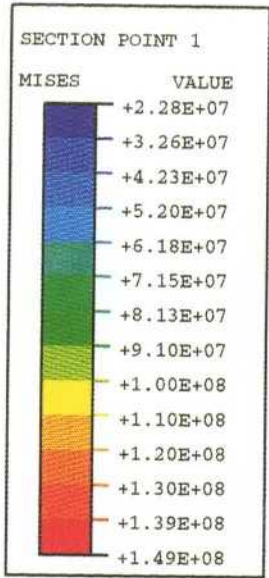


*Figure 5-20. Mises stress in the copper overpack using the 'upper bound' properties for the corrosion product.*

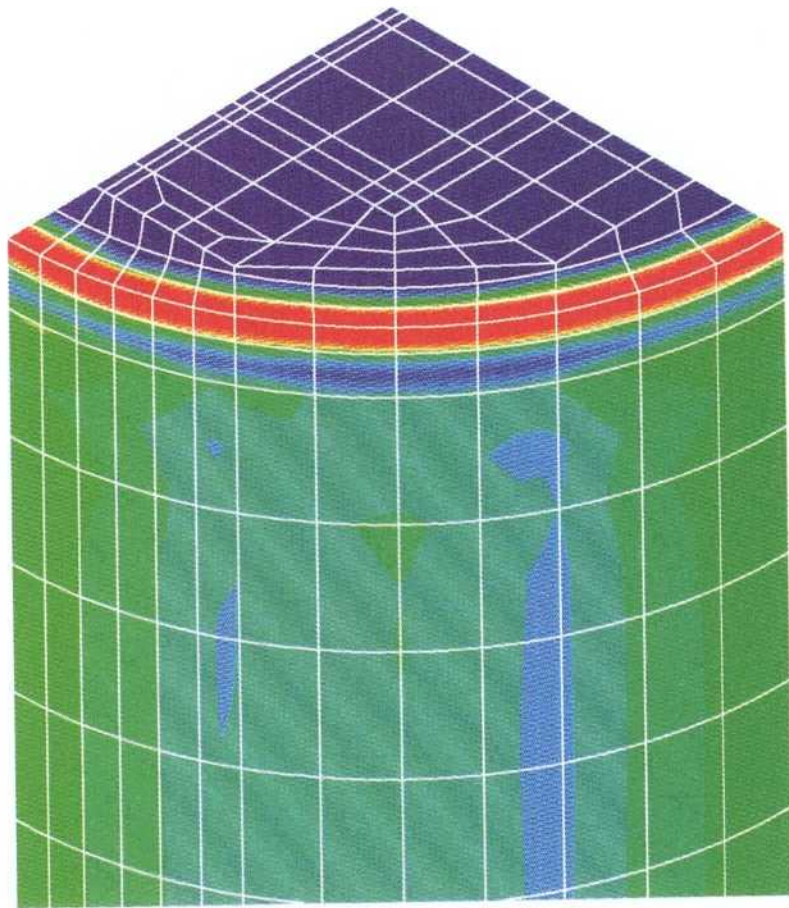
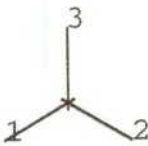
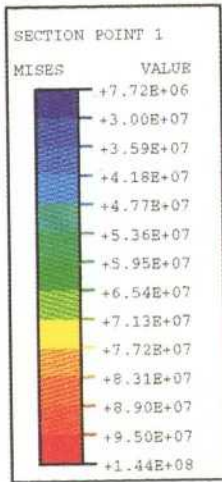


*Figure 5-21. Mises stress in the copper overpack using the 'lower bound' properties for the corrosion product.*

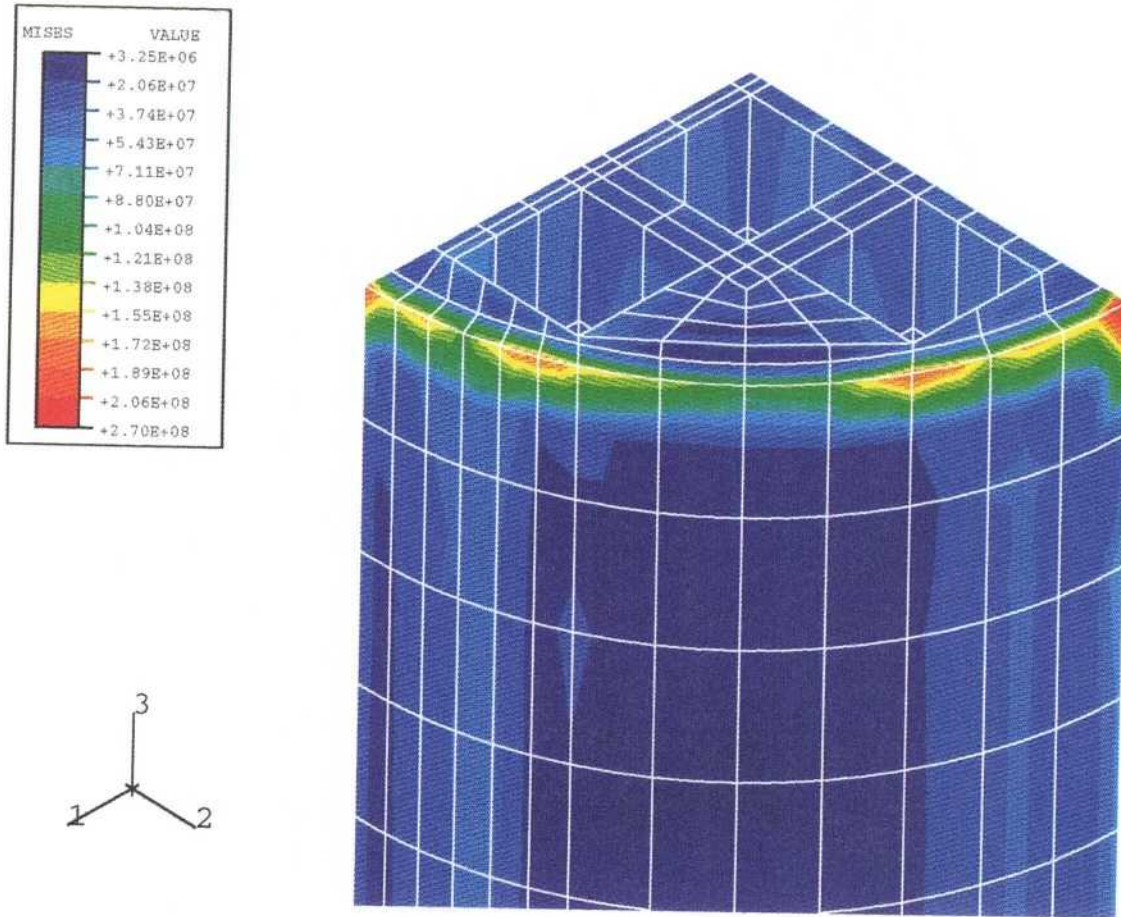


*Figure 5-22. Mises stress in the inner container using the 'lower bound' properties for the corrosion product.*

## 5.5 DETAILED ANALYSES

The purpose of the ‘detailed’ analyses was to determine how corrosion affects the region local to the penetration in the copper overpack; in particular, will the hole yawn. A penetration in the wall of the canister was modelled, because:

- it is the worst case for deformations of the copper overpack;
- the hoop stresses in the copper overpack will create stress concentrations local to the hole.

### 5.5.1 Model

The model was constructed from second order 3D brick elements, and is independent of the differences in BWR/PWR canister design. The finite element mesh is shown in Figure 5-23. The large central elements model the corrosion product, the inner elements model the steel container and the outer elements model the copper overpack. The ‘canister’ analyses showed little difference in the deformation of the copper overpack for the BWR and PWR designs, justifying a single detailed model. The model region includes the penetration and symmetrical constraints. The inner surface of the model (which represents the steel container) is constrained in the radial direction. The effect is to make the model slightly over-stiff in this direction, in effect a worst case scenario for the modelled region. The bentonite backfill is not modelled.

Both global and restricted corrosion scenarios were modelled. The case of global corrosion was relatively straightforward to model, as the magnetite layer was assumed to have uniform properties. The case of restricted corrosion required more care. Although, by assumption, corrosion occurs within an area of 4 cm radius around the penetration (see Section 5.2.5), the corrosion does not stop suddenly at 4 cm, i.e. there will be a transition region. The way in which this transition region is modelled will significantly affect the deformation of the copper overpack. The corroded area of 4 cm radius was modelled as stiff and expanding. In the transition region, between a radius of 4 cm and 8 cm, the stiffness was decreased from 205 GPa (i.e. steel) to 0 GPa in six steps, and no expansion was modelled.

A 0.5 mm expansion in the annular gap was modelled by an orthotropic thermal expansion of the corrosion product (cf. Section 5.3).

In the case of global corrosion, a second model (with a refined finite element mesh) was used to predict the stresses near the penetration. Only a section

of the copper overpack was modelled, with boundary constraints determined by the first model.

The steel container was modelled as a linear elastic material. The corrosion product was modelled with very high stiffness and, within a distance of 4 cm of the penetration, orthotropic expansion properties. Preliminary analyses indicated that substantial local yield would occur in the copper overpack, and so the copper was modelled as a multi-linear plastic material (see Table 5-1).

## 5.5.2 Results

In the global corrosion scenario, Figure 5-23 shows the displacements in the model (magnified by a factor 200). The wide elements in the centre of the model represent the expansion of the corrosion product. The copper overpack expands radially, generating hoop stresses. Figure 5-24 shows the Mises stress in the copper overpack. The bulk of the material is at stresses between 115 MPa and 136 MPa, and so general yield has occurred. Yield begins to occur for an expansion of the annulus by about 0.25 mm. A more detailed study of the stresses around the penetration (Figure 5-25) shows that the stress concentration factor is about 2.5, which is correct for a thick isotropic material. The major contribution is from the hoop stresses. The stress concentration factor reduces to 1.0 within a distance of a hole diameter. There is no significant dilation of the penetration.

In the restricted corrosion scenario, Figure 5-26 shows the displacements in the model. The copper overpack is significantly deformed. The stresses on both the outer and inner surfaces of the copper overpack are shown in the Mises plots, Figures 5-27 and 5-28 respectively. Since the copper overpack has been modelled as a plastic material, the plastic strain (Figure 5-29) is more useful in determining whether failure is likely to occur. The maximum plastic strain is 5.78%, corresponding to a total strain of 5.82%, which is well below the strain to failure of copper, 29%. The maximum strain is at the edge of the corroded area, about 4 cm from the penetration. There is no significant dilation of the penetration.

Figure 5-30 shows that the displacements in the steel container are small. The displacements become insignificant halfway through the modelled thickness of steel (50 mm). This suggests that the model is sufficiently thick, and that the geometry of the inner container (BWR or PWR design) does not affect the results.

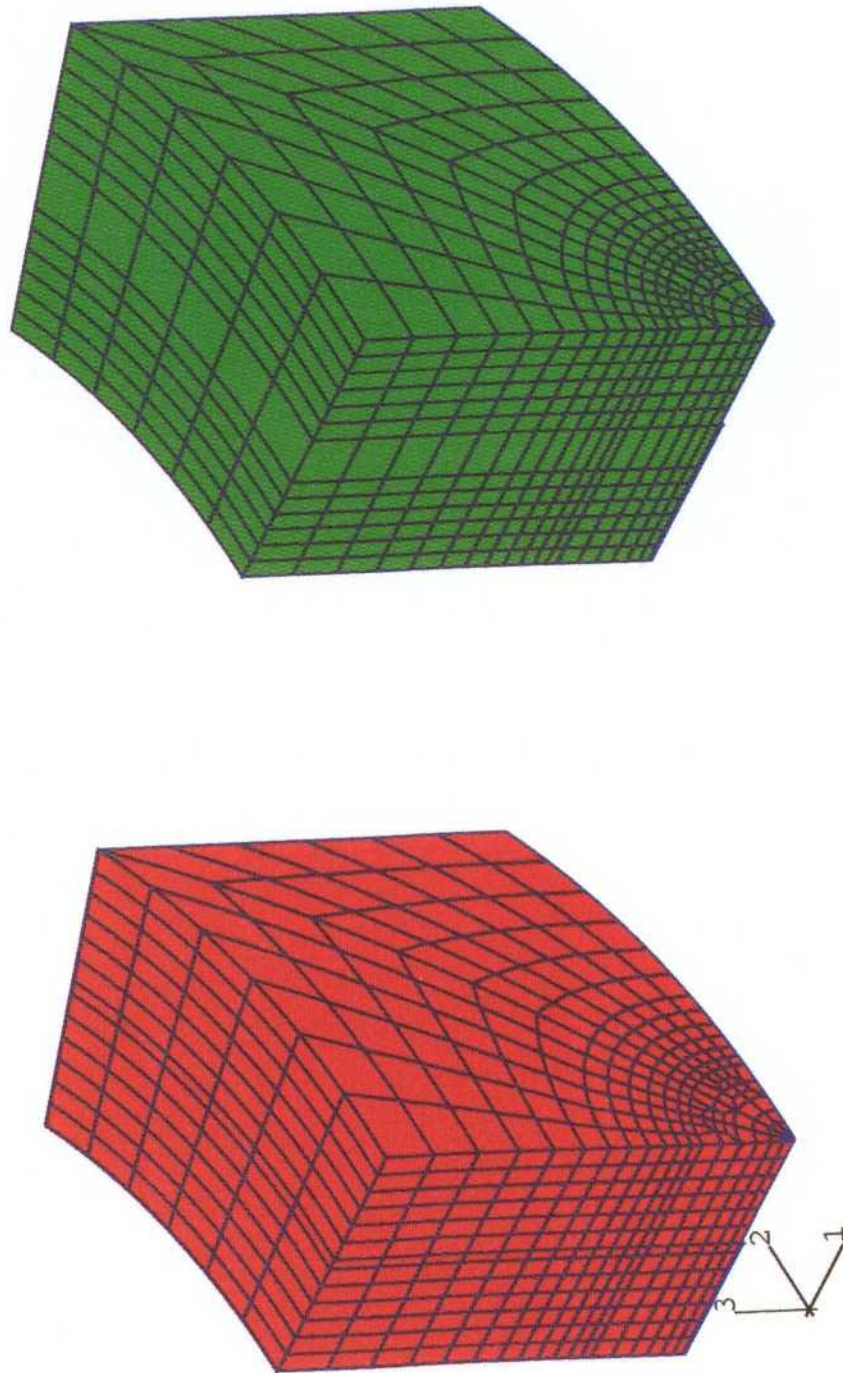


*Figure 5-23. Detailed model: original finite element mesh and displaced shape for global corrosion scenario and 0.5 mm displacement load.*

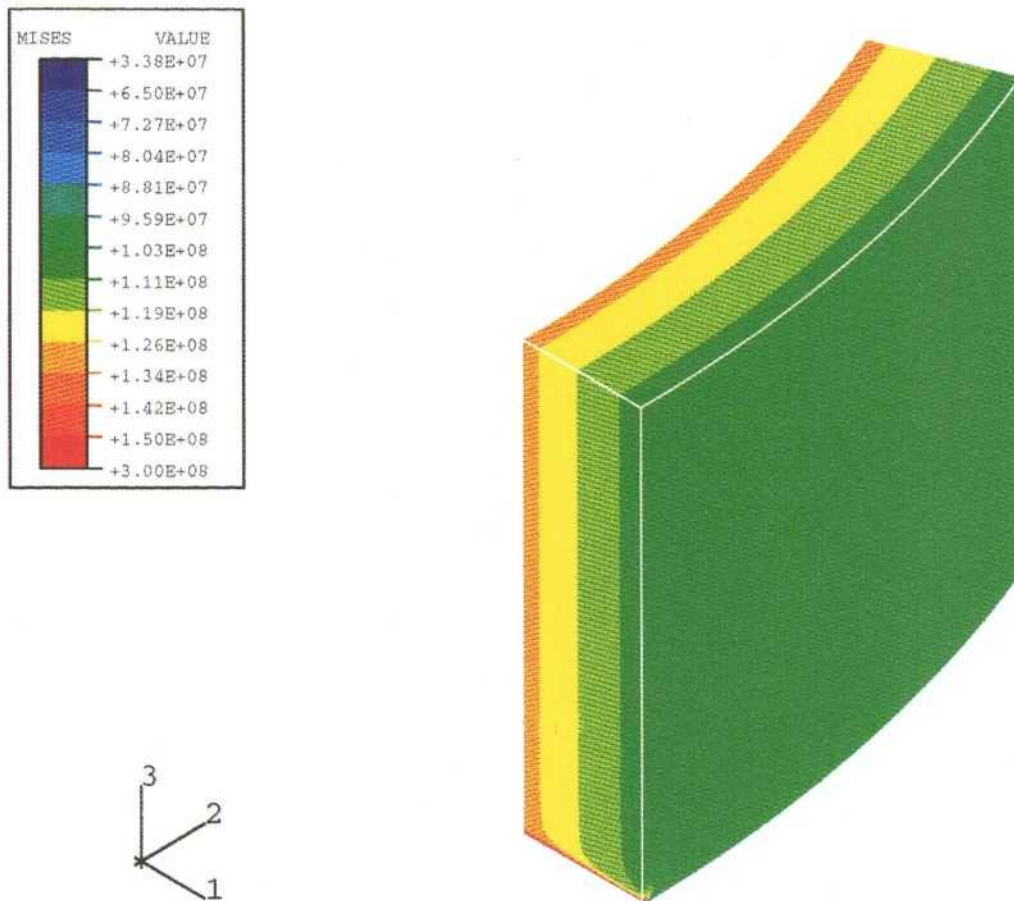


*Figure 5-24. Mises stress in the copper overpack for global corrosion scenario and 0.5 mm displacement load.*

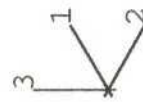
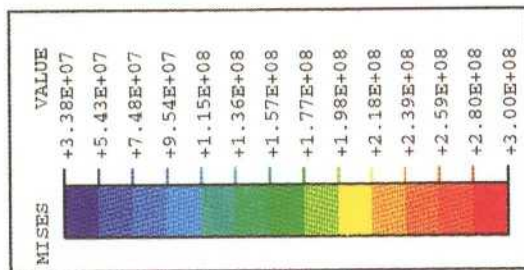
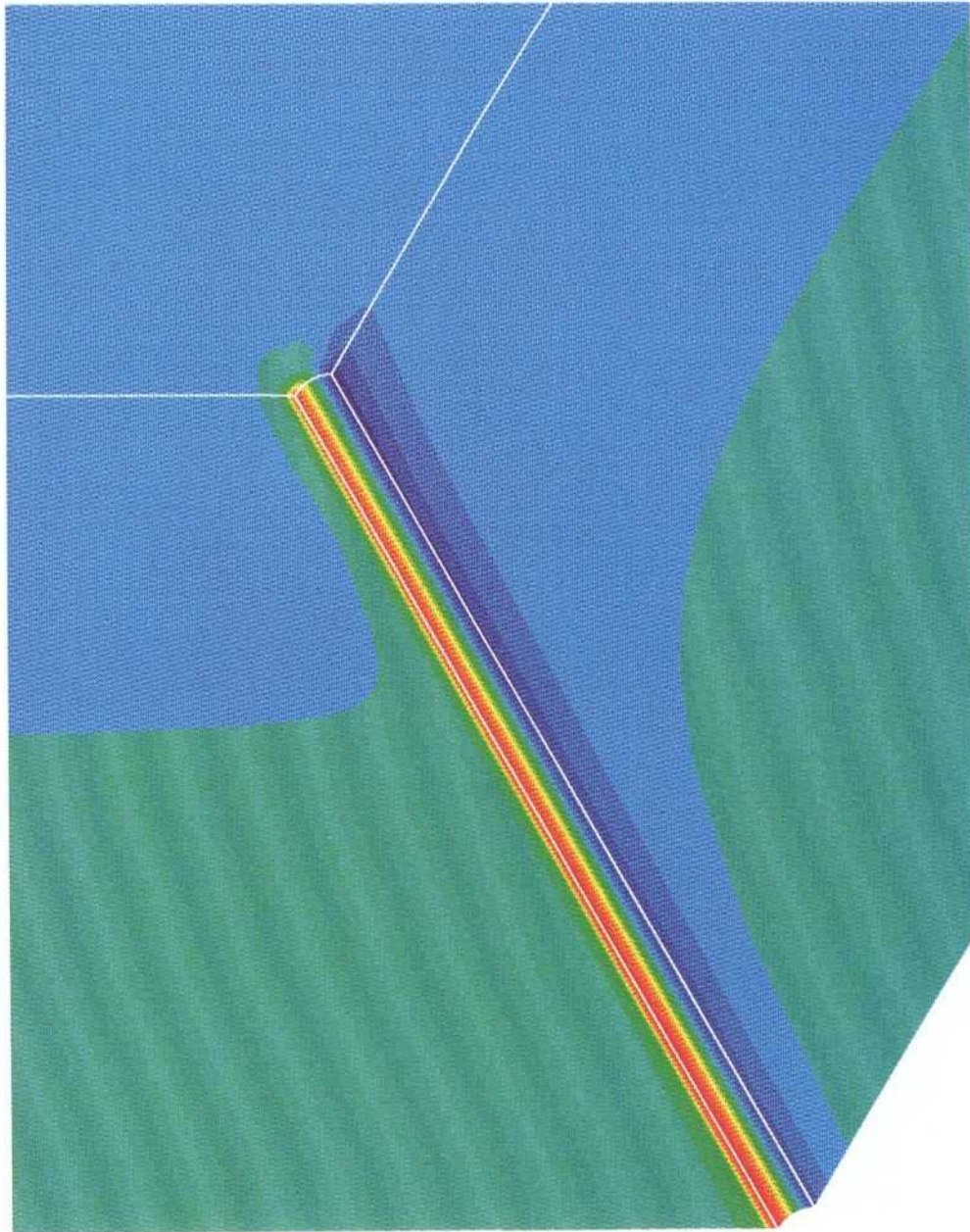


**Figure 5-25.** Mises stress in the copper overpack near the penetration for global corrosion scenario and 0.5 mm displacement load.

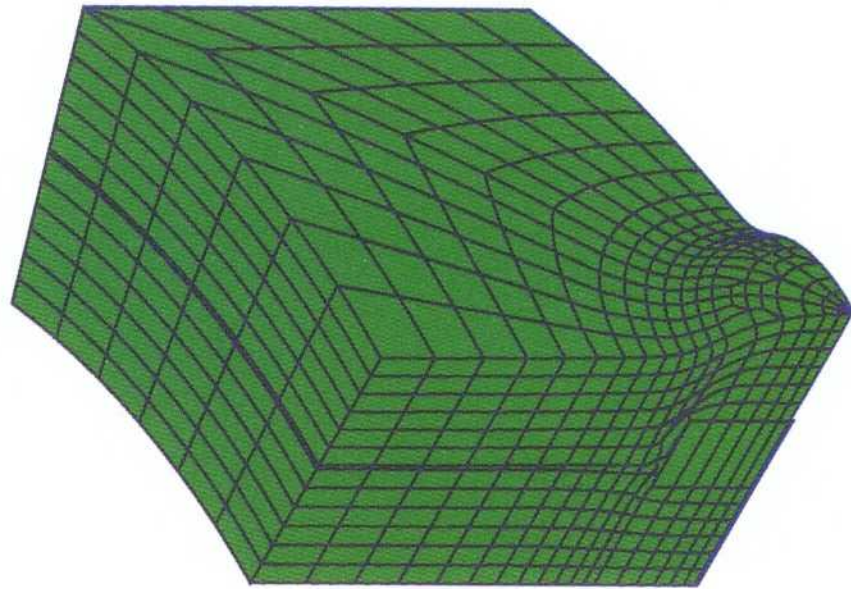


*Figure 5-26. Detailed model: displaced shape for restricted corrosion scenario and 0.5 mm displacement load.*

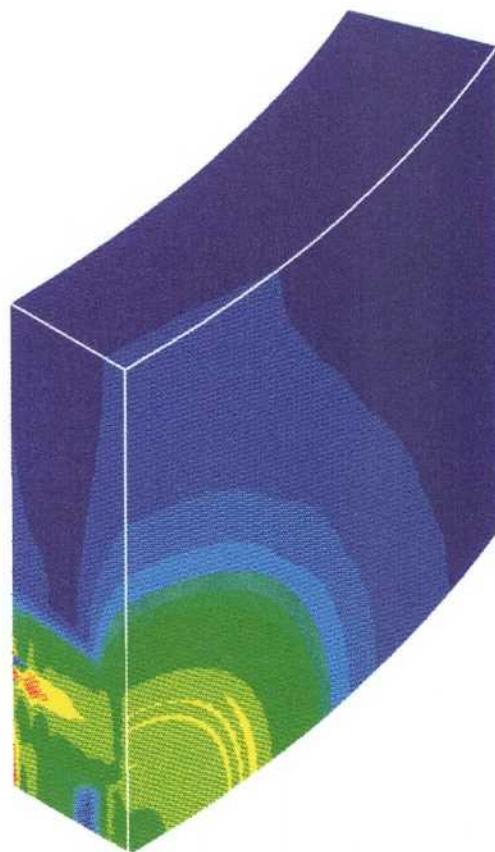
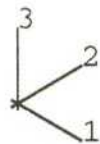
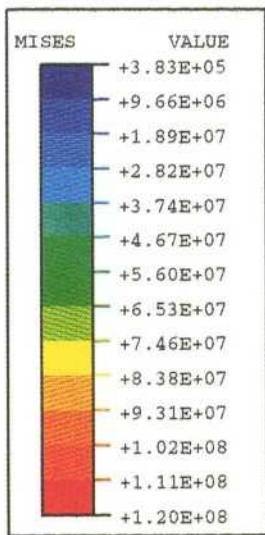


*Figure 5-27. Mises stress in the copper overpack for restricted corrosion scenario and 0.5 mm displacement load.*

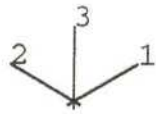
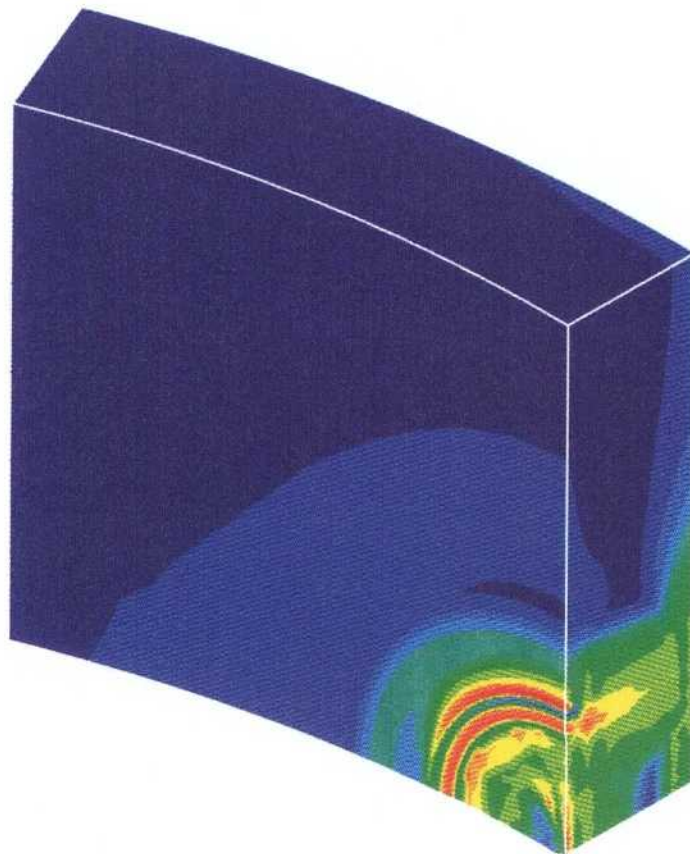
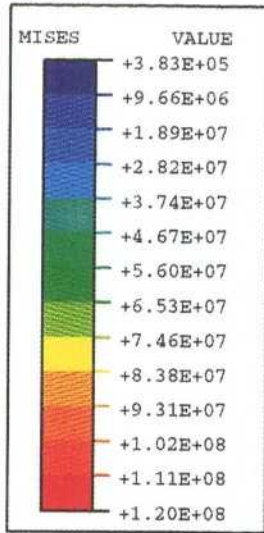


**Figure 5-28.** Mises stress in the copper overpack for restricted corrosion scenario and 0.5 mm displacement load.

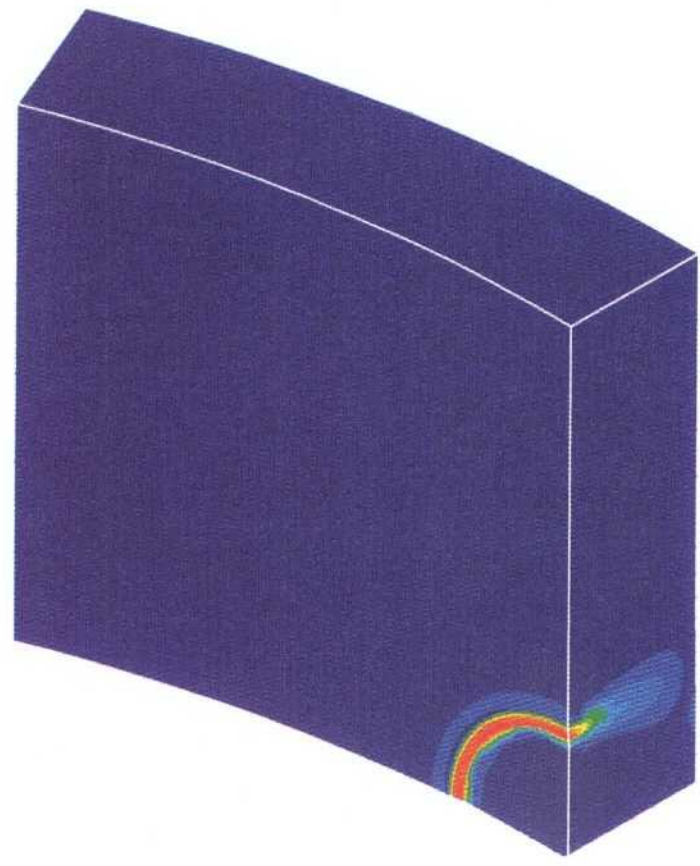
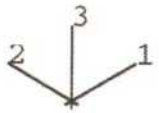
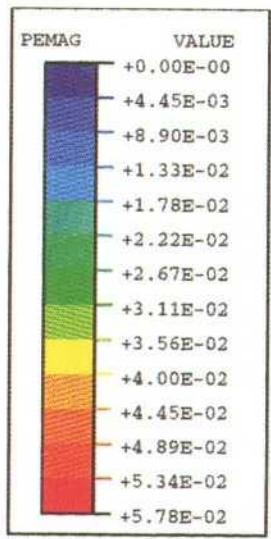


*Figure 5-29. Plastic strain in the copper overpack for restricted corrosion scenario and 0.5 mm displacement load.*

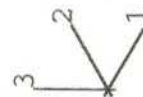
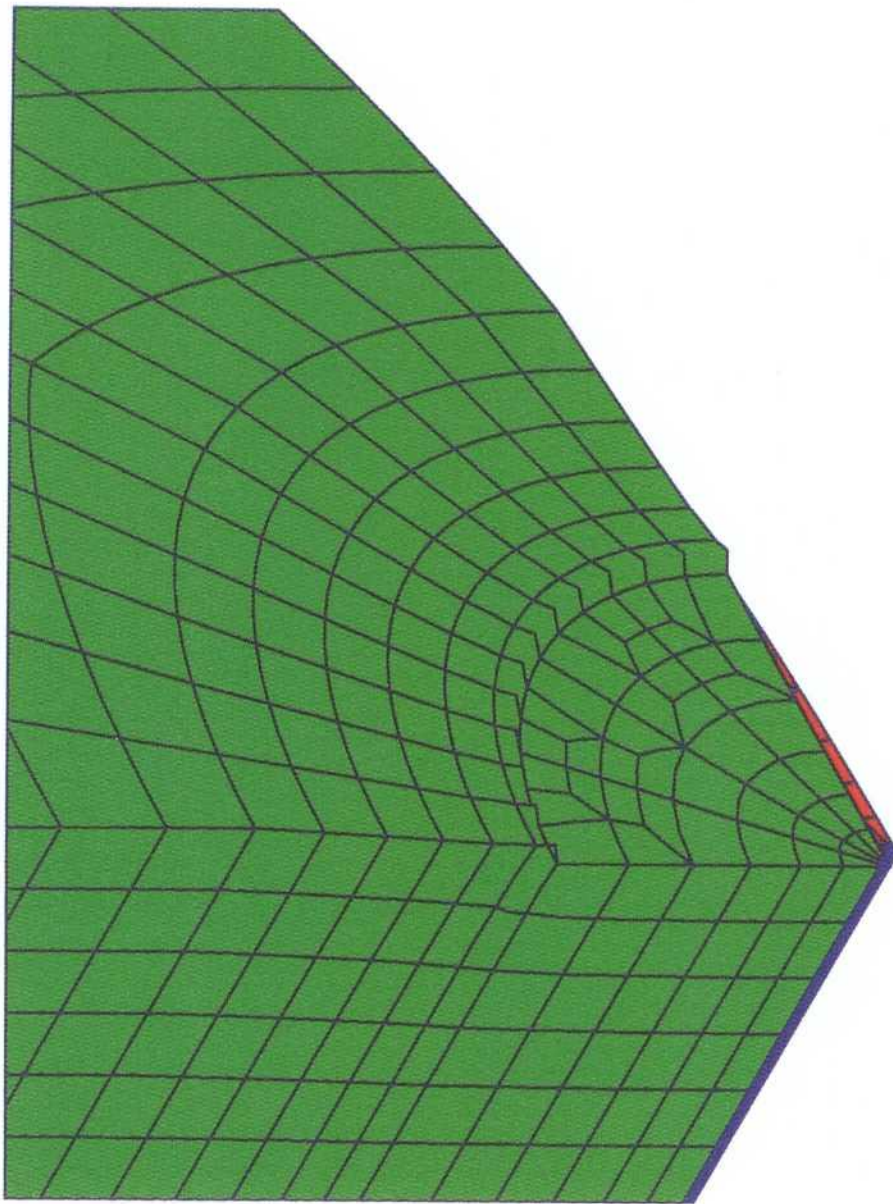


**Figure 5-30.** Detailed model: displacement of inner container for restricted corrosion scenario and 0.5 mm displacement load.

### 5.5.3 Discussion

The penetration does not increase significantly in size for either the global or restricted corrosion scenarios. Since there is no dilation, the stresses do not cause a change in the corrosion regime.

The global corrosion case produces stress concentrations within one diameter of the penetration which are due to the effect of the hoop stresses generated in the copper. The concentration is slightly higher than might be expected for a thick walled structure, showing that limited deformation of the area surrounding the penetration has occurred (i.e. the penetration is ovalised). The copper overpack shows general yield for an expansion of the annulus of about 0.25 mm. Plastic strains in the copper vary with the position of the penetration because of the different stiffnesses in the cross section of the inner container.

The restricted corrosion case does not affect the overall structural integrity of the canister. The main phenomenon is a local plasticity in the copper overpack at the outer radius of the corroded area (it is believed that this will occur provided that  $r_c > 10r_p$ , where  $r_c$  is the radius of the corroded area and  $r_p$  is the radius of the penetration). A long time after the first onset of plasticity, the build-up of corrosion product might cause the copper overpack to fail by pushing out a disc of material. This would cause a change to the global corrosion regime, i.e. local corrosion in the canister delays the onset of more widespread corrosion.

In the restricted corrosion case, the results show that the displacements, and therefore stresses, in the steel container are localised. This justifies the size of the region modelled in this section. It also justifies the assumption in Section 5.3 (for the 'canister' analyses) that modelling a second symmetrical penetration does not distort the results.

## 5.6 INFLUENCE OF DEFECT GEOMETRY

In the above models, the penetration in the copper overpack was circular. This section examines the effect of changing the shape of the defect in the copper overpack; specifically, it assumes that the defect is a longitudinal crack (considered to be a worst case for the development of stresses).

### 5.6.1 Model

As before, a segment of the copper overpack was modelled using second order brick elements. In order to reduce the model size neither the steel container nor corrosion product were modelled explicitly. This means that the results are independent of the design of the inner container. Although some of the detail of how the canister reacts to corrosion has been lost, the

model does give a fair indication of the significance of the initial defect geometry. Symmetry was assumed so that only a quarter of the defect was modelled. Symmetry constraints were applied around the boundary of the copper overpack.

Two defect geometries were considered:

- a circular penetration of area  $5 \text{ mm}^2$  (i.e. diameter 2.46 mm as modelled previously);
- a longitudinal through-thickness crack of length 10 mm (the model assumes that the crack thickness is infinitesimally small; assuming an elliptical crack of the same area as the circular penetration would give a width of 0.62 mm).

For a given cross-sectional area, a circular penetration is the defect geometry that presents the least restriction on the flow of water to and from the inner container.

The alternative geometry that was considered is a long thin crack. The analysis assumes that the maximum area for an undetected crack is the same as for a circular defect. Since the hoop stresses generated by the expansion of corrosion product are approximately twice the longitudinal stresses, it was felt that a longitudinal crack was the most severe orientation. This is also the most likely orientation for any cracks formed in the material during construction.

Transverse cracking is possibly more likely at the lid welds; however, it is assumed that these regions will be routinely inspected using a non-destructive technique, and that any defects will be repaired prior to emplacement of the canister. Stresses in the region of a transverse crack are likely to lie somewhere between those for a circular penetration and a longitudinal crack.

### **5.6.2 Method of analysis**

In both linear-elastic and elastic-plastic models, there is a singularity at the tip of a crack. There are a number of methods that are used to model this with reasonable accuracy without using a large numbers of finite elements /5-10, 5-11/. The simplest (used here) is to move the mid-side nodes of the finite elements adjacent to the crack tip to a point a quarter along the edge of the element from the crack tip. Although this generates a square root strain singularity along the edges of the element, the singularity does not extend into the interior of the element. This method gives an improvement in the calculated displacements, and hence a better estimate of the crack aperture (which is important because it controls the rate of water ingress). Since the copper overpack material is 'tough' and brittle crack growth is unlikely, a

highly refined calculation of the stresses at the crack tip is not needed, and the J-integral around the crack tip is not required.

Both global and restricted corrosion scenarios were considered for the crack geometry.

In the global case, a radial displacement of 0.5mm was applied to the inner surface of the overpack. This displacement is a result of the build-up of corrosion product. It is assumed that the steel container is rigid, and that all of the displacement is taken up by the copper. This assumption leads to larger predicted stresses in the copper.

In the restricted case, the radial displacement of 0.5mm was applied only within a distance of 4 cm of the defect, and was linearly reduced to zero in the next 4 cm. The rest of the inner surface of the overpack was kept fixed, with zero radial displacement. This is different to the method used before, where the steel container and the corrosion product were modelled explicitly, and the transition region was modelled by a reduction in the stiffness of the corrosion product.

Elastic material properties were used for the global cases. Elastic-plastic material properties were used for the restricted cases, as extensive yielding of the material is expected.

### **5.6.3 Results**

In the global corrosion scenario, the results for the case with a circular penetration are virtually identical to the previous analysis, showing that the change in method, while reducing the size of the model, has not significantly degraded the results. Figure 5-31 shows the Mises stress in the vicinity of the penetration. There is a stress concentration around the hole of about 2.5-3.0, which is typical for isotropic materials. The copper overpack has generally yielded with the Mises stress between 90MPa and 140MPa. The hole does not dilate significantly; hence, the stresses do not alter the corrosion behaviour of the canister. Figure 5-32 shows the Mises stress for the crack defect. Again, the stress concentration around the crack is very localised, and the stresses elsewhere are similar to the case of a circular penetration. The dilation of the crack is negligible.

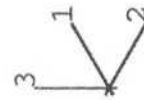
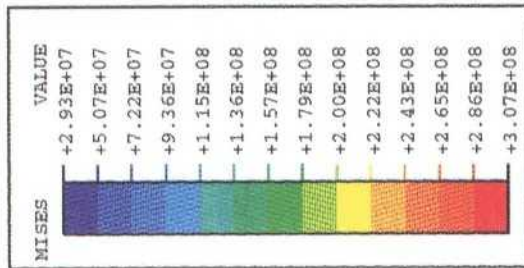
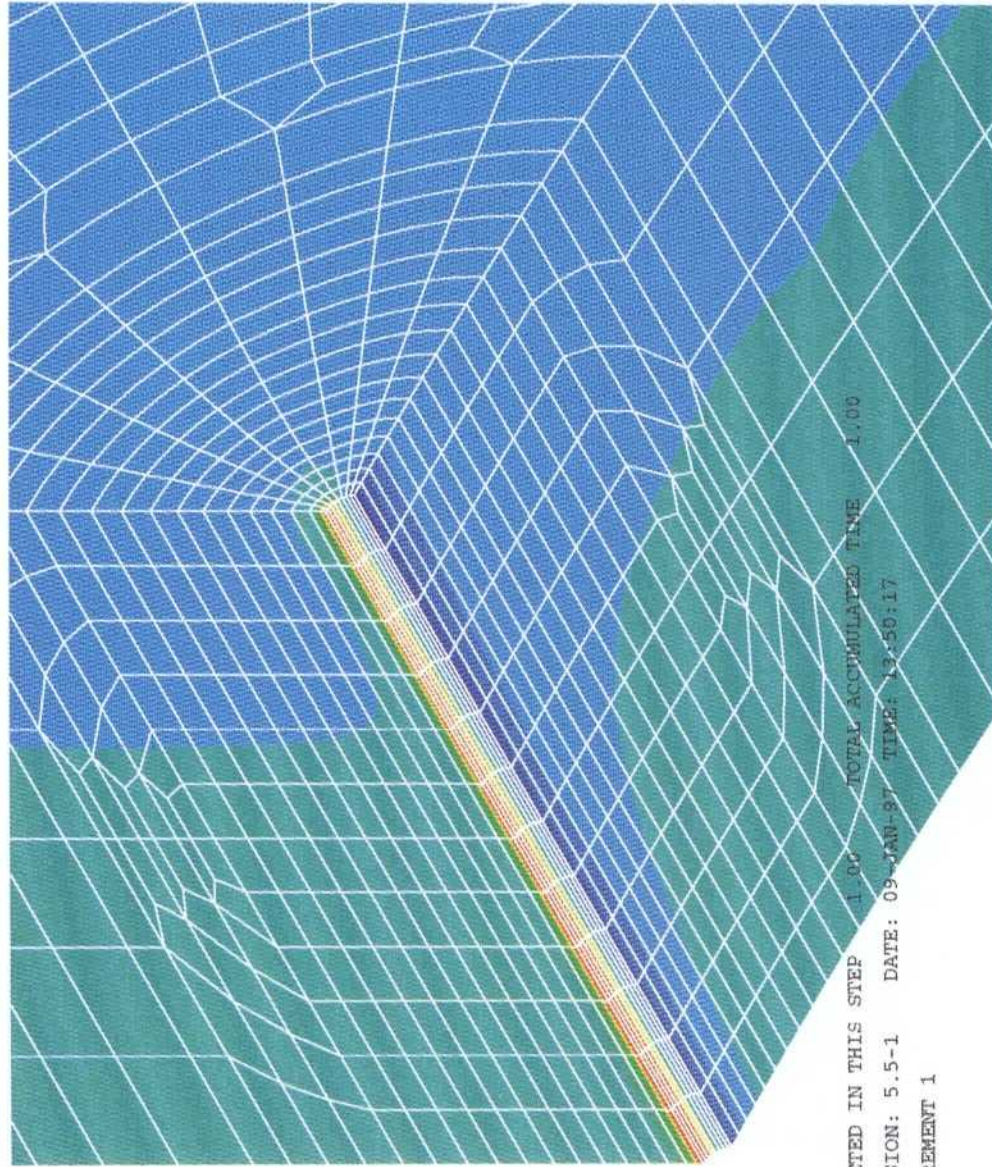
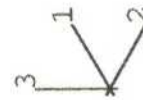
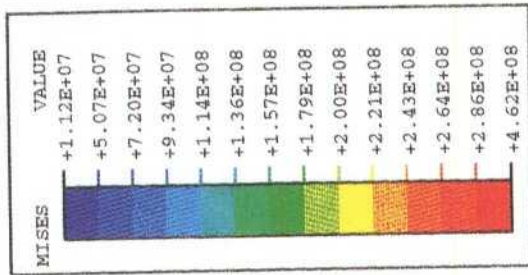
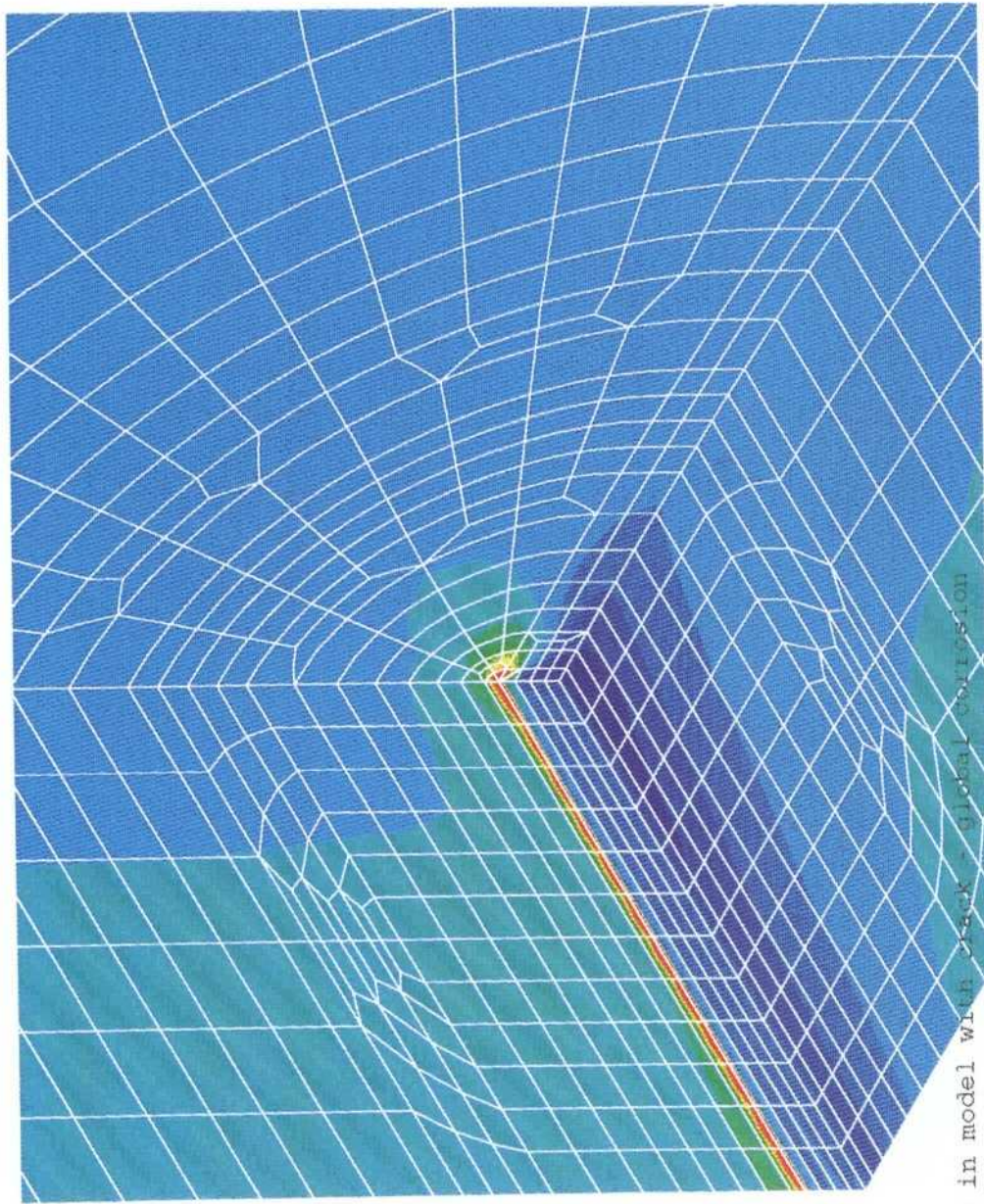


**Figure 5-31.** Mises stress in a model with a circular penetration and global corrosion scenario.



Mises stress in model with crack + global corrosion

**Figure 5-32.** Mises stress in a model with a crack penetration and global corrosion scenario.

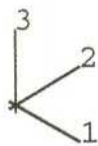
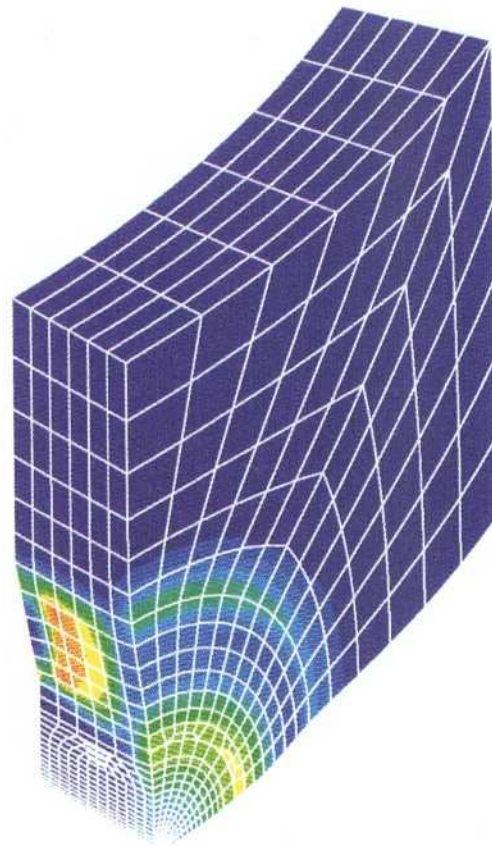
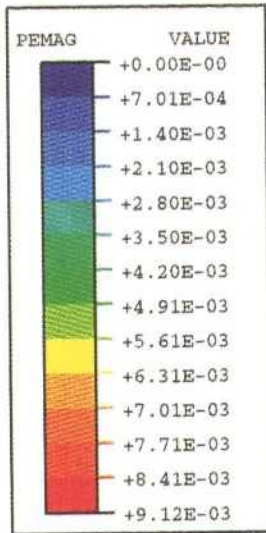


*Figure 5-33. Plastic strain in a model with a circular penetration and restricted corrosion scenario.*

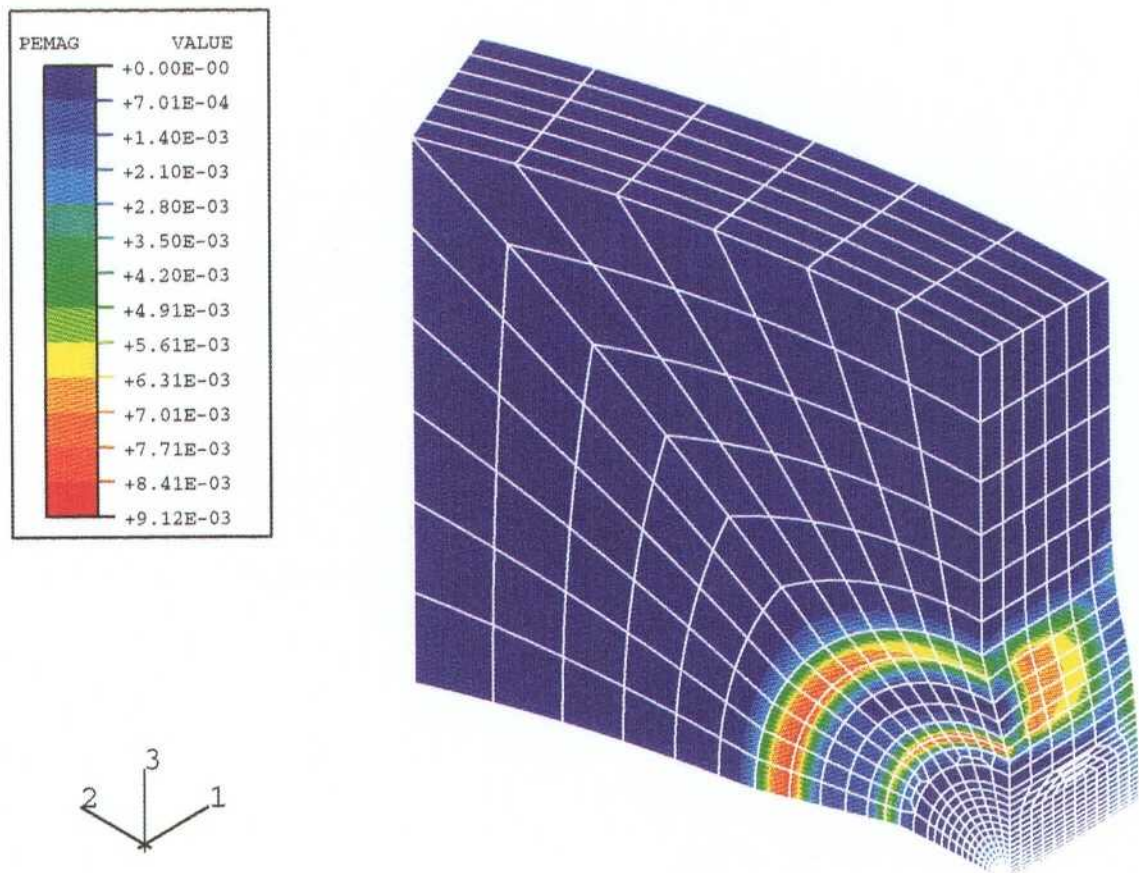


*Figure 5-34. Plastic strain in a model with a circular penetration and restricted corrosion scenario.*

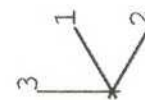
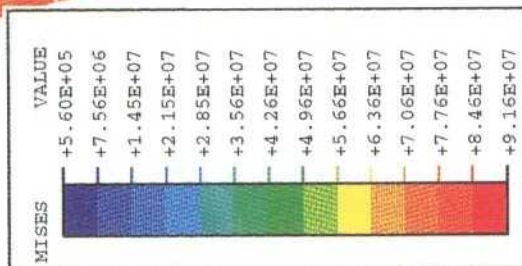
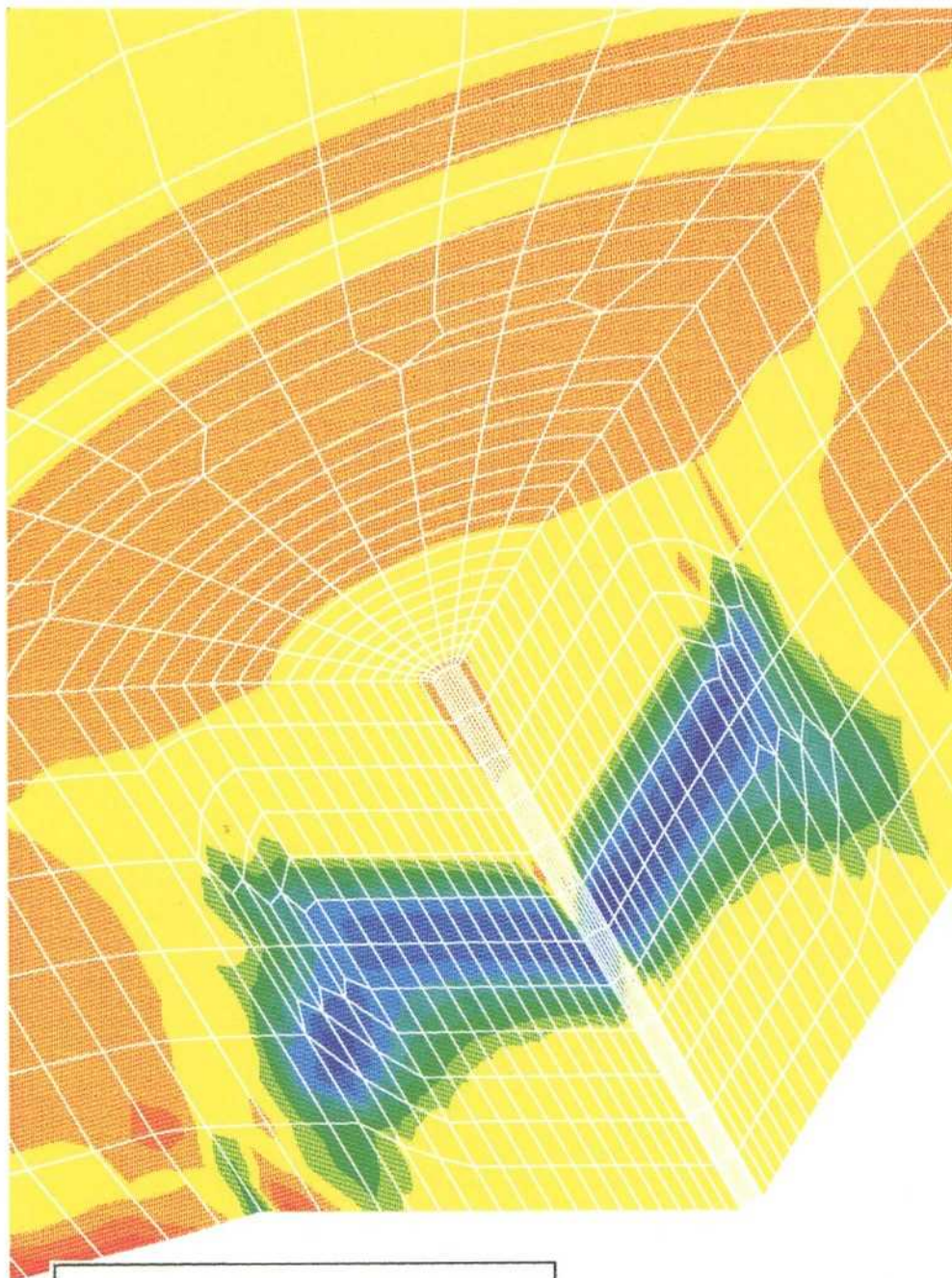


**Figure 5-35.** Mises stress in a model with a circular penetration and restricted corrosion scenario.

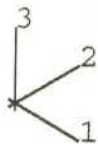
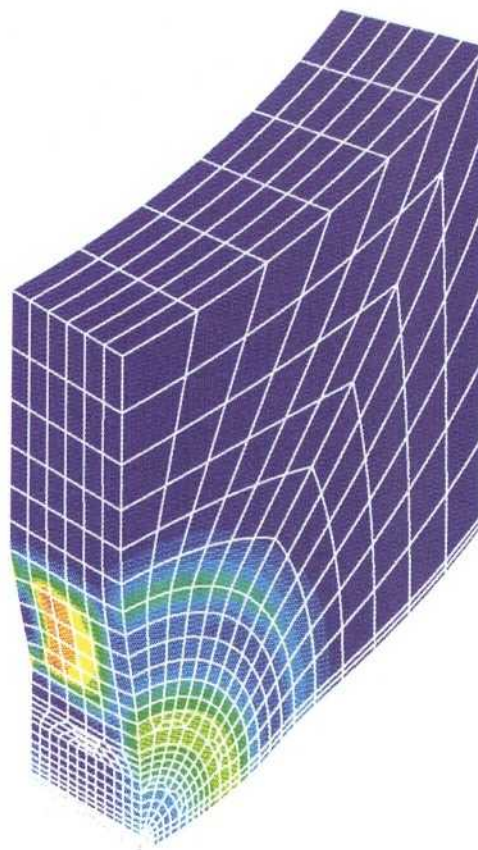
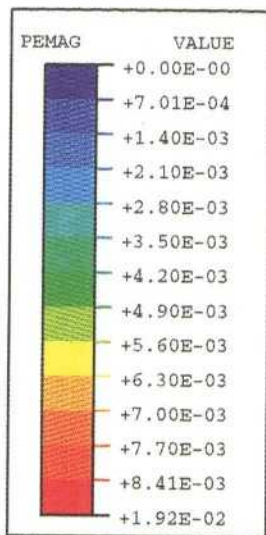


*Figure 5-36. Plastic strain in a model with a crack penetration and restricted corrosion scenario.*

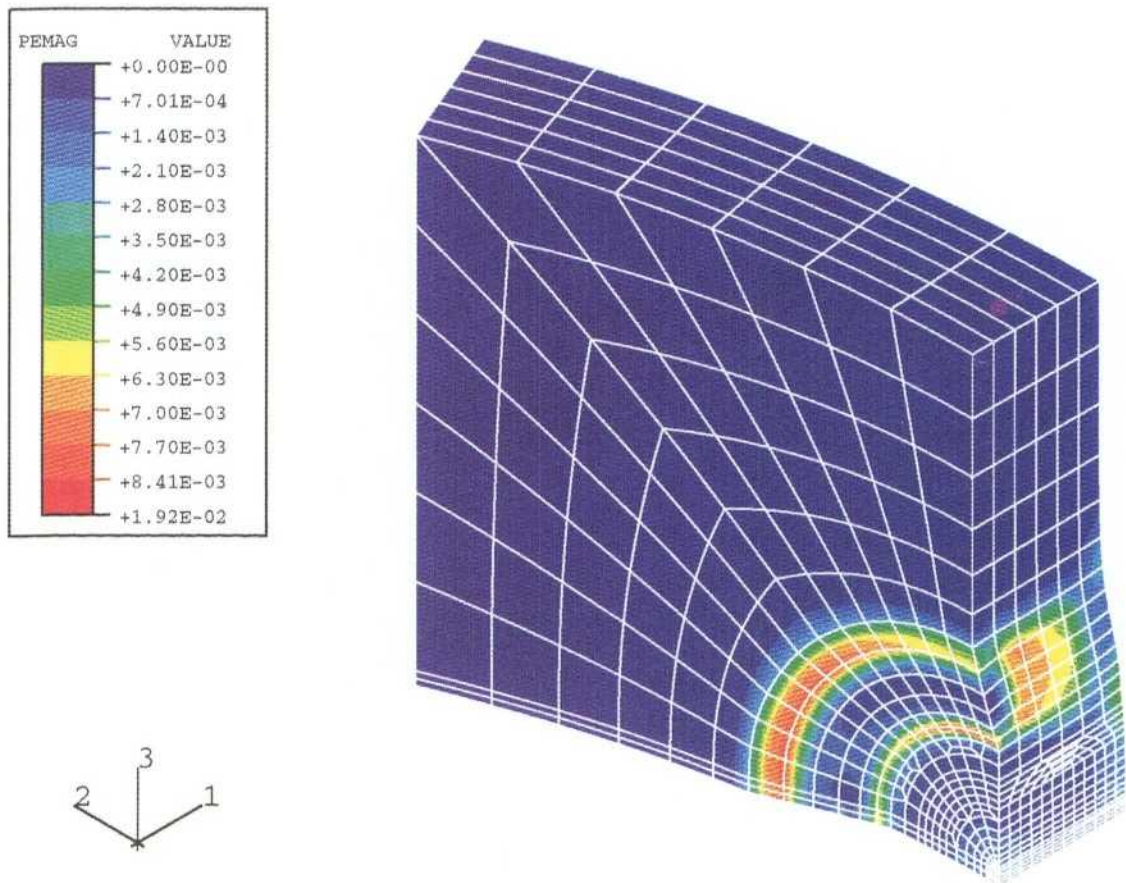


**Figure 5-37.** Plastic strain in a model with a crack penetration and restricted corrosion scenario.

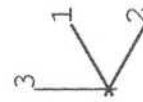
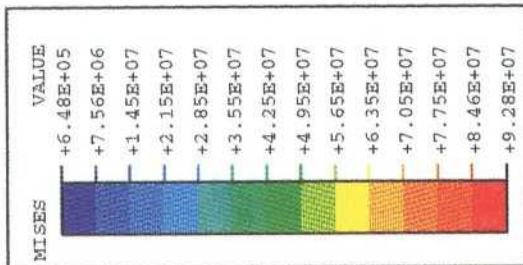
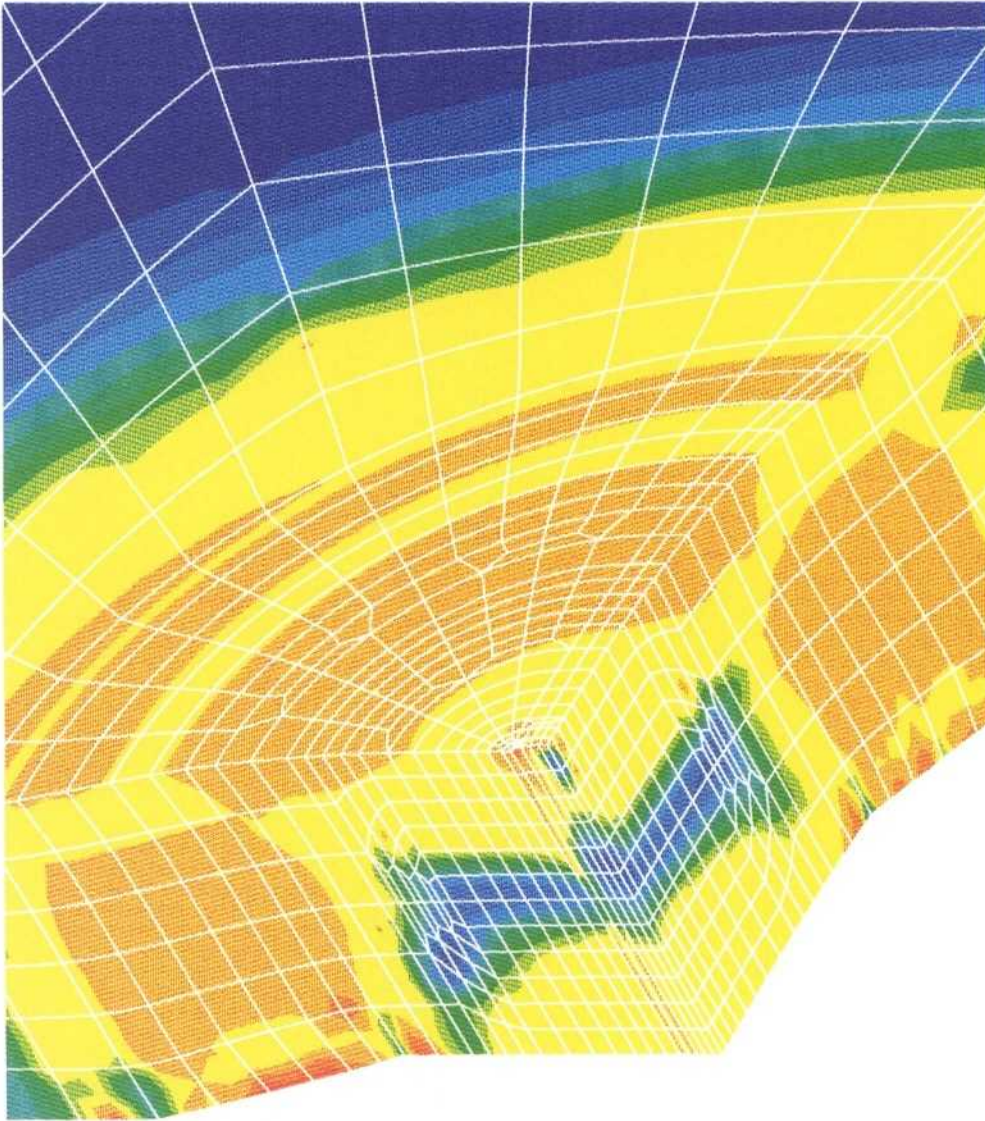


*Figure 5-38. Mises stress in a model with a crack penetration and restricted corrosion scenario.*

In the restricted case, Figures 5-33 and 5-34 show plastic strain for the model with the circular penetration, and indicate that the copper overpack has yielded where the local deformation due to corrosion has occurred. However, the maximum plastic strain is less than 1%, and so the copper is far from failure. Figure 5-35 shows a close up of the Mises stress in the region of the hole. The stresses around the hole are not significantly higher than the stresses elsewhere in the copper overpack. The hole does not dilate significantly; hence, the stresses do not alter the corrosion behaviour of the canister.

Figures 5-36 and 5-37 show the plastic strain for the model with a crack. Overall there is little difference in the strain compared to the model with a circular penetration. The peak, of nearly 2%, is in a very localised region around the tip of the crack. Figure 5-38 shows that the crack has little effect on the Mises stress in the overpack. Again, dilation of the defect is negligible.

## **5.7 VAULT ANALYSES**

The purpose of the 'vault' analyses was to determine how deformations of the canister might affect the surrounding bentonite and rock.

### **5.7.1 Model**

The copper overpack, a 0.5 m thickness of bentonite and a 0.2 m thickness of rock were modelled. Only the bottom half of the deposition hole was modelled: there is less bentonite beneath the canister, and it is expected that the largest stresses in the rock will be generated by corrosion of the bottom lid of the canister. The deposition hole was modelled using second order axisymmetric elements.

The finite element mesh used for the global corrosion case is shown in Figure 5-39, based on the geometry presented in reference /5-2/. The red finite elements correspond to the copper overpack, the green elements to the bentonite and the blue elements to the rock. The model used for the restricted corrosion case was very similar, although additional refinement was needed near the penetration. Symmetry was used to model the top half of the canister, and the boundary conditions applied to the rock assumed that the geology extended to infinity.

As final details of the procedure used to drill the deposition holes were not available, the corner at the base of the hole was assumed to have a radius of curvature of 500 mm. This:

- gives a minimum thickness of bentonite between the canister and the rock, thus reducing the buffering effect of the clay and increasing the stresses in the rock;
- but underestimates the stress concentration factor.

Since the stress concentration factor decreases more slowly at large radii of curvature, the effect of an overestimate of this radius on the predicted stresses is less than had a small radius (i.e. sharp corner) been assumed (note that typical corner radii for holes drilled in rock are of the order of 50 – 100 mm).

In the global corrosion case, the deformation of the copper overpack was determined from the results of the ‘canister’ analyses (Section 5.3). The largest displacements occur for the PWR canister design. Values from this model corresponding to an expansion of the annular gap of 0.5 mm were interpolated at the nodal positions of the ‘vault’ model. In addition, an extreme case in which the copper overpack was deformed uniformly by 55 mm was analysed (this would correspond to corrosion of a 51.8 mm thickness of steel, i.e. penetration of a fuel channel). This latter case was intended to provide a worst case prediction for the stresses in the rock (it allows for neither the deformation nor reducing stiffness of the steel container). The restricted corrosion case was handled similarly.

The copper overpack was modelled as an elastic multi-linear plastic material (see Table 5-1). The bentonite backfill was modelled as an elastic plastic material with Drucker-Prager hardening. The effects of the bentonite swelling pressure on the material properties were included as an initial condition. It is probable that the rock will contain fissures, but these were not explicitly represented, and the rock was modelled as a linear elastic material (see Table 5-1).

### 5.7.2 Results

For the case of global corrosion, Figure 5-40 shows the maximum principal stresses in the rock. In most areas the stress on the rock is compressive. However, localised regions of tensile stress, extending to a depth of 100 mm, occur at the corners of the deposition hole. Fissures in the rock are most likely to propagate in this area. The bentonite, because of the Drucker-Prager characteristics, shows only extremely limited local yield. Figure 5-41 shows the Mises stress distribution in the bentonite. As almost no plasticity occurs, even for relatively large displacements, it is clear that the bentonite is able to ‘absorb’ most of the copper overpack deformation. The representation of the copper overpack is consistent with the results in Section 5.3. In particular, plasticity is visible in the canister rim and there is some yield in the canister wall. The deformation of the canister is radial (axial on the lid), with bending effects creating the stress concentrations at the rim.

For the extreme displacement scenario, Figure 5-42 is a plot of the maximum principal stresses in the rock. It shows that the peak compressive stresses have increased by 2.98 MPa to 4.19 MPa, and the peak tensile stresses have increased by 0.37 MPa to 1.42 MPa. Figure 5-43 shows the plastic strain in the copper overpack, indicating that the rim has failed and there is significant plastic deformation in the rest of the canister. The bentonite has deformed plastically, as shown in Figure 5-44, with peak stresses at the canister rim.

For the case of restricted corrosion on the canister lid, Figure 5-45 shows the maximum principal stresses in the rock. The stresses are similar to those in Figure 5-40. Figure 5-46 shows the deformation of the canister (magnified by a factor 20). The behaviour of the copper overpack is consistent with the results in Section 5.3. In the bentonite, plastic strain is localised to within 1 cm of the penetration in the copper overpack.

### 5.7.3 Discussion

The results show that bentonite will act as an efficient buffer for the stresses induced by corrosion of the canister. The hydrostatic yield and hardening characteristics of bentonite prevented the onset of general yield in all but the most extreme case modelled. The (low) elastic modulus of saturated bentonite allowed deformations to occur without significantly stressing the rock.

Compressive stresses in the rock are unlikely to cause failure. Localised tensile stresses in the rock occur at the corners of the deposition hole. It is possible that these stresses will cause cracking in the rock to a depth of about 100 mm. The possibility that the tensile stresses will propagate fissures in the rock has not been addressed by the modelling.

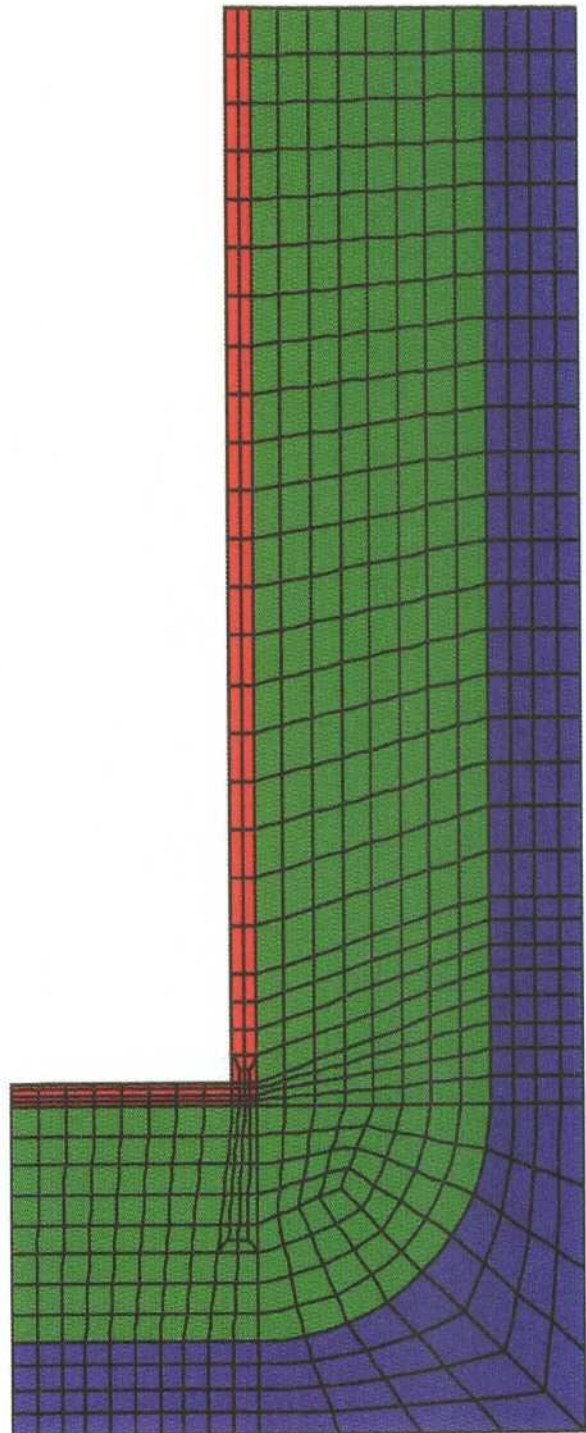


Figure 5-39 Global model mesh

*Figure 5-39. Vault model: finite element mesh.*

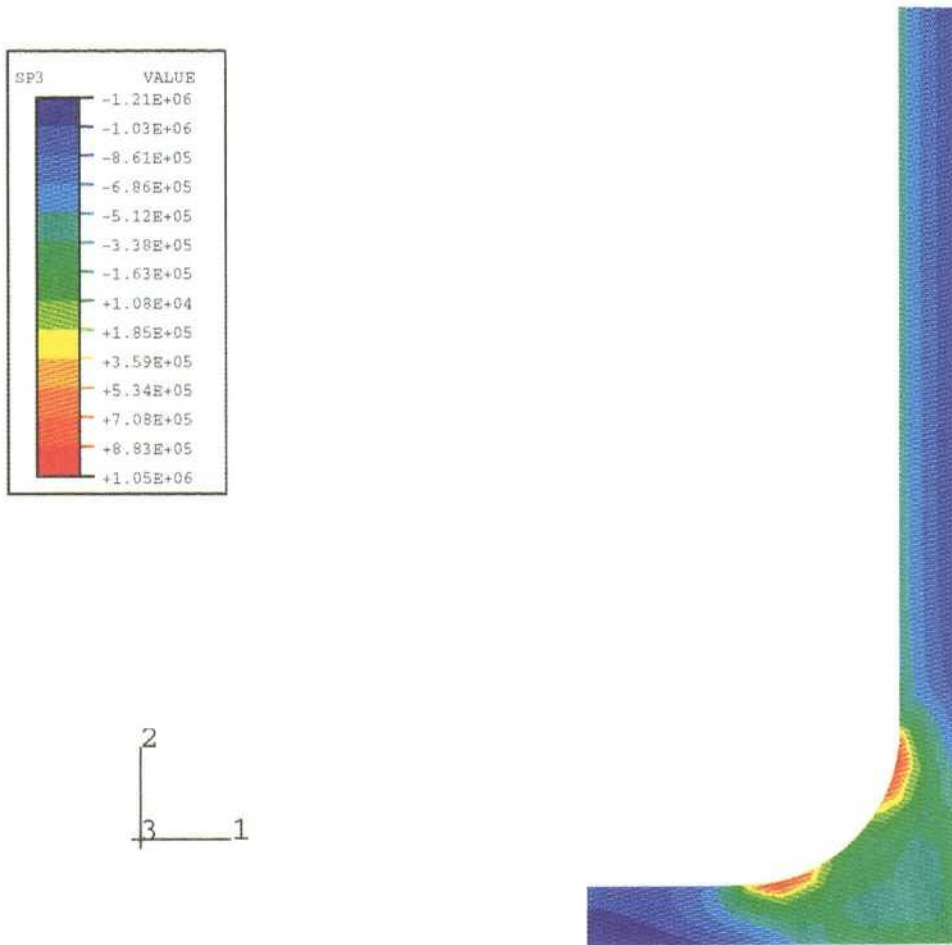


Figure 5-40: Maximum principal stress in rock at load extracted from core model

*Figure 5-40. Maximum principal stresses in the rock for global corrosion scenario.*

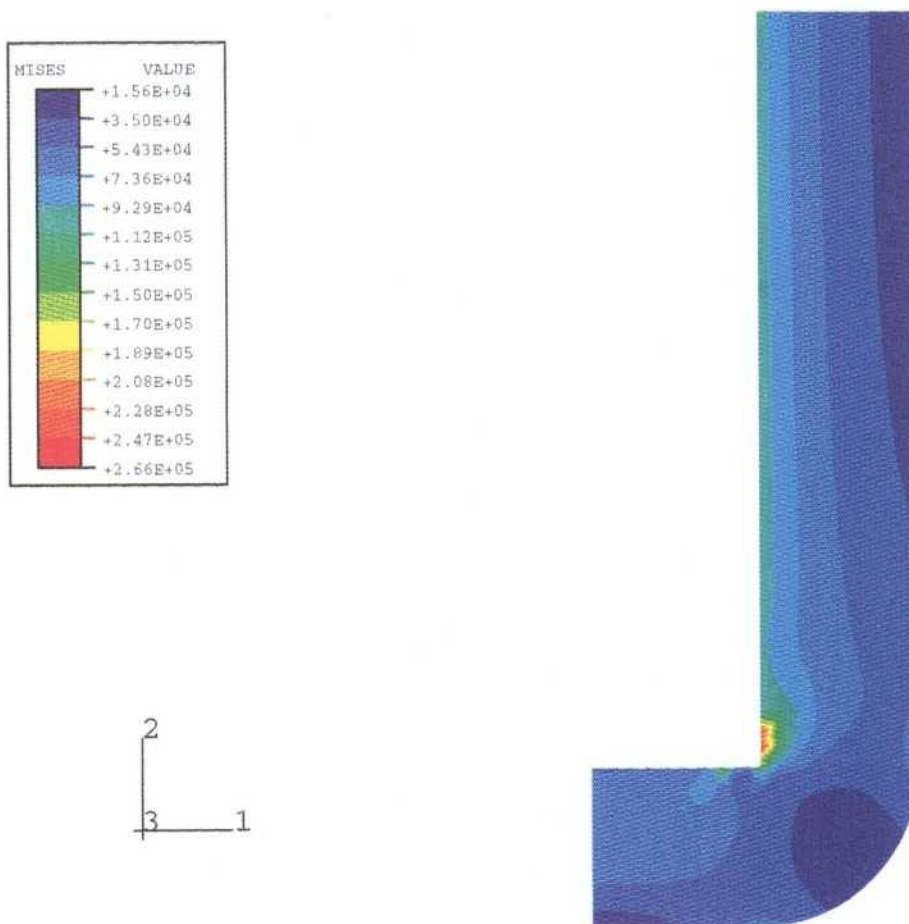
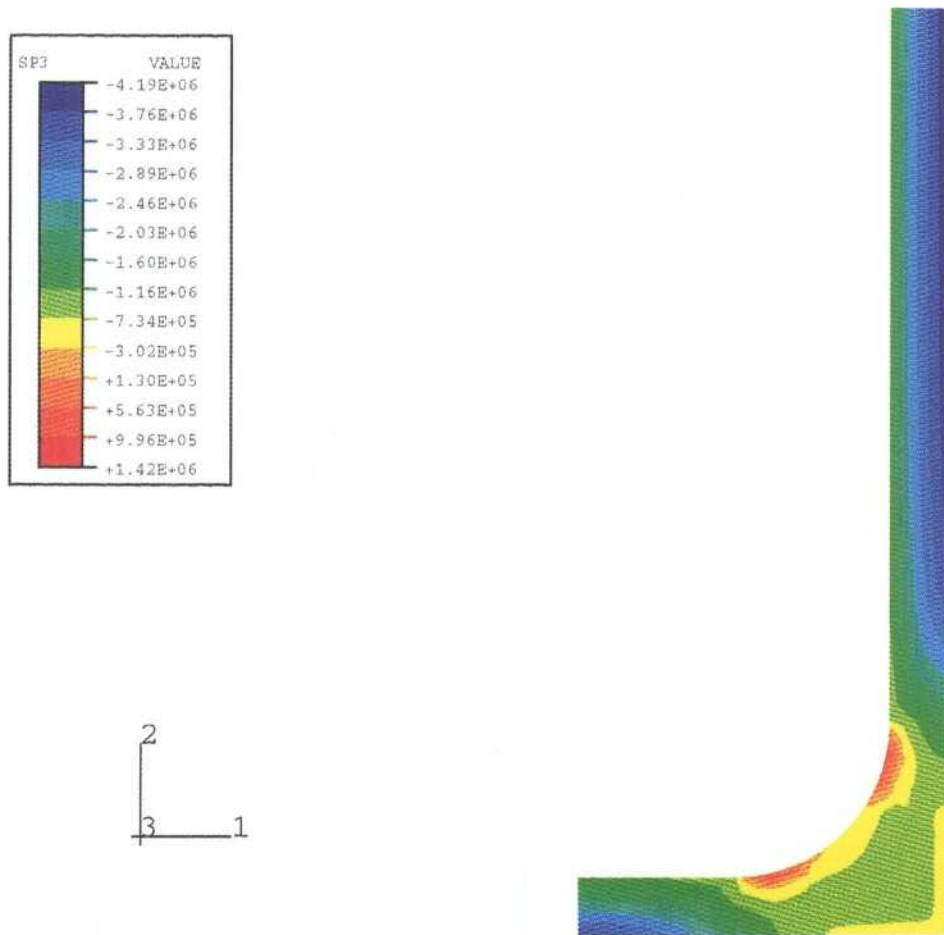
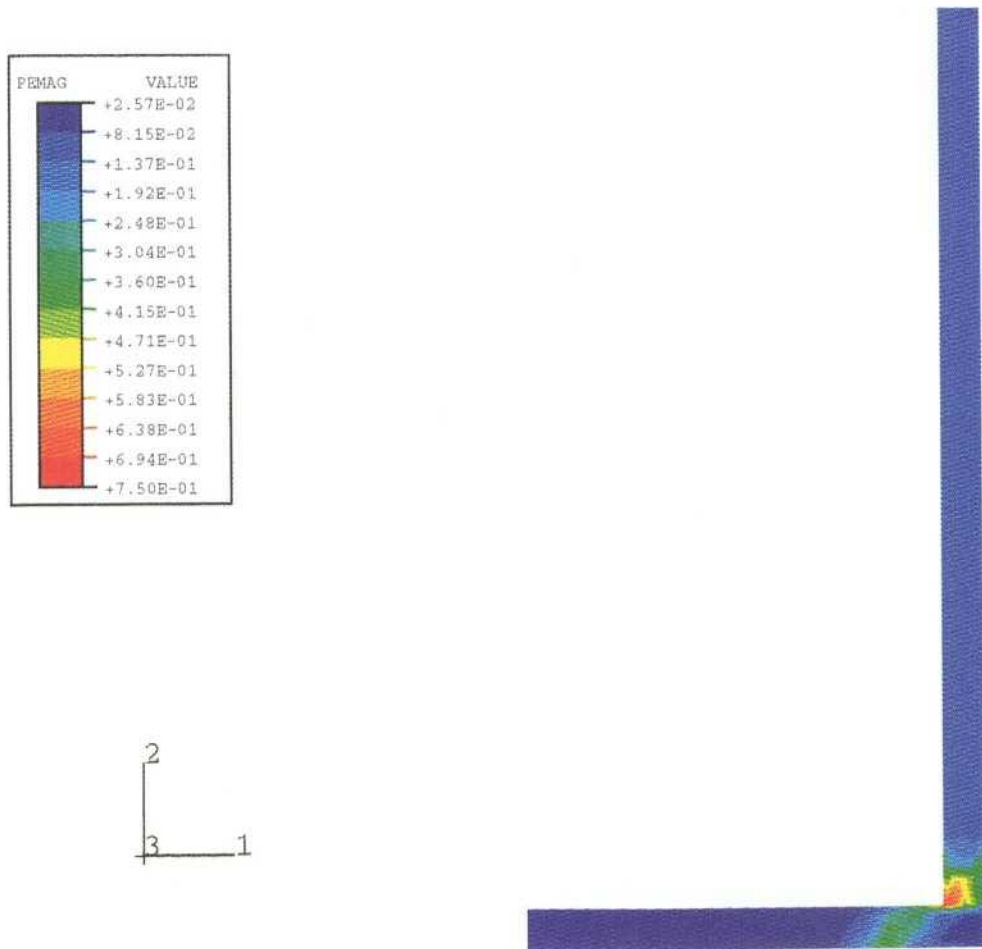


Figure 5-41: Mises stress in bentonite at load extracted from core model

*Figure 5-41. Mises stress in the bentonite for global corrosion scenario.*



*Figure 5-42. Maximum principal stresses in the rock for extreme global displacement.*



*Figure 5-43. Plastic strain in the copper overpack for extreme global displacement.*

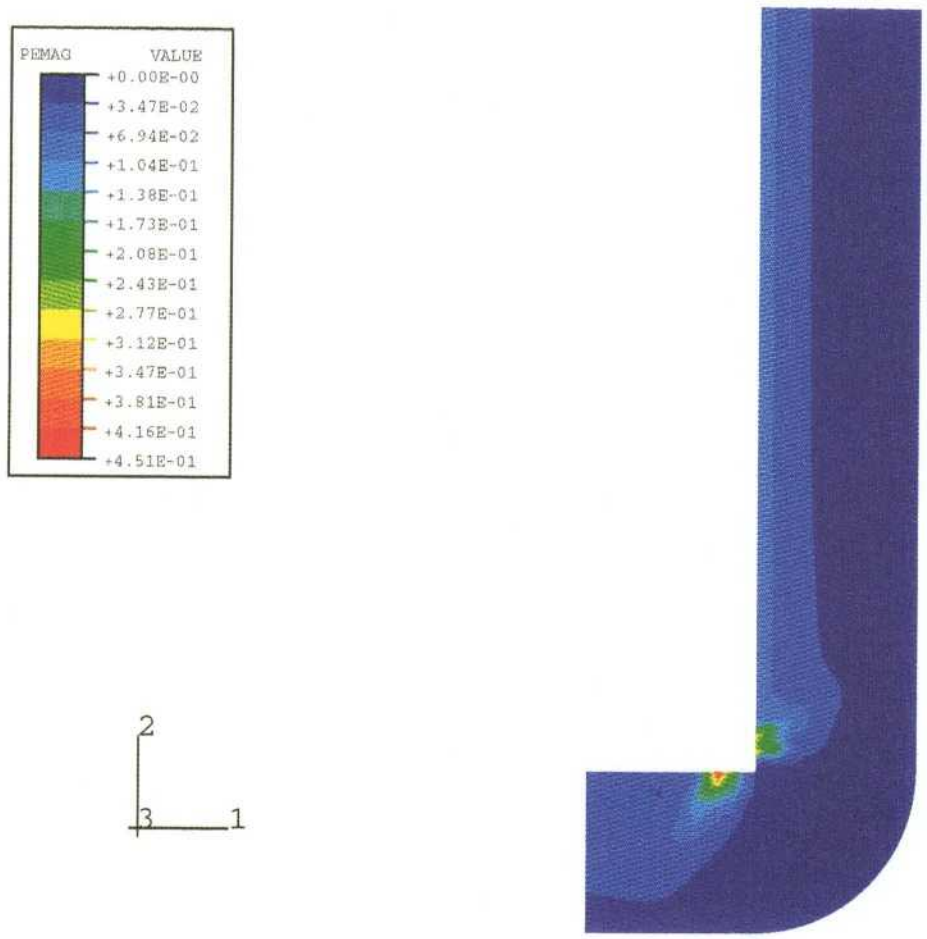
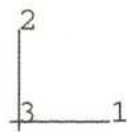
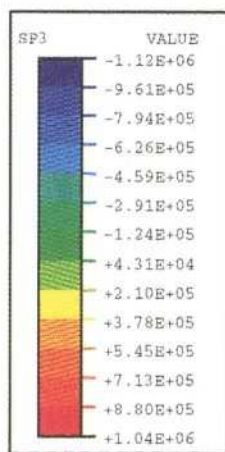
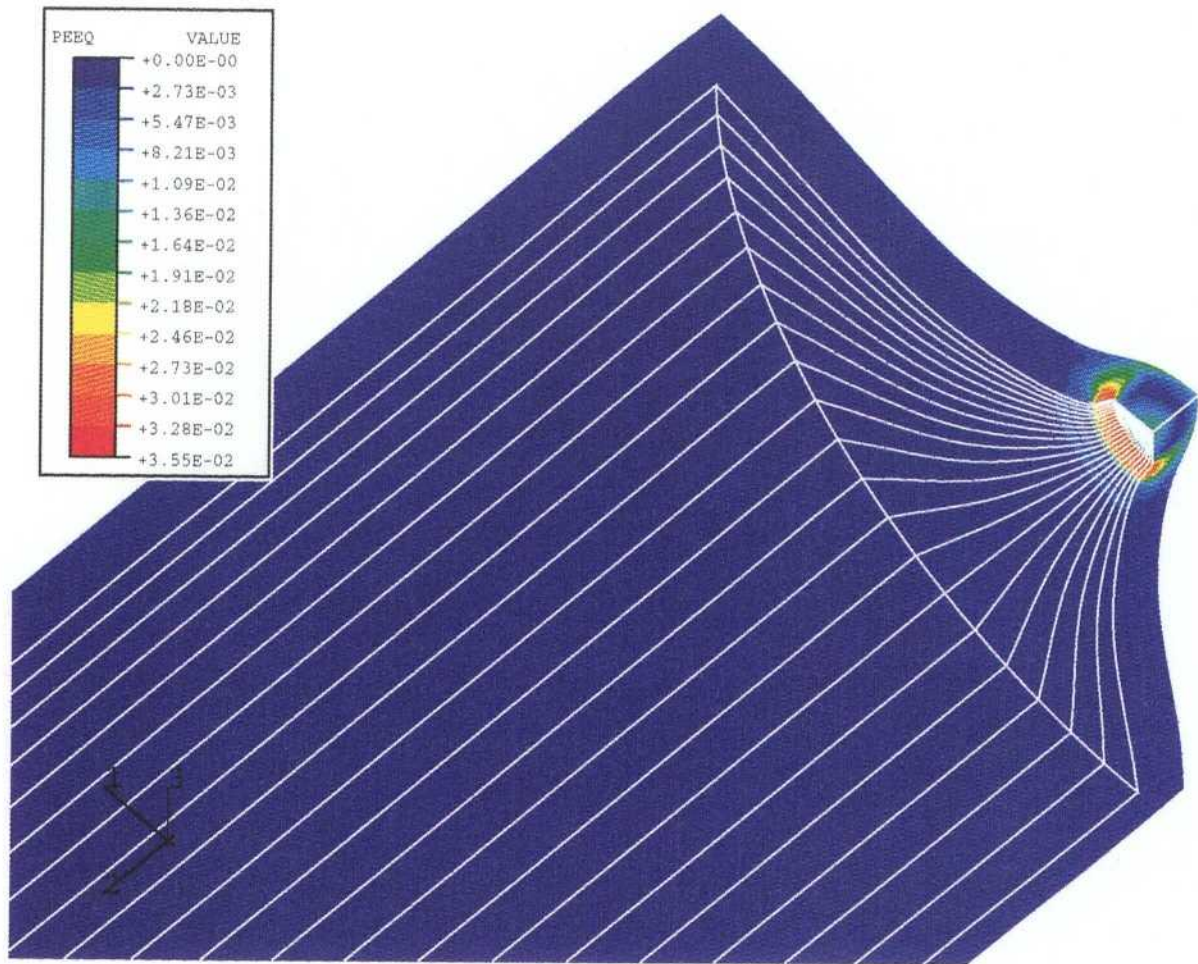


Figure 5-44: Plastic strain in bentonite at extreme global corrosion loadcase

*Figure 5-44. Plastic strain in the bentonite for extreme global displacement.*



*Figure 5-45. Maximum principal stresses in the rock for restricted corrosion scenario.*



*Figure 5-46. Plastic strain in the copper overpack for restricted corrosion scenario.*

## 5.8 CORROSION AT THE LID INTERFACE

### 5.8.1 Introduction

The finite element calculations performed so far were concerned with the effects of corrosion on the external surfaces of the canister. As such, they did not consider the lid fixing in detail. It is likely that corrosion will take place at the interface between the steel container and its lid, inducing bending stresses in the lid and tensile stresses in its fixing bolt. An issue is whether the build-up of stress can be sufficient to cause the lid fixing to fail, allowing the lid to come free and giving the groundwater access to the exposed fuel channels.

The design of the lid fixing is different for the BWR and PWR canister inserts. It is the BWR design, with its single central bolt, that is likely to produce the highest bending stresses in the lid and tensile stresses in its fixing bolt. For this reason, the calculations concentrated on this design.

Although a detailed finite element calculation was beyond the scope of this report, a series of analyses of the lid and its fixing arrangement were carried out to provide an indication of whether the lid is likely to come free. The analyses apply up to the time at which corrosion product has filled the annular gap; thereafter the copper overpack and bentonite backfill exert a force on the lid, and a detailed finite element analysis is needed to handle this interaction.

### 5.8.2 Results

The calculations to determine the bending stresses in the insert lid and the load on the central bolt are based on standard engineering equations /5-12/. The full calculations are presented as an annex (Appendix C) to this report.

The calculations show that the load on the central bolt is likely to be between  $10^5$  N and  $2.55 \cdot 10^5$  N, depending on the closeness of the fit of the lid in its recess. This is significantly below the proof load for the bolt, and failure is unlikely.

The combined bending stresses in the steel lid lie between 155.8MPa and 340.7MPa. Although the peak stress is above the yield stress for steel (200MPa), it remains sufficiently below the ultimate tensile strength (400MPa) that failure of the lid is unlikely at these deflection levels. An additional aspect to the problem is that as the lid bows, the lower corner of the lid will rotate and tend to dig into the side wall of the lid recess, thus restricting the flow of groundwater and reducing the rate at which corrosion product builds up.

## 6

# TIME SCALE FOR THE STRESS MODEL

### 6.1 INTRODUCTION

The work described in Section 5 calculates the stress distribution in a spent fuel disposal canister as a function of:

- the depth of steel that has been removed by corrosion;
- the type of corrosion, whether restricted or global.

A best estimate of the corrosion rate is  $0.1 \mu\text{m/year}$ , and this can be used to present the evolution of the canister as a function of time.

In order to provide a more complete description of the behaviour of the canister, two of the stress analyses had to be extended.

For the restricted corrosion scenario, the displacement of the annulus (due to the formation of corrosion product) was increased up to the point where local failure of the copper overpack occurs. Copper fails when the plastic strain reaches 29% (see Table 5-1). Since the defect geometry has little effect on the overall stress distribution (see Section 5.6) only the case of a circular penetration was considered.

The 'canister' model with compressible corrosion product was modified to use elastic-plastic properties for the copper instead of linear elastic properties. Also, 'upper bound' properties (see Section 5-4) were assumed for the corrosion product, since this generates the highest stresses (i.e. this choice leads to a conservative estimate of the canister life). The displacement load in the annulus was then increased until failure occurred.

### 6.2 RESULTS

Figure 6-1 depicts the sequence of events during the lifetime of a spent fuel disposal canister, in relation to its design life of  $10^5$  years. The Figure numbers identify contour plots that show the results of stress analyses at a particular time.

Initially it is assumed that there is a small penetration in the copper overpack, and restricted corrosion starts. The annular gap between the copper overpack and the inner container fills with corrosion product locally to the hole. This takes  $0.18 \cdot 10^5$  years, during which time no load is applied to the copper overpack. A 1000 years after the gap has filled, the copper

overpack starts to yield. The plastic strain distribution in the overpack is shown in Figures 6-2 and 6-3 (front and back views respectively). The greatest strain is around the penetration. Figures 6-4 and 6-5 show the corresponding Mises stress distribution.

After  $2.16 \cdot 10^5$  years (i.e.  $10^5$  years beyond the design life of the canister), the overpack in the region where the restricted corrosion is occurring reaches the strain to failure for copper, at which point a 'plug' of copper is detached from the overpack (Figures 6-6 to 6-9). This increase in the size of the penetration is accompanied by a change from restricted to global corrosion.

The rest of the annulus has to fill with corrosion product, which takes a further  $0.18 \cdot 10^5$  years, before any significant additional force is exerted on the copper overpack (it is recognised that in the region where the restricted corrosion was occurring, corrosion will continue and will expand the hole in the copper; however, this expansion is likely to be small)

During this period of global corrosion, the copper overpack starts to yield at its rim (i.e. at the joint between the lid and the rest of the overpack) after  $2.36 \cdot 10^5$  years, as shown in Figure 6-10. Compared to the results from the linear elastic model used in the earlier 'canister' analyses, there is a reduction in the stress concentration because of the introduction of plasticity (see Figure 6-11).

The lid fails after  $4.02 \cdot 10^5$  years, at which time 18.4 mm of corrosion product has built up. The plastic strain and Mises stress distributions are shown in Figures 6-12 and 6-13 respectively.

After  $7.16 \cdot 10^5$  years, the steel inner container has corroded through to its fuel channels. General yielding of the copper has occurred by this stage (see Figure 6-14), but the plastic strains (with the exception of those at the rim) are less than 20% so general failure has not occurred. General yielding of the bentonite, which acts as a buffer between the canister and the rock, has also occurred (Figure 6-15). The rock is mainly in a state of low compressive stress, and so is unlikely to fail. Tensile stresses in the rock are very localised, as shown in the plot of the maximum principal stresses (Figure 6-16).

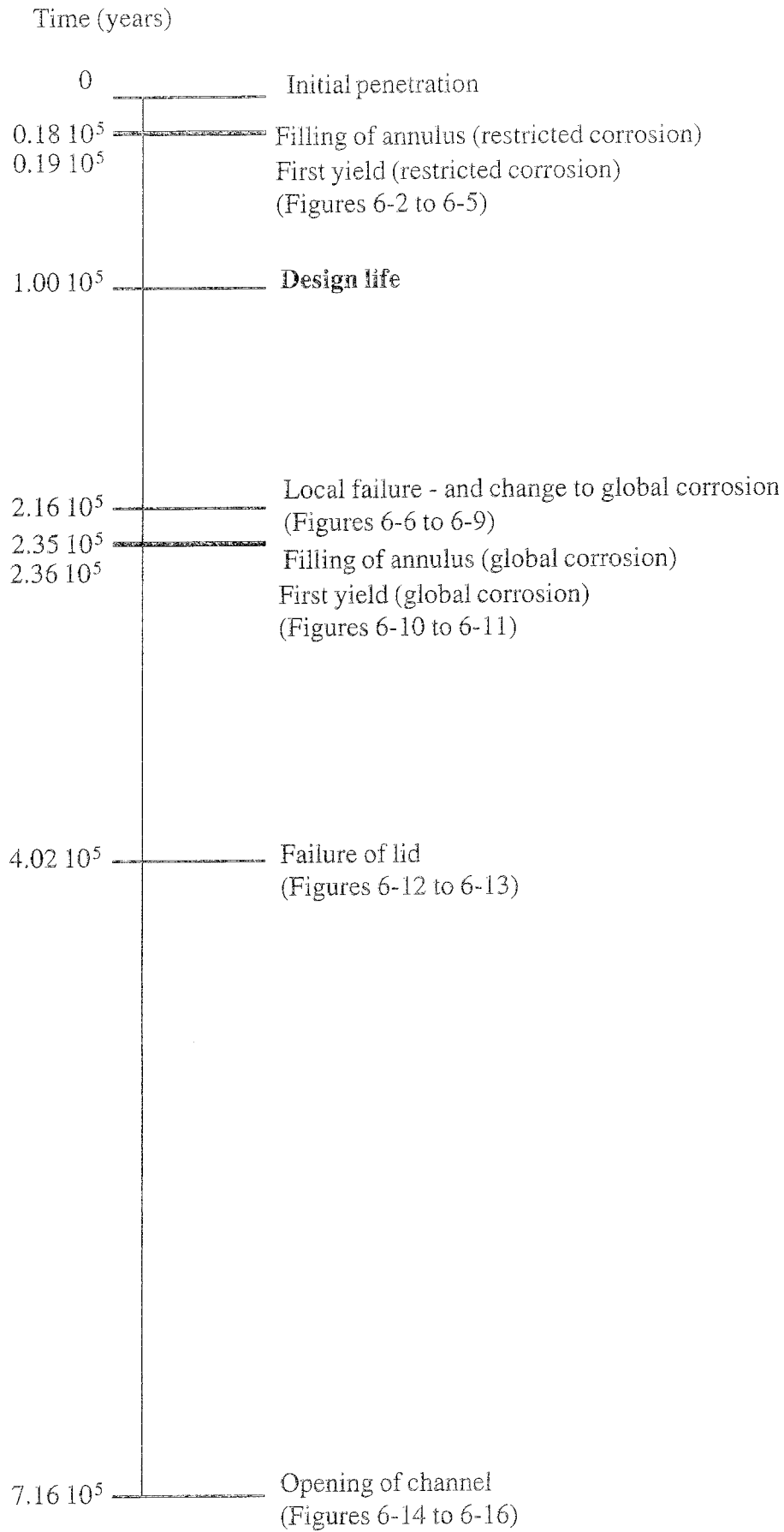


*Figure 6-1. Life history of a spent fuel disposal canister.*

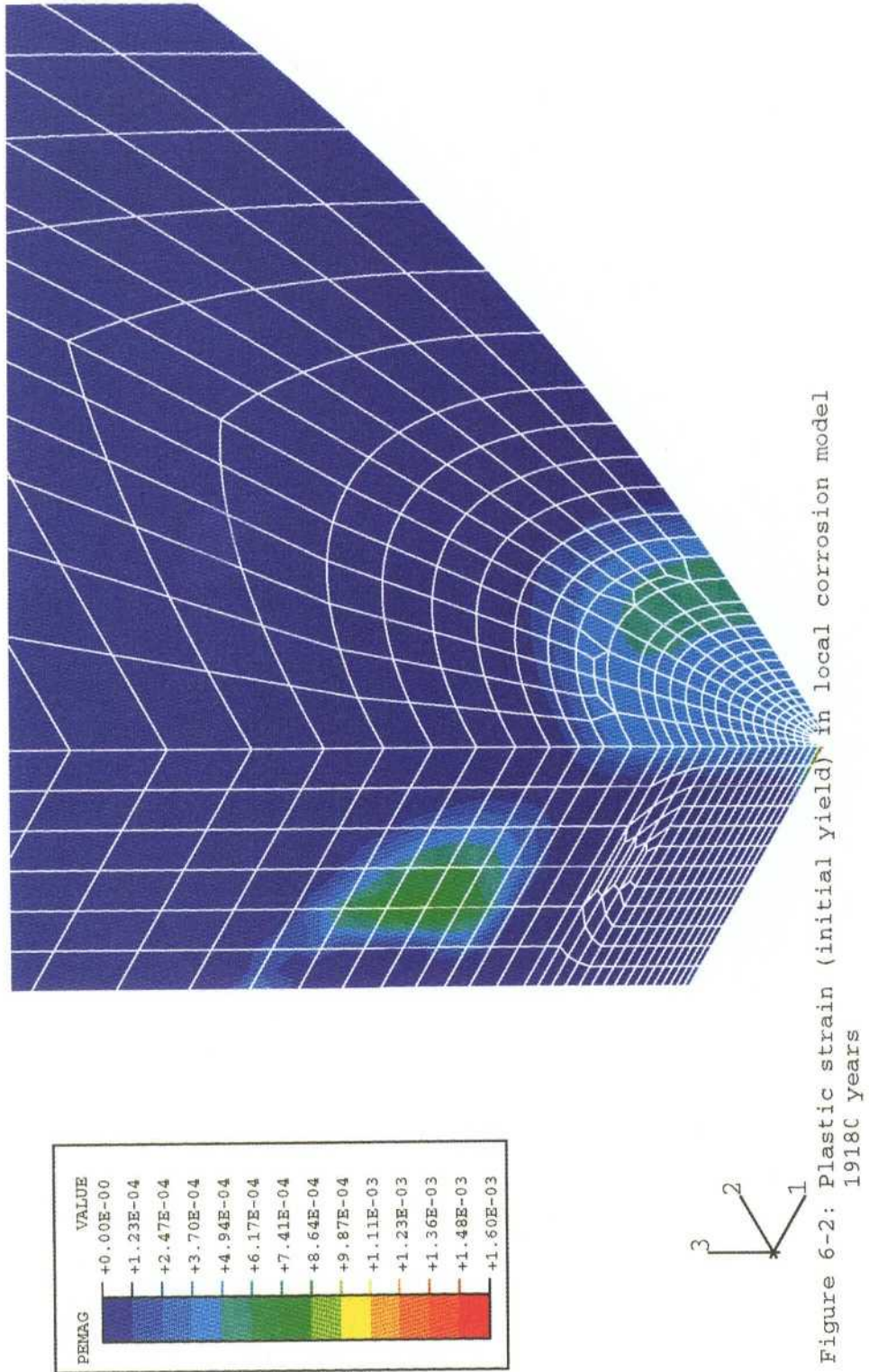


Figure 6-2: Plastic strain (initial yield) in local corrosion model 1918C years

Figure 6-2. Plastic strain in the copper overpack for restricted corrosion scenario (first yield).

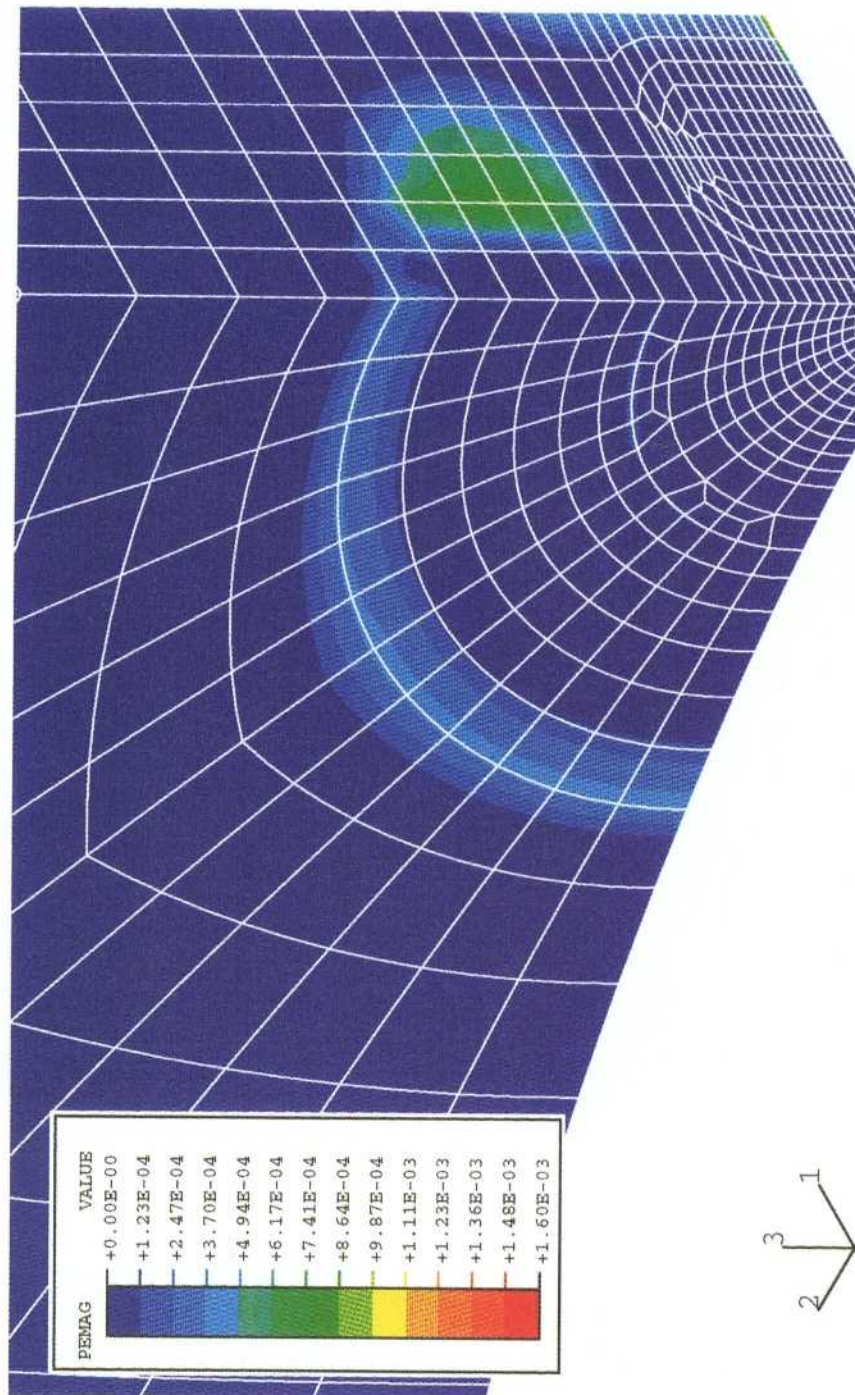


Figure 6-3: Plastic strain (initial yield) in local corrosion model (back view) 19180 years

Figure 6-3. Plastic strain in the copper overpack for restricted corrosion scenario (first yield).

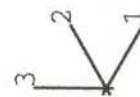
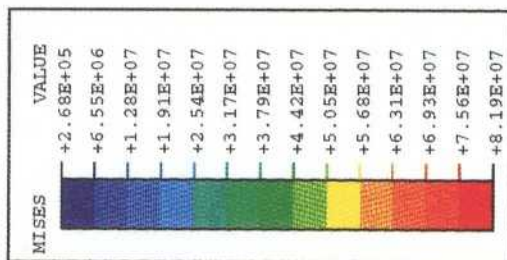
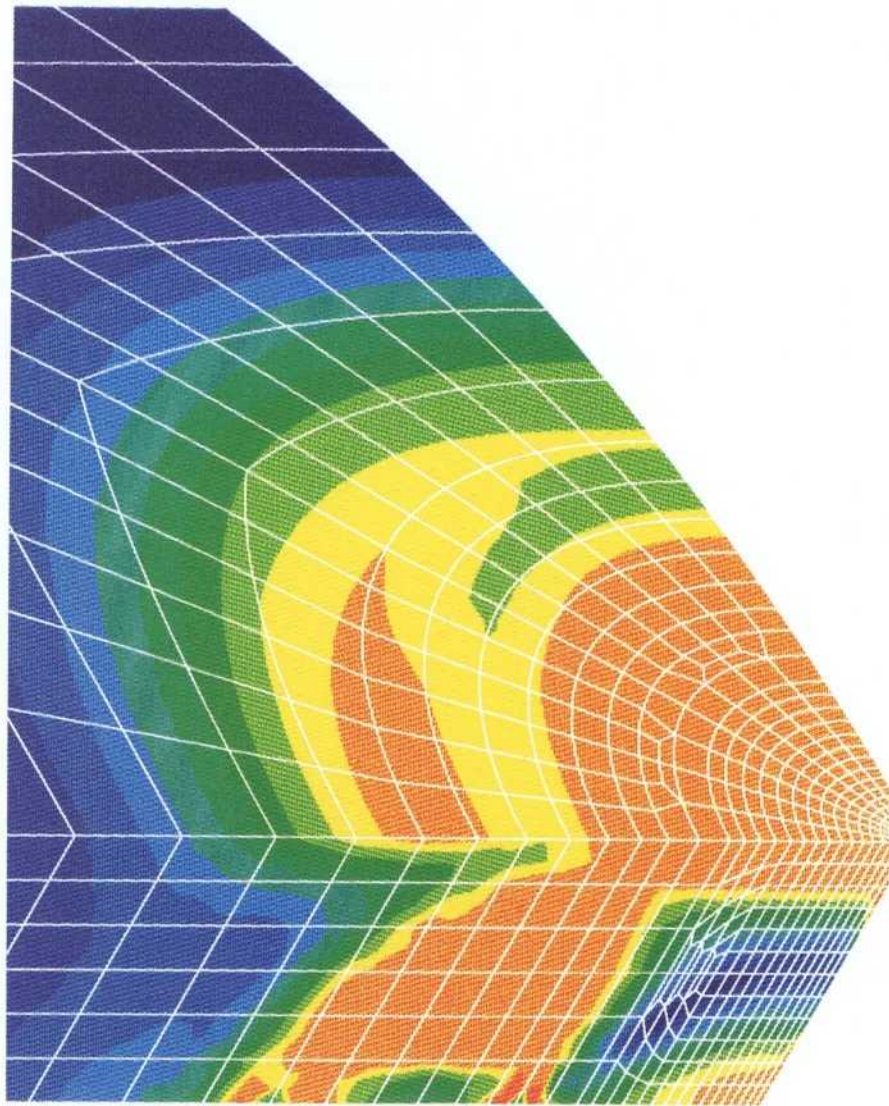


Figure 6-4: Von Mises stress (initial yield) in local corrosion model 19180 years

Figure 6-4. Mises stress in the copper overpack for restricted corrosion scenario (first yield).

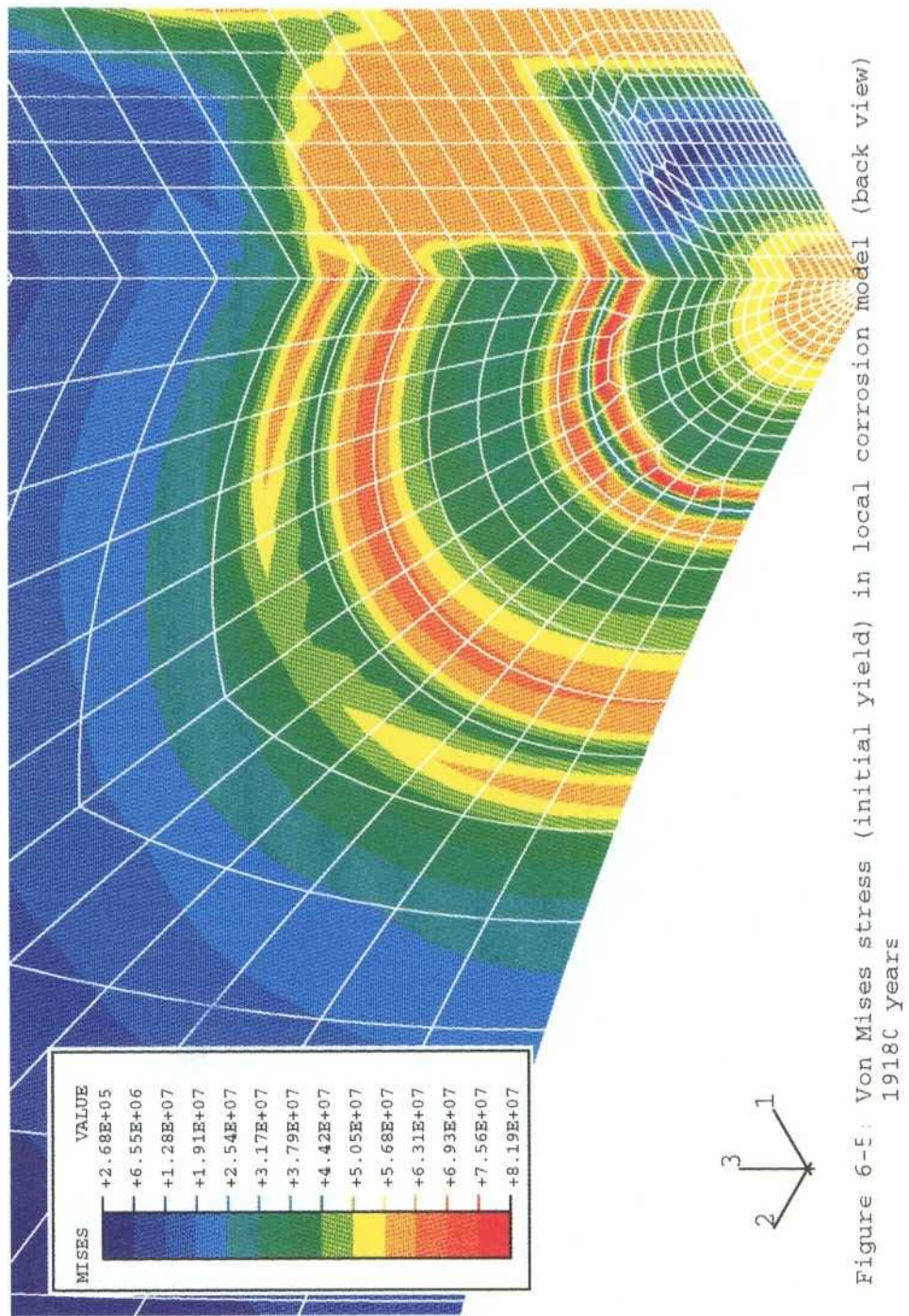


Figure 6-5: Von Mises stress (initial yield) in local corrosion model (back view) 19180 years

Figure 6-5. Mises stress in the copper overpack for restricted corrosion scenario (first yield).

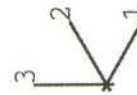
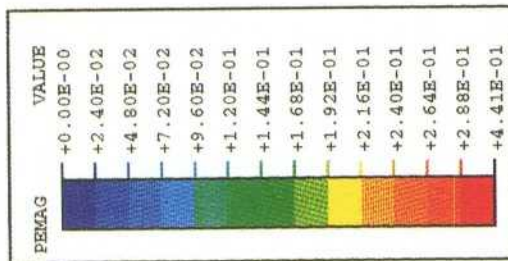
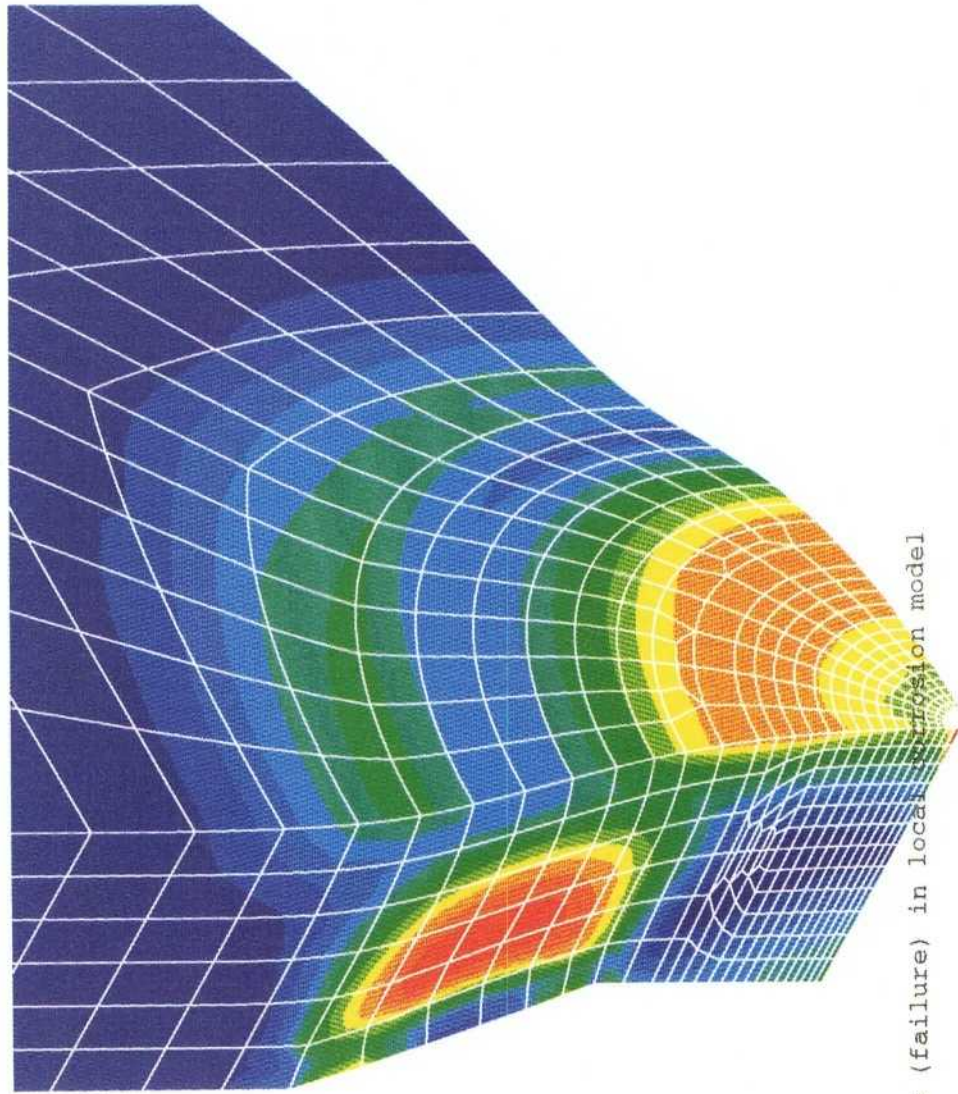


Figure 6-6: Plastic strain (failure) in local corrosion model  
216360 years

*Figure 6-6. Plastic strain in the copper overpack for restricted corrosion scenario (strain to failure).*

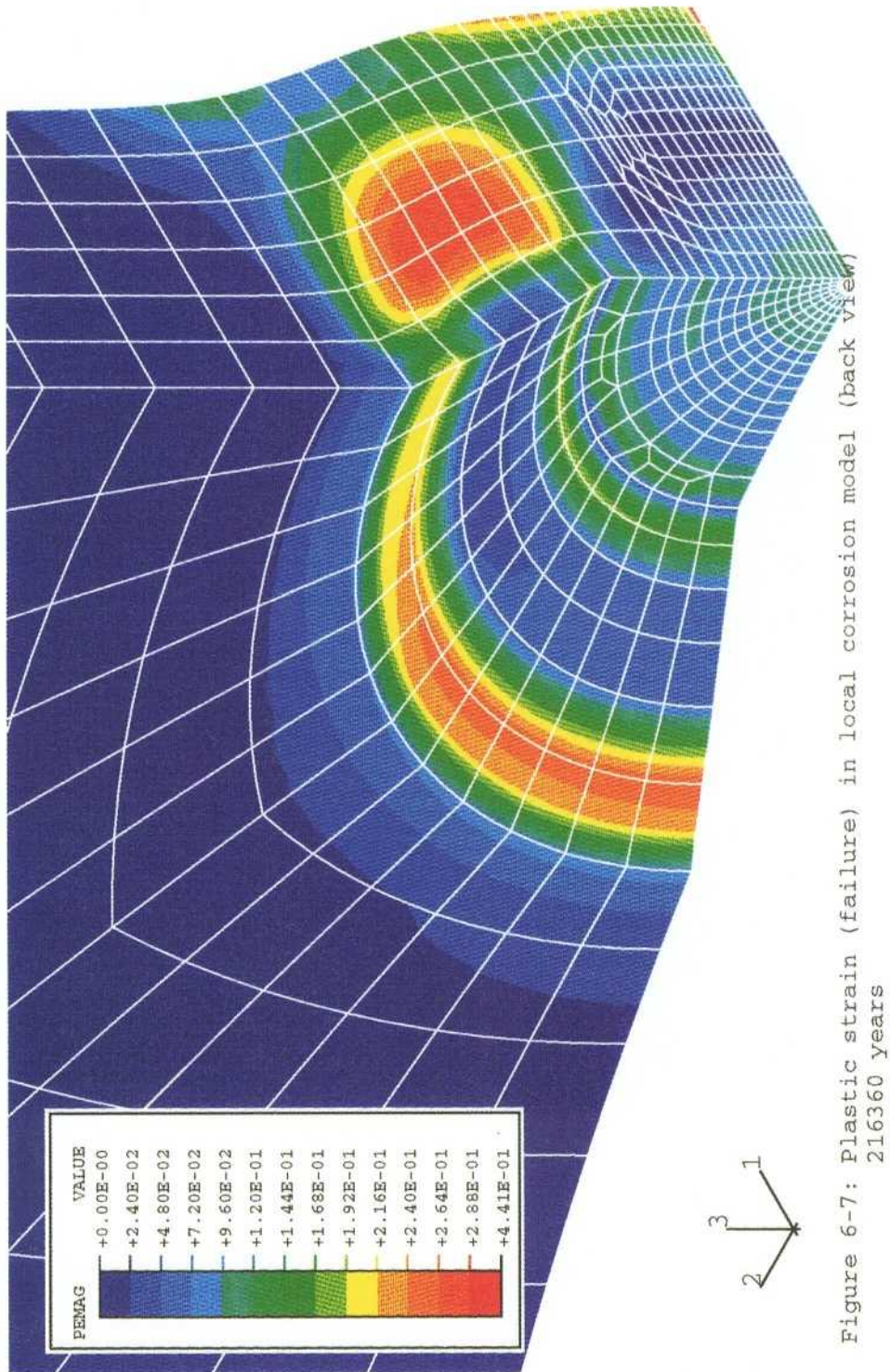


Figure 6-7: Plastic strain (failure) in local corrosion model (back view)  
216360 years

*Figure 6-7. Plastic strain in the copper overpack for restricted corrosion scenario (strain to failure).*

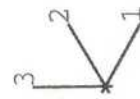
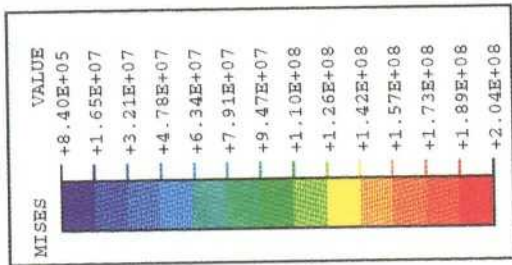
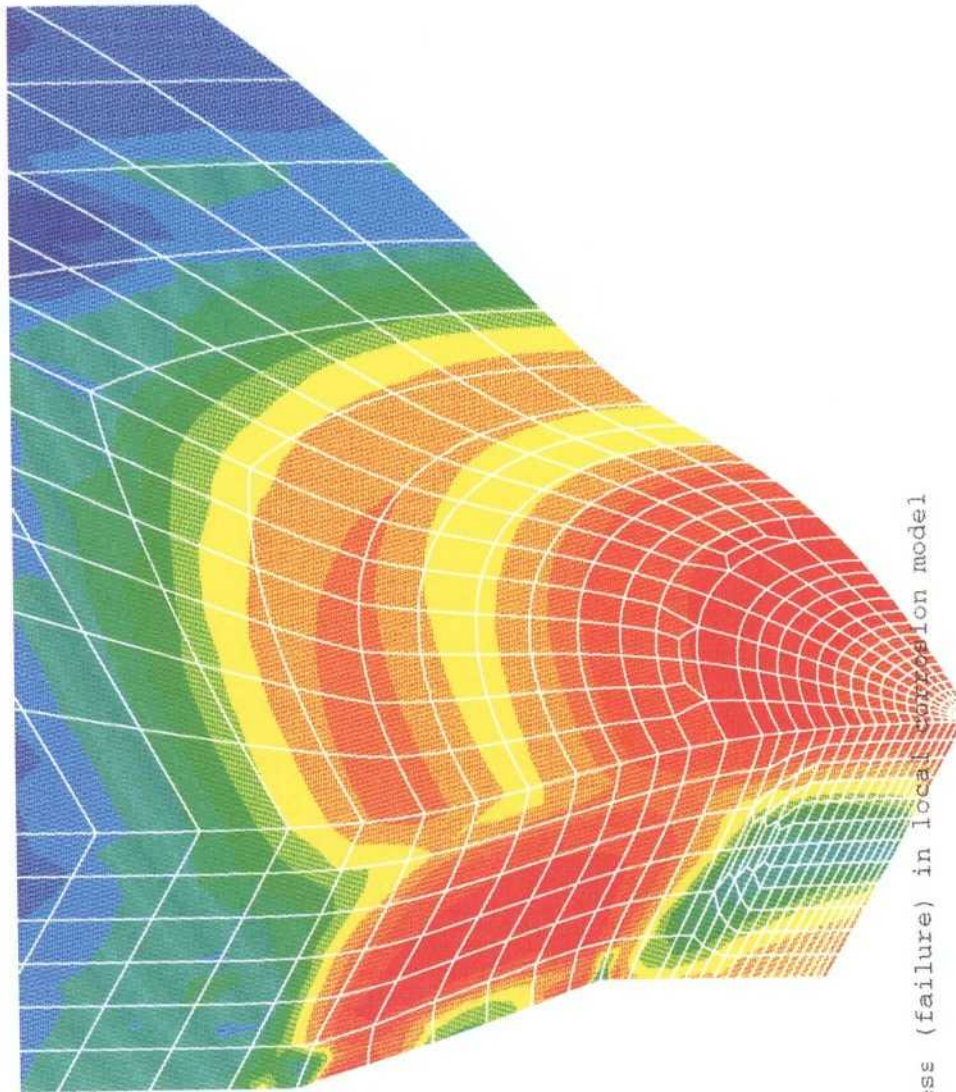


Figure 6-8: Von Mises stress (failure) in local corrosion model 216360 years

Figure 6-8. Mises stress in the copper overpack for restricted corrosion scenario (strain to failure).

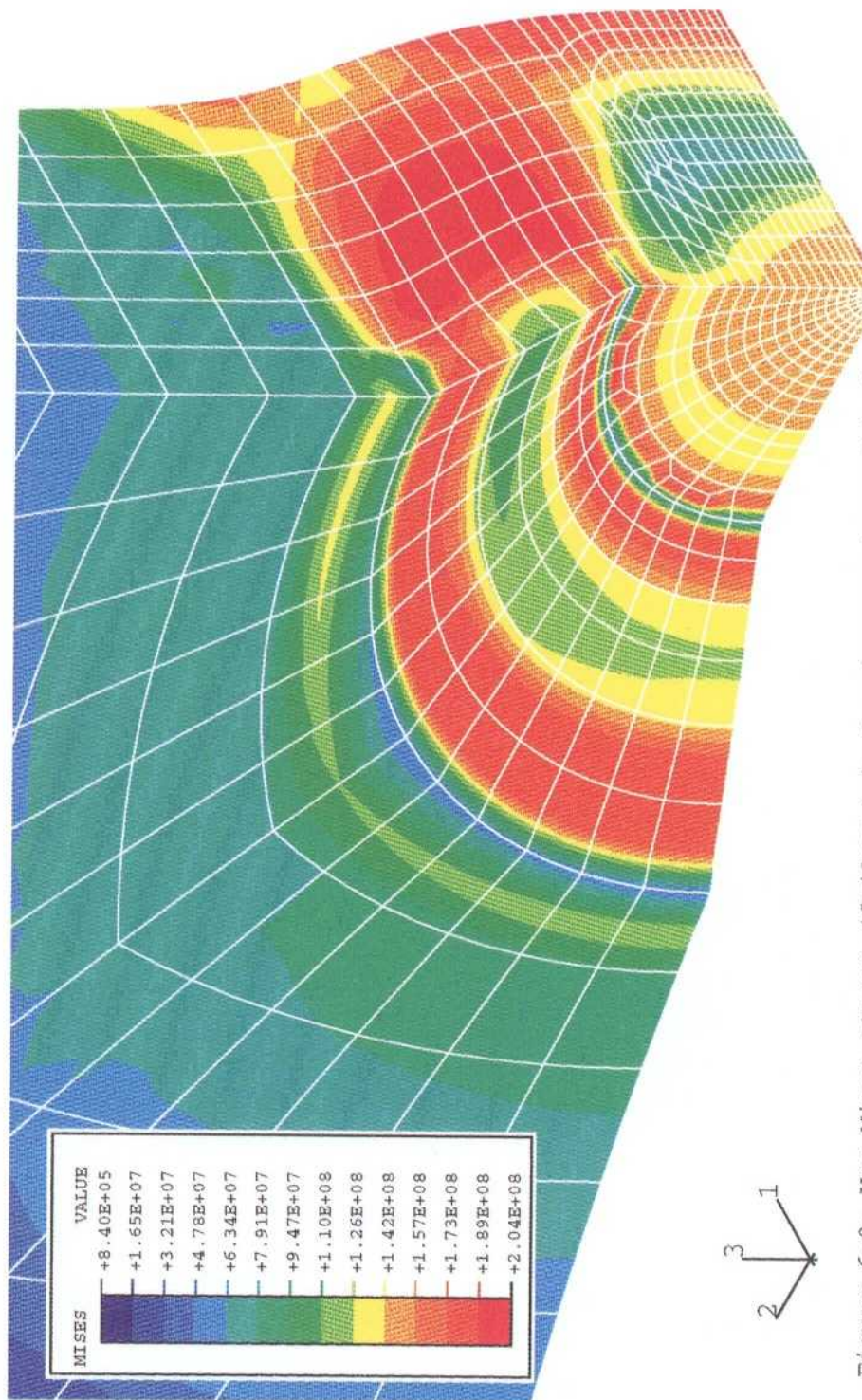


Figure 6-9: Von Mises stress (failure) in local corrosion model (back view) 216360 years

**Figure 6-9.** Mises stress in the copper overpack for restricted corrosion scenario (strain to failure).

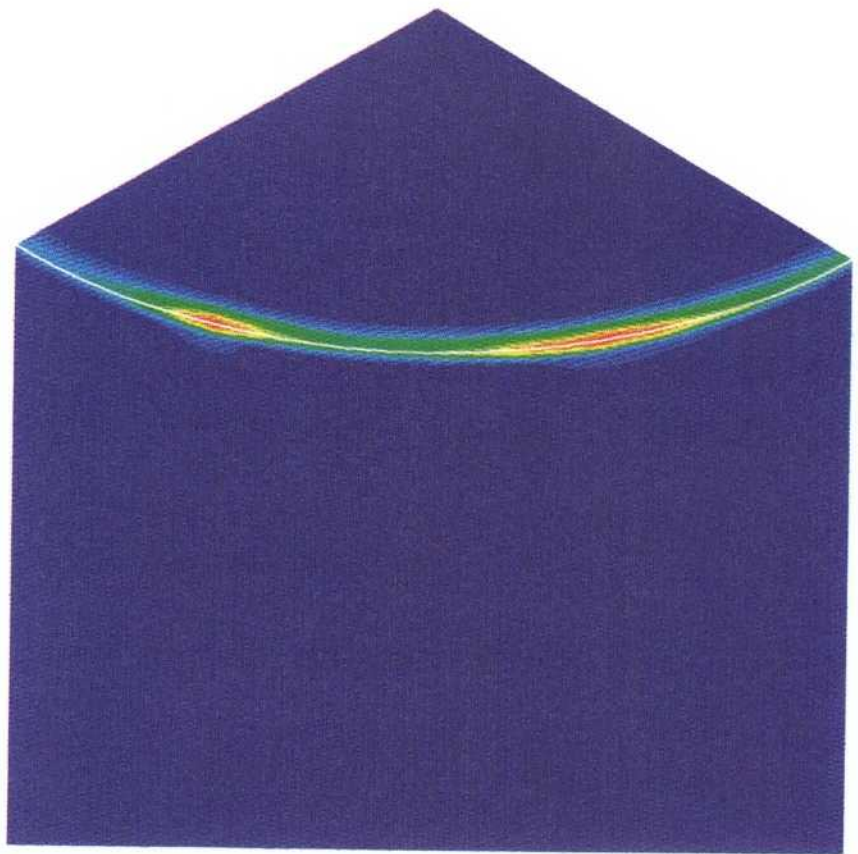
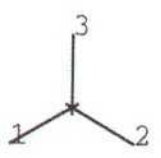
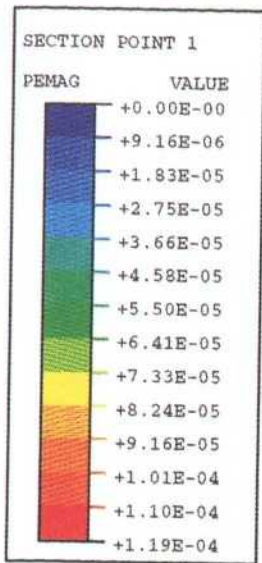


Figure 6-10: Plastic strain in copper jacket (initial yield)  
236050 Years

*Figure 6-10. Plastic strain in the copper overpack for global corrosion scenario (first yield).*

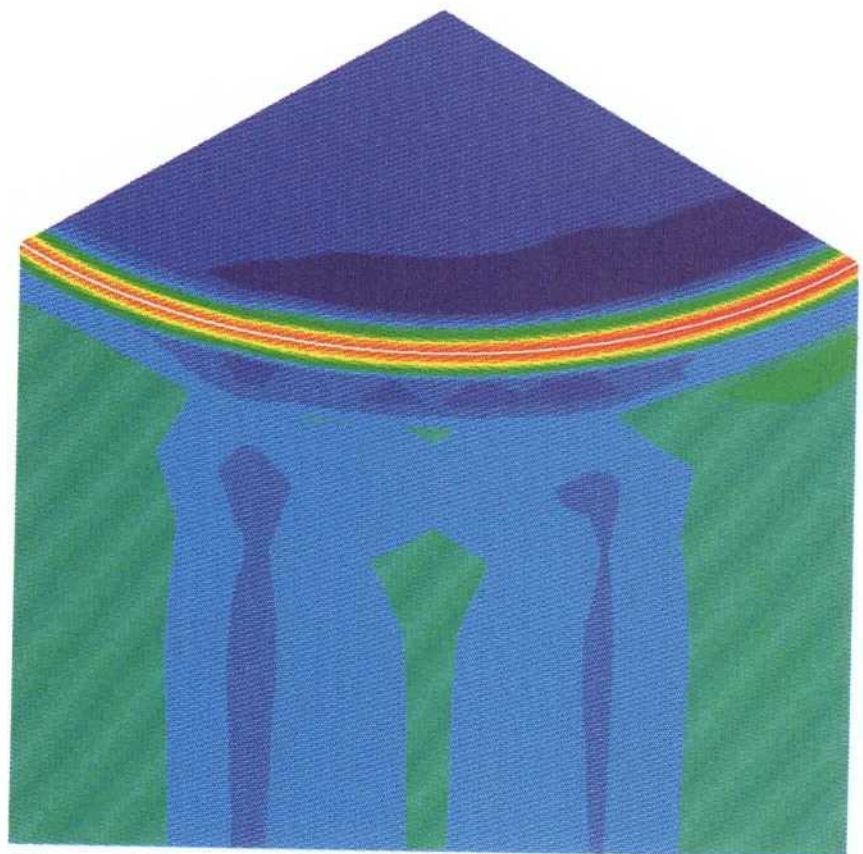
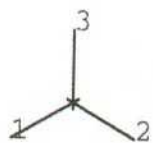
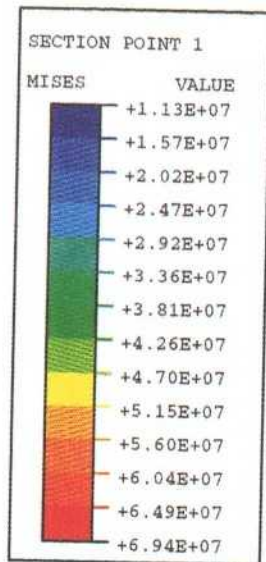


Figure 6-11: Von Mises stress in copper jacket (initial yield)  
236050 Years

*Figure 6-11. Mises stress in the copper overpack for global corrosion scenario (strain to failure).*

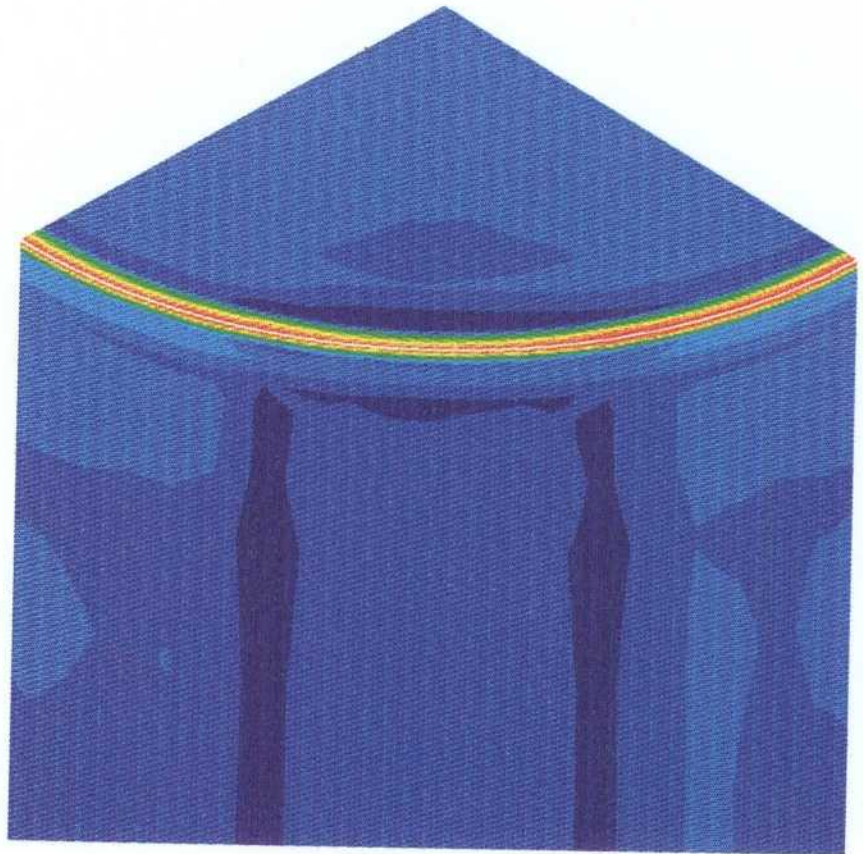
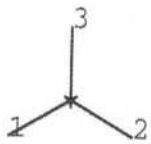
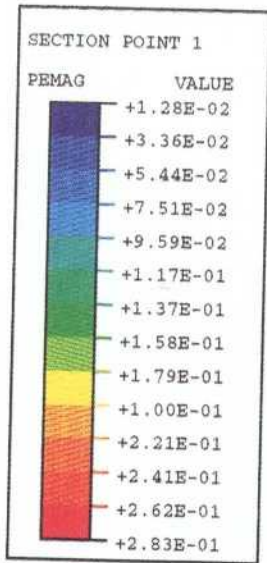


Figure 6-12: Plastic strain in copper jacket (failure of lid)  
401820 years

*Figure 6-12. Plastic strain in the copper overpack for global corrosion scenario (failure of the lid).*

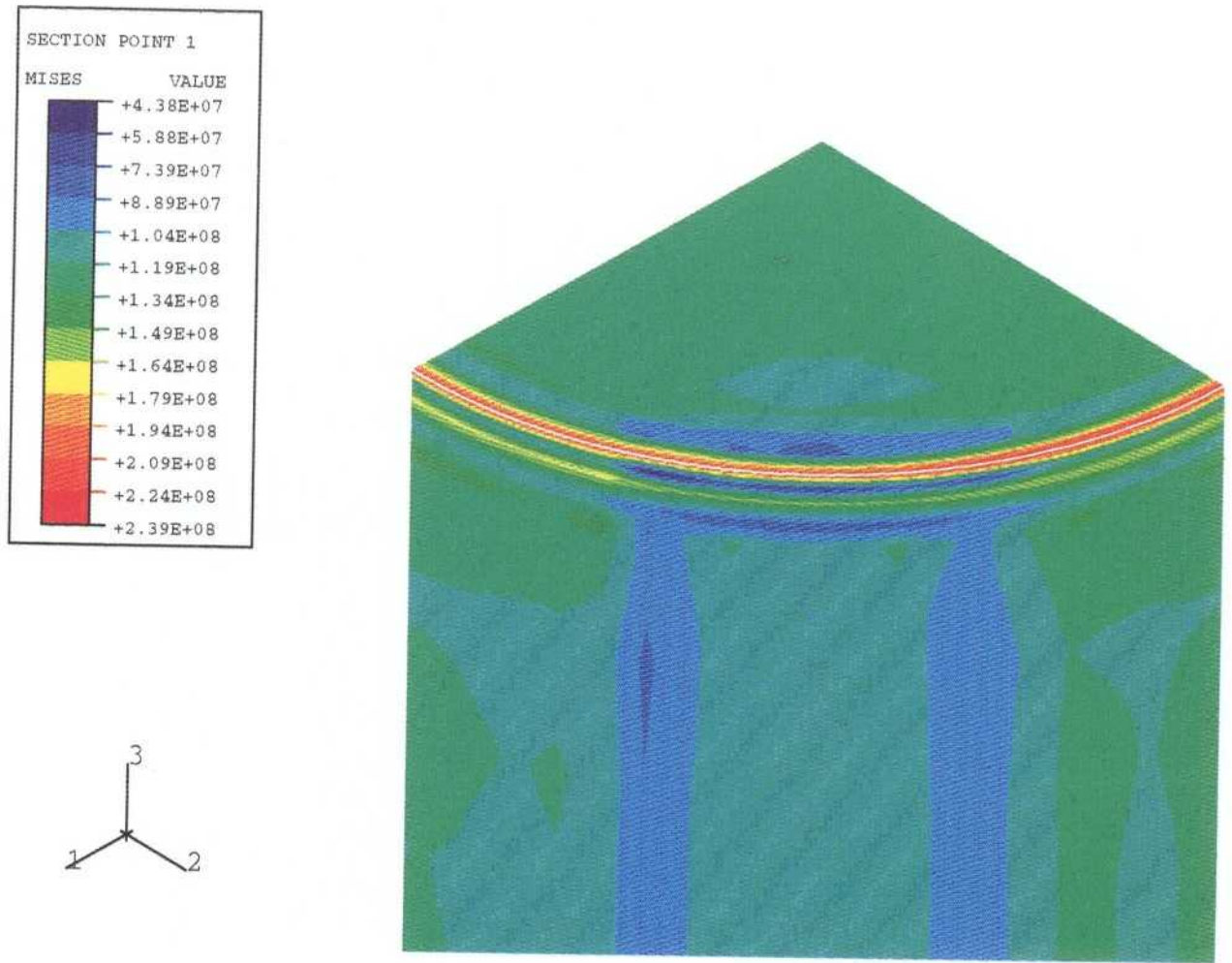


Figure 6-13: Von Mises stress in copper jacket (failure of lid)  
401820 years

*Figure 6-13. Mises stress in the copper overpack for global corrosion scenario (failure of the lid).*

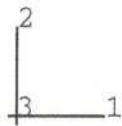
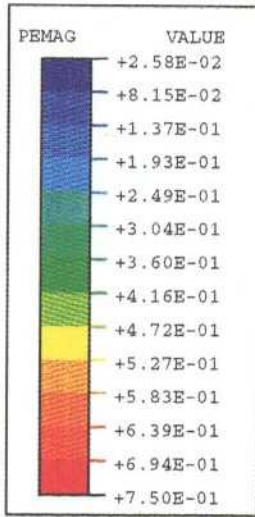


Figure 6-14 : Plastic strain in copper jacket for extreme global corrosion case 734550 years

*Figure 6-14. Plastic strain in the copper overpack for extreme corrosion scenario.*

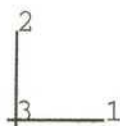
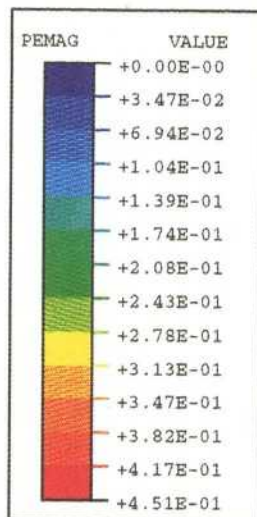


Figure 6-15: Plastic strain in bentonite for extreme global corrosion case 734550 years

*Figure 6-15. Plastic strain in the bentonite for extreme corrosion scenario.*

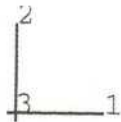
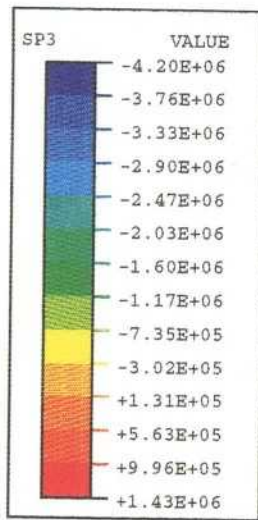


Figure 6-16: Maximum principal stress in rock for extreme global corrosion case 734550 years

*Figure 6-16. Maximum principal stresses in the rock for extreme corrosion scenario.*

A model has been developed for the inflow of water to a canister with a penetration in its copper overpack, resulting in anaerobic corrosion of the cast steel inner container and the generation of hydrogen. This model describes the interactions between the supply of water, corrosion, hydrogen production, pressure inside the canister and the flows of water and hydrogen.

Broadly, the sequence of events is as follows:

- Water flows into the annulus through the penetration in the copper overpack, causing anaerobic corrosion on the outer and inner surfaces of the inner container. This generates hydrogen which causes the pressure inside the canister to rise, thereby gradually reducing the rate of water inflow. Since water is being consumed by corrosion at an almost constant rate, the internal water inventory reaches a maximum and then declines. Depending on the hole size, the corrosion rate, and the height of the crack in the inner container, the water in the annulus may also spill over into the inner container.
- What happens next is determined by the maximum water inventory inside the canister, which depends mainly on the hole size and the corrosion rate. The distribution of water between the annulus and inner container is relatively unimportant. There are three possibilities:
  - (1) If the hole is so small that the initial (i.e. peak) rate of water ingress cannot match the corrosion rate, then there is no build-up of liquid water in the vessel. Corrosion proceeds at a rate limited by the supply of water, which decreases as the hydrogen pressure inside the canister rises. The internal pressure approaches the external pressure asymptotically from below, while the corrosion rate falls asymptotically to zero. No hydrogen escapes from the canister. Assuming a hole of circular cross-section, a simple calculation based on the rate of water supply that is required to support the postulated corrosion rate, shows that the hole radius is directly proportional to the corrosion rate and inversely proportional to the external pressure. At a corrosion rate of  $10^{-7}$  m/year and a pressure of 5MPa, the hole radius below which no water collects in the canister is calculated as 1.62 mm, corresponding to an area of  $8.25 \text{ mm}^2$ .
  - (2) If the hole is larger in comparison with the corrosion rate than in case (1), but still sufficiently small, there will be a build-up of liquid water inside the canister, but this water will be

completely consumed before the pressure inside the canister reaches the external pressure. After this, corrosion proceeds at a rate limited by the supply of water to the canister, which decreases as the internal pressure rises, as in case (1). Thus, as before, the internal pressure approaches the external pressure asymptotically from below, while the corrosion rate falls asymptotically to zero. Once again, no hydrogen escapes from the canister.

- (3) If the hole is sufficiently large in comparison with the corrosion rate, the hydrogen pressure inside the canister will reach the external pressure while there is still water left in the vessel. If the water level in the annulus is below the penetration in the copper overpack, hydrogen starts to escape, keeping the internal pressure constant and cutting off the external pressure-driven water supply. However, if the water level in the annulus is above the penetration, the pressure inside the canister rises further, and water is expelled until the water level in the annulus falls below the penetration. At this point the excess pressure is relieved, and hydrogen is vented. In both cases, once hydrogen is being expelled from the canister, corrosion proceeds as before until the water inventory inside the canister is exhausted. The total amount of hydrogen expelled from the canister is largely determined by the water inventory inside the canister at the point when hydrogen starts to escape.

The calculation halts when

- either the internal water inventory is exhausted, and diffusion suddenly becomes the sole means of water supply;
- or the annulus fills with corrosion residue.

After any liquid water in the canister has been consumed, corrosion of the steel container continues because water vapour can diffuse into the canister from outside. A numerical model of this diffusion limited corrosion process, which took into account:

- the change in size of the annular gap as corrosion progresses;
- possible suppression of the corrosion rate;
- the flow of hydrogen generated by the corrosion process;

was developed to predict the corrosion residue profile in the annulus. Suppression of the corrosion rate, characterised by a length scale of the order of  $1\ \mu\text{m}$ , has a considerable influence on the build-up of corrosion residue in the annulus.

The annular fitting gap between the cast steel inner container and the copper overpack eventually fills with magnetite ( $\text{Fe}_3\text{O}_4$ ). A set of finite element calculations has analysed the implications of the build-up of corrosion product for the structural integrity of the canister.

The analyses considered an extreme corrosion scenario, with corrosion occurring globally on the outer surface of the cast insert, and a more likely scenario, with corrosion restricted to a region around the initial defect. Additional aspects of the long-term behaviour of the canister that have been considered include: the influence of the initial defect geometry, and the effect of assuming more realistic mechanical properties for the corrosion product.

In the case of restricted corrosion, the stress analyses showed no loss of long term structural integrity of the canister. The copper overpack fails locally when the strain reaches 50%. This occurs at the edge of the region of corrosion product build-up, when the displacement in the copper overpack is 0.5 mm. At this point the groundwater gains access to the fuel channels in the cast insert, and corrosion starts to occur globally.

In the case of restricted corrosion, the geometry of the initial defect could have been important. The results of a stress analysis showed that, other than locally near the edge of the defect, plastic strains were low for both a circular hole and a longitudinal crack in the copper overpack. The stresses near the defect were not significantly larger than the stresses elsewhere, and so significant dilation of the hole is unlikely. The copper overpack is likely to fail locally near the edge of the region of corrosion product build-up, regardless of the geometry of the initial defect, and corrosion then starts to occur globally.

In the case of global corrosion, the inner container maintains its structural integrity for a displacement loading of at least 0.5 mm. For a displacement loading of 0.2 mm, stress concentrations in the rim of the copper overpack cause plasticity. The copper overpack yields more generally at a displacement loading of 0.25 mm. Despite this plasticity, the copper overpack is likely to remain intact until after the time at which corrosion of the inner container causes a breach of the fuel storage channels.

Allowing for compression of the corrosion product did not lead to a significant decrease in the stresses as compared with the previous study, which assumed that the corrosion product was rigid. The introduction of voids in the corrosion product resulted in a slight reduction in the maximum stresses in the inner container and the copper overpack. This reduction is small, about 1%, although using an extreme bound on the properties of the corrosion product did give a 10% reduction in the stresses in the copper overpack and in the inner container. Basing our estimate of the lifetime of the canister on the time at which the copper overpack begins to fail, thus

allowing the groundwater access to the fuel channels in the cast insert, we note that:

- the lifetime is unchanged if we assume that the corrosion product is compressible;
- the lifetime is a factor 1.03 greater if the corrosion product is assumed to have voids.
- the lifetime is a factor 1.1 greater if an extreme bound is used to define the properties of the corrosion product.

It is likely that corrosion will take place at the interface between the steel container and its lid, inducing bending stresses in the lid and tensile stresses in its fixing bolt. This build-up of stress could be sufficient to cause the lid fixing to fail, allowing the lid to come free and giving the groundwater access to the exposed fuel channels. Indeed, the assessment model assumes (conservatively) that there is a 1 mm wide crack in the inner container. A stress analysis showed that the central bolt fixing the lid of the BWR canister insert is likely to resist the loads induced by the build-up of corrosion product at the interface, at least until the point when the build-up of corrosion product on the external surface of the lid has started to exert a balancing force. The flow of groundwater through the fuel channels of the canister will be restricted. It is likely that the PWR canister design will be similarly satisfactory.

Finally, a previous study considered the effect on the repository of the expansion of the canister due to corrosion. The results of an analysis that assumed corrosion was occurring globally on the outer surface of the cast insert (a worst case), identified regions of the rock where cracks might initiate. Compression of the rock is unlikely to cause failure of the storage hole. Bentonite acts as an extremely efficient buffer for displacement loadings of up to 55mm (equivalent to corrosion of the entire thickness of steel to the fuel storage channels).

## REFERENCES

- 2-1 Werme L and Eriksson J**  
**March 1995**  
Copper Canister with Cast Inner Component: Amendment to Project on Alternative Systems Study (PASS)  
SKB Technical Report 95-02  
SKB Technical Report 93-04
- 2-2 Pusch R, Neretnieks I and Sellin P**  
**December 1991**  
Description of Transport Properties in a KBS-3 Type Repository  
SKB Technical Report 91-49
- 3-1 Blackwood D, Hoch A, Naish C, Rance A and Sharland S**  
**1994**  
Research on Corrosion Aspects of the Advanced Cold Process Canister  
SKB Technical Report 94-12
- 3-2 Bond A, Hoch A and Tomczyk A**  
**1996**  
Stresses in a Spent Fuel Disposal Canister  
AEAT-0510
- 3-3 Wikramaratna R, Goodfield M, Rodwell W, Nash P and Agg P**  
**November 1993**  
A Preliminary Assessment of Gas Migration from the Copper/Steel Canister  
SKB Technical Report 93-31
- 3-4 Henshaw J, Hoch A and Sharland S**  
**1990**  
Further Assessment Studies of the Advanced Cold Process Canister  
AEA-D&R-0060
- 3-5 Wikramaratna R**  
**May 1997**  
Private Communication.
- 5-1 Werme L**  
**March 1996**  
Private Communication.

- 5-2 Borgesson L**  
**July 1992**  
 Interaction between Rock, Bentonite Buffer and Canister  
 SKB Technical Report 92-30
- 5-3 Howatson A M, Lund P G and Todd J D**  
**1972**  
 Engineering Tables and Data  
 Chapman and Hall
- 5-4 Makurat A and Backer L**  
**September 1993**  
 DECOVALEX Test Case 1:2  
 AEA Technology
- 5-5 Werme L**  
**May 1996**  
 Private Communication.
- 5-6 Blackwood D, Naish C C, Platts N, Taylor K and Thomas M**  
**1993**  
 The Anaerobic Corrosion of Carbon Steel in Granitic Groundwaters  
 AEA InTec 1414
- 5-7 Nicholls J, Hall D and Tortorelli P**  
**1994**  
 Hardness and Modulus Measurement on Oxide Scales  
 Materials at High Temperatures, **12**, 141
- 5-8 Nagl M, Saunders S and Guttman V**  
**1994**  
 Experimental Data on Oxide Fracture  
 Materials at High Temperatures, **12**, 163
- 5-9 Nagl M, Evans W, Hall D and Saunders S**  
**1994**  
 An In Situ Investigation of the Tensile Failure of Oxide Scales  
 Oxidation of Metals, **42**, 431
- 5-10 Henshall R and Shaw K**  
**1975**  
 Crack Tip Finite Elements are Unnecessary  
 International Journal for Numerical Methods in Engineering, **9**, 495
- 5-11 Hibbitt, Karlsson and Sorenson**  
**1996**  
 ABAQUS/Standard Version 5.5 User's Manual, and Examples Manual

**5-12 Reark R and Young W**  
**1989**

Formulas for Stress and Strain (6th edition)  
McGraw Hill

**D-1 Platts N, Blackwood D and Naish C**  
**1994**

Anaerobic Oxidation of Carbon Steel in Granitic Groundwaters: a Review  
SKB Technical Report 94-01

# APPENDIX A

## A.1 SUMMARY OF MODEL OF HYDROGEN PRODUCTION

In the assessment model, the proposed spent fuel canister is represented as having an internal depth of 4.47m and an outer radius of 0.525m. It consists of a cast steel inner container of 0.473m radius inside a 50mm thick copper overpack. There is an annular gap of 2mm between the inner container and the overpack /2-1/. In the BWR canister type investigated here, the spent fuel is contained in 12 square section vertical channels of width 0.156m. On closure the remaining void volume in the inner container will be 0.4m<sup>3</sup>.

The canister is assumed to be buried in granite at a depth of 500m inside a vertical hole backfilled with compacted sodium bentonite to a thickness of 0.5m. The hydrostatic pressure of water at this depth is 5MPa, and in all the calculations involving water or hydrogen flow into or out of the canister this is taken as the effective external pressure. The bentonite swelling pressure of 5MPa is resisted by solid surfaces (the canister overpack and the surrounding granite) and plays no part in the flow processes of concern here.

As in previous corrosion studies /3-1/, the inner canister is assumed to be penetrated by a circumferential crack of width 1mm at height  $h_1$ ; this height is one of the key parameters in the model. However, by contrast we now assume the copper overpack to be penetrated by a hole rather than a circumferential crack. The reference value for the cross sectional area of the hole is 5mm<sup>2</sup>, in agreement with the value used in a recent stress analysis study /3-2/, but the effect of increasing the hole size is also investigated in the present model. A further model parameter is  $h_2$ , the height of the hole.

### A.1.1 Equations

The model is characterised by the following variables, which are functions of time only. A subscript, 1, is attached to variables associated with the inner canister, and 2 to variables associated with the annulus. Units of measurement are given in brackets:

- $hw_1(t)$  the water depth in the inner canister (m);

- $hw_2(t)$  the water depth in the annulus (m);
- $t_1(t)$  the net thickness of magnetite residue in the inner canister (m);
- $t_2(t)$  the net thickness of magnetite residue in the annulus (m);
- $n_i(t)$  the number of kilogram-moles of hydrogen in the canister;
- $n_e(t)$  the number of kilogram-moles of hydrogen expelled from the canister;
- $V_{hi}(t)$  the volume of hydrogen in the canister (m<sup>3</sup>);
- $p_i(t)$  the internal canister pressure (Pa).

Initially the pressures and hydrogen inventories in the inner canister and annulus were distinguished, but numerical checks showed that the internal transport processes were so rapid compared to the changes due to corrosion that within sensible timesteps for the computer model ( $\approx 1$  year) they could be treated as instantaneous, and the distinctions were dropped.

The interacting processes of corrosion, hydrogen production, pressure rise and the transport of hydrogen and water within the canister are described in terms of first order differential equations in time expressing mass balances for the water, hydrogen, iron and magnetite.

### **Growth of corrosion residue**

The equation for the growth of the magnetite layer in the inner canister is

$$\frac{dt_1}{dt} = 10^{-6} \gamma \mu_{mag} \quad \text{A-1}$$

where  $\gamma$  is a corrosion rate reduction factor ( $0 \leq \gamma \leq 1$ ), and  $\mu_{mag}$  is the effective growth rate (in microns/year) of the magnetite layer after taking account of the consumption of steel by corrosion. As long as there is liquid water in the canister,  $\gamma$  has the value 1.0; otherwise it takes a value determined by the ratio of the actual water supply rate and that required to support corrosion at the postulated rate. If the corrosion rate of steel is  $\mu$  (in microns/year),  $\mu_{mag}$  is given by

$$\mu_{mag} = \mu \left( \frac{\sigma_{mag} M_{mag}}{v_{mFe} \rho_{mag}} - 1 \right) \quad \text{A-2}$$

where  $\sigma_{mag} = 1/3$  is the stoichiometric ratio of magnetite with respect to iron in the anaerobic corrosion reaction (Equation 3-4),  $M_{mag} = 231.54$  is the relative molecular mass of magnetite,  $v_{mFe} = 7.105 \cdot 10^{-3} \text{ m}^3/\text{kg} \cdot \text{mol}$  is the kg-molar volume of iron, and  $\rho_{mag} = 5180 \text{ kg/m}^3$  is the density of magnetite. The expression in brackets in Equation A-2 has the value 1.097.

The corresponding equation for the growth of magnetite in the annulus is

$$\frac{dt_2}{dt} = 10^{-6} \gamma \mu_{mag} \frac{A_{w2}}{A_2} \quad \text{A-3}$$

where  $A_2$  is the area of the corroding surface in the annulus, and  $A_{w2}$  is an enhanced area which takes into account the increase in corrosion due to galvanic coupling below the water surface. Given a radius  $R_c = 0.473 \text{ m}$  for the inner canister, and an annulus height  $H = 4.47 \text{ m}$ , we have

$$A_2 = 2 \pi R_c H \quad \text{A-4}$$

and

$$A_{w2} = A_2 + 2 \pi R_c (\alpha - 1) h w_2 \quad \text{A-5}$$

where  $\alpha \approx 2.0$  is a galvanic enhancement factor.

### Water balance

The total liquid water inventory inside the canister is subject to the following balance equation

$$\frac{d}{dt} (A_{c1} h w_1 + A_{c2} h w_2) = Q_e - 10^{-6} \gamma \mu_w (A_1 + A_{w2}) \quad \text{A-6}$$

where  $A_{c1}$  and  $A_{c2}$  are the free cross-section areas of the inner canister and the annulus respectively,  $Q_e$  is the influx of water from outside the canister ( $\text{m}^3/\text{year}$ ),  $\mu_w$  is the rate of consumption of water by corrosion (microns/year), and  $A_1$  is the area of the corroding surface in the inner canister ( $\text{m}^2$ ).  $\mu_w$  is given by

$$\mu_w = \mu \frac{\sigma_w M_w}{v_{mFe} \rho_w} \quad \text{A-7}$$

where  $\sigma_w = 4/3$  is the stoichiometric ratio of water with respect to iron in the anaerobic corrosion reaction,  $M_w = 18.015$  is the relative molecular

mass of water, and  $\rho_w = 995.7 \text{ kg/m}^3$  is the density of water at  $30^\circ\text{C}$ . The influx of water is given by

$$Q_e = c_{sy} K^* (p_e - p_i) \quad \text{A-8}$$

where  $c_{sy} = 3.15576 \cdot 10^7 \text{ s}$  is the number of seconds in a year, the factor  $K^*$  is based on an analysis by Wikramaratna et al /3-3/ and is given by

$$K^* = \frac{2 \pi k r_h}{\eta_w} \quad \text{A-9}$$

$k = 10^{-20} \text{ m}^2$  is the permeability of the bentonite,  $r_h$  is the radius of the hole and  $\eta_w = 10^{-3} \text{ Pa s}$  is the dynamic viscosity of water.

Note that once the water inside the canister has dried out,  $\gamma$  is evaluated by setting the right-hand side of A-6 to zero.

In the computer code, apportionment of changes in the water inventory between the inner container and annulus is based on the following principles:

- inflowing water from outside the canister is initially assigned to the annulus;
- if the water level in the annulus reaches the circumferential crack in the inner container, any excess will spill over
- if the levels of water in both the annulus and inner container are above the circumferential crack, then the levels rise and fall together (i.e.  $hw_1 = hw_2$ ) subject only to Equation A-5. This state continues until one or other of the levels falls below the crack;
- if there is water in both the annulus and the inner container, then its consumption by corrosion is apportioned in such a way that the drop in water levels *from this cause alone* is the same in both regions (i.e. it is assumed that the corrosion process in general involves water vapour);

Except in the third case, the computer code works by updating either  $hw_1$  or  $hw_2$  first (whichever is the simplest), and then updating the other variable through the water balance Equation A-6. This approach ensures that water is conserved at every timestep, with the isolated exception of the point at which the inside of the canister dries out.

### Hydrogen production

The equation for hydrogen production is

$$\frac{d}{dt}(n_i + n_e) = \gamma \mu_h (A_1 + A_{w2}) \quad \text{A-10}$$

where

$$\mu_h = 10^{-6} \mu \frac{\sigma_h}{V_{mFe}} \quad \text{A-11}$$

$\sigma_h = 4/3$  is the stoichiometric ratio of hydrogen with respect to iron in the anaerobic corrosion reaction. Note that  $\mu_h$  has dimensions of  $\text{kg} \cdot \text{mol}/\text{m}^2/\text{year}$ . The internal volume of hydrogen,  $V_{hi}$ , is simply the volume occupied neither by water nor corrosion product, and the internal pressure is determined by the ideal gas law

$$p_i = \frac{n_i RT}{V_{hi}} \quad \text{A-12}$$

While  $p_i < p_e$  we set  $n_e = 0$ ; once the condition  $p_i \geq p_e$  has been reached, the internal pressure is kept practically constant and  $n_i$  is determined by  $V_{hi}$ . The balance of the hydrogen production calculated using Equation A-10 is assigned to  $n_e$  (this is a simplification of what actually occurs).

### A.1.2 The computer model and its solution

The computer model is based on the conceptual model of the corroding canister described in Equations A-1 to A-12. Starting from a reasonable set of initial values for the time-dependent variables, and using a timestep size  $\Delta t$  of order 1 year (which is short compared to the time for significant changes in the canister dimensions due to corrosion, but long compared to the time for internal mass transfer), the program updates each variable at each timestep according to the model equations.

There are choices as to how the updating should be done:

- should the values of variables on the ‘right-hand sides’ of the equations be taken from the previous timestep or from the current timestep (i.e. should the updating scheme be respectively explicit or implicit)? Since implicit schemes tend to be more stable than explicit schemes, we chose an implicit scheme. However, by their nature, implicit schemes require the updating scheme to be iterated (a process known as ‘inner iteration’) two or more times at each timestep in order to obtain convergence. There are several branches in the execution of the computer code; any condition which determines whether a branch is taken or not is evaluated using the values of variables at the end of the previous timestep (otherwise

switching between different conditions could occur in successive inner iterations, preventing convergence)

- in what order should the variables be updated? We chose to update the variables according to their sensitivity to the values of the remaining variables. Thus, magnetite thicknesses, which are nearly independent of the other variables, were updated first; followed by the depths of water; and then by the hydrogen volume, hydrogen inventory, and the pressure. This order in which to update the variables is believed to be the most stable.

### A.1.3 Comparison of time scales for corrosion and water vapour diffusion

It has been assumed in both Section 3 (on corrosion due to liquid water ingress) and in Section 4 (on diffusion-limited corrosion) that the transport of water vapour within the canister is practically instantaneous compared to the timesteps used in calculating the growth of magnetite on corroding surfaces, implying that the distributions of water vapour flux and water vapour density may, to a good approximation, be treated as steady-state. We now examine the validity of this assumption.

When liquid water is entering the canister and causing one or both internal water levels to rise, transport of the incoming water is controlled either by pressure forces or by gravity, and the assumption of instantaneous transport is justified. However when either the incoming liquid water evaporates completely as it enters the canister or the water supply is due mainly to vapour diffusing through the penetration we must assume for conservatism that there is no convective transport within the canister, i.e. diffusion is the only effective transport mechanism.

To assess the validity of assuming steady state conditions when the water supply is diffusion controlled we compare the time required for a change in corrosion radius to register in the  $\rho_2(r)$  profile against the timestep size.

In general, the outward diffusion of water vapour in the annulus competes with the consumption of water vapour by corrosion; the former process tends to increase the corrosion radius  $r_c$  and the latter to reduce it. When  $r_c$  is increasing diffusion is the dominant physical process, but when  $r_c$  is decreasing corrosion dominates. We therefore distinguish between the cases of increasing and decreasing  $r_c$ .

*For the case when  $r_c$  is increasing* we note that a typical relationship between the penetration distance  $x$  of a diffusion process and  $t$ , the time taken is

$$x^2 \sim 4Dt$$

A-13

where  $D$  is the diffusion constant. Hence the time interval required for an increase in penetration  $\Delta x$  is

$$\Delta t \sim \frac{x\Delta x}{2D} \tag{A-14}$$

Given that  $D \sim 9 \cdot 10^{-7} \text{ m}^2/\text{s}$  and that the largest increase in corrosion radius is always at the beginning of a calculation (i.e. when the initial water vapour distribution is set up), we use  $\Delta x = x = L + r_{ci}$  (where  $r_{ci}$  is the initial value of corrosion radius) in A-14 to estimate the maximum value of  $\Delta t$  required for each case and to compare this with the timestep size. The worst case is at the highest corrosion rate considered with no corrosion suppression ( $\mu = 25.845 \text{ microns/year}$  and  $l_s \rightarrow \infty$ ), for which the timestep is  $7.05 \cdot 10^{-4} \text{ year}$  and  $\Delta t$  from A-14 is  $8.1 \cdot 10^{-5} \text{ year}$ . In all other cases, the timestep is more than an order of magnitude larger than  $\Delta t$ . Hence the time scale for water vapour transport in the annulus appears to be negligibly small in comparison with the timestep.

*For the case when  $r_c$  is decreasing* the dominant process is the consumption of water vapour in the annulus by corrosion. The time constant for this  $t_c$  is approximately

$$t_c = \frac{\rho_2(r_c)h_g(r_c)}{S_c(r_c)} \tag{A-15}$$

An order of magnitude estimate of  $t_c$  is given by setting  $\rho_2(r_c) = \rho_{sv}$ ,  $h_g(r_c) = h_2$  and by assigning the unsuppressed corrosion flux to  $S_c(r_c)$ . For the worst case, corresponding to the maximum corrosion rate ( $\mu = 25.845 \text{ microns/year}$ ), this gives  $t_c \sim 7 \cdot 10^{-4} \text{ year}$ , comparable with the time step. However  $\rho_2(r_c)$  is zero, so even if a more realistic formula for  $t_c$  (say with  $\rho_2$  evaluated at a slightly smaller radius) is used instead of A-15, the value of  $t_c$  is clearly going to be much smaller than the figure quoted. Thus again the time scale for water vapour transport in the annulus appears to be negligibly small in comparison with the timestep.

*For the case when  $r_c$  is constant (or nearly constant)* the question of a time scale for the redistribution of water vapour does not arise.

In order to compare the time scales more rigorously, it is necessary to solve the full time-dependent diffusion equation for water vapour in the annulus (subject to a gap that varies with radius and time, and a corrosion radius that varies with time). This is beyond the scope of the present work. However, the above analysis is thought to justify the assumption of a quasi steady-state distribution of water vapour in the annulus for all the cases covered by our calculations.

## APPENDIX B

### B.1 MODEL OF DIFFUSION LIMITED CORROSION

#### B.1.1 Equations and solutions with no corrosion inhibition

The equation for the flow of water vapour through the penetration from outside (against the counterflow of hydrogen produced by corrosion) is simply that of constant flux  $F_1$  (kg/m<sup>2</sup> s). Assuming that  $x$  is measured upwards from the junction with the annulus, the flow is in the negative  $x$ -direction and is therefore given by

$$-F_1 = \rho_1 V_1 - D \frac{d\rho_1}{dx} \quad \text{B-1}$$

where the subscript 1 distinguishes quantities in the penetration from those in the annulus,  $\rho_1$  (kg/m<sup>3</sup>) is the water vapour density,  $V_1$  (m/s) is the outflowing hydrogen velocity and  $D$  (m<sup>2</sup>/s) is the diffusion coefficient of water vapour in hydrogen. The boundary condition at the outer end of the penetration ( $x = L$ ) is saturated vapour density, so  $\rho_1(L) = \rho_{sv}$ . Assuming that the corrosion reaction is



the molar fluxes of water vapour and hydrogen are equal and opposite. Combining this fact with the ideal gas law for hydrogen then leads to

$$V_1 = \frac{F_1}{\rho_F} \quad \text{B-3}$$

where  $\rho_F \equiv \frac{p_e M_w}{RT}$  has the dimensions of a density (kg/m<sup>3</sup>). At an external pressure  $p_e$  of 10 MPa,  $\rho_F$  has the value 71.48 kg/m<sup>3</sup> which is more than 3 orders of magnitude larger than  $\rho_{sv}$ . Combining B-3 with B-1 and integrating gives

$$\rho_1(x) = \rho_F \left[ \left( 1 + \frac{\rho_{sv}}{\rho_F} \right) \exp \left\{ \frac{F_1(x-L)}{D\rho_F} \right\} - 1 \right] \quad \text{B-4}$$

whence the density at the junction is

$$\rho_{10} \equiv \rho_1(0) = \rho_F \left[ \left( 1 + \frac{\rho_{sv}}{\rho_F} \right) \exp \left\{ \frac{-F_1 L}{D \rho_F} \right\} - 1 \right] \quad \text{B-5}$$

Note that B-5 allows us to define a maximum possible value of  $F_1$  corresponding to the limit  $\rho_{10} = 0$ ; thus

$$\max F_1 = \frac{D \rho_F}{L} \ln \left( 1 + \frac{\rho_{sv}}{\rho_F} \right) \quad \text{B-6}$$

which evaluates to  $5.536 \cdot 10^{-7} \text{ kg/m}^2 \text{ s}$  for  $L = 0.05 \text{ m}$  (cf. equation A-20).

The expression for the outward flux of water vapour in the annulus is similar to B-1, namely

$$F_2 = \rho_2 V_2 - D \frac{d\rho_2}{dr} \quad \text{B-7}$$

In the annulus the water vapour mass balance includes a sink term describing the consumption of water vapour by corrosion. If the corrosion rate of iron in the inner canister is  $\mu$  microns/year, the corresponding water vapour flux  $S_c$  ( $\text{kg/m}^2 \text{ s}$ ) is

$$S_c = \frac{10^{-6} \mu \sigma_w M_w}{V_{mFe} S_y} \quad \text{B-8}$$

where all quantities have been defined previously (see Appendix A.1) except for  $S_y$ , the number of seconds in a year. If  $\mu$  is 1 micron/year,  $S_c$  has the value  $1.071 \cdot 10^{-10} \text{ kg/m}^2 \text{ s}$ . The corrosion rate parameter  $\Lambda$  ( $\text{m}^{-1}$ ), defined in Section 5.2.5, may be written in terms of  $S_c$ :

$$\Lambda = \frac{S_c}{\rho_{sv} D} \quad \text{B-9}$$

B-7 and B-8 imply an upper limit on the corrosion radius  $r_c$ , since the water vapour mass balance requires that the ratio  $F_1/S_c$  must equal the ratio of the total corroding area to the penetration area, i.e.  $r_c^2/r_0^2$  where  $r_0$  is the radius of the penetration. Thus, if the penetration has the standard area  $5 \text{ mm}^2$  so that  $r_0 = 1.26 \text{ mm}$ , the upper limit on  $r_c$  is  $90.7 \text{ mm}$  assuming a uniform corrosion rate of 1 micron/year. This upper limit on  $r_c$  is proportional to  $r_0/\mu^{0.5}$  (cf. the discussion in Section 4-5).

In order to write down the water vapour mass balance equation for the annulus, we also define the quantities  $h_a$  (m) for the size of the uncorroded annular gap (a constant throughout the calculations) and  $h_g(r, t)$  (m) for the size of the gap as a function of radius and time. If  $t_2(r, t)$  (m) is the net thickness of corrosion residue defined in Appendix A.1 then clearly

$$h_g = h_a - t_2 \quad \text{B-10}$$

at all  $r$  and  $t$ . Water vapour mass balance is therefore expressed by

$$\frac{1}{r} \frac{d}{dr} (rF_2) = -\frac{S_c}{h_g} \quad \text{B-11}$$

The boundary condition on the flux at the junction with the penetration is again based on water vapour mass balance, and is given by

$$F_{20} = \frac{r_0}{2h_{g0}} (F_1 - S_c) \quad \text{B-12}$$

where  $F_{20}$  is the value of  $F_2$  and  $h_{g0}$  is the annular gap at radius  $r_0$ , i.e. at the junction. If the gap is constant from radius  $r_0$  to radius  $r$ , then B-11 may be integrated subject to B-12 to give

$$F_2(r) = \frac{r_0 F_{20}}{r} - \frac{S_c}{2h_g} \left( r - \frac{r_0^2}{r} \right) \quad \text{B-13}$$

Finally, in order to obtain the water vapour density  $\rho_2$  as a function of radius we note that, in the same way as for the penetration (cf. equation B-2),

$$V_2(r) = -\frac{F_2(r)}{\rho_F} \quad \text{B-14}$$

and using this in B-7, rearranging and integrating we obtain, again assuming that the gap is constant over the radius interval of interest,

$$\rho_2(r) = \rho_J + \left( 1 - \frac{\rho_J}{\rho_F} \right) \frac{1}{4Dh_g} \left[ S_c (r^2 - r_0^2) - 2r_0^2 F_1 \ln \left( \frac{r}{r_0} \right) \right] \quad \text{B-15}$$

where  $\rho_J \equiv \rho_{10}$  is the density at the junction, which assumes continuity of density there. Note that this formula is approximate, being correct to order  $(\rho_J/\rho_F)$ , which is better than about  $4 \cdot 10^{-4}$ .

### B.1.2 Finding the flux and the corrosion radius

Since  $G_2 \equiv rF_2$  has the derivative properties  $dG_2/dr < 0$  and  $d^2G_2/dr^2 < 0$  (see B-11), there must be a finite radius at which  $G_2$  and hence  $F_2$  are zero. We note from B-14 that  $V_2 = 0$  and hence from B-7 that  $d\rho_2/dr = 0$  at the same point. We identify this point with the corrosion radius  $r_c$ . On physical grounds  $\rho_2$  must also fall to zero at this radius, and the solutions for  $F_2$  in B-13 and  $\rho_2$  in B-15 only apply up to  $r_c$ ; beyond this there is no corrosion taking place and all variables fall to zero.

The values of  $r_c$  and  $F_1$ , which are not known a priori, can be determined simultaneously by setting  $F_2(r_c) = 0$  in B-13 and  $\rho_2(r_c) = 0$  in B-15. The first of these gives

$$F_1 r_0^2 = S_c r_c^2 \quad \text{B-16}$$

Thus we write  $q \equiv F_1/S_c = (r_c/r_0)^2$  and substitute into the density condition which gives

$$\rho_J + \left(1 - \frac{\rho_J}{\rho_F}\right) \frac{S_c r_0^2}{4Dh_g} [q - 1 - q \ln(q)] = 0 \quad \text{B-17}$$

We may introduce dimensionless numbers  $Na, Nb, Nc$ :

$$Na \equiv \frac{4h_g D \rho_F}{r_0^2 S_c}, \quad Nb \equiv 1 - \frac{\rho_{sv}}{\rho_F}, \quad Nc \equiv \frac{S_c L}{D \rho_F} \quad \text{B-18}$$

whence

$$\rho_J = \rho_F (1 - Nb \exp(Nc q)) \quad \text{B-19}$$

and finally B-17 may be written

$$q - 1 - q \ln(q) - Na \left[ 1 - \frac{1}{Nb \exp(Nc q)} \right] = 0 \quad \text{B-20}$$

For a given set of parameter values  $Na, Nb, Nc$ ,  $q$  may be found from B-20 by an iterative method, for example Newton-Raphson iteration.

If  $r_c$  as determined by the above procedure exceeds the maximum possible corrosion radius  $r_{\max}$  (corresponding to the total outer surface area of the inner canister) then  $r_c$  is reset to  $r_{\max}$ ,  $F_1$  is determined directly from B-16 and  $\rho_J$ ,  $F_2(r)$  and  $\rho_2(r)$  follow at once. In this case the condition of zero

water vapour density at  $r_c$  no longer applies;  $\rho_2$  is non-zero over the whole outer surface of the canister.

### B.1.3 The effect of corrosion inhibition

The corrosion rate may be suppressed by the presence of a thick magnetite layer. Qualitative insight into this behaviour can be gained by assuming a simple model for the corrosion rate

$$\frac{\mu}{1 + \frac{t_R}{l_s}} \quad \text{B-21}$$

where  $\mu$  is the initial corrosion rate,  $t_R$  is the thickness of the magnetite layer and  $l_s$  is a 'suppression length'.

It should be noted that  $t_R \neq t_2$  since the magnetite takes up space originally occupied by the corroded iron as well as part of the annulus. Since the product is 2.097 times thicker than the layer of iron removed by corrosion (see Appendix A.1), the relationship between these quantities is

$$t_R = \frac{2.097}{1.097} t_2 \approx 1.912 t_2 \quad \text{B-22}$$

Thus we write  $t_R = c_R t_2$  with  $c_R = 1.912$ .

In the absence of suppression of the corrosion rate, the equation for the growth of the magnetite is equation A-3 (neglecting galvanic coupling effects) i.e.

$$\frac{dt_2}{dt} = 10^{-6} \mu_{mag} = 1.097 \times 10^{-6} \mu \quad \text{B-23}$$

and the time taken for corrosion product to fill the annulus is

$$T_0 = \frac{10^6 h_a}{1.097 \mu} \quad \text{B-24}$$

where  $\mu$  is in microns/year and  $h_a$  is in metres;  $T_0$  is in years.

If there is suppression of the corrosion rate B-23 has to be modified according to B-21 and B-22 to give

$$\frac{dt_2}{dt} = \frac{1.097 \times 10^{-6} \mu}{\left(1 + \frac{c_R t_2}{l_s}\right)} \quad \text{B-25}$$

In this case, integration of B-25 gives for the time  $T_s$  required to fill the annulus opposite the penetration

$$T_s = T_0 \left( 1 + \frac{c_R h_a}{2l_s} \right) \quad \text{B-26}$$

In the computer model equation B-25 is used to update the residue thickness (and hence gap width) at each timestep for all points within the current corrosion radius  $r_c$ . If the corrosion rate is suppressed equation B-11 becomes

$$\frac{1}{r} \frac{d}{dr} (rF_2) = - \frac{S_c}{(h_a - t_2) \left( 1 + \frac{c_R t_2}{l_s} \right)} \quad \text{B-27}$$

Writing

$$h_{eff} \equiv (h_a - t_2) \left( 1 + \frac{c_R t_2}{l_s} \right) \quad \text{B-28}$$

we see that for the case of constant gap width the solution of B-27 has the same form as B-13 with  $h_g$  replaced by  $h_{eff}$ . Similarly the solution B-15 for  $\rho_2$  and the procedure outlined in Section B.1.2 for finding  $F_1$  and  $r_c$  hold provided that  $h_g$  is replaced by  $h_{eff}$ .

As described in the main text, numerical integration for  $F_2$  and  $\rho_2$  is used instead of the above formulae when the gap varies with radius as a result of the corrosion history.

#### B.1.4 Predicting the variation of the corrosion radius with time

We first note that equation B-27 may be written in the form

$$\frac{dG_2}{dr} = - \frac{rS_c}{h_{eff}} \quad \text{B-29}$$

which shows that  $dG_2/dr < 0$  for all radii. Taking the partial derivative of B-29 with respect to  $h_{eff}$  at fixed radius and then the derivative of  $h_{eff}$  with respect to  $t_2$  gives

$$\frac{\partial}{\partial t_2} \left( \frac{dG_2}{dr} \right) = \frac{rS_c}{h_{eff}^2} \frac{dh_{eff}}{dt_2} = \frac{rS_c}{h_{eff}^2} \left[ -1 + \frac{c_R}{l_s} (h_a - 2t_2) \right] \quad \text{B-30}$$

We consider two cases:

- no corrosion suppression;
- finite corrosion suppression.

In the first case (no corrosion suppression) we may write simply

$$\frac{\partial}{\partial t_2} \left( \frac{dG_2}{dr} \right) = \frac{rS_c}{h_{eff}^2} \frac{dh_{eff}}{dt_2} = -\frac{rS_c}{h_{eff}^2} \quad \text{B-31}$$

This implies that  $dG_2/dr$  decreases (becomes larger in magnitude) everywhere as  $t_2$  increases. Hence  $G_2$  will fall to zero more rapidly, and therefore  $r_c$  will decrease as time progresses. Note that since we are merely seeking the direction of change in  $r_c$  as a function of  $t_2$ , and hence of time, it is not necessary to consider how the flux of water vapour ( $F_1$  or  $F_{20}$ ) varies with  $t_2$ . This also applies to the finite corrosion suppression case.

In the second case (finite corrosion suppression) we note that the right-hand side of B-30 is zero when

$$t_2 = t_{2c} = \frac{1}{2} \left( h_a - \frac{l_s}{c_R} \right) \quad \text{B-32}$$

which to a good approximation in cases of interest gives  $t_{2c} \approx h_a/2$ ; at smaller values of  $t_2$  the right-hand side of B-30 is positive and at larger values it is negative. Thus at early times before the corrosion residue has filled half the annulus opposite the penetration  $r_c$  will increase as time progresses. The analysis becomes more subtle beyond this since at a given point in time  $t_2$  is generally a decreasing function of radius such that the right-hand side of B-30 is negative at small radii and positive at larger radii; the variation of  $r_c$  with time is then not immediately clear. We have not pursued this analysis further. Our predictions for this case are therefore limited to  $t_2(r_0) < t_{2c} \approx h_a/2$ .

## APPENDIX C

**CALCULATION SHEET**

<b>Project Title</b>	SKB CANISTER ASSESSMENT		
<b>Calculation Title</b>	LID INTERFACE CORROSION ASSESSMENT		
<b>Calculation Ref</b>	14182001/C1		
<b>Issue</b>	A		
<b>Calc by</b>	AE Bond	<b>Date</b>	12-01-96
<b>Checked by</b>	AJ Tomczyk	<b>Date</b>	12-01-96
<b>Appd by</b>	AE Bond	<b>Date</b>	12-01-96

**1 - INTRODUCTION**

Stresses will be introduced into the insert lid due to corrosion at the interface of the insert lid and the top of the side walls, on which the seals contact. Stresses will increase until such time that the top of the insert lid and any corrosion build up on the top surface contacts the copper overpack.

The design of the insert for the BWR type fuel has a single, central bolt to hold down the insert lid. This calculation aims to assess the loads in this central bolt.

**1.1 - DESIGN REFERENCES**

The dimensions used in this calculation have been taken from drawing number :  
278 Skiss 002 B (96 02 22)

**1.2 - DIMENSIONS**

Insert lid dimensions:

- Thickness:  $t := 50 \cdot \text{mm}$
- Radius:  $a := 950 \cdot \text{mm}$
- Maximum edge deflection  $y_c := 2 \cdot \text{mm}$

**1.3 - MATERIAL PROPERTY DATA**

- Modulus of elasticity:  $E := 200 \cdot \text{GPa}$
- Poisson's ratio:  $\nu := 0.3$

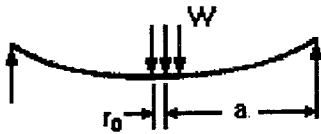
**1.4 - STANDARD DATA**

- $\text{GPa} \equiv \text{Pa} \cdot 10^9$
- $\text{MPa} \equiv \text{Pa} \cdot 10^6$
- $\text{N} \equiv \text{newton}$
- $\text{kN} \equiv \text{N} \cdot 10^3$

## 2 - BOLT LOADS (Simply Supported Edge)

A lower bound calculation of the load on the central bolt can be achieved by assuming that the edge of the insert lid is free to rotate, and is thus simply supported.

Using the equations derived in Roark Table 24 Case 16:



Uniform load over a very small central circular area of radius  $r_o$ ; edge simply supported

Constants

$$D := \frac{E \cdot t^3}{12 \cdot (1 - \nu^2)}$$

Radial position of applied load  $r_o := 15 \cdot \text{mm}$  (Needed to avoid singularity at  $r=0$ )

$$r'_o := \left( \sqrt{1.6 \cdot r_o^2 + t^2} - 0.675 \cdot t \right) \cdot \left( r_o < \frac{t}{2} \right) + r_o \cdot \left( r_o \geq \frac{t}{2} \right)$$

Load required to apply edge displacement

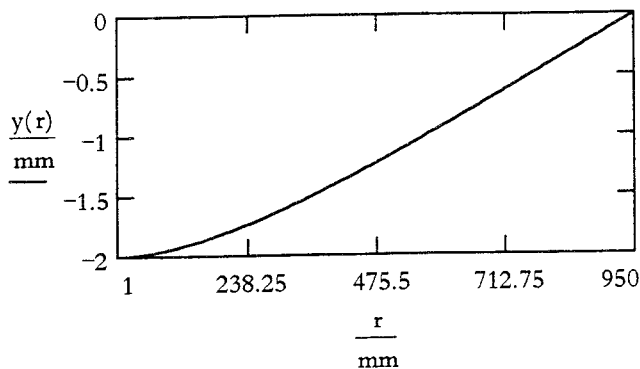
$$W := \frac{16 \cdot \pi \cdot D \cdot y_c}{a^2} \cdot \left( \frac{1 + \nu}{3 + \nu} \right) \quad W = 100.5 \cdot \text{kN}$$

General formulae and graphs for deflection, slope, moment and stress as a function of  $r$ :

Define  $r$ , the range of the radius  $r := 1 \cdot \text{mm}, \frac{a}{99} \dots a$

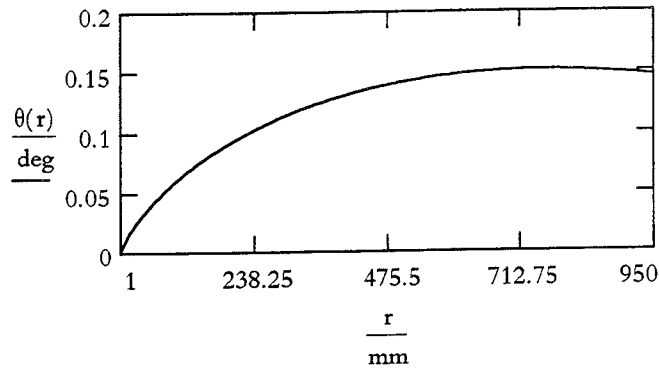
**Deflection:**

$$y(r) := \frac{-W}{16 \cdot \pi \cdot D} \cdot \left[ \frac{3 + \nu}{1 + \nu} \cdot (a^2 - r^2) - 2 \cdot r^2 \cdot \ln \left( \frac{a}{r} \right) \right]$$



Slope:

$$\theta(r) := \frac{W \cdot r}{4 \cdot \pi \cdot D} \cdot \left( \frac{1}{1 + \nu} + \ln\left(\frac{a}{r}\right) \right)$$



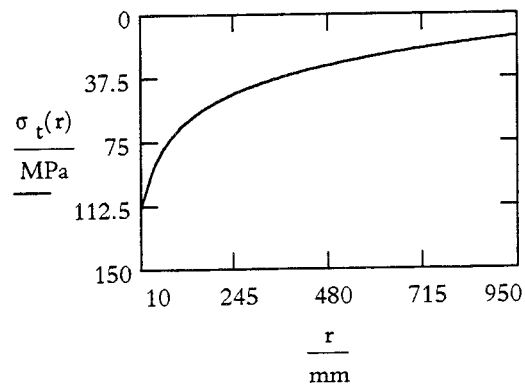
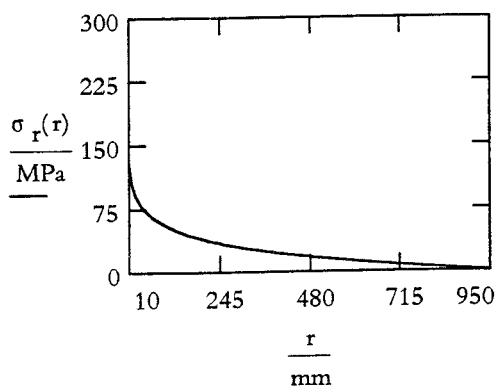
Bending stresses; radial and tangential:

$$M_r(r) := \frac{W}{16 \cdot \pi} \left[ 4 \cdot (1 + \nu) \cdot \ln\left(\frac{a}{r}\right) + (1 - \nu) \cdot \left( \frac{a^2 - r^2}{a^2} \right) \cdot \frac{r_o'^2}{r^2} \right]$$

$$M_t(r) := \frac{W}{16 \cdot \pi} \left[ 4 \cdot (1 + \nu) \cdot \ln\left(\frac{a}{r}\right) + (1 - \nu) \cdot \left( 4 - \frac{r_o'^2}{r^2} \right) \right]$$

$$\sigma_r(r) := \frac{6 \cdot M_r(r)}{t^2}$$

$$\sigma_t(r) := \frac{6 \cdot M_t(r)}{t^2}$$



Radial and tangential stress at center and outer radius:

$$\sigma_r(r_o) = 109.28 \cdot \text{MPa}$$

$$\sigma_r(a) = 0 \cdot \text{MPa}$$

$$\sigma_t(r_o) = 111.1 \cdot \text{MPa}$$

$$\sigma_t(a) = 13.4 \cdot \text{MPa}$$

Combined bending stress

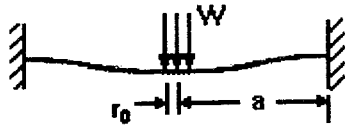
$$\sigma_c := \sqrt{(\sigma_r(r_o))^2 + (\sigma_t(r_o))^2}$$

$$\sigma_c = 155.8 \cdot \text{MPa}$$

### 3 - BOLT LOADS (Built-in Edge)

An upper bound calculation of the load on the central bolt can be achieved by assuming that the edge of the insert lid built-in. If the lid is a close fit in its recess, this may well be the appropriate load case to assume.

Using the equations derived in Roark Table 24 Case 17:



Uniform load over a very small central circular area of radius  $r_0$ ; edge fixed

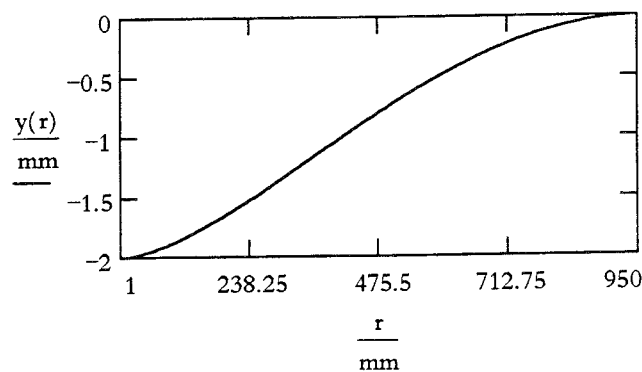
Load required to apply edge displacement

$$W := \frac{16 \cdot \pi \cdot D \cdot y_c}{a^2} \quad W = 255 \cdot \text{kN}$$

General formulae and graphs for deflection, slope, moment and stress as a function of r:

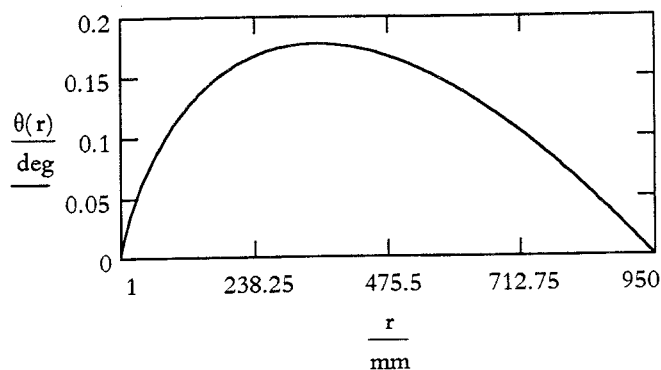
**Deflection:**

$$y(r) := \frac{-W}{16 \cdot \pi \cdot D} \cdot \left[ a^2 - r^2 \cdot \left( 1 + 2 \cdot \ln \left( \frac{a}{r} \right) \right) \right]$$



**Slope:**

$$\theta(r) := \frac{W \cdot r}{4 \cdot \pi \cdot D} \cdot \ln \left( \frac{a}{r} \right)$$



Slope at center and outer radius:

$$\theta(0 \cdot \text{mm}) = 0 \cdot \text{deg}$$

$$\theta(a) = 0 \cdot \text{deg}$$

Maximum slope (magnitude):

$$j := 1..100$$

$$S_{(j)} := \theta(r)$$

$$A := \max(S)$$

$$B := \min(S)$$

$$\theta_{\max} := (A > B) \cdot A + (A \leq B) \cdot B$$

$$\theta_{\max} = 1.7462 \cdot 10^{-3} \cdot \text{deg}$$

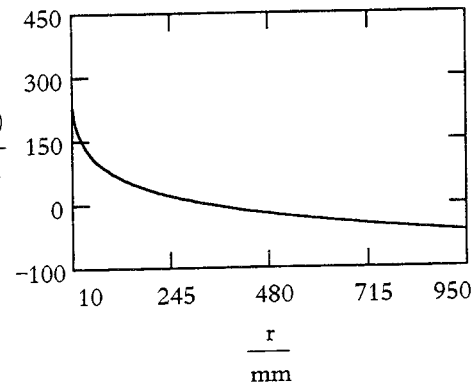
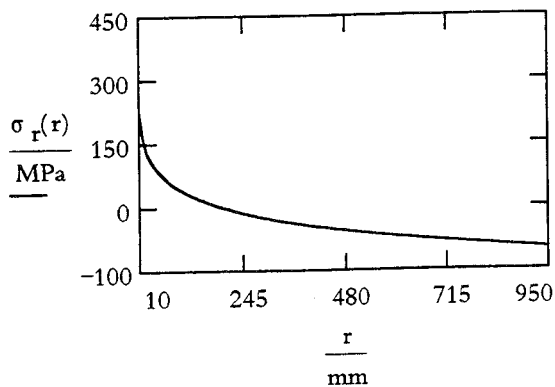
**Bending stresses; radial and tangential:**

$$M_r(r) := \frac{W}{4 \cdot \pi} \cdot \left[ (1 + \nu) \cdot \ln\left(\frac{a}{r}\right) - 1 + \frac{(1 - \nu) \cdot r_o'^2}{4 \cdot r^2} \right]$$

$$M_t(r) := \frac{W}{4 \cdot \pi} \cdot \left[ (1 + \nu) \cdot \ln\left(\frac{a}{r}\right) - \nu + \frac{\nu \cdot (1 - \nu) \cdot r_o'^2}{4 \cdot r^2} \right]$$

$$\sigma_r(r) := \frac{6 \cdot M_r(r)}{t^2}$$

$$\sigma_t(r) := \frac{6 \cdot M_t(r)}{t^2}$$



Radial and tangential stress at center and outer radius:

$$\sigma_r(r_o) = 228.702 \cdot \text{MPa}$$

$$\sigma_r(a) = -48.7 \cdot \text{MPa}$$

$$\sigma_t(r_o) = 252.5 \cdot \text{MPa}$$

$$\sigma_t(a) = -14.6 \cdot \text{MPa}$$

Combined bending stress

$$\sigma_c := \sqrt{(\sigma_r(r_o))^2 + (\sigma_t(r_o))^2}$$

$$\sigma_c = 340.7 \cdot \text{MPa}$$

# APPENDIX D

## D.1 TIME TO FIRST RELEASE OF RADIONUCLIDES

A key question in assessing the safety of the repository is the time at which radionuclides are first released from a spent fuel disposal canister. Release can occur only after the canister has filled with groundwater and a pathway has been established between the spent fuel and the geosphere. If there is a crack in the inner container (as assumed in Section 3), the release of radionuclides will occur after the copper overpack has failed, but otherwise is delayed until the inner canister has corroded through.

### D.1.1 Time

Initially it is assumed that there is a small penetration in the copper overpack, and restricted corrosion starts. We consider the two cases:

#### Crack in the inner container

The copper overpack will fail after corrosion residue has closed the 2 mm annular fitting gap, and the copper around the penetration has been strained to failure (i.e. displaced by 21.8 mm, as calculated in Section 5). The reference corrosion rate assumed in this report is  $0.1 \mu\text{m}/\text{year}$ , and the relative densities of carbon steel and corrosion product (magnetite) are about 2.1. It follows that the time to failure of the copper overpack, and hence the time at which radionuclides are first released from the canister, is

$$\frac{(21.8 + 2.0) 10^{-3}}{(2.1 - 1.0) 10^{-7}} = 2.16 10^5 \text{ years} \quad \text{D-1}$$

#### No crack in the inner container

In this case, radionuclides will be released to the geosphere only after the inner container has corroded through. The relevant thickness of the inner container is 45.76 mm for the BWR canister, and 50.15 mm for the PWR canister.

The inner container undergoes restricted corrosion until the copper overpack fails after  $2.16 10^5$  years. The associated increase in the size of the penetration in the copper overpack is accompanied by a change from restricted to global corrosion (i.e. the inner container undergoes corrosion

over most of its surface). In addition, the annular fitting gap fills with water, and as a result the corrosion rate may be galvanically enhanced; we conservatively assume that the rate is enhanced by a factor 2. It follows that the time for the inner container to corrode through, and hence the time at which radionuclides are first released, is

$$2.16 \cdot 10^5 + \frac{45.76 \cdot 10^{-3}}{2.0 \cdot 10^{-7}} = 4.45 \cdot 10^5 \text{ years} \quad \text{D-2}$$

for the BWR canister, and

$$2.16 \cdot 10^5 + \frac{50.15 \cdot 10^{-3}}{2.0 \cdot 10^{-7}} = 4.67 \cdot 10^5 \text{ years} \quad \text{D-3}$$

for the PWR canister.

### Comment

Provided that there are no complications with the above picture for the failure of containment (e.g. due to ‘early’ liquid water ingress, which can occur at lower corrosion rates), **the time at which radionuclides are first released from a canister is inversely proportional to the corrosion rate.**

#### *The effect of uncertainty in the corrosion rate*

If the uncertainty in the corrosion rate is scoped by carrying out a calculation using a lower value of  $0.01 \mu\text{m}/\text{year}$ , the above times increase by a factor 10. However, at this corrosion rate liquid water can enter the canister during its ‘dynamic’ corrosion phase (as described in Section 3). In one scenario (Scenario 3 of Section 3.4.4, in which the penetration in the copper overpack and the crack in the inner container are both at the bottom of the canister), water makes contact with the spent fuel before being expelled when the pressure in the canister exceeds the external hydrostatic pressure. In this scenario, a small amount of contaminated water reaches the geosphere between  $8.26 \cdot 10^3$  years and  $1.48 \cdot 10^4$  years, after which release stops until the copper overpack fails.

#### *The effect of uncertainty in the penetration size*

If the corrosion rate is  $0.1 \mu\text{m}/\text{year}$ , and the initial (circular cross-section) penetration in the copper overpack has an area that is smaller than  $8.25 \text{ mm}^2$ , liquid water doesn’t enter the canister (see Section 3.3); corrosion is limited by the diffusion of water vapour, and is restricted to a small area around the penetration. It follows that for a penetration smaller than the reference ( $5 \text{ mm}^2$ ), the annular gap will fill and the copper

overpack will be breached at practically the same times as those given above.

If the penetration in the copper overpack has an area that is somewhat larger than  $8.25 \text{ mm}^2$ , liquid water can enter the canister; if the penetration and the crack in the inner container are both near the bottom of the canister, a small amount of contaminated water reaches the geosphere at an early stage (cf. the discussion for a lower corrosion rate). However, the annular gap will fill and the copper overpack will be breached at roughly the same times as for the case of a smaller penetration.

For even larger penetrations, liquid water enters the canister at an early stage, and global corrosion starts immediately. If the inner container also has a crack, the time at which radionuclides are first released from the canister is short. Otherwise the inner container has to corrode through, and the time at which radionuclides are first released, is

$$\frac{45.76 \cdot 10^{-3}}{2.0 \cdot 10^{-7}} = 2.29 \cdot 10^5 \text{ years} \quad \text{D-4}$$

for the BWR canister, and

$$\frac{50.15 \cdot 10^{-3}}{2.0 \cdot 10^{-7}} = 2.51 \cdot 10^5 \text{ years} \quad \text{D-5}$$

for the PWR canister. However, a large initial penetration in the copper overpack is regarded as extremely improbable.

The effect of varying the penetration size may be summarised by noting that

- the ratio of penetration size to corrosion rate determines how much water can enter the canister, and whether corrosion is limited by the diffusion of water vapour;
- time scales are inversely proportional to the corrosion rate.

### **D.1.2 Data Uncertainties**

The key parameter in the above time calculations is the anaerobic corrosion rate of carbon steel. The discussion of data uncertainties therefore focuses on this parameter.

#### **The corrosion rate**

The corrosion rate of  $0.1 \mu\text{m}/\text{year}$  used in the above calculations is derived from hydrogen evolution measurements by Blackwood et al /5-6/. The

experiment looked at the anaerobic corrosion of type BS4360 grade 43A carbon steel wires in synthetic Swedish granitic groundwater with an initial pH of 8.1. Four cases were investigated, being characterised by two different pre-treatments of the wires (either pickled in HCl or degreased in absolute alcohol) and two different temperatures (either 30°C or 50°C). The data was obtained over a period (500 days) which is very short compared to the canister corrosion time scale of order 10<sup>5</sup> years.

Since the corrosion rate is expected to decrease with time, 0.1 µm/year is thought to represent an upper limit for the long-term corrosion of the inner container (/5-6/, /D-1/, /3-1/). However, given the extreme extrapolation involved in using this data (or any other laboratory data), considerable uncertainty must attach to this number. It is recommended that, for the purpose of a Safety Assessment, the uncertainty can be quantified by carrying out parallel calculations using a corrosion rate of 0.01 µm/year (this value represents the lower end of the range of corrosion rates measured at the end of the experiment).

### **The corrosion rate in a humid atmosphere**

Blackwood et al /3-1/ report that the long-term rate of hydrogen production from carbon steel in a high-humidity anaerobic atmosphere is the same as for a sample completely submerged in a synthetic Swedish granitic groundwater. Hence *the long-term corrosion rate is the same (0.1 µm/year) for the two cases.* The time to reach the long-term rate is also similar. However, for partially submerged samples this 'settling' time is considerably longer (the inferred corrosion rate on these samples is 0.15 µm/year after 5000 hours). Despite their comment that this may be relevant to corrosion in disposal canisters, we note that

- the corrosion rate was still decreasing at the end of the experiment;
- there is again an extreme extrapolation involved in applying the data on a relevant time scale.

### **Factors influencing the corrosion rate**

In general, the corrosion rate of carbon steel submerged in groundwater will depend on temperature, salinity, pH and hydrogen overpressure. In the case of the copper canister with cast steel inner component, galvanic coupling may also affect the corrosion rate. We summarise the experimental evidence relating to the influence of these factors below.

### *Temperature*

In the experiments cited by Platts et al /D-1/, the corrosion rate of carbon steel under demineralised water is practically independent of temperature in the range 25°C–100°C. It appears that *below 100°C temperature does not significantly influence the corrosion rate.*

### *Salinity*

Weight loss and hydrogen production experiments looking at the corrosion of carbon steel in deaerated water typical of Swiss granitic formations show (broadly) that the concentrations of dissolved salts (mainly  $\text{HCO}_3^-/\text{CO}_3^{2-}$ ,  $\text{Cl}^-$  and  $\text{SO}_4^{2-}$ ; with  $\text{Na}^+$ ,  $\text{Mg}^{2+}$  and  $\text{Ca}^{2+}$  as the balancing anions) do not significantly affect the corrosion rate /D-1/. However, a measurement of the effect of ionic strength on corrosion using a solution of SKB synthetic groundwater 10 times stronger than usual (but still at a pH of 8.1) gave a corrosion rate about an order of magnitude higher than in the standard groundwater /3-1/; this result is not fully understood.

### *pH*

Under acidic conditions (0.1M  $\text{HCO}_3^-$ ), the corrosion rate of carbon steel appears to be similar (or even lower) to that for demineralised water /D-1/. Blackwood et al /3-1/ conducted experiments on the effects of dissolved ammonia and nitric acid (in quantities corresponding to the maximum expected to be produced by radiolysis over the lifetime of the canister) in synthetic Swedish granitic groundwater. The rates of hydrogen production were initially reduced, but later reached the usual long-term value. Taken together, these results suggest that *for a fairly wide range of initial pH values (approximately 3–10), the long-term corrosion rate is practically independent of pH.* It should be noted that in the (closed) experimental cells the final pH was between 9 and 10. However, in a perforated canister the groundwater inventory would not be limited, and therefore the long-term chemical environment would be different from that seen in the laboratory. This may affect the long-term corrosion rate.

### *Hydrogen overpressure*

The theory of electrochemical kinetics suggests that anaerobic corrosion reactions might be retarded by increasing hydrogen overpressure ('activity'). This was investigated by Blackwood et al /5-6/ by comparing the weight loss of carbon steel coupons exposed to synthetic Swedish granitic groundwater at 90°C under atmospheres with a hydrogen overpressure of 1, 10 and 100 atmospheres. Corrosion rates were generally less than 1  $\mu\text{m}/\text{year}$  and decreased with time, but contrary to expectations were higher at 10 atmospheres than at 1 atmosphere. However, the weight losses

were small and difficult to measure, and therefore caution is necessary in drawing conclusions.

#### *Galvanic coupling*

The calculations described in Section D.1.1 (conservatively) allow for galvanic coupling between the copper overpack and the cast steel inner container.

#### *Summary*

From the evidence cited above, it appears that the long-term anaerobic corrosion rate of carbon steel in synthetic Swedish granitic groundwater may (within limits) be treated as independent of temperature and pH. The influence of salinity and hydrogen overpressure is not entirely clear.

The corrosion rate in an anaerobic humid atmosphere may be affected by temperature and by hydrogen overpressure; in this case, there is no evidence relating to the effect of hydrogen overpressure.

### **D.1.3 Recommendations regarding safety assessment modelling**

It is recommended that, for the purpose of a Safety Assessment, a corrosion rate of  $0.1 \mu\text{m}/\text{year}$  should be adopted as a reference value. Uncertainty can be addressed by carrying out parallel calculations using a lower corrosion rate of  $0.01 \mu\text{m}/\text{year}$ . There is no evidence to suggest that a corrosion rate significantly higher than  $0.1 \mu\text{m}/\text{year}$  will be sustained under likely repository conditions. The greatest uncertainty is associated with the very large extrapolation in time made in using experimental data (measured over periods of the order of a few years) as the basis for estimating the corrosion rate on time scales of the order of  $10^5$  years.

# List of SKB reports

## Annual Reports

1977-78

TR 121

### **KBS Technical Reports 1 – 120**

Summaries

Stockholm, May 1979

1979

TR 79-28

### **The KBS Annual Report 1979**

KBS Technical Reports 79-01 – 79-27

Summaries

Stockholm, March 1980

1980

TR 80-26

### **The KBS Annual Report 1980**

KBS Technical Reports 80-01 – 80-25

Summaries

Stockholm, March 1981

1981

TR 81-17

### **The KBS Annual Report 1981**

KBS Technical Reports 81-01 – 81-16

Summaries

Stockholm, April 1982

1982

TR 82-28

### **The KBS Annual Report 1982**

KBS Technical Reports 82-01 – 82-27

Summaries

Stockholm, July 1983

1983

TR 83-77

### **The KBS Annual Report 1983**

KBS Technical Reports 83-01 – 83-76

Summaries

Stockholm, June 1984

1984

TR 85-01

### **Annual Research and Development Report 1984**

Including Summaries of Technical Reports Issued during 1984. (Technical Reports 84-01 – 84-19)

Stockholm, June 1985

1985

TR 85-20

### **Annual Research and Development Report 1985**

Including Summaries of Technical Reports Issued during 1985. (Technical Reports 85-01 – 85-19)

Stockholm, May 1986

1986

TR 86-31

### **SKB Annual Report 1986**

Including Summaries of Technical Reports Issued during 1986

Stockholm, May 1987

1987

TR 87-33

### **SKB Annual Report 1987**

Including Summaries of Technical Reports Issued during 1987

Stockholm, May 1988

1988

TR 88-32

### **SKB Annual Report 1988**

Including Summaries of Technical Reports Issued during 1988

Stockholm, May 1989

1989

TR 89-40

### **SKB Annual Report 1989**

Including Summaries of Technical Reports Issued during 1989

Stockholm, May 1990

1990

TR 90-46

### **SKB Annual Report 1990**

Including Summaries of Technical Reports Issued during 1990

Stockholm, May 1991

1991

TR 91-64

### **SKB Annual Report 1991**

Including Summaries of Technical Reports Issued during 1991

Stockholm, April 1992

1992

TR 92-46

### **SKB Annual Report 1992**

Including Summaries of Technical Reports Issued during 1992

Stockholm, May 1993

1993

TR 93-34

### **SKB Annual Report 1993**

Including Summaries of Technical Reports Issued during 1993

Stockholm, May 1994

1994

TR 94-33

**SKB Annual Report 1994**

Including Summaries of Technical Reports Issued during 1994  
Stockholm, May 1995

1995

TR 95-37

**SKB Annual Report 1995**

Including Summaries of Technical Reports Issued during 1995  
Stockholm, May 1996

1996

TR 96-25

**SKB Annual Report 1996**

Including Summaries of Technical Reports Issued during 1996  
Stockholm, May 1997

**List of SKB Technical Reports 1997**

TR 97-01

**Retention mechanisms and the flow wetted surface – implications for safety analysis**

Mark Elert  
Kemakta Konsult AB  
February 1997

TR 97-02

**Äspö HRL – Geoscientific evaluation 1997/1. Overview of site characterization 1986–1995**

Roy Stanfors<sup>1</sup>, Mikael Erlström<sup>2</sup>,  
Ingemar Markström<sup>3</sup>  
<sup>1</sup> RS Consulting, Lund  
<sup>2</sup> SGU, Lund  
<sup>3</sup> Sydkraft Konsult, Malmö  
March 1997

TR 97-03

**Äspö HRL – Geoscientific evaluation 1997/2. Results from pre-investigations and detailed site characterization. Summary report**

Ingvar Rhén (ed.)<sup>1</sup>, Göran Bäckblom (ed.)<sup>2</sup>,  
Gunnar Gustafson<sup>3</sup>, Roy Stanfors<sup>4</sup>, Peter Wikberg<sup>2</sup>  
<sup>1</sup> VBB Viak, Göteborg  
<sup>2</sup> SKB, Stockholm  
<sup>3</sup> VBB Viak/CTH, Göteborg  
<sup>4</sup> RS Consulting, Lund  
May 1997

TR 97-04

**Äspö HRL – Geoscientific evaluation 1997/3. Results from pre-investigations and detailed site characterization. Comparison of predictions and observations. Geology and mechanical stability**

Roy Stanfors<sup>1</sup>, Pär Olsson<sup>2</sup>, Håkan Stille<sup>3</sup>  
<sup>1</sup> RS Consulting, Lund  
<sup>2</sup> Skanska, Stockholm  
<sup>3</sup> KTH, Stockholm  
May 1997

TR 97-05

**Äspö HRL – Geoscientific evaluation 1997/4. Results from pre-investigations and detailed site characterization. Comparison of predictions and observations. Hydrogeology, groundwater chemistry and transport of solutes**

Ingvar Rhén<sup>1</sup>, Gunnar Gustafson<sup>2</sup>, Peter Wikberg<sup>3</sup>  
<sup>1</sup> VBB Viak, Göteborg  
<sup>2</sup> VBB Viak/CTH, Göteborg  
<sup>3</sup> SKB, Stockholm  
June 1997

TR 97-06

**Äspö HRL – Geoscientific evaluation 1997/5. Models based on site characterization 1986–1995**

Ingvar Rhén (ed.)<sup>1</sup>, Gunnar Gustafson<sup>2</sup>,  
Roy Stanfors<sup>3</sup>, Peter Wikberg<sup>4</sup>  
<sup>1</sup> VBB Viak, Göteborg  
<sup>2</sup> VBB Viak/CTH, Göteborg  
<sup>3</sup> RS Consulting, Lund  
<sup>4</sup> SKB, Stockholm  
October 1997

TR 97-07

**A methodology to estimate earthquake effects on fractures intersecting canister holes**

Paul La Pointe, Peter Wallmann, Andrew Thomas,  
Sven Follin  
Golder Associates Inc.  
March 1997

TR 97-08

**Äspö Hard Rock Laboratory Annual Report 1996**

SKB  
April 1997

TR 97-09

**A regional analysis of groundwater flow and salinity distribution in the Äspö area**

Urban Svensson  
Computer-aided Fluid Engineering AB  
May 1997

TR 97-10

**On the flow of groundwater in closed tunnels. Generic hydrogeological modelling of nuclear waste repository, SFL 3–5**

Johan G Holmén  
Uppsala University/Golder Associates AB  
June 1997

TR 97-16

**Groundwater flow through a natural fracture. Flow experiments and numerical modelling**

Erik Larsson  
Dept. of Geology, Chalmers University of Technology, Göteborg, Sweden  
September 1997

TR 97-11

**Analysis of radioactive corrosion test specimens by means of ICP-MS. Comparison with earlier methods**

R S Forsyth  
Forsyth Consulting  
July 1997

TR 97-17

**A site scale analysis of groundwater flow and salinity distribution in the Äspö area**

Urban Svensson  
Computer-aided Fluid Engineering AB  
October 1997

TR 97-12

**Diffusion and sorption properties of radionuclides in compacted bentonite**

Ji-Wei Yu, Ivars Neretnieks  
Dept. of Chemical Engineering and Technology, Chemical Engineering, Royal Institute of Technology, Stockholm, Sweden  
July 1997

TR 97-18

**Release of segregated nuclides from spent fuel**

L H Johnson, J C Tait  
AECL, Whiteshell Laboratories, Pinawa, Manitoba, Canada  
October 1997

TR 97-13

**Spent nuclear fuel – how dangerous is it? A report from the project "Description of risk"**

Allan Hedin  
Swedish Nuclear Fuel and Waste Management Co,  
Stockholm, Sweden  
March 1997

TR 97-14

**Water exchange estimates derived from forcing for the hydraulically coupled basins surrounding Äspö island and adjacent coastal water**

Anders Engqvist  
A & I Engqvist Konsult HB, Vaxholm, Sweden  
August 1997

TR 97-15

**Dissolution studies of synthetic soddyite and uranophane**

Ignasi Casas<sup>1</sup>, Isabel Pérez<sup>1</sup>, Elena Torrero<sup>1</sup>, Jordi Bruno<sup>2</sup>, Esther Cera<sup>2</sup>, Lara Duro<sup>2</sup>  
<sup>1</sup> Dept. of Chemical Engineering, UPC  
<sup>2</sup> QuantiSci SL  
September 1997